



저작자표시-비영리-변경금지 2.0 대한민국

이용자는 아래의 조건을 따르는 경우에 한하여 자유롭게

- 이 저작물을 복제, 배포, 전송, 전시, 공연 및 방송할 수 있습니다.

다음과 같은 조건을 따라야 합니다:



저작자표시. 귀하는 원저작자를 표시하여야 합니다.



비영리. 귀하는 이 저작물을 영리 목적으로 이용할 수 없습니다.



변경금지. 귀하는 이 저작물을 개작, 변형 또는 가공할 수 없습니다.

- 귀하는, 이 저작물의 재이용이나 배포의 경우, 이 저작물에 적용된 이용허락조건을 명확하게 나타내어야 합니다.
- 저작권자로부터 별도의 허가를 받으면 이러한 조건들은 적용되지 않습니다.

저작권법에 따른 이용자의 권리는 위의 내용에 의하여 영향을 받지 않습니다.

이것은 [이용허락규약\(Legal Code\)](#)을 이해하기 쉽게 요약한 것입니다.

[Disclaimer](#)

공학박사학위논문

**Behavior and Analysis of Transfer Zone in
Pretensioned Prestressed Concrete
Members**

프리텐션 프리스트레스트 콘크리트
부재의 전달영역 거동 및 해석

2015년 2월

서울대학교 대학원
건설환경공학부
박 호

**Behavior and Analysis of Transfer Zone in
Pretensioned Prestressed Concrete Members**

**프리텐션 프리스트레스트 콘크리트 부재의
전달영역 거동 및 해석**

지도교수 조재열

이 논문을 공학 박사 학위논문으로 제출함
2014년 10월

서울대학교 대학원
건설환경공학부
박 호

박호의 박사학위논문을 인준함
2015년 1월

위 원 장 _____ (인)

부위원장 _____ (인)

위 원 _____ (인)

위 원 _____ (인)

위 원 _____ (인)

Abstract

Behavior and Analysis of Transfer Zone in Pretensioned Prestressed Concrete Members

Ho Park

Department of Civil and Environmental Engineering

The Graduate School

Seoul National University

Transfer length is defined as the distance over which prestressing steel should be bonded to concrete to transfer the effective prestress in the prestressing steel. Estimation of transfer length can greatly affect cracking moment at service limit state as well as shear strength and development length at ultimate limit state due to the lower prestressing force within the transfer zone.

Many empirical equations have been proposed for transfer length, however it is well known that there is a significant discrepancy between the predictions from the equations. The first goal of this study is to reassess the influences of the well-known test variables on transfer length and to examine new experimental factors that might affect the estimation of transfer length. In addition, the previous empirical equations assumed a constant bond stress distribution along the transfer zone. This assumption was made based on the observation of a linear distribution of concrete strain. The second goal is to propose a transfer length equation based on the actual distribution of bond stress. The last goal was to evaluate transfer length of high-strength strands that have been recently developed.

For the purposes, an extensive experimental program was conducted. Strand strains were measured on the helical wires with electrical resistance strain gauges (ERSGs). Applicability of ERSGs to transfer length test and analytical model for behavior of strand were discussed. Influences of the test variables on transfer length were identified and the empirical equations including the current code provisions were evaluated. Finally, a novel bond model and transfer length equation was proposed based on the actual bond behavior of strand.

Test results showed that the effects of initial prestress, concrete compressive strength at transfer, and strand diameter could be accounted for by the equation proposed by Oleśniewicz. It implies a linear distribution of bond stress and a parabolic distribution of strand strain. In the considered range of cover depth, cross section size, and strand spacing, the effects of these factors were negligible if conforming to the current code provisions. The effects of curing condition, debonding, reinforcement spacing, and prestress release method were examined.

The current code provisions provided conservative estimates for transfer length of high strength strand. The cover depth and strand spacing of the current code are also feasible to high strength strand.

Based on the measured strand strain, a novel bond-slip-strain relationship for a strand in the transfer zone of a pretensioned concrete member is presented. Estimates obtained from the proposed model were in good agreement with the test results from other studies as well as those from this work.

Keywords: pretension, transfer length, high strength strand, bond stress, strand strain, bond-slip-strain relationship

Student number: 2009-30232

Table of Contents

Abstract	i
List of Table	ix
List of Figure	xiii
Notations	xxi
1. Introduction	1
1.1 Research Background.....	1
1.1.1 Definition and Importance of Transfer Length	1
1.1.2 Problems with the Previous Research on Transfer Length	3
1.2 Scope and Objectives of the Thesis.....	4
1.3 Organization of the Thesis.....	6
2. Literature Review	9
2.1 Introduction	9
2.2 Bond Mechanism of Prestressing Strand.....	11
2.2.1 Adhesion	11
2.2.2 Friction.....	12
2.2.3 Mechanical Interlocking	13
2.3 Bond Models for Prestressing Strand	14
2.3.1 Balázs (1992)	14
2.3.2 Den Uijl (1992)	21
2.4 Theoretical Analyses Based on Concrete Confinement	25

2.4.1 Weerasekera and Loov (1990)	26
2.4.2 Den Uijl and Bigaj (1996)	27
2.4.3 Oh and Kim (2006)	27
2.4.4 Comparison of Analytical Results.....	27
2.5 Empirical Equations for Transfer Length	32
2.5.1 Design Code.....	32
2.5.1.1 <i>ACI318-11 (2011)</i>	32
2.5.1.2 <i>AASHTO LRFD Bridge Design Specifications (2010)</i>	34
2.5.1.3 <i>Eurocode2 (2004)</i>	35
2.5.2 Empirical Equations from Previous Research.....	38
2.5.2.1 <i>Oleśniewicz (1975)</i>	38
2.5.2.2 <i>Zia and Mostafa (1977)</i>	39
2.5.2.3 <i>Cousins et al. (1990a)</i>	39
2.5.2.4 <i>Mitchell et al. (1993)</i>	41
2.5.2.5 <i>Russell and Burns (1993)</i>	42
2.5.2.6 <i>Deatherage and Burdette (1994)</i>	44
2.5.2.7 <i>Buckner (1995)</i>	45
2.5.2.8 <i>Tadros and Baishya (1996)</i>	46
2.5.2.9 <i>Mahmoud et al. (1999)</i>	47
2.5.2.10 <i>Barnes et al. (2003)</i>	48
2.5.2.11 <i>Kose and Burkette (2005)</i>	50
2.5.2.12 <i>Martí-Vargas et al. (2007b)</i>	50
2.5.3 Factors Affecting Transfer Length	52
2.5.3.1 <i>Compressive Strength of Concrete</i>	52

2.5.3.2 <i>Initial Prestress</i>	56
2.5.3.3 <i>Strand Diameter</i>	56
2.5.3.4 <i>Strand Surface Condition</i>	58
2.5.3.5 <i>Cover Depth and Strand Spacing</i>	59
2.5.3.6 <i>Top Bar Effect</i>	61
2.5.3.7 <i>Time-Dependent Effect</i>	62
2.5.3.8 <i>Prestress Release Method</i>	63
3. High Strength Prestressing Strand	65
3.1 Introduction	65
3.2 Mechanical Properties of High Strength Prestressing Strand	65
4. Experimental Program	73
4.1 Introduction	73
4.2 Transfer Length Test for Grade 1,860 Strands	74
4.2.1 Test Variables	74
4.2.2 Material Properties	85
4.2.2.1 <i>Concrete</i>	85
4.2.2.2 <i>Prestressing Strand and Reinforcing Steel Bars</i>	86
4.2.3 Fabrication of Test Specimens	88
4.2.4 Instrumentation	93
4.2.4.1 <i>DEMEC gauge</i>	93
4.2.4.2 <i>ERSGs for strand and concrete</i>	94
4.2.4.3 <i>LVDTs for end slip and Load cells</i>	100
4.3 Transfer Length Test for Grade 2,400 Strands	101

4.3.1 Test Variables	101
4.3.2 Material Properties.....	108
4.3.2.1 Concrete	108
4.3.2.2 Prestressing Strand	109
4.3.3 Fabrication of Test Specimens	110
4.3.4 Instrumentation	114
5. Experimental Results	117
5.1 Introduction	117
5.2 Applicability of ERSGs to Transfer Length Test.....	117
5.2.1 Comparison of Strain Measurements using DEMEC and ERSG	117
5.2.2 Applicability of ERSGs for Strand	122
5.2.2.1 Loss of Bonds due to Gauge Attachment.....	123
5.2.2.2 Stability under High Temperatures	125
5.3 Estimation of Initial Prestress.....	128
5.3.1 Behavior of Seven-Wire Strand Subject to Axial and Torsional Displacement.....	128
5.3.2 Estimation of Prestress at Each Fabrication Stage.....	134
5.3.2.1 Relationship between Measured Strain, Axial Force, and Twisting Moment	134
5.3.2.2 Jacking Force and Anchorage Seating Loss	139
5.3.2.3 Time-Dependent Losses and Prestress just before Release.....	145
5.3.2.4 Loss due to Elastic Shortening of Specimen and Initial Prestress	147
5.4 Transfer Length	157
5.4.1 Determination of Transfer Length.....	157
5.4.2 Effect of Test Variables on Transfer Length.....	165

5.4.2.1 Initial Prestress	165
5.4.2.2 Concrete Compressive Strength at Transfer.....	169
5.4.2.3 Strand Diameter.....	173
5.4.2.4 Cover Depth and Cross Section Size.....	175
5.4.2.5 Strand Spacing.....	185
5.4.2.6 Curing Condition	188
5.4.2.7 Debonding.....	190
5.4.2.8 Reinforcement Spacing.....	191
5.4.2.9 Prestress Release Method	192
5.4.3 Comparison with Empirical Equations	195
5.4.3.1 ACI318-11 (2011)	195
5.4.3.2 Eurocode2 (2004).....	198
5.4.3.3 Oleśniewicz (1975)	199
5.4.3.4 Zia and Mostafa (1977)	200
5.4.3.5 Balázs (1992)	201
5.4.3.6 Mitchell et al. (1993)	202
5.4.3.7 Mahmoud et al. (1999)	203
5.4.3.8 Barnes et al. (2003)	204
5.4.3.9 Kose and Burkette (2005)	205
5.4.3.10 Martí-Vargas et al. (2007b)	206
5.5 Concluding Remarks	207
6. Bond-slip-strain Model of Strand.....	209
6.1 Introduction	209
6.2 Bond Stress and Slip of Test Specimens	212

6.2.1 Test Specimens Included in This Analysis.....	212
6.2.2 Calculation of Bond Stress, Slip, and Transfer Length.....	214
6.3 Bond-Slip-Strain Relationship	215
6.3.1 Derivation of the Relationship between Bond, Slip, and Strain	215
6.3.2 Bond Stress Distribution	218
6.3.3 Slip Distribution.....	221
6.3.4 Determination of Coefficients and Transfer Length	222
6.3.5 Comparison of the Proposed Model and Experimental Result	224
6.4 Verification of the Proposed Model.....	227
6.5 Concluding Remarks	233
7. Conclusions	235
7.1 Methodology of Measurement	235
7.2 Resolution of Discrepancies in Previous Equations	236
7.3 Transfer Length of High Strength Strand	237
7.4 Proposal of New Transfer Length Equation	237
Reference	239
Appendix A.....	253
Appendix B.....	267
국문초록.....	287

List of Tables

Table 2.1	Empirical equations for transfer length and their parameters (Martí-Vargas et al., 2007b).....	54
Table 3.1	Specifications for the mechanical properties of the high strength prestressing strands (KATS, 2011).....	68
Table 3.2	Measured mechanical properties of SWPC7CL strand (Choi, 2015) ...	69
Table 3.3	Measured mechanical properties of SWPC7DL strand (Choi, 2015) .	70
Table 3.4	Stress corrosion test of high strength prestressing strands (Kim et al., 2014).....	71
Table 4.1	Test variables for Grade 1,860 strands.....	77
Table 4.2	Test variables considered in each test series	79
Table 4.3	Specimens of test series 1~3	80
Table 4.4	Specimens of test series 4	81
Table 4.5	Specimens of test series 5	82
Table 4.6	Specimens of test series 6	83
Table 4.7	Specimens of test series 7	84
Table 4.8	Concrete mix proportion for tests of Grade 1,860 strands.....	85
Table 4.9	Average compressive strength and elastic moduli of concrete at transfer and after 28 days (test series 1~7).....	86
Table 4.10	Mechanical properties of Grade 1,860 strand.....	87
Table 4.11	Test variables for Grade 2,400 strands.....	103
Table 4.12	Specimens of test series 8	105
Table 4.13	Specimens of test series 9	106
Table 4.14	Specimens of test series 10	107

Table 4.15	Concrete mix proportion for tests of Grade 2,400 strands.....	108
Table 4.16	Average compressive strength and elastic moduli of concrete at transfer and after 28 days (test series 8~10).....	109
Table 4.17	Mechanical properties of Grade 2,400 strand.....	110
Table 5.1	Comparison of the measured and calculated elongations of the strands tensioned in the prestressing bed for transfer length specimens with single strand.....	143
Table 5.2	Comparison of the measured and calculated elongations of the strands tensioned in the prestressing bed for development length specimens.....	144
Table 5.3	Stress in strand and prestress losses at each fabrication stage (test series 1 and 2).....	150
Table 5.4	Stress in strand and prestress losses at each fabrication stage (test series 3 and 4).....	151
Table 5.5	Stress in strand and prestress losses at each fabrication stage (test series 5).....	152
Table 5.6	Stress in strand and prestress losses at each fabrication stage (test series 6 and 7).....	153
Table 5.7	Stress in strand and prestress losses at each fabrication stage (test series 8).....	154
Table 5.8	Stress in strand and prestress losses at each fabrication stage (test series 9).....	155
Table 5.9	Stress in strand and prestress losses at each fabrication stage (test series 10).....	156
Table 5.10	Measured transfer length (test series 1 ~ 4).....	161
Table 5.11	Measured transfer length (test series 5 ~ 6).....	162

Table 5.12	Measured transfer length (test series 7 ~ 8).....	163
Table 5.13	Measured transfer length (test series 9 ~ 10).....	164
Table 5.14	Influence of initial prestress on transfer length.....	166
Table 5.15	Influence of initial prestress on transfer length of high strength strand	168
Table 5.16	Influence of concrete compressive strength at transfer on transfer length of specimens with a single strand	171
Table 5.17	Influence of concrete compressive strength at transfer on transfer length of specimens with two strands	172
Table 5.18	Influence of strand diameter on transfer length	173
Table 5.19	Influence of cover depth on transfer length of fully bonded Grade 1,860 strand.....	177
Table 5.20	Influence of cover depth on transfer length of partially debonded Grade 1,860 strand.....	178
Table 5.21	Influence of cross section size on transfer length of fully bonded Grade 1,860 strand.....	180
Table 5.22	Influence of cross section size on transfer length of partially debonded Grade 1,860 strand.....	181
Table 5.23	Influence of cover depth on transfer length of high strength strand embedded in normal strength concrete	183
Table 5.24	Influence of cover depth on transfer length of high strength strand embedded in high strength concrete	184
Table 5.25	Influence of strand spacing on transfer length of fully bonded Grade 1,860 strand.....	185
Table 5.26	Influence of strand spacing on transfer length of high strength strand	

	embedded in normal strength concrete	187
Table 5.27	Influence of strand spacing on transfer length of high strength strand embedded in high strength concrete	188
Table 5.28	Influence of curing conditions on transfer length	190
Table 5.29	Influence of debonding on transfer length	190
Table 5.30	Influence of reinforcement spacing on transfer length	191
Table 5.31	Influence of prestress release method on transfer length.....	194
Table 6.1	Test specimens included in the analysis.....	213
Table 6.2	Comparison of the calculated and measured transfer lengths in this study.....	225
Table 6.3	Comparison of the proposed model and the transfer lengths measured by Kim (2000).....	228
Table 6.4	Comparison of the proposed model and the slip measured by Kim (2000).....	228
Table 6.5	Comparison of the proposed model and the transfer lengths measured by Mitchell et al. (1993)	230
Table 6.6	Comparison of the proposed model and the transfer lengths measured by Russell and Burns (1997).....	232

List of Figures

Figure 2.1	Rigid-brittle behavior of adhesion (Russell and Burns, 1993).....	12
Figure 2.2	Wedge action from Hoyer's effect (Kim, 2000)	13
Figure 2.3	Calculated bond behaviors of prestressing strand: (a) bond-slip relationship; (b) bond stress distribution; (c) slip distribution; and (d) strand stress distribution (Balázs, 1992)	20
Figure 2.4	Set-up of pull-out and push-in tests: (a) pull-out fixed; (b) pull-out free; and (c) push-in (Den Uijl, 1992).....	22
Figure 2.5	Relationship among bond stress, slip, and strand stress: (a) push-in; (b) pull-out free; and (c) pull-out fixed ($k = 30$ kN/mm); and (d) pull-out fixed ($k = 165$ kN/mm) (Den Uijl, 1992).....	24
Figure 2.6	Analytical results of concrete confinement models: (a) strand strain distribution; (b) bond stress distribution; (c) crack penetration depth; (d) crack width at surface; (e) radial strand strain; and (f) radial stress-strain relationship.....	28
Figure 2.7	Radial and circumferential stress at elastic section: (a) Oh and Kim (2006); (b) Weerasekera and Loov (1990); (c) Den Uijl and Bigaj (1996)	29
Figure 2.8	Radial and circumferential stress at partially cracked section: (a) Oh and Kim (2006); (b) Weerasekera and Loov (1990); (c) Den Uijl and Bigaj (1996).....	30
Figure 2.9	Radial and circumferential stress at fully cracked section: (a) Oh and Kim (2006); (b) Weerasekera and Loov (1990); (c) Den Uijl and Bigaj (1996)	31

Figure 2.10	Assumed bond distribution in Cousins et al. model (Cousins et al., 1990a)	40
Figure 2.11	Set-up of ECADA test method (Martí-Vargas et al., 2007a).....	51
Figure 3.1	Measured stress-strain curves of high strength prestressing strands.....	67
Figure 3.2	Methods of determining yield point of prestressing strand.....	67
Figure 4.1	Specimen designation for transfer length test of Grade 1,860 strands..	78
Figure 4.2	Illustrative cross sections of test specimens with Grade 1,860 strands.	79
Figure 4.3	Drawings and picture of prestressing bed 1	90
Figure 4.4	Drawings and picture of prestressing bed 2	91
Figure 4.5	Procedure of specimen fabrication: (a) formwork; (b) concrete placement; (c) steam curing; (d) compressive strength test; (e) form removal; and (f) prestress release by disk cutting.....	92
Figure 4.6	Set-up of transfer length test (Grade 1,860 strand).....	92
Figure 4.7	DEMEC gauge: (a) digital dial gauge; and (b) disks	93
Figure 4.8	Strain gauge attachments on helical wires of strand	94
Figure 4.9	Instrumentation: (a) ERSG for strand; and (b) ERSG for concrete	95
Figure 4.10	Gauge arrangements of the specimens of the test series 1: (a) N45S150-B70F-1; (b) N45S150-B70F-2; and (c) N45S150-B70F-3	96
Figure 4.11	Gauge arrangements of the specimens of the test series 2: (a) N45S150-B70F-4 and N45S150-B70F-R60; and (b) the rest of the specimens ...	97
Figure 4.12	Gauge arrangements of the specimens of the test series 3 and 4: (a) N45S150-B70F-S45; (b) N45S150-B70F-C30 and N45S60-B70F; and (c) the rest of the specimens	98
Figure 4.13	Gauge arrangements of the specimens of the test series 5, 6 and 7: (a) typical pattern; and (b) N45S150-B70F-5	99

Figure 4.14 Instrumentation of transfer length test for Grade 1,860 strands: (a) Loadcell; and (b) LVDT for end slip of strand	100
Figure 4.15 Illustrative cross sections of test specimens with Grade 2,400 strands	103
Figure 4.16 Specimen designation for transfer length test of Grade 2,400 strands	104
Figure 4.17 Drawing of prestressing bed for transfer length specimens with single prestressing strand.....	112
Figure 4.18 Drawing of prestressing bed for transfer length specimens with two prestressing strands	113
Figure 4.19 Gauge arrangements of test series 8 and 9: (a) test specimen with Grade 2,400 strands; and (b) test specimen with Grade 1,860 strands.....	115
Figure 4.20 Gauge arrangements of test series 10: (a) test specimen with Grade 2,400 strands; and (b) test specimen with Grade 1,860 strands.....	115
Figure 4.21 Instrumentation of transfer length test for Grade 2,400 strands: (a) Loadcell; and (b) LVDT for end slip of strand	116
Figure 5.1 Concrete strains of N45S150-B70F-1 measured by DEMEC gauges along specimen length: (a) full range; and (b) magnified.....	118
Figure 5.2 Concrete strains of N45S150-B70F-2 measured by DEMEC gauges along specimen length	119
Figure 5.3 Concrete strains of N45S150-B70F-3 measured by DEMEC gauges along specimen length: (a) full range; and (b) magnified.....	119
Figure 5.4 Strain profile measured by ERSGs for the specimen N45S150-B70F-1 with 15 gauges attached to strand.....	120
Figure 5.5 Strain profile measured by ERSGs for the specimen N45S150-B70F-2 with 7 gauges attached to strand.....	121

Figure 5.6	Comparison of strain profiles obtained by ERSGs on concrete and strands	123
Figure 5.7	Influence of number of ERSGs attached to strand surface on: (a) concrete strain profile; and (b) strand strain profile.....	124
Figure 5.8	Temperatures inside and outside the specimen during steam curing	126
Figure 5.9	Strain histories during steam curing: (a) bare strand; (b) N45S150-B70F-1; (c) N45S150-B70F-2; and (d) N45S150-B70F-4	127
Figure 5.10	Geometry of a helical wire wrapped around a center wire (Machida and Durelli, 1973)	129
Figure 5.11	Elongation and rotation in a helical wire (Machida and Durelli, 1973)	130
Figure 5.12	Installation locations of ERSGs on the transverse cross section of the strand.....	135
Figure 5.13	Hydraulic jack for single strand.....	137
Figure 5.14	Measured strand strain with respect to jacking force (N45S150-B70F-2)	138
Figure 5.15	Comparison of the target values and the actual values of the prestressing force	139
Figure 5.16	Strand strain measured during jacking with respect to elapsed time (N40A200-D70-S50-1).....	140
Figure 5.17	Comparison of the measured and calculated elongation for: (a) N40A200-D70-C40-2; and (b) all the specimens in the test series 8, 9, and 10.....	142
Figure 5.18	Comparison of the measured and calculated residual prestressing force after seating.....	145

Figure 5.19 Comparison of the measured and calculated residual prestressing force just before release	147
Figure 5.20 Comparison of the measured and calculated concrete strain at the center of the specimen just after release	148
Figure 5.21 Illustration of smoothing technique	157
Figure 5.22 Determination of transfer length from the measured strain profile: (a) slope-intercept method (Deatherage and Burdette, 1994); and (b) AMS method (Russell and Burns, 1997)	158
Figure 5.23 Effect of smoothing on measured transfer length (Russell and Burns, 1993)	159
Figure 5.24 Influence of initial prestress on transfer length.....	167
Figure 5.25 Influence of initial prestress on transfer length of high strength strand	169
Figure 5.26 Influence of concrete compressive strength at transfer on transfer length of specimens with a single strand	171
Figure 5.27 Influence of concrete compressive strength at transfer on transfer length of specimens with two strands	172
Figure 5.28 Influence of strand diameter on transfer length	174
Figure 5.29 Damage due to sudden release of prestress: (a) N45S150-B70F-C30S; and (b) N45S60-B70F.....	175
Figure 5.30 Influence of cover depth on transfer length of fully bonded Grade 1,860 strand.....	177
Figure 5.31 Influence of cover depth on transfer length of partially debonded Grade 1,860 strand.....	178
Figure 5.32 Influence of cross section size on transfer length of fully bonded Grade	

1,860 strand.....	180
Figure 5.33 Influence of cross section size on transfer length of partially debonded Grade 1,860 strand.....	181
Figure 5.34 Influence of cover depth on transfer length of high strength strand embedded in normal strength concrete	183
Figure 5.35 Influence of cover depth on transfer length of high strength strand embedded in high strength concrete	184
Figure 5.36 Influence of strand spacing on transfer length of fully bonded Grade 1,860 strand.....	185
Figure 5.37 Influence of strand spacing on transfer length of high strength strand embedded in normal strength concrete	187
Figure 5.38 Influence of strand spacing on transfer length of high strength strand embedded in high strength concrete	188
Figure 5.39 Temperatures inside and outside specimen during air curing	189
Figure 5.40 Influence of debonding on transfer length.....	191
Figure 5.41 Influence of reinforcement spacing on transfer length	192
Figure 5.42 Influence of prestress release method on transfer length.....	193
Figure 5.43 Comparison of the measured transfer lengths and the predictions by the ACI318-11 Eq.(12-4) (2011)	196
Figure 5.44 Comparison of the measured transfer lengths and the predictions by the ACI318-11 Shear design (2011)	197
Figure 5.45 Comparison of the measured transfer lengths and the predictions by the Eurocode2 (2004)	198
Figure 5.46 Comparison of the measured transfer lengths and the predictions by Oleśniewicz (1975).....	199

Figure 5.47 Comparison of the measured transfer lengths and the predictions by Zia and Mostafa (1977).....	200
Figure 5.48 Comparison of the measured transfer lengths and the predictions by Balázs (1992).....	201
Figure 5.49 Comparison of the measured transfer lengths and the predictions by Mitchell et al. (1993)	202
Figure 5.50 Comparison of the measured transfer lengths and the predictions by Mahmoud et al. (1999).....	203
Figure 5.51 Comparison of the measured transfer lengths and the predictions by Barnes et al. (2003).....	204
Figure 5.52 Comparison of the measured transfer lengths and the predictions by Kose and Burkette (2005).....	205
Figure 5.53 Comparison of the measured transfer lengths and the predictions by Martí-Vargas et al. (2007b).....	206
Figure 6.1 Deviation of strain curves in transfer zone due to boundary condition	211
Figure 6.2 Bond stress distributions of the test specimens excluded from and included in the analysis.....	213
Figure 6.3 Curve fitting for measured strain values of specimen N45S150-B70F-1	215
Figure 6.4 Transfer bond-slip-strain relationship of the pretensioned tendon.....	217
Figure 6.5 Strain distributions of the tendon and concrete along the transfer zone	218
Figure 6.6 Deformation of the concrete surrounding the tendon when slip occurs	220

Figure 6.7	Comparison of the test results and the proposed model for specimen N45S150-B70-1: (a) Bond stress distribution; (b) Strand strain distribution; (c) Slip distribution; and (d) Bond-slip relationship.....	226
Figure 6.8	Comparison of test results from Kim (2000) and proposed model: (a) M12-N-C4-2; (b) M12-H-C5-1; (c) M15-N-C5-2; and (d) M15-H-C4-2	229
Figure 6.9	Comparison of test results from Mitchell et al. (1993) and proposed model: (a) 9.5/89-825; and (b) 9.5/31-1200.....	230
Figure 6.10	Comparison of test results from Russell and Burns (1997) and proposed model: (a) SS150-4; and (b) SS160-6.....	232

Notations

A_c	= cross sectional area of concrete, mm ²
A_p	= cross sectional area of prestressing tendon, mm ²
A_{pc}	= cross sectional area of center wire of strand, mm ²
A_{ph}	= cross sectional area of helical wire of strand, mm ²
B	= bond modulus, MPa
B_b	= coefficient given by equation (2.12), MPa
C	= multiplication factor of bond-slip relationship in equation (2.6), MPa
C_A	= coefficient given by equation (5.6b)
C_B	= coefficient given by equation (5.6c)
C_C	= coefficient given by equation (5.7b)
C_D	= coefficient given by equation (5.7c)
C_E	= coefficient given by equation (5.10b)
C_F	= coefficient given by equation (5.10c)
C_G	= coefficient given by equation (5.11b)
C_H	= coefficient given by equation (5.11c)
C_1	= a factor for strand surface condition in equation (2.46)
C_2	= a factor for concrete confinement in equation (2.46)
E_c	= elastic modulus of concrete, MPa
E_{ci}	= elastic modulus of concrete at transfer, MPa

E_p	= elastic modulus of prestressing strand, MPa
G_p	= shear modulus of prestressing strand, MPa
I	= moment of inertia of the cross section of the helical wire, mm ⁴
I_c	= moment of inertia of concrete section, mm ⁴
I_p^c	= polar moment of inertia of the cross section of the center wire, mm ⁴
K	= ratio of twisting moment and axial force developing during tensioning
K_p	= coefficient given by equation (2.5), MPa ⁻¹
K_1	= coefficient for equation (2.13)
M	= bending moment acting on helical wire, kN·m
M_{cr}	= cracking moment, kN·m
M_d	= moment due to the self-weight. , kN·m
M_u	= ultimate moment, kN·m
M_n	= nominal flexural strength, kN·m
N	= number of crack
P	= total axial force acting on prestressing strand, kN
P_c	= axial force acting on center wire of prestressing strand, kN
P_h	= axial force acting on helical wire of prestressing strand, kN
R	= radius of reference cylinder, mm
T	= total twisting moment acting on prestressing strand, kN·m
T_c	= twisting moment acting on center wire of prestressing strand, kN·m
T_h	= twisting moment acting on helical wire of prestressing strand, kN·m
U_t	= plastic transfer bond stress, MPa

- U'_t = plastic transfer bond stress normalized by f'_{ci}
- U'_d = plastic flexural bond stress normalized by f'_c
- a_0 = 1.0, coefficient of the bond characteristic
- a_1 = coefficient that represents increasing slope of bond stress, mm^{-2}
- a_2 = coefficient that represents bond stress by adhesion, mm^{-1}
- a_3 = coefficient that represents elastic deformation of a member
- a_4 = coefficient that represents initial difference between concrete and tendon strain
- a_5 = coefficient that represents initial slip, mm
- b = width of cross section of specimen, mm
- c = $C\sqrt{f'_{ci}}$, $\text{MPa}^{1/2}$
- c_b = distance from centroid of prestressing strand to the closest face of concrete, mm
- c_c = clear cover depth, mm
- c_{eff} = effective cover depth given by equation (2.56)
- d_b = nominal diameter of reinforcing bar or prestressing tendon, mm
- e_p = eccentricity of centroid of prestressing tendon, mm
- f_{bpd} = plastic flexural bond stress in equation (2.27), MPa
- f_{bpt} = plastic transfer bond in equation (2.22), MPa
- $f_{c,avg}$ = average stress over concrete section, MPa
- f_{cm} = mean concrete compressive strength at 28 days, MPa
- f_{ct} = splitting tensile strength of concrete, MPa

f_{ctdi}	= design tensile strength of concrete at time of release, MPa
f_{ctm}	= mean tensile strength of concrete at 28 days, MPa
f_{ctmi}	= tensile strength of concrete at time of release, MPa
f'_c	= specified compressive strength of concrete, MPa
f'_{ci}	= compressive strength of concrete at detensioning, MPa
f_p	= stress in prestressing strand, MPa
f_{pi}	= initial prestress, MPa
$f_{pi,1}$	= stress in prestressing tendon just after anchorage seating, MPa
$f_{pi,2}$	= stress in prestressing tendon prior to detensioning, MPa
f_{pj}	= stress in prestressing tendon at jacking, MPa
f_{ps}	= stress in prestressing tendon at nominal flexural strength, MPa
f_{pu}	= tensile strength of tendon, MPa
f_{se}	= effective prestress, MPa
f_{py}	= yielding stress of prestressing tendon
f_{px}	= strand stress considered in each equation listed in Table 2.1
h	= height of cross section of specimen, mm
k_1, k_2, k_3	= fitting factors for equation (2.55)
l_d	= development length, mm
l_{db}	= debonded length of prestressing tendon, mm
l_e	= embedment length, mm
l_{fb}	= flexural bond length, mm

l_t	= transfer length, mm
$l_{t,c}$	= transfer length at cut end, mm
$l_{t,d}$	= transfer length at dead end, mm
m_p	= number of strands in the considered row
n	= modulus ratio for prestressing strand ($= E_p / E_c$)
p	= pitch length of seven-wire strand, mm
r	= radial distance on the transverse cross section of helical wire from its centroid, mm
r_c	= radius of gyration of concrete cross section, mm
s	= slip, mm
s_{cm}	= coefficient for type of cement in equation (2.24);
s_n	= $1000 s / d_b$, non-dimensional slip
s_p	= center-to-center spacing of prestressing tendon, mm
s_r	= center-to-center spacing of reinforcing bars, mm
t	= concrete age, day
t_i	= time of release, day
x	= longitudinal location from end of strain plateau zone, mm
$\Delta f_{pi,1}$	= anchorage seating loss of prestress, MPa
$\Delta f_{pi,2}$	= loss of prestress between anchorage seating and detensioning, MPa
$\Delta f_{pi,3}$	= prestress loss due to elastic shortening of specimen, MPa
$\Delta \varepsilon_{pr}$	= change in strain of pretensioned tendon due to detensioning
Θ	= $\pi d_b^2 / 4 A_p$

- Σ_o = perimeter of prestressing strand, mm
- Ψ = relative transfer length in equation (2.29)
- α = coefficient for development of tensile strength with time in equation (2.24)
- α_b = coefficient in equation (2.51)
- α_{ct} = coefficient for long term effects on the tensile strength and for unfavorable effects from the way the load is applied in equation (2.23)
- α_s = coefficient for design situation in equation (2.26)
- α_t = coefficient for material type of tendon in equation (2.50)
- α_1 = coefficient for type of release in equation (2.26)
- α_2 = coefficient for type of tendon in equation (2.26)
- β = lay angle of helical wire, degree
- γ = normalized rotation per undeformed pitch length of prestressing strand
- γ_c = partial safety factor for concrete
- $\gamma_{s\theta}^{th}$ = shear strain on transverse cross section of helical wire associated with twisting moment T_h acting on the helical wire
- $\gamma_{z\theta}^{tc}$ = shear strain on transverse cross section of center wire associated with twisting moment T_c acting on the center wire
- δ = nondimensional slip normalized by diameter of prestressing strand
- ε = axial displacement per unit length
- ε_c = concrete strain
- ε_{el} = elastic strain of concrete in strain plateau zone by prestressing force

- ε_p = strain in prestressing strand
- ε_{pl} = proportional strain limit of prestressing strand
- ε_{pr} = strain of pretensioned tendon just before detensioning
- ε_{ps} = strain corresponding to f_{ps}
- ε_{pu} = strain in prestressing strand at rupture
- ε_{py} = strain corresponding to f_{py}
- ε_s = strain of reinforcing bar embedded in concrete
- ε_z^{ac} = axial strain in center wire of prestressing strand associated with axial force P_c acting on the center wire
- ε_s^{ah} = axial strain in helical wire of prestressing strand associated with axial force P_h acting on the helical wire
- ε_s^{bh} = axial strain in helical wire of prestressing strand associated with bending moment M acting on the helical wire
- η = distance on transverse cross section of helical wire from its neutral axis for bending
- η_{p1} = coefficient for type of tendon in equation (2.22)
- η_{p2} = coefficient for type of tendon and bond situation at anchorage in equation (2.27)
- η_1 = coefficient for bond condition in equation (2.22)
- κ = coefficient to take into account effect of position of prestressing strand equation (2.21)
- κ_b = coefficient given by equation (2.9)

- μ = coefficient of friction
- λ = factor to take into account effect of strain in prestressing strand at failure
in equation (2.44)
- λ_m = coefficient in equation (2.54)
- ξ = nondimensional coordinate in longitudinal direction of prestressing
strand ($= x/d_b$)
- ρ_p = ratio of cross sectional area of prestressing strand to concrete ($= A_p/A_c$)
- σ_z^{ac} = normal stress in center wire of prestressing strand associated with axial
force P_c acting on the center wire
- σ_s^{ah} = normal stress in helical wire of prestressing strand associated with axial
force P_h acting on the helical wire
- σ_s^{bh} = normal stress in helical wire of prestressing strand associated with
bending moment M acting on the helical wire
- τ_{ad} = adhesion bond, MPa
- τ_b = bond stress, MPa
- $\tau_{s\theta}^{th}$ = shear stress on transverse cross section of helical wire associated with
twisting moment T_h acting on the helical wire, MPa
- $\tau_{z\theta}^{tc}$ = shear stress on transverse cross section of center wire associated with
twisting moment T_c acting on the center wire
- τ_0 = bond stress when strain of reinforcement is zero, MPa
- ψ = coefficient to take into account the scatter of the bond stress

1. Introduction

1.1 Research Background

1.1.1 Definition and Importance of Transfer Length

In pretensioned prestressed concrete members, prestressing force is transferred from prestressing tendons into concrete by direct bond between the two materials rather than by anchorage devices. This force transfer mechanism inevitably requires a certain embedment length of the prestressing tendons to fully transfer the prestressing force to the concrete. The embedment length required for full transfer is called transfer length. According to ACI318 code (ACI Committee 318, 2011), transfer length is defined as the distance over which a prestressing strand should be bonded to concrete so as to develop an effective prestress in the prestressing steel.

The prestressing force begins to be transferred at the end of the concrete member and reaches the maximum value at the transfer length. Beyond the transfer zone, stress in the prestressing tendons remains constant because there is no longer bond action transferring the prestressing force. In the transfer zone, on the other hand, the prestressing force is lower than the value intended by the designer and it depends on the distance from the end of the member. Most empirical equations including the current design code provisions for transfer length assume a linear variation in the prestressing force along the transfer zone.

In general design cases, transfer length may not be a controlling factor (Russell and Burns, 1993). Only a rough and conservative estimation will be sufficient for these cases. However, in some cases, a section within the transfer zone can be a

primary concern and a reasonable estimate for transfer length becomes a crucial factor for safety design. For pretensioned concrete structures such as short cantilevers, railroad ties, truss members, and footing beams, a large bending moment is likely to occur near the ends of the structures (Oh and Kim, 2000). Within the transfer zone, the value of the prestressing force greatly affects the behavior of pretensioned concrete structures at service limit state because the prestressing force plays a dominant role in determining the cracking moment of the sections (Barnes et al., 2003). In these cases, an unreasonable estimation of transfer length will cause unconservative design.

Another case where an emphasis should be given to the accuracy of the estimation of the transfer length is shear design. The shear demand is normally greatest in the transfer zone of prestressed concrete structures (Barnes et al., 2003) and the contribution of concrete to the sectional shear strength is significantly affected by the value of the prestressing force (Russell and Burns, 1993).

Similarly to reinforcing steel bars, the prestressing tendons should also be bonded over a certain distance to provide bond integrity for the strength of the pretensioned concrete structures (ACI committee 318, 2011). The required distance is called development length. The current code provisions for development length usually comprise of two terms, which respectively represent transfer length and flexural bond length. The flexural bond length is defined as an additional length over which the prestressing strands should be bonded so that a stress in the prestressing steels at nominal strength of the member may develop (ACI committee 318, 2011). As a part of development length, transfer length is of primary importance in accurately estimating development length. Therefore, transfer length can be a crucial factor for the ultimate behavior as well as the serviceability of pretensioned concrete structures.

1.1.2 Problems with the Previous Research on Transfer Length

A large number of experiments have been performed for the purpose of directly determining the transfer length under specific experimental conditions and variables. In these experiments, attempts were made to identify the effects of test variables on the transfer length and, based on the test results, several empirical equations were proposed to best fit the measured transfer lengths. However, such an approach has a fundamental limitation in that the experimental conditions impose restrictions on its application. Martí-Vargas et al. (2007) showed that the previous empirical formulae result in significantly discrepant estimates under the same conditions. Kose (2007) also indicated that the proposed formulae do not predict transfer length accurately for other than the experimental data used in their developments. It is because most studies rely on empirical assessments that were performed under different conditions and variables, rather than solid theoretical backgrounds.

Another problem with the formulation of the empirical equations is the assumption of bond stress over the transfer zone. The previous equations postulated different relationships between the maximum bond stress within the transfer zone and the compressive strength of concrete, which is one of the most important factors to cause different results from each other.

However, it is common that the equations assumed a constant bond stress over the transfer zone. Historically, the current ACI318 code provision on the transfer length was first introduced in the 1963 version (Tabatabai and Dickson, 1993; Martí-Vargas et al., 2007). It was based on the research by Hanson and Kaar (1959) which stated that the average bond stress over the transfer zone is found to be 2.76 MPa (400 psi). The constant bond stress was justified by the strain distribution measured

on concrete surface and later it was widely accepted by several design codes and researchers. There has been a general consensus that the distribution of bond stress is likely to be constant and it was supported by the measured concrete strain profiles that shows linearity. However, this constant bond stress distribution is inconsistent with the results from analytical approaches conducted in the 1990s based on bond-slip relationship of prestressing strands or concrete confinement. According to the approaches, bond stress varies within the transfer zone rather than remains constant. The actual distribution of bond stress over the transfer zone has been rarely measured because there has been a concern that installing an instrument on the prestressing tendons might disrupt developing bond stress between the prestressing tendons and concrete. For obtaining the actual distribution of bond stress, however, measurement should be taken on the surface of the prestressing tendons.

1.2 Scope and Objectives of the Thesis

In order to more accurately estimate transfer length, experiments that include a wide variety of variables that affect the transfer length should be based on solid theoretical foundations that describe bond mechanisms of prestressing strands and actual bond stress distribution within the transfer zone. Electrical resistance strain gauges (ERSG) were extensively utilized to capture the actual distribution of strain in the prestressing strands and bond stress over the transfer zone. Traditionally, detachable mechanical strain (DEMEC) gauge has been used for the measurement of transfer length. To reevaluate the current state of the art for the transfer length of pretensioned concrete, a series of experimental frameworks was planned and conducted assessing the effects of a material, geometric, methodological and

environmental factors, some of which were not considered in the previous studies. Based on the experimental results, a new bond-slip-strain model of prestressing strands was proposed and an equation for transfer length was also derived from the proposed bond model.

This work is highly opportune because high-strength prestressing strands have been recently developed in some countries. High-strength prestressing strands have improved yield and tensile strengths than those of the existing prestressing strands, Grade 1,860 (Grade 270), thus can contain higher stress at transfer. Through the comprehensive experimental research, it was evaluated whether the existing code provisions, previous empirical equations, and theoretical analyses are applicable to high-strength prestressing strands.

In summary, there are five primary objectives in this thesis:

1. To reevaluate important test variables currently known as affecting the transfer length of pretensioned concrete member and to evaluate test variables not considered in the previous experimental research.
2. To obtain the actual distribution of strain in the prestressing strands and bond stress over the transfer zone.
3. To measure the transfer length of high-strength prestressing strands.
4. To evaluate the existing code provisions, previous empirical equations, and theoretical analyses based on the comprehensive experimental works.
5. To propose a new equation for transfer length based on the bond mechanisms of prestressing strands and actual bond stress within the transfer zone.

1.3 Organization of the Thesis

In this thesis, extensive experimental works were conducted to investigate the transfer length of pretensioned concrete structures reinforced with Grade 1,860 strands as well as newly developed high-strength prestressing strands. The research background for the study was discussed in Chapter 1.

Chapter 2 provides a brief review of the fundamental bond mechanism of the prestressing seven-wire strands. In addition, Chapter 2 provides a review on the previous research and empirical equations for transfer length and development length of pretensioned concrete structures. Bond-slip relationships proposed for prestressing strands are also reviewed. Theoretical analyses based on concrete confinement are introduced and representative methods are briefly summarized. Lastly, factors influencing the transfer length are identified and briefly discussed.

Chapter 3 briefly introduces the mechanical properties of high-strength prestressing strands developed in South Korea.

The experimental program performed in this research is detailed in Chapter 4. Totally, 66 specimens were fabricated and tested through 10 concrete batches. Included were 11 test variables: initial prestress, concrete compressive strength, strand diameter, cover depth, cross section size, strand spacing, curing condition, debonding, reinforcement spacing, prestress release method, and tensile strength of strand. Curing condition and reinforcement spacing in the vicinity of prestressing strand are test variables that have not considered in the previous research. Remaining test variables are generally accepted as major test variables on transfer length.

Chapter 5 presents the results obtained from the transfer length test. Several issues

regarding the suitability of ERSGs to measuring transfer length are discussed. The behavior of the prestressing strands is examined using the measurement of ERSGs attached on the strand surface. The influences of the test variables are investigated and the existing code provisions and empirical equations are evaluated by comparing with the measured transfer lengths.

The derivation of a bond-slip-strain model for prestressing strands is presented in detail in Chapter 6. The model is formulated based on the experimental results of the test specimens. The proposed model is verified by comparing with other experimental results collected by literature survey.

Finally, the conclusions drawn from this study are summarized in Chapter 7.

2. Literature Review

2.1 Introduction

This chapter summarizes current methodologies of determining transfer length of pretensioned concrete structures. Roughly, there are 3 types of methodology to determine the transfer length. First one is based on the fundamental bond mechanism of prestressing strand. In this methodology, a governing equation that represents the behavior of a single prestressing strand embedded in concrete is formulated considering equilibrium, compatibility, and elastic behavior of steel and concrete (Balázs, 1992; fib, 2000). The governing equation is exactly same as that of reinforcing steel bars. To solve the governing equation, a particular bond-slip relationship is adopted. This means that the bond characteristics of reinforcements are reflected by the bond-slip relationship.

It should be noted that prestressing strands experience two distinct bond situations: push-in and pull-out (Den Uijl, 1998). The prestressing strand enters into concrete in the push-in situation and slips out of concrete in the pull-out situation. The two situations simulate the transfer and flexural bond action of the prestressing strand, respectively. Abrishami and Mitchell (1993) reported that the bond stiffness is greater in the transfer length simulation than in the flexural bond simulation.

An exact solution may exist or not depending on the mathematical form of the bond-slip relationship. If there is no exact solution, numerical analysis such as finite difference method is carried out to obtain an approximate solution.

The bond mechanism of the prestressing strand within transfer zone is provided in

Section 2.2 and bond-slip relationships of the prestressing strand are given in Section 2.3.

The second methodology is to calculate the transfer length numerically based on concrete confinement. The variation in the diameter of the prestressing strand during transfer causes radial compressive stress and circumferential tensile stress on the concrete surrounding the prestressing strand. The concrete confinement capacity and the resulting bond stress are expressed by these stresses in the two directions. Depending on the solution procedure, a second order ordinary differential equation with respect to the radial displacement of the concrete may be solved by a numerical technique. A detailed description and analytical results are provided in Section 2.4.

The last methodology of determining the transfer length is to use empirical equations. It is most practical and popular method to obtain the transfer length because of its convenience. Many empirical equations have been proposed by researchers for decades. The researchers have considered various factors in their experimental programs and successfully identified the effect of the factors on the transfer length. However, the basic form of the proposed empirical equations still resembled the current code provision. Only several factors such as compressive strength of concrete, prestress level, and diameter of prestressing tendon are exclusively included in the empirical equations and the effect of the other factors merged into a coefficient as a lump-sum.

In Section 2.5, some empirical equations for transfer length are introduced and factors affecting the transfer length are briefly summarized.

2.2 Bond Mechanism of Prestressing Strand

Bond mechanism of prestressing strand is partly different from that of reinforcing steel ribbed bars. It is mainly because the prestressing strand has a unique geometric characteristic of a helical pattern of outer wires. It is generally accepted that there are 3 elements of bond to contribute the transfer bond between concrete and prestressing strand (fib, 2000). They are adhesion, friction, and mechanical interlocking. The transfer bond is developed by combined action of these elements (Russell and Burns, 2003). However, the contribution of each element to the transfer bond is still not known quantitatively. Each element is separately discussed in the following sections.

2.2.1 Adhesion

A very thin cementitious layer around the prestressing strand combines the concrete and the prestressing strand chemically and physically. Adhesion is the resistance of the layer against the relative movement of the prestressing strand. It generates the transfer bond at a very small slip but completely fails once the bond stress reaches a critical value. Russell and Burns (1993) stated that the adhesion behaves in a rigid-brittle way and it does not recover after the failure. Figure 2.1 shows the rigid-brittle behavior of adhesion. The contribution of the adhesion is small and it is replaced by friction after the failure (fib, 2000).

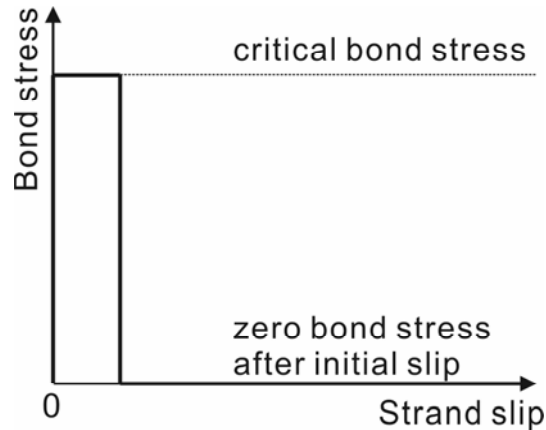


Figure 2.1 Rigid-brittle behavior of adhesion (Russell and Burns, 1993)

2.2.2 Friction

In pretensioned concrete structures, a prestressing strand is tensioned before concrete placement. Tensioning causes the longitudinal elongation and the radial reduction of the prestressing strand due to Poisson's effect. At transfer of prestress, the prestressing strand struggles to return to the unstressed state but it is impossible because the concrete surrounding the prestressing strand is hardened. Radial expansion of the prestressing strand imposes a radial compressive stress on the surrounding concrete. The compressive stress acts as a normal pressure and hence friction is activated when the relative movement of the prestressing strand in the concrete begins to occur. This effect is called Hoyer's effect or wedge action (Russell and Burns, 2003). Figure 2.2 shows Hoyer's effect on the prestressing strand schematically. Another mechanism such as shrinkage can also cause the radial compressive stress at the interface of the concrete and the prestressing strand (fib, 2000).

There are few researches on the coefficient of friction. Baltay and Gjelsvik (1990)

reported that the coefficient of friction for mild steel varies between 0.3 and 0.6. The average value was found to be 0.47. Bogaerts and Brosens (1995) found in a push-in test of seven-wire strand with short embedment length that the coefficient of friction decreased as the slip increased and remained constant after the slip of 1 mm. It ranged approximately from 0.2 to 0.6.

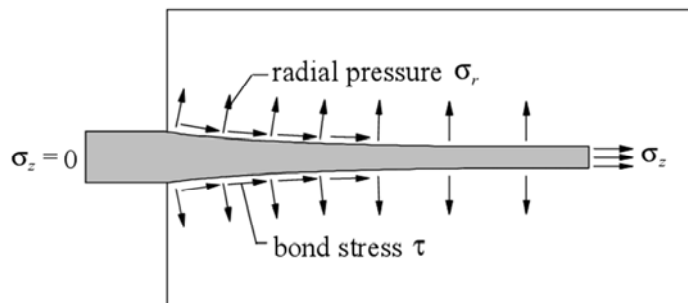


Figure 2.2 Wedge action from Hoyer's effect (Kim, 2000)

2.2.3 Mechanical Interlocking

The helical outer wires of the seven-wire strand form a furrow between the two adjacent wires. The furrow is filled with concrete and becomes a hump to restraint the change in the pitch of the seven-wire strand in the concrete (fib, 2000). This restraint is called mechanical interlocking. It is a similar action to the rib bearing of reinforcing steel bars. The mechanical interlocking restrains the twist of the strand and generates a twisting moment in the strand (fib, 2000; Russell and Burns, 2003).

The influence of the mechanical interlocking had been ignored because the seven-wire strand has a low torsional stiffness (Stocker and Sozen, 1970). However, Russell and Burns (1993) insisted that the previous test program had not been

appropriate for the evaluation of the mechanical interlocking and that mechanical interlocking plays a significant role in the flexural bond as well as the transfer bond of actual pretensioned concrete structures.

Den Uijl (1992) postulated another mechanism to formulate his bond model from the experimental results. The mechanism is called pitch effect and assumed to be proportional to the absolute value of the change in the strand stress. Unfortunately, there was no physical description on the pitch effect (fib, 2000).

2.3 Bond Models for Prestressing Strand

In this section, two bond models for prestressing strand are introduced. The first model, which was proposed by Balázs (1992), has the form of a power function with respect to the slip. This form allowed an exact solution of the governing equation for the bond behavior of the prestressing strand and a closed form of the transfer length was drawn. The second bond model was formulated by Den Uijl (1992). The most distinctive feature of this bond model is that it includes terms of the local stress in the prestressing strand. With these terms, the fundamental bond mechanisms mentioned in the previous section were expressed in mathematical forms and incorporated into the bond model.

2.3.1 Balázs (1992)

Force equilibrium on the surface of a prestressing strand embedded in concrete within an infinitesimal distance dx can be expressed as follows:

$$A_p \frac{df_p}{dx} = -\Sigma_o \tau_b (s) \quad (2.1)$$

where, A_p is cross sectional area of a prestressing strand; f_p is stress in the prestressing strand; Σ_o is a perimeter of the prestressing strand; τ_b is bond stress; and s is slip.

The slip s has the following relationship with the strain in the concrete and the prestressing strand:

$$\varepsilon_p - \varepsilon_c = -\frac{ds}{dx} \quad (2.2)$$

where, ε_p and ε_c is the strain in the prestressing strand and the concrete, respectively.

The forces acting on the prestressing strand and the concrete section at a specific x should be in equilibrium:

$$A_c \frac{df_{c,avg}}{dx} = -A_p \frac{df_p}{dx} \quad (2.3)$$

where, A_c is cross sectional area of the concrete; and $f_{c,avg}$ is an average stress over the concrete section.

With the assumption of the elastic behavior of the concrete and the prestressing strand, substituting equations (2.1) and (2.2) into equation (2.3) gives the governing equation for the behavior of the prestressing strand embedded in concrete:

$$\frac{d^2\delta}{d\xi^2} - K_p\tau_b(\delta) = 0 \quad (2.4)$$

where, δ is the nondimensional slip normalized by the diameter of the prestressing strand ($=s/d_b$); and ξ is the nondimensional coordinate in the longitudinal direction of the prestressing strand ($=x/d_b$). Equating the perimeter of the prestressing strand Σ_o with πd_b gives the coefficient of K_p as follows:

$$K_p = \frac{4(1+n\rho_p)}{E_p} \Theta \quad (2.5)$$

where, n is the ratio of the elastic modulus of the prestressing strand to the concrete ($=E_p/E_c$); ρ_p is the ratio of the cross sectional area of the prestressing strand to the concrete ($=A_p/A_c$); and Θ is the ratio of the circular section calculated with the nominal diameter of the prestressing strand d_b to the actual cross sectional area of the prestressing strand ($=\pi d_b^2/4A_p$).

In equation (2.4), bond stress τ_b is given as a function of slip s . Balázcs proposed a power function for a prestressing seven-wire strand:

$$\tau_b = C\delta^a \quad (2.6)$$

The value of C and a was found to be 13 and 0.25 from the test results of the prestressing strands pushed into the concrete with the compressive strength of 40

MPa. The diameter and the area of the prestressing strand were 12.8 mm and 100 mm², respectively. Balázs assumed a linear relationship between the bond stress and the square root of the concrete compressive strength at time of transfer f'_{ci} . Considering this linear relationship and the scatter of the test results, equation (2.7) was rewritten as:

$$\tau_b = \psi c \sqrt{f'_{ci}} \sqrt{\delta} \quad (2.7)$$

where, $c = 2.055 \text{ MPa}^{1/2}$; and

$$\psi = \begin{cases} 1.00 & \text{for average value} \\ 1.35 & \text{for upper bound value} \\ 0.65 & \text{for lower bound value} \end{cases}$$

The governing equation can be solved by substituting equation (2.7) into equation (2.4) and taking the initial condition of $\delta(\xi=0)=0$ and $\delta'(\xi=0)=0$.

$$\delta = \kappa_b \xi^{\frac{2}{1-a}} \quad (2.8)$$

The coefficient κ_b is given by:

$$\kappa_b = \left[\frac{\psi c (1-a)^2}{2(1+a)} K_p \sqrt{f'_{ci}} \right]^{\frac{1}{1-a}} \quad (2.9)$$

Substituting equation (2.8) into equation (2.6) gives the bond distribution over the transfer zone:

$$\tau_b = \psi c \sqrt{f'_{ci}} \kappa_b^a \xi^{\frac{2a}{1-a}} \quad (2.10)$$

The distribution of the stress in the prestressing strand can be obtained by substituting equation (2.10) into equation (2.1):

$$f_p(\xi) = f_p(0) - B_b \xi^{\frac{1+a}{1-a}} \quad (2.11)$$

Note that $f_p(0)$ means the effective prestress f_{se} . The coefficient B_b is given by:

$$B_b = \frac{4(1-a)}{1+a} \Theta \kappa_b^a \psi c \sqrt{f'_{ci}} \quad (2.12)$$

Transfer length can be calculated from equation (2.11) using the boundary condition of zero stress in the prestressing strand at the end of the member, $f_p(l_t/d_b) = 0$:

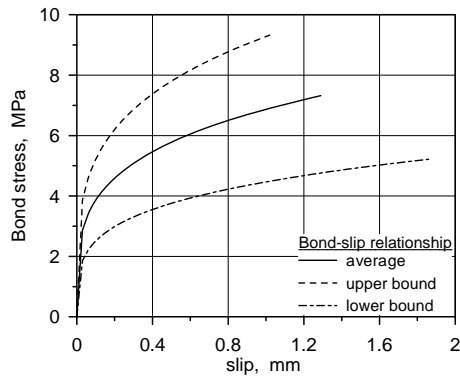
$$\frac{l_t}{d_b} = \left(\frac{f_{se}}{B_b} \right)^{\frac{1-a}{1+a}} = K_1 \sqrt[5]{\frac{f_{se}^3}{f'_{ci}{}^2}} \quad (2.13)$$

where,

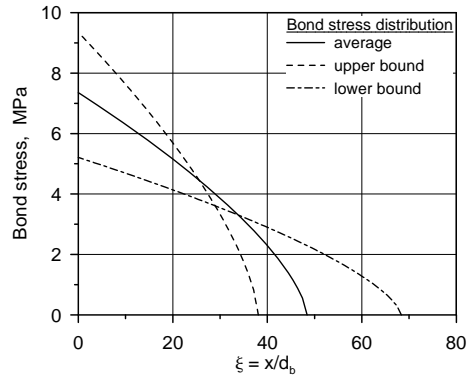
$$K_1 = \begin{cases} 3.15 \text{ MPa}^{-1/5} & \text{for average value} \\ 3.11 \text{ MPa}^{-1/5} & \text{when } n\rho_p = 0.1 \\ 3.17 \text{ MPa}^{-1/5} & \text{when } n\rho_p = 0 \end{cases}$$

The upper bound and lower bound of the bond stress yield the corresponding values for transfer length. The upper bound and lower bound of transfer length are $0.79l_t$ and $1.4l_t$, respectively.

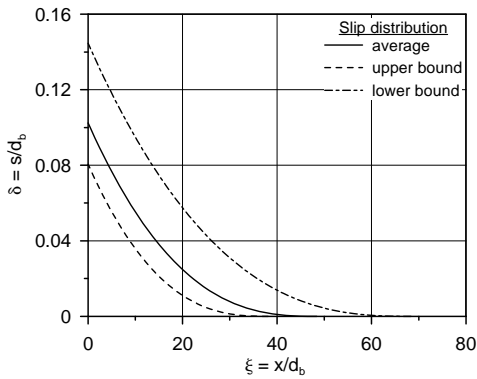
The distributions of the slip, bond stress, and stress in the prestressing strand were calculated using equation (2.8), (2.10), and (2.11) with the conditions of $d_b = 12.8 \text{ mm}$, $A_p = 100 \text{ mm}^2$, $E_p = 195,000 \text{ MPa}$, $n\rho_p = 0$, $f_{se} = 1,100 \text{ MPa}$, and $f'_{ci} = 40 \text{ MPa}$. The average transfer length was $48.4d_b$ (620 mm). The upper bound and lower bound value were $68.4d_b$ (875 mm) and $38.1d_b$ (488 mm), respectively. The current ACI318-11 code provision gives $52.4d_b$ (670 mm), which is very close to the average value. The results are presented in figure 2.3 along with the bond-slip relationship of equation (2.6). Though the resulting transfer length is similar to the value from the code provision, the bond stress distribution keeps increasing within the transfer zone rather than remains constant. The bond stress is zero at the end of the transfer zone and reaches the maximum value at the end of the member. If splitting cracks develop significantly, the bond stress would diminish to a lower value. Balázs did not take into account the effect of the concrete confinement. The increasing bond stress results in the parabolic shape of the strand stress distribution.



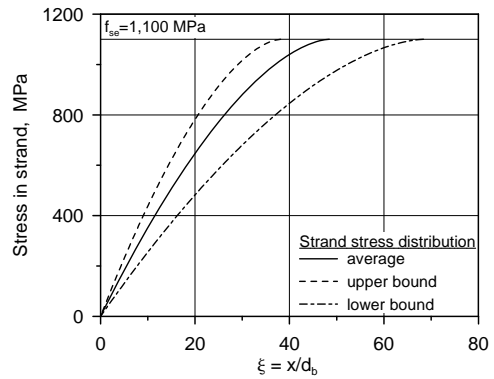
(a)



(b)



(c)



(d)

Figure 2.3 Calculated bond behaviors of prestressing strand: (a) bond-slip relationship; (b) bond stress distribution; (c) slip distribution; and (d) strand stress distribution (Balázs, 1992)

2.3.2 Den Uijl (1992)

Den Uijl (1992) performed a series of experiments that simulated two bond situations of the prestressing strands: pull-out and push-in situation. The pull-out test had a fixed or free boundary condition at the unloaded end of the prestressing strand. The different boundary conditions in the pull-out test varied the stress in the prestressing strand and helped to identify the effect of the strand stress on the bond-slip relationship. The test set-up is presented in figure 2.4.

The test specimens were designed to have short embedment lengths for a uniform bond distribution along the prestressing strand embedded in the concrete. The prestressing strands were bonded over 50 mm or 88 mm in the concrete cylinders with the length of 100 mm and the diameter of 103 mm. The debonded regions of 12 mm or 50 mm were provided at the bottom part of the test specimens by a PVC tube or molded wax cone. The cube strength of concrete was 55.4 MPa and the splitting tensile strength was 3.12 MPa in average. A single prestressing strand with the diameter of 9.3 mm and the tensile strength of 1,950 MPa was located at the center of the concrete cylinder. Totally, 24 pull-out specimens and 20 push-in specimens were tested through 6 test series.

The test results exhibited that the bond situation strongly affects the stress in the prestressing strand as well as the bond-slip relationship. This meant that the bond situation might be simulated by the stress in the prestressing strand. The measured bond-slip relationships were approximately bi-linear and consisted of two linear phases. In the first phase, the bond stress rapidly increased with slip. However, this phase finished at a small slip and was followed by the second phase. Den Uijl stated that the friction is the main factor to contribute to the bond stress in the second phase.

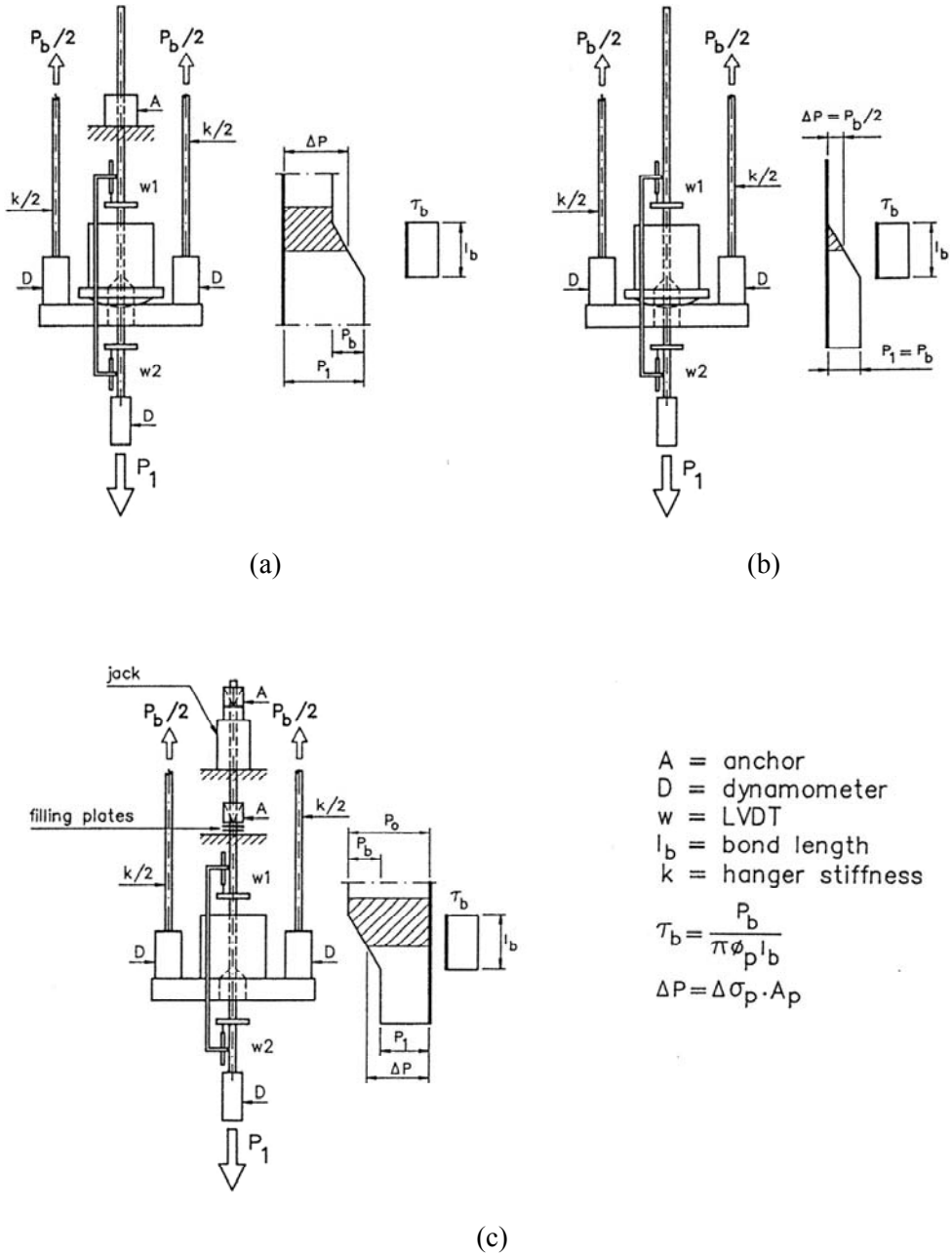


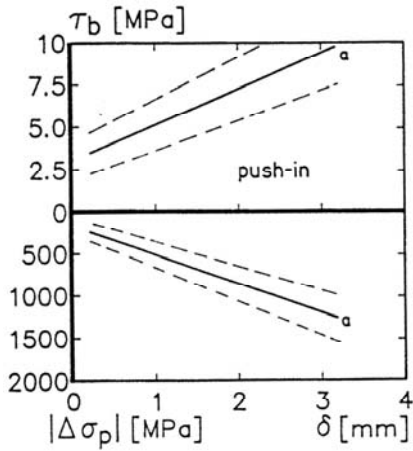
Figure 2.4 Set-up of pull-out and push-in tests: (a) pull-out fixed; (b) pull-out free; and (c) push-in (Den Uijl, 1992)

Den Uijl formulated his bond model only for the second phase and ignored the first phase in a practical view. The bond model included two terms of the stress in the prestressing strand to fit best the test results. The proposed bond-slip-stress model is as follows:

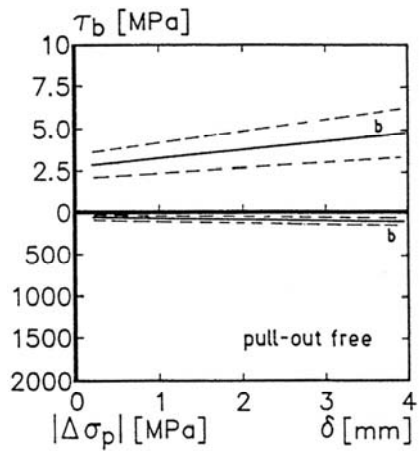
$$\tau_b = 3 + 0.4s - 2.5 \times 10^{-3} \Delta f_p + 1.5 \times 10^{-3} |\Delta f_p| \quad (2.14)$$

where, Δf_p is the change in the stress in the prestressing strand. The four terms of the equation reflected the effect of the fundamental bond mechanisms. The first two terms represent the combined contribution of the adhesion and lack-of-fit effect. Lack-of-fit effect is a wedging action caused by small changes in the cross section of the prestressing strand when a slip occurs (Barnes et al., 2003). Stocker and Sozen (1970) neglected the mechanical interlocking and instead regarded the lack-of-fit effect as the major factor to enhance the bond performance of the seven-wire strand. Den Uijl followed the same line. The third term and the last term corresponded to the friction (Poisson effect) and pitch effect, respectively (Den Uijl, 1998). Den Uijl briefly mentioned that the pitch effect is related to the contact stress caused by the helical shape of the seven-wire strands.

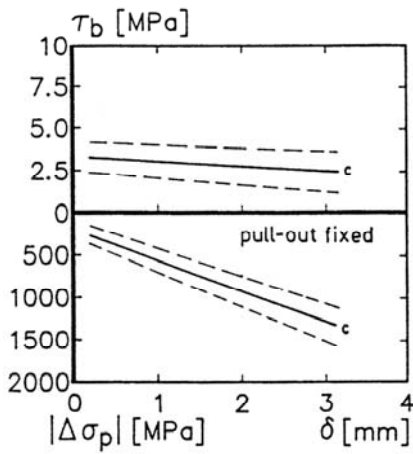
Figure 2.5 presents the bond stresses calculated by equation (2.14) under various bond situations. Solid lines represent the average values while dotted lines means the bounds on which 90% of the test results ranged. Figure 2.5(c) and (d) shows the effect of the hanger stiffness of the loading frame on the test results. The hanger stiffness varied with the area of the hanger and its influence was carefully investigated in his research.



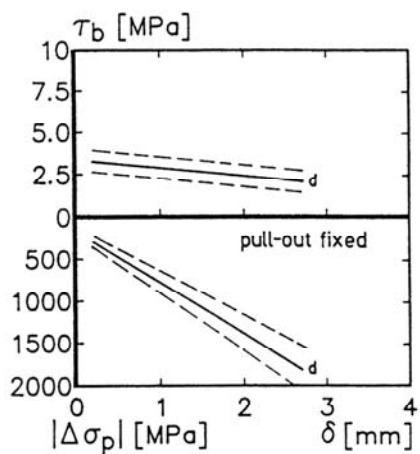
(a)



(b)



(c)



(d)

Figure 2.5 Relationship among bond stress, slip, and strand stress: (a) push-in; (b) pull-out free; and (c) pull-out fixed ($k = 30 \text{ kN/mm}$); and (d) pull-out fixed ($k = 165 \text{ kN/mm}$) (Den Uijl, 1992)

2.4 Theoretical Analyses Based on Concrete Confinement

The prestressing force is transferred from a strand to concrete by radial compressive stresses without regard to the transfer mechanism. These compressive stresses act as an internal pressure to restrain the radial deformation of the strand and induce circumferential tensile stresses in concrete. If the maximum tensile stress exceeds the splitting tensile strength of concrete, radial cracks are initiated along the strand. Since the radial compressive stresses and the circumferential tensile stresses are in equilibrium, the propagation of the radial cracks weakens the magnitude of the maximum radial compressive stresses that are the confining capacity of the concrete to determine the bond resistance. This confining capacity can be evaluated by considering the concrete around the strand as a thick-walled cylinder.

Tepfer (1973) assumed a circumferential stress distribution over the cracked part of the concrete cylinder to obtain analytical solutions for the internal pressure acting on the strand. With this assumption, the internal pressure was linked to the crack penetration depth. Later, several researchers adopted fictitious crack model to reasonably describe the softening behavior of concrete. The fictitious crack model indicated that concrete tensile stresses are able to be transmitted across a certain width of crack. Because the magnitudes of the circumferential tensile stresses directly depend on the crack width in the fictitious crack model, the resulting stress-strain relationship varies with the gauge length. Gopalaratnam and Shah (1985) experimentally showed that concrete tensile stress has a unique relationship with crack width rather than tensile strain after cracking. For the concrete cylinder, radial cracks penetrate from the interface between the strand and concrete to the surface of the concrete cylinder. The crack width varies radially and thus the resulting stress-

strain relationship varies along the radial locations in the cracked part of the concrete cylinder. Noghabai (1995) has surveyed methods to obtain analytical and numerical solutions for concrete confinement.

2.4.1 Weerasekera and Loov (1990)

Weerasekera and Loov (1990) used an identical concrete tensile stress-strain relationship in their thick-walled cylinder analysis. Thus, the concrete circumferential stresses over the cracked part of the concrete cylinder were determined by a unique stress-strain relationship, irrespective of crack width. It did not represent the actual tensile behavior of concrete but provided a simple and robust solution procedure. The tensile stress-strain relationship was proposed in the form of hyperbola based on the experimental results by Gopalaratnam and Shah (1985). After cracking, concrete was regarded as an anisotropic material with respect to radial and circumferential directions. Elastic modulus along the circumferential direction was stress-dependent and the radial and the circumferential stresses were given in terms of the radial and the circumferential strain. A second order non-linear differential equation was constructed using equilibrium and then it was numerically solved until the compatibility condition at the interface between the strand and concrete was satisfied within a certain tolerance. It was assumed that the bond stress is only generated by the internal pressure and they are connected by a constant coefficient of friction. Finally, longitudinal distributions of bond stress and strand stress along the transfer zone are analyzed using the finite difference method.

2.4.2 Den Uijl and Bigaj (1996)

Den Uijl and Bigaj (1996) derived analytical solutions for the bond behavior of ribbed bars using a thick-walled cylinder model. They took into account the wedge action of the ribs and the Poisson effect. Concrete softening behavior was described by a bi-linear fictitious crack model. In their analysis, the radial compressive stress at the interface was expressed by the radial displacement of the interface.

2.4.3 Oh and Kim (2006)

Oh and Kim (2006) followed the same analytical approach as Weeraseker and Loov (1990). The important feature of their analysis is that a tensile stress-crack width relationship was employed to simulate cracking behavior of circumferential concrete fibers. The tensile softening behavior of concrete was expressed by a hyperbolic equation into which the tensile stress-crack width relationship proposed by Gopalaratnam and Shah (1985) was transformed. A second order non-linear non-homogeneous differential equation with respect to a radial displacement was derived and numerically solved by using the fourth order Runge-Kutta method.

2.4.4 Comparison of Analytical Results

For comparison of the analytical models, consider an example with the following properties and dimensions:

Strand: $d_b = 15.2 \text{ mm}$, $f_{pu} = 1,860 \text{ MPa}$, $f_{pi} = 1,300 \text{ MPa}$

Concrete: $f'_{ci} = 40 \text{ MPa}$, $f_{ct} = 3.54 \text{ MPa}$, $c_c = 40 \text{ mm}$, $\mu = 0.4$, $N = 4$

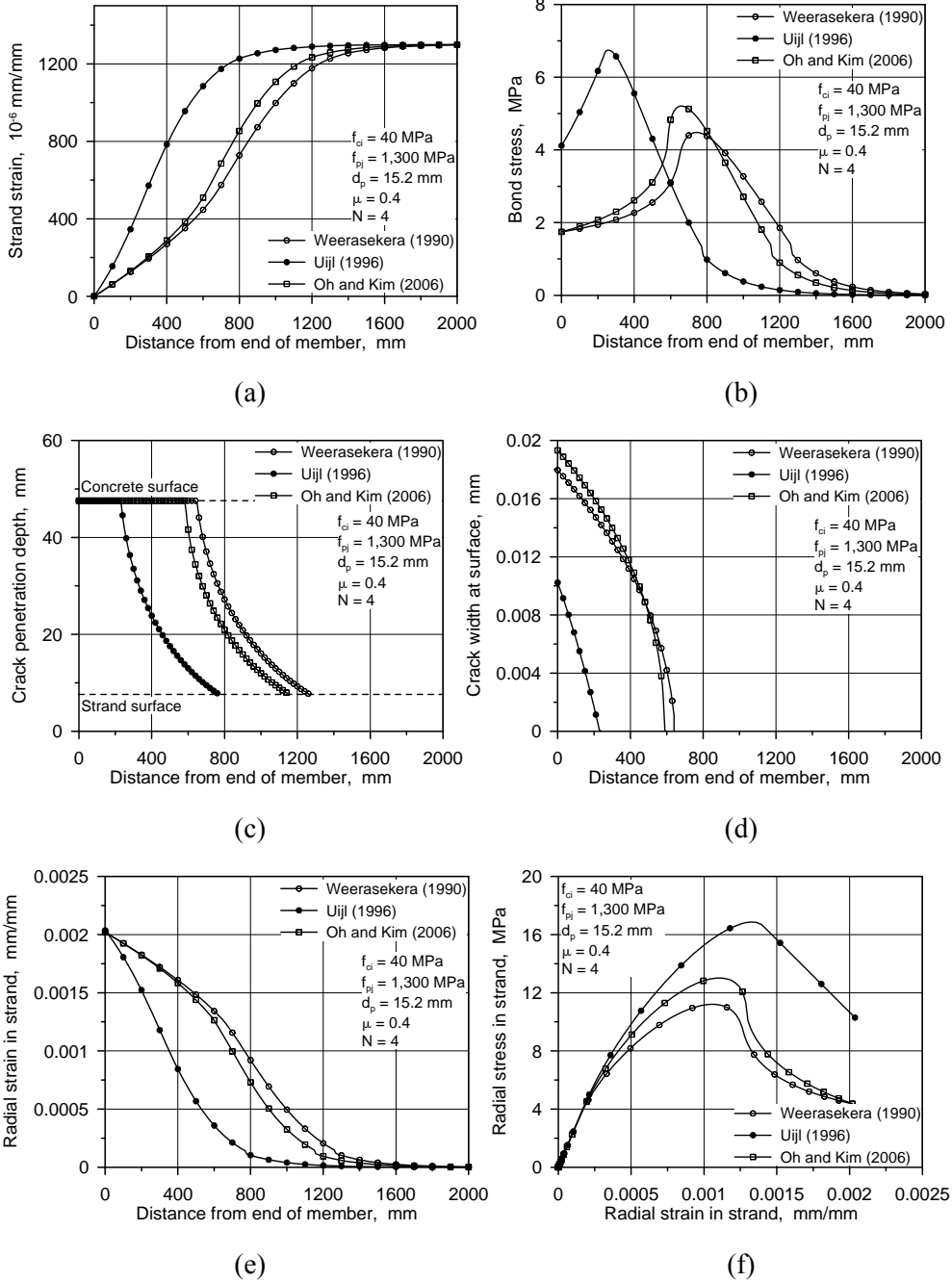
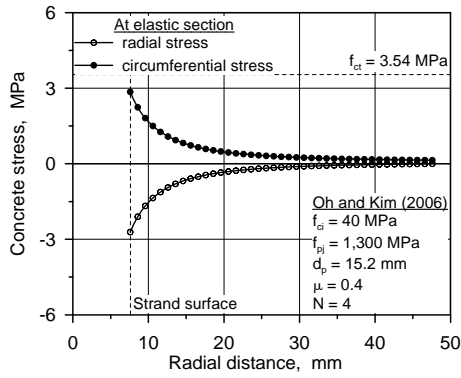
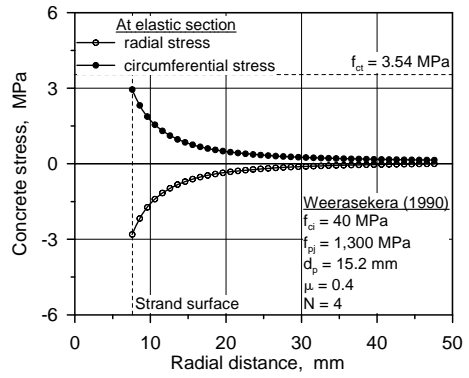


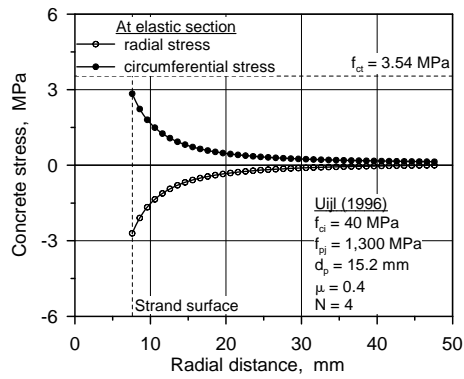
Figure 2.6 Analytical results of concrete confinement models: (a) strand strain distribution; (b) bond stress distribution; (c) crack penetration depth; (d) crack width at surface; (e) radial strand strain; and (f) radial stress-strain relationship



(a)

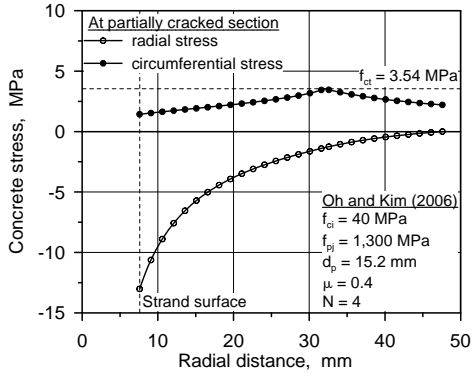


(b)

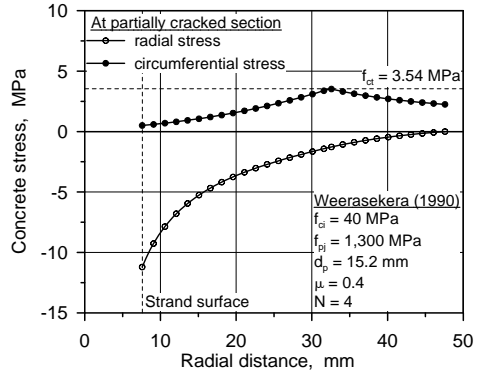


(c)

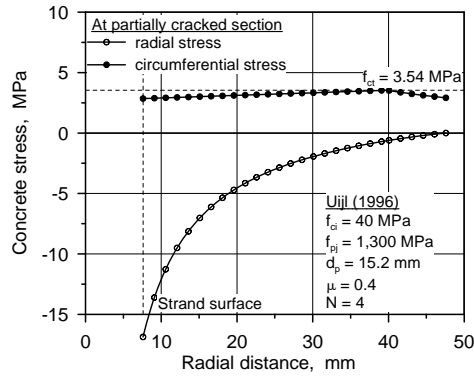
Figure 2.7 Radial and circumferential stress at elastic section: (a) Oh and Kim (2006); (b) Weerasekera and Loov (1990); (c) Den Uijl and Bigaj (1996)



(a)

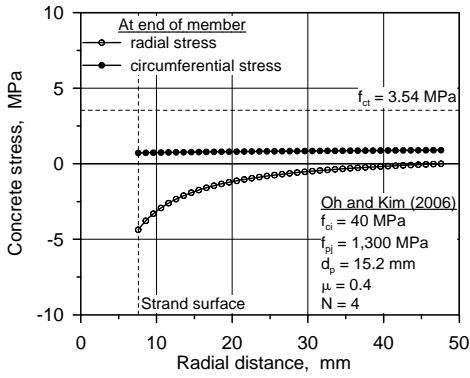


(b)

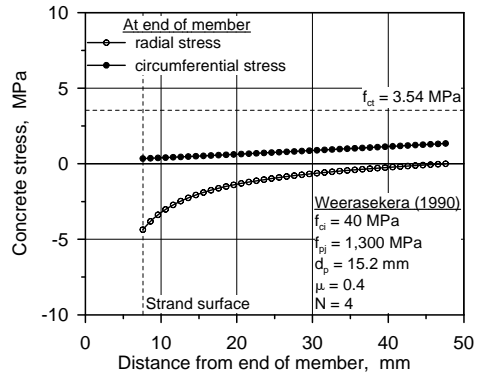


(c)

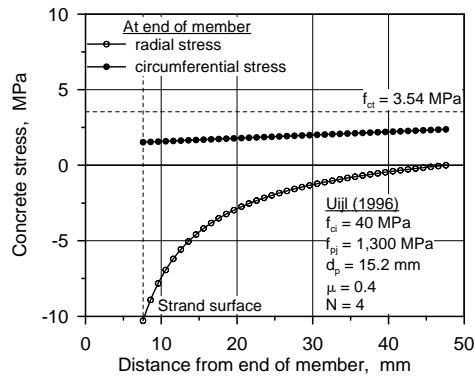
Figure 2.8 Radial and circumferential stress at partially cracked section: (a) Oh and Kim (2006); (b) Weerasekera and Loov (1990); (c) Den Uijl and Bigaj (1996)



(a)



(b)



(c)

Figure 2.9 Radial and circumferential stress at fully cracked section: (a) Oh and Kim (2006); (b) Weerasekera and Loov (1990); (c) Den Uijl and Bigaj (1996)

2.5 Empirical Equations for Transfer Length

Several empirical equations for transfer have been proposed to modify the ACI318 code provision. In this section, the provisions of ACI318, AASHTO LRFD, and Eurocode2 with regard to transfer length are briefly introduced. Also several important research works and their proposed equations are summarized. In many empirical equations, transfer length was considered as a part of development length. Thus, complete forms of the equations are introduced in this section.

2.5.1 Design Code

2.5.1.1 ACI318-11 (2011)

The current code equation for transfer and development length, ACI Eq. (12-4), was first appeared in ACI318-63 code. Using the assumption of a constant transfer bond distribution, Mattock (1962) developed the equation. The equilibrium condition at the transfer length is given by:

$$(U_t \Sigma_o) l_t = A_p f_{se} \quad (2.15)$$

The value of the constant transfer bond U_t was found to be 2.76 MPa, which was derived from the test results conducted at Portland Cement Association (PCA) (Hanson and Kaar, 1959; and Kaar et al., 1963). Hanson and Kaar (1959) stated that the average transfer bond stress amounted to 2.76 MPa and Mattock (1962) agreed with it. Note that the average value for transfer bond stress was used to derive the equation rather than a conservative value (Tabatabai and Dickson, 1993). Regarding

Σ_o and A_p , the actual values for Grade 1,720 prestressing seven-wire strand were used: $A_p = 0.725(\pi d_b^2/4)$ and $\Sigma_o = (4/3)\pi d_b$. Substituting U_t , A_p and Σ_o into equation (2.15) gives the ACI Eq. (12-4):

$$l_t = \frac{f_{se}}{20.3} d_b \approx \frac{f_{se}}{21} d_b \quad (2.16)$$

In order to take into account the effect of a low prestressing force within the transfer zone on the shear strength, Section 11.3.4 of the ACI318-11 code makes the following statement with regard to transfer length:

The prestress force shall be assumed to vary linearly from zero at end of the prestressing steel, to a maximum at a distance from end of the prestressing steel equal to the transfer length, assumed to be 50 diameters for strand and 100 diameters for single wire.

Because the stress in the Grade 1,720 prestressing seven-wire strands for the test at the PCA was approximately 1,030 MPa, the expression of $50d_b$ yielded almost the same results to the ACI Eq. (12-4).

Mattock (1962) proposed the development length equation based on the test results conducted by Hanson and Kaar (1959) and obtained by American Association of Railroads:

$$l_d = \frac{1}{7} (1.11 f_{ps} - 0.77 f_{se}) d_b \quad (2.17)$$

This equation can be rewritten by using equation (2.16) as:

$$\frac{f_{ps} - f_{se}}{7} = 0.9 \left(\frac{l_d - l_t}{d_b} \right) \quad (2.18)$$

In 1962, ACI Committee removed the coefficient of 0.9 in equation (2.18) and modified it to the current equation for development length, ACI Eq. (12-4):

$$l_d = l_t + \frac{1}{7} (f_{ps} - f_{se}) d_b = \frac{1}{7} \left(f_{ps} - \frac{2}{3} f_{se} \right) d_b \quad (2.19)$$

Note that equation (2.19) was formulated to best fit the test results. It means that the equation represents average values rather than conservative values.

2.5.1.2 AASHTO LRFD Bridge Design Specifications (2010)

Article 5.11.4.1 of AASHTO LRFD suggests an equation that is similar to but more conservative than the ACI318 code provision:

$$l_t = 60d_b \quad (2.20)$$

$$l_d = \frac{1}{7} \kappa \left(f_{ps} - \frac{2}{3} f_{se} \right) d_b \quad (2.21)$$

where,

$$\kappa = \begin{cases} 1.0 & \text{for pretensioned panels, piling, and other pretensioned} \\ & \text{members with a depth of less than or equal to 610 mm} \\ 1.6 & \text{for pretensioned members with a depth greater than} \\ & \text{610 mm} \end{cases}$$

2.5.1.3 Eurocode2 (2004)

The equation suggested by Eurocode2 is also established on the assumption of the constant plastic bond stress. However, the constant plastic bond stress is affected by concrete tensile strength:

$$f_{bpt} = \eta_{pl} \eta_1 f_{ctdi} \quad (2.22)$$

where, η_{pl} is a coefficient for type of tendon;

$$\eta_{pl} = \begin{cases} 2.7 & \text{for indented wires} \\ 3.2 & \text{for three and seven-wire strands} \end{cases}$$

η_1 is a coefficient for bond condition;

$$\eta_1 = \begin{cases} 1.0 & \text{for good bond condition} \\ 0.7 & \text{otherwise} \end{cases}$$

and f_{ctdi} is the design tensile strength of concrete at time of release.

Bond condition is defined depending on the vertical position of a tendon. If the height of a section is less than 250 mm, all the tendons in the section are considered in a good bond condition regardless of their position. For a section with the height greater than 250 mm, tendons over 250 mm from the bottom of the section are considered in a poor bond condition. The height of this zone for poor bond condition does not exceed 300 mm. The design tensile strength of concrete at time of release f_{ctdi} is given by:

$$f_{ctdi} = \alpha_{ct} \frac{0.7 f_{ctmi}}{\gamma_c} \quad (2.23)$$

where, α_{ct} is a coefficient for long term effects on the tensile strength and for unfavorable effects from the way the load is applied; γ_c is partial safety factor for concrete; f_{ctmi} is the tensile strength of concrete at time of release:

$$f_{ctmi} = \left\{ \exp \left[s_{cm} \left(1 - \sqrt{\frac{28}{t_i}} \right) \right] \right\}^\alpha \cdot f_{ctm} \quad (2.24)$$

with

$$s_{cm} = \begin{cases} 0.30 f_{ck}^{2/3} & \text{for } f_{ck} \leq 50 \text{ MPa} \\ 2.12 \ln(1 + 0.1 f_{cm}) & \text{for } f_{ck} > 50 \text{ MPa} \end{cases} \quad (2.25)$$

where, s_{cm} is a coefficient for type of cement;

$$s_{cm} = \begin{cases} 0.20 & \text{for Class R} \\ 0.25 & \text{for Class N} \\ 0.38 & \text{for Class S} \end{cases}$$

t_i is time of release;

α is a coefficient for development of tensile strength with time;

$$\alpha = \begin{cases} 1.0 & \text{for } t < 28 \text{ days} \\ 2/3 & \text{for } t \geq 28 \text{ days} \end{cases}$$

f_{ctm} is the mean tensile strength of concrete at 28 days;

and f_{cm} is the mean compressive strength of concrete at 28 days

Transfer length is calculated by the following equation:

$$l_t = \alpha_s \alpha_1 \alpha_2 \frac{f_{pi}}{f_{bpt}} d_b \quad (2.26)$$

where, α_s is a coefficient for design situation;

$$\alpha_s = \begin{cases} 0.8 & \text{for verifications of local stresses at release} \\ 1.2 & \text{for ultimate limit states} \end{cases}$$

α_1 is a coefficient for type of release;

$$\alpha_1 = \begin{cases} 1.0 & \text{for gradual release} \\ 1.25 & \text{for sudden release} \end{cases}$$

and α_2 is a coefficient for type of tendon;

$$\alpha_2 = \begin{cases} 0.25 & \text{for tendons with circular section} \\ 0.19 & \text{for three and seven-wire strands} \end{cases}$$

Equation (2.26) considers the factors regarding design situation, type of release, and type of tendon. For verifications of local stresses at release, a shorter transfer length would give conservative results. At ultimate limit state, on the contrary, a longer transfer length would be favorable.

The constant flexural bond stress can be obtained in a similar way to equation (2.22):

$$f_{bpd} = \eta_{p2} \eta_1 f_{ctd} \quad (2.27)$$

where, η_{p2} is a coefficient for type of tendon and bond situation at anchorage;

$$\eta_{p2} = \begin{cases} 1.4 & \text{for indented wires} \\ 1.2 & \text{for seven-wire strands} \end{cases}$$

Like the ACI318 and AASHTO LRFD, development length is expressed as the sum of transfer length and flexural bond length:

$$l_{bpd} = 1.2l_t + \alpha_2 \frac{(f_{ps} - f_{se})}{f_{bpd}} d_b \quad (2.28)$$

2.5.2 Empirical Equations from Previous Research

2.5.2.1 Oleśniewicz (1975)

Oleśniewicz (1975) statistically investigated transfer lengths measured in fields and laboratories. The cube compressive strength of concrete at time of transfer ranged from 20 MPa to 50 MPa. In the proposed equation, transfer length was proportional to a diameter of prestressing strand and a square root of ratio of the initial prestress to concrete compressive strength at time of transfer. The proposed equation also accounted for a scatter of the measured transfer lengths by adopting a factor Ψ :

$$l_t = \Psi d_b \sqrt{\frac{f_{pi}}{f_{ci}}} \quad (2.29)$$

where, f_{pi} is initial prestress; and

$$\Psi = \begin{cases} 10 & \text{for average value} \\ 13 & \text{for upper bound value} \\ 7 & \text{for lower bound value} \end{cases}$$

2.5.2.2 Zia and Mostafa (1977)

Zia and Mostafa (1977) collected extensive test results of transfer and development length that had been reported in the literature. The concrete compressive strength at time of transfer ranged from 14 MPa to 56 MPa in their literature survey. They proposed an equation for transfer length and flexural bond length by linear regression analysis on the collected test results. The proposed equation for transfer length took into account the effect of concrete compressive strength at time of transfer, initial prestress, diameter of prestressing strand, and type of release:

$$l_t = 1.5 \frac{f_{pi}}{f'_{ci}} d_b - 117 \quad \text{for sudden release} \quad (2.30)$$

$$l_t = 1.3 \frac{f_{pi}}{f'_{ci}} d_b - 58 \quad \text{for gradual release} \quad (2.31)$$

The proposed equation for flexural bond length was more conservative than the ACI318 code provision:

$$l_{fb} = \frac{1.25}{7} (f_{ps} - f_{se}) d_b \quad (2.32)$$

2.5.2.3 Cousins et al. (1990a)

Cousins et al. (1990a, 1990b, and 1990c) conducted several experiments to measure transfer and development lengths of epoxy coated and uncoated

prestressing strands. Three different quantities of epoxy grit were considered: low, medium, and high density. Based on their test results, they proposed new equations for transfer and development length, which are capable of applying to epoxy coated and uncoated seven-wire strands. In their proposal, they assumed that the transfer zone is divided by two zones, elastic zone and plastic zone (see figure 2.6). Each zone has different bond distribution. In the elastic zone, transfer bond stress increases linearly with a bond modulus B . The plastic zone, which takes majority of the transfer zone, had a constant transfer bond.

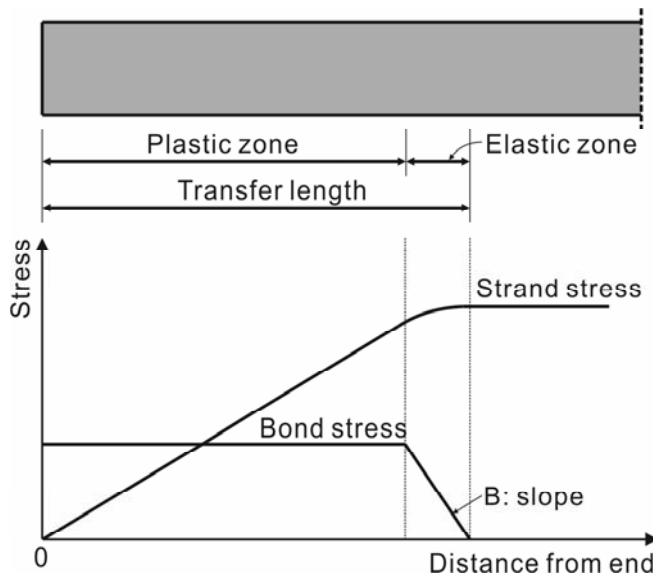


Figure 2.10 Assumed bond distribution in Cousins et al. model (Cousins et al., 1990a)

Under the assumption of the transfer bond distribution, the following equation was derived for transfer length:

$$l_t = 0.5 \left(\frac{U'_t \sqrt{f'_{ci}}}{B} \right) + \frac{f_{se} A_p}{\pi d_b U'_t \sqrt{f'_{ci}}} \quad (2.33)$$

where, U'_t is plastic transfer bond stress normalized by f'_{ci} ; and B is bond modulus.

Similarly, a new development length equation was also proposed:

$$l_{fb} = (f_{ps} - f_{se}) \left(\frac{A_p / \pi d_b}{U'_d \sqrt{f'_c}} \right) \quad (2.34)$$

where, U'_d is plastic bond stress for development length normalized by f'_c . The value of U'_t , B , and U'_d were determined from the measured concrete strain profiles of the test specimens.

2.5.2.4 Mitchell et al. (1993)

In the experimental research of Mitchell et al. (1993), twenty two pretensioned concrete beams with a rectangular section were fabricated and tested to investigate the effect of concrete compressive strength on transfer and development length. The concrete compressive strength at 28 days ranged from 31 MPa to 89 MPa. Stress-relieved strands had the diameter of 9.5 mm and the tensile strength of 1,813 MPa while low-relaxation strands with the diameter of 12.7 mm and 15.2 mm had the tensile strength of 1,903 MPa and 1,793 MPa. Prestress was gradually released by hydraulic rams.

The test specimens were tested with varying embedment lengths by 3 or 4 point

loading after transfer of prestress. Concrete and strand strain were measured through the whole tests. Mitchell et al. (1993) found that transfer and flexural bond length were inversely proportional to a square root of concrete compressive strength at time of transfer. They also suggested that the transfer length should be a function of initial prestress f_{pi} rather than effective prestress f_{se} , which was previously adopted by Zia and Mostafa (1977). Based on their test results, they modified the ACI318 code provisions to include the effect of concrete compressive strength:

$$l_t = \frac{f_{pi} d_b}{21} \sqrt{\frac{20}{f'_{ci}}} \quad (2.35)$$

$$l_{fb} = 0.145(f_{ps} - f_{se}) \sqrt{\frac{30}{f'_{ci}}} \quad (2.36)$$

2.5.2.5 Russell and Burns (1993)

Russell and Burns (1993) performed an extensive experimental program to determine transfer and development length of prestressing strands with a diameter of 15.2 mm and to establish a design guideline for debonded strands. At that time, 15.2 mm strands were considered large and there were still a widespread concern about the use of the prestressing strands with a large diameter after the Federal Highway Administration (FHWA) issued a moratorium prohibiting the use of 15.2 mm strands in 1988 (Russell and Burns, 1997). The moratorium was lifted in 1996 as a result of extensive research on 15.2 mm strands.

Totally, 65 beams were fabricated with the test variables including number of strands, diameter of strand, debonding, confining reinforcement, and size and shape

of cross section. Three of the beams were full-sized AASHTO type C composite girders. Nineteen development length tests were performed on 13 beams. It was achieved by loading each end of one test specimen. Concrete compressive strengths at time of transfer and 28 day were 28 MPa and 41 MPa, respectively. Grade 1,860 prestressing strands with the diameter of 12.7 mm and 15.2 mm were used for the fabrication of the beams. Prestress was suddenly released by flame cutting.

Excessive transfer lengths were measured from some of the test specimens, which led to the proposal of a more conservative equation than the ACI318 code provision:

$$l_t = \frac{f_{pe}}{14} d_b \quad (2.37)$$

Equation (2.37) gives longer transfer length than the ACI318 code provision by 50%.

Development length test revealed that the failure mode of the I-type section girders is controlled by web shear cracking within the transfer zone. The web shear cracking weakened the anchorage capacity of the prestressing strand and eventually led to a bond failure. Based on these observations, Russell and Burns (1993) made several recommendations to prevent the anchorage failure in case where the shear resistance of a member is controlled by web shear cracking. The other case where web shear cracking does not occur, the following expression was proposed to estimate the development length:

$$l_d = \frac{M_u}{M_{cr}} l_t \quad (2.38)$$

The above equation (2.38) can be transformed into a criterion not allowing flexural cracks to develop within the transfer zone:

$$M_{cr} > l_t \cdot V_u \quad (2.39)$$

2.5.2.6 Deatherage and Burdette (1994)

In response of the FHWA moratorium in 1988, Deatherage and Burdette (1994) conducted an experiment for transfer and development length of 22 full scale AASHTO type I beams with various diameter of prestressing strands. The prestressing strands investigated were Grade 1,860 low-relaxation type with the diameter of 13 mm, 13.3 mm, 14 mm, and 15 mm. Concrete compressive strength at 28 days was 34.5 MPa. Prestress was suddenly released by flame cutting.

Based on the test results and other researcher's discussion, Deatherage and Burdette (1994) insisted that an equation for longer transfer and development length is desirable. For this purpose, they made some modifications to the ACI318 code provision. In their proposed equation, the term of f_{se} was replaced by f_{si} for transfer length and a factor of 1.5 was introduced for flexural bond length:

$$l_t = \frac{f_{pi}}{21} d_b \quad (2.40)$$

$$l_{fb} = \frac{1.5}{7} (f_{ps} - f_{se}) d_b \quad (2.41)$$

2.5.2.7 Buckner (1995)

Buckner (1995) reviewed extensive researches that had been performed on transfer and development length since the FHWA moratorium. He attempted to formulate a unifying theory that explains the conflicting conclusions and suggestions of the previous researches.

After analyzing the data in the literature, he proposed the following equations for transfer and flexural bond length:

$$l_t = \frac{f_{pi}}{21} d_b \quad (2.42)$$

$$l_{fb} = \lambda (f_{ps} - f_{se}) d_b \quad (2.43)$$

Comparing the proposal of Deatherage and Burdette (1994), the transfer length equation is exactly same as equation (2.40) but the flexural bond length equation includes a factor of λ rather than the factor of 1.5 in equation (2.41). Buckner found that the development length increased with the strain in the prestressing strand at failure of the members. He stated that it was because the average bond stress over the anchorage zone became lower as the strand strain increased. Thus, the factor λ was given as a function of ε_{ps} that is a strand strain corresponding to f_{ps} :

$$1.0 \leq \lambda = 0.6 + 40\varepsilon_{ps} \leq 2.0 \quad (2.44)$$

The factor λ has the lower bound value of 1.0, which corresponds to the yield strain of the strand of 0.01, and the upper bound value of 2.0, which corresponds to

an assumed ultimate strain of 0.035. The expression for the factor λ was derived from the analysis of the data of the previous researches.

2.5.2.8 Tadros and Baishya (1996)

Tadros and Baishya (1996) simplified the proposal of Buckner (1995) to avoid the inconvenience of calculating ε_{ps} . The factor λ was expressed with the term f_{ps} rather than the term ε_{ps} by using the approximate relationship:

$$\lambda = \frac{1}{7} \left(\frac{f_{ps}}{27} - 55 \right) \geq 1.0 \quad (2.45)$$

Considering other factors affecting the bond of prestressing strands, the development length equation was modified to be:

$$l_d = C_1 C_2 l_{db} \quad (2.46)$$

where, C_1 is a factor for strand surface condition; and C_2 is a factor for concrete confinement. The value of C_1 and C_2 is set 1.0 under the standard condition of Grade 1,860 low-relaxation strand; 13 mm diameter; smooth uncoated; 50 mm spacing; 34.5 MPa normal weight concrete; and regular bottom location. Under different conditions, however, the values of C_1 and C_2 were open to discussion. The basic development length l_{db} was provided as:

$$l_{db} = \begin{cases} l_t + \frac{1}{49} \left(\frac{\bar{f}_{ps}}{27} - 55 \right) (\bar{f}_{ps} - 1,100) d_b & \text{for } 1,675 \leq \bar{f}_{ps} \leq 1,860 \text{ MPa} \\ l_t + \frac{1}{7} (\bar{f}_{ps} - 1,100) d_b & \text{for } 1,100 \leq \bar{f}_{ps} \leq 1,675 \text{ MPa} \\ \frac{1}{7} \left(\frac{3}{8} \bar{f}_{ps} d_b \right) & \text{for } 0 \leq \bar{f}_{ps} \leq 1,100 \text{ MPa} \end{cases} \quad (2.47)$$

As a part of development length calculation, they argued that it is reasonable that transfer length is expressed by f_{pe} rather than f_{pi} . Their argument was supported by several factors that the external loads are usually applied after all prestress losses occurred; that transfer length varies with time and the applied load; and that the range of the variation is wider in the value of f_{pe} than f_{pi} . Thus, the expression for transfer length was modified to be:

$$l_t = \frac{f_{pe}/0.8}{21} d_b \quad (2.48)$$

More simply, transfer length was calculated as:

$$l_t = 60d_b \quad (2.49)$$

2.5.2.9 Mahmoud et al. (1999)

Mahmoud et al. (1999) tested 52 specimens to measure transfer and development length of two types of carbon fiber reinforced polymer (CFRP), Leadline bars and carbon fiber composite cables (CFCC), as well as steel strand. The test specimens

had rectangular sections and 50 mm or 100 mm debonding regions at both ends. Prestress was gradually released by a cylindrical hydraulic jack. ERSGs and DEMEC gauges were used together to measure the concrete strains and tendon strains during the test. The range of concrete compressive strength was 22 ~ 48 MPa at time of release and 31 ~ 63 MPa at 28 days. The Grade 1,860 prestressing strands with the diameter of 9.6 mm and 12.7 mm were used. To determine development length, a one-point or two-point static loading was applied up to failure in a displacement controlled manner.

As a result, they proposed a unifying transfer length equation applicable to CFRP as well as steel strand:

$$l_t = \frac{f_{pi}}{\alpha_t f_{ci}^{0.67}} d_b \quad (2.50)$$

where, α_t is a coefficient for material type of tendon.

$$\alpha_t = \begin{cases} 2.4 & \text{for steel strands} \\ 1.9 & \text{for Leadline bars} \\ 4.8 & \text{for CFCC strands} \end{cases}$$

A development length equation was also proposed but unfortunately it was applicable only to CFRP tendons.

2.5.2.10 Barnes et al. (2003)

In the experimental program performed by Barnes et al. (2003), 36 full-scale AASHTO type I girders were fabricated. Multiple transfer zones were created with

staggered debonding patterns in one test specimen. As a result, totally 192 transfer zones were created and transfer length were measured for 184 of these zones. Main test variables were concrete compressive strength, release method, and surface conditions of the prestressing strand. The investigated concrete compressive strengths at time of prestress were 27.6, 48.3, and 62.1 MPa. Two different surface conditions were included: as-received condition and rusted condition. Half of the prestressing strands were stored indoors during the test and free from rust. It was defined as the as-received condition. The other half were exposed to weather in the yard for several months and covered with rust. It was defined as the rusted condition. Prestress was released by flame-cutting however there were two types of release method. Approximately 2/3 test specimens were simultaneously cut at both ends and the rest were done at one end. The prestressing strands were Grade 1,860 low-relaxation seven-wire strand with a diameter of 15.2 mm, and were spaced in 50 mm for all the specimens.

The test results showed a significant scatter and thus Barnes et al. made an attempt to find a general trend. The following equation was proposed to explain the trend of the measured transfer length:

$$l_t = \alpha_b \frac{f_{pi}}{\sqrt{f_{ci}}} d_b \quad (2.51)$$

where,

$$\alpha_b = \begin{cases} 0.13 \text{ MPa}^{-0.5} & \text{for average value} \\ 0.22 \text{ MPa}^{-0.5} & \text{for upper bound value} \\ 0.06 \text{ MPa}^{-0.5} & \text{for lower bound value} \end{cases}$$

2.5.2.11 Kose and Burkette (2005)

Kose and Burkette (2005) collected data for transfer and development lengths in the research conducted after the FHWA memorandum (Castrodale et al., 1988; Abdalla et al., 1993; Cousins et al., 1993; Burdette et al., 1994; Tawfiq, 1995; Jabson, 1997; Kilgore, 1997; Grove, 1998; Lane, 1998; Kose, 1999; and Gross and Burns, 1995) and formulate a new equation for development length including transfer length. Totally, 313 transfer length data and 95 development length data were considered in the linear regression analysis. Concrete compressive strength ranged from 34.8 to 91.1 MPa. The Grade 1,860 low-relaxation prestressing strands with the diameter of 12.7 mm and 15.2 mm were used in the research. The proposed formulae represented the upper bound of 95% confidence interval for the data:

$$l_t = 0.045 \frac{f_{pi}}{\sqrt{f'_{ci}}} (1 - d_b)^2 \quad (2.52)$$

$$l_{db} = 200 + 0.19 \frac{(f_{pu} - f_{pi})}{\sqrt{f'_{ci}}} (1 - d_b)^2 \quad (2.53)$$

2.5.2.12 Martí-Vargas et al. (2007b)

Martí-Vargas et al. (2007a) developed a new method of measuring transfer length of pretensioned concrete members, which is called ECADA test method. It consists of repeated measurements of the force supported by the strand with varying embedment lengths. For the measurements, an anchorage-measurement-access (ANA) system is placed at the stressed end to simulate the sectional rigidity of the test specimens.

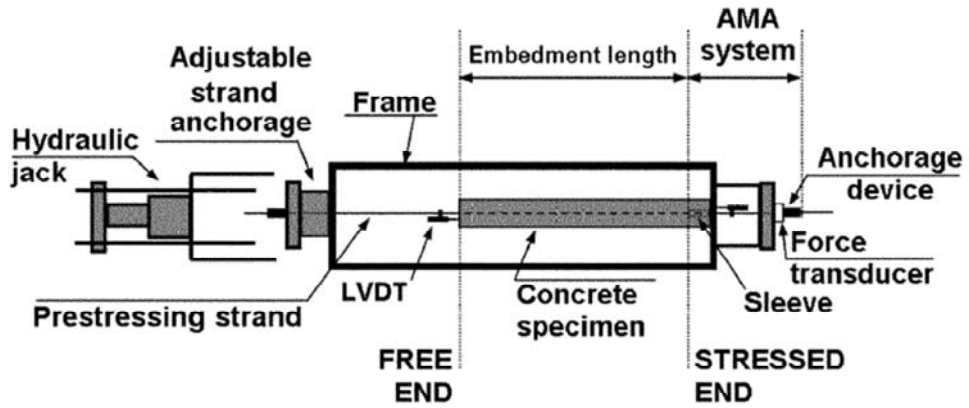


Figure 2.11 Set-up of ECADA test method (Martí-Vargas et al., 2007a)

Using the ECADA test method, they measured the transfer lengths for the test specimens with a rectangular section of 100×100 mm and a single prestressing strand concentrically located. The concrete compressive strength at time of prestress ranged from 24 to 55 MPa and Grade 1,860 low-relaxation seven-wire strands of 12.9 mm diameter were used. Based on the test results from this study and other researches, an equation was proposed to estimate transfer length:

$$l_t = \lambda_m \frac{4.7 f_{pi}}{f_{ci}^{0.67}} d_b \quad (2.54)$$

where,

$$\lambda_m = \begin{cases} 1.0 & \text{for average value} \\ 1.5 & \text{for upper bound value} \\ 0.5 & \text{for lower bound value} \end{cases}$$

2.5.3 Factors Affecting Transfer Length

2.5.3.1 Compressive Strength of Concrete

Though the current ACI318 code does not take into account the effect of concrete compressive strength on transfer and development length of prestressing strands, concrete compressive strength has been regarded as one of the most important factors. Various researchers investigated the effect of concrete compressive strength at time of transfer and found a consistent trend that transfer and development lengths decrease as concrete compressive strength increases (Oleśniewicz, 1975; Zia and Mostafa, 1977; Castrodale et al., 1988; Cousins et al., 1990a, 1990b, and 1990c; Balázs, 1992; Mitchell et al., 1993; Den Uijl, 1996; Mahmoud et al., 1999; Oh and Kim, 2000; Barnes et al., 2003; Kose and Burkette, 2005; and Martí-Vargas et al., 2007b).

With the assumption of the uniform bond stress distribution along the transfer zone, the effect of the concrete compressive strength can be interpreted as the effect of the uniform bond stress U_t . This idea was reflected in equation (2.33) and (2.34) by Cousins et al. (1990a). In the equations, it was assumed that the uniform bond stress is proportional to a square root of the concrete compressive strength.

The relationship between the bond stress and the concrete compressive strength can be also explained as a confining action of concrete. Concrete in the majority of transfer zone is thought to be in an inelastic state, where transverse cracks develop alongside the prestressing strand. The radial expansion of the strand at transfer causes a high level of radial compressive stress on the surrounding concrete, which should be equilibrated by circumferential tensile stress. Since concrete has much weaker properties for tensile behavior, radial cracks occur through the inelastic part

of the transfer zone. With these radial cracks, the response of the concrete to the radial displacement of the strand is weakened. The radial response of the concrete determines the radial compressive stress that is a main cause of the concrete confining action and the frictional bond stress (Barnes et al., 2003).

Consequently, the basic form of an equation for transfer and development length depends on which relationship is adopted between the uniform bond stress and the compressive strength of concrete. According to Martí-Vargas et al. (2007b), the many transfer length equations found in the literature can be appeared in a single form:

$$l_t = \frac{f_{px}^{k_1} A_p}{(k_2 \pi d_b) U_t} + k_3 \quad (2.55)$$

where, f_{px} is strand stress considered in each equation; and k_1 , k_2 and k_3 are fitting factors. Using $A_p = 0.779 \pi d_b^2 / 4$ and $k_1 = 4/3$, Martí-Vargas et al. (2007b) obtained the uniform bond stress U_t as a function of concrete compressive strength. In cases that specific values for A_p and k_1 were reported, those values were used for the calculation of U_t . The values of k_1 , k_2 , k_3 , and U_t for the transfer length equations in Section 2.5.2 are summarized in Table 2.1, which does not include equation (2.52) proposed by Kose and Burkette (2005) because it does not fit the structure of equation (2.55). Table 2.1 shows that various functions with respect to concrete compressive strength at transfer have been used to calculate the uniform bond stress.

Table 2.1 Empirical equations for transfer length and their parameters (Martí-Vargas et al., 2007b)

Reference	Equation	Parameters				
		f_{px}	k_1	U_t	k_2	k_3
ACI318-11 (2011)	$l_t = \frac{f_{pe}}{21} d_b$	f_{pe}	1	2.76	4/3	–
Eurocode2 (2004)	$l_t = \alpha_1 \alpha_2 \frac{f_{pi}}{\eta_{p1} \eta_1 f_{ctdi}} d_b$	f_{pi}	1	$\frac{\eta_{p1} \eta_1}{\alpha_1} f_{ctdi}$	1	–
Oleśniewicz (1975)	$l_t = 10 d_b \sqrt{\frac{f_{pi}}{f'_{ci}}}$	f_{pi}	0.5	$0.015 f'_{ci}{}^{0.5}$	4/3	–
Zia and Mostafa – sudden release (1977)	$l_t = 1.5 \frac{f_{pi}}{f'_{ci}} d_b - 117$	f_{pi}	1	$0.097 f'_{ci}$	4/3	-117
Zia and Mostafa – gradual release (1977)	$l_t = 1.3 \frac{f_{pi}}{f'_{ci}} d_b - 58$	f_{pi}	1	$0.112 f'_{ci}$	4/3	-58
Cousins et al. (1990a)	$l_t = 0.5 \left(\frac{U_t \sqrt{f'_{ci}}}{B} \right) + \frac{f_{se} A_p}{\pi d_b U_t \sqrt{f'_{ci}}}$	f_{pe}	1	$0.556 f'_{ci}{}^{0.5}$	1	$3.4 f'_{ci}{}^{0.5}$
Balazs (1992)	$l_t = 3.15 \sqrt[5]{\frac{f_{pe}^3}{f'_{ci}{}^{12}}}$	f_{pe}	0.6	$0.046 f'_{ci}{}^{0.4}$	4/3	–
Mitchell et al. (1993)	$l_t = \frac{f_{pi} d_b}{21} \sqrt{\frac{20}{f'_{ci}}}$	f_{pi}	1	$0.674 f'_{ci}{}^{0.5}$	4/3	–

Table 2.1 Empirical equations for transfer length and their parameters (Martí-Vargas et al., 2007b) (Continued)

Reference	Equation	Parameters				
		f_{px}	k_1	U_t	k_2	k_3
Russell and Burns (1993)	$l_t = \frac{f_{pe}}{14} d_b$	f_{pe}	1	1.84	4/3	–
Deatherage and Burdette (1994) Buckner (1995)	$l_t = \frac{f_{pi}}{21} d_b$	f_{pi}	1	2.76	4/3	–
Tadros and Baishya (1996)	$l_t = \frac{f_{pe}/0.8}{21} d_b$	$f_{pe}/0.8$	1	2.76	4/3	–
Mahmoud et al. (1999)	$l_t = \frac{f_{pi}}{2.4 f_{ci}^{0.67}} d_b$	f_{pi}	1	$0.350 f_{ci}^{0.67}$	4/3	–
Barnes et al. (2003)	$l_t = 0.13 \frac{f_{pi}}{\sqrt{f_{ci}}} d_b$	f_{pi}	1	$1.124 f_{ci}^{0.5}$	4/3	–
Martí-Vargas et al. (2007b)	$l_t = \frac{4.7 f_{pi}}{f_{ci}^{0.67}} d_b$	f_{pi}	1	$0.031 f_{ci}^{0.67}$	4/3	–

2.5.3.2 Initial Prestress

When Grade 1,720 strands were commonly used for pretensioned concrete structures, Janney (1963) investigated transfer lengths of high strength prestressing strand, Grade 1,860 strand. He observed a small increase of transfer length in the test result of Grade 1,860 strands and concluded that the effect of higher prestress was insignificant. On the other hand, Karr et al. (1963) stated that transfer length has a linear relationship with initial prestress.

With the assumption of the constant bond distribution along the transfer region and negligence of the effect of the change in the radial strain of the strand, transfer length is linearly varied with initial prestress. Most empirical equations have been derived on this assumption and thus have the term of f_{pi} or f_{se} . Exceptional cases were the equations proposed by Oleśniewicz (1975) and Balázs (1992). In their equations, transfer length is proportional to strand stress to power of 0.5 and 0.6, respectively. These values give the bond distribution in a parabolic shape along the transfer zone.

2.5.3.3 Strand Diameter

Generally, strand diameter has been also recognized as a major parameter to affect transfer and development length because it determines the perimeter of the strand and thus the contact area to the surrounding concrete. Increase in strand diameter directly means increase in the contact area on which bond acts. In most empirical equations, therefore, transfer length is proportional to strand diameter.

It has been supported by the experimental observations. In Janney's experiment on wires with the diameter of 2.5 ~ 7.0 mm, transfer length was moderately

increased as the wire diameter increased (Janney, 1954). Hanson and Kaar (1959) investigated the influence of the strand diameter on flexural bond length up to 12.7 mm and revealed that the strand diameter has a considerable effect on the average bond stress at which general bond slip occurs. Over and Au (1965) concluded that transfer length required for the large diameter is greater than that of the smaller diameter. Cousins et al. (1990b) found in their experiment for epoxy-coated and uncoated strands that the uncoated strands with 9.5, 12.7, and 15.2mm diameter have a much larger transfer length than the value calculated by the ACI318 code provision by 60%. This report led to the FHWA's memorandum, which put the complete restriction of using the prestressing strand with 15.2 mm diameter in pretensioned concrete structures in 1988. Oh and Kim (2000) stated that transfer length of 15.2 mm strand is 25% larger than that of 12.7 mm. This value was close to the increase in the strand diameter, 20%, which implied the linear relationship between transfer length and strand diameter.

On the other hand, there are some researches that reported no or opposite influence of strand diameter. In the experiments performed by Deatherage and Burdette (1994), transfer length of 12.7 mm and 14.3 mm diameter strands were approximately proportional to the strand diameter, however this relationship could not be found in 15.2 mm diameter strands. Kose and Burkette (2005) revealed that the some empirical equations including the design code provisions underestimated transfer lengths of 12.7 mm diameter strands but overestimated transfer lengths of 15.2 mm diameter strands, which questioned the widely accepted linear relationship between transfer length and strand diameter.

2.5.3.4 Strand Surface Condition

Many researchers have reported that surface roughness can improve bond properties of prestressing strands. In their research, rusted and deformed conditions were often considered as viable means to improve the surface roughness of the prestressing strands. Comparing intentionally roughened conditions, reference conditions were called in various ways: ‘clean strand’, ‘bright strand’, ‘as-received condition’, or ‘mill condition’. The reference condition, however, does not mean that strand surface is completely clean because there are residual lubricants, usually stearates, resulting from the wire drawing process (Deatherage and Burdette, 1994).

Janney (1954) found that rusted wires exhibited transfer and flexural bond performances superior to that of clean wires. He attributed this enhanced performance of the rusted wires to the reduction in the coefficient of friction. Hanson (1969) investigated the effect of the surface roughness of the prestressing strand. He considered as-received, partially rusted, rusted, and deformed conditions. The test results showed that rusted and deformed conditions reduced average transfer lengths of 11.1 mm diameter strands, which amounted to 711 mm for as-received, 584 mm for partially rusted, 483 mm for fully rusted, and 559 mm for deformed conditions. Cousins et al. (1990b and 1990c) observed that epoxy coating on strand significantly reduced transfer and development length. They sawed some ends of specimens to examine the surface between the strand and the concrete. In the specimens with the coated strand, many scratches were found in the direction of strand movement and cement particles adhered onto the surface of the coated strand. Based on these observations, they noted that bond mechanism of coated strands mainly relies on adhesion and grit-paste interlock. Deatherage and Burdette (1994)

prepared the prestressing strands in 3 conditions: mill condition, 1-day weathering, and 3-day weathering. Visible rust was not created but they stated that the strands were microscopically roughened. Transfer lengths of 1-day weathered and 3-day weathered strands were reduced respectively by 27.9% and 40%. This reduction was attributed to increased adhesion of the concrete and increased coefficient of friction between the concrete and the strand. Barnes et al. (2003) also observed that transfer lengths of rusted strands are shorter than those of bright strands in average. However, the scatter of the results was much wider and in some cases longer transfer lengths were measured in the rusted strand specimens. They concluded that there was no clear relationship between the surface roughness and transfer length.

2.5.3.5 Cover Depth and Strand Spacing

Concrete cover and strand spacing should be sufficiently provided to prevent splitting cracks of concrete surrounding a strand. Regarding strand spacing, the current ACI318 code requires that center-to-center spacing of pretensioning tendons at each end of a member be not less than $4d_b$ for strands. Cousins et al. (1993 and 1994) and Deatherage and Burdette (1994) investigated the feasibility of a reduced spacing of $3.5d_b$ (44.5 mm) for 12.7 mm diameter strands. They found no sign of splitting cracks and no significant effects of the reduced strand spacing on transfer and development lengths. Russell and Burns (1993 and 1996) carried out a similar experiment for 15.2 mm diameter strands. They tested pretensioned members with the strand spacing of 50 mm, which corresponds to $3.3d_b$ for 15.2 mm diameter strands. The test results clearly proved that the strand spacing of 50 mm can be safely applied to 15.2 mm diameter strands. Based on their research, the current

ACI318 code allows a reduced spacing of 45 mm for strands of 12.7 mm diameter or smaller and 50 mm for strands of 15.2 mm diameter if concrete compressive strength at time of prestress exceeds 28 MPa. On the contrary, Oh and Kim (2000) observed that a reduced spacing increases transfer length for 12.7 mm and 15.2 mm diameter strands. A reduction of center-to-center strand spacing from $4d_b$ to $3d_b$ led to 15 ~ 20% increase in transfer length of 12.7 mm diameter strands and 18 ~ 22% for 15.2 mm diameter strands. Wider spacing of $5d_b$, on the other hand, only caused 5 ~ 6% decrease in transfer length.

The current ACI318 code requires a minimum clear cover depth of 40 mm for a prestressing tendon embedded in cast-in-place concrete not exposed to weather or in contact with ground. Den Uijl (1992 and 1996) performed a series of experiments to examine the effect of concrete cover depth on bond behavior of prestressing strands. In his experiments, two groups of concrete were investigated: normal strength concrete (NSC) and high strength concrete (HSC). NSC had the cube strength at transfer of 33 ~ 44.5 MPa and the splitting strength of 2.3 ~ 2.6 MPa. HSC had the cube strength at transfer of 40.5 and 70.8 MPa and the splitting strength of 4.1 and 5.2 MPa. The diameter of the prestressing strands was 9.5 mm and 12.7 mm. Based on the test results, criteria of clear cover to prevent splitting cracks were established to be more than $2.5d_b$ for NSC and $1.5d_b$ for HSC. The requirement of $2.5d_b$ for NSC gives 38 mm for 15.2 mm diameter strands, which agrees well with the minimum cover depth of the current ACI318 code provision, 40 mm. In the experiment performed by Oh and Kim (2000), cover depth was investigated in the range of 30 ~ 50 mm. No visible cracks were developed on the concrete surfaces. A reduction of clear cover from 40 mm to 30 mm led to 13 ~ 26% increase in transfer length of 12.7 mm diameter strands and 22 ~ 27% for 15.2 mm diameter strands.

Clear cover of 50 mm, on the other hand, caused relatively minor decreases in transfer length, 7 ~ 11% for 12.7 mm diameter strands and 16 ~ 19% for 15.2 mm diameter strands.

Den Uijl (1996 and 1998) suggested a concept of effective cover depth to represent the contribution of concrete in the cover and between strands:

$$c_{eff} = \frac{2c_c + 1.5(m_p - 1)s_c}{2m_p} \quad (2.56)$$

where, c_c is clear cover depth; m_p is number of strands in the considered row; and s_c is clear strand spacing. The coefficient of 1.5 was arbitrary determined to take into account a more beneficial effect of the concrete between strands in carrying the circumferential tensile stress. A clear tendency was found between the relative transfer length Ψ and the effective cover depth (Den Uijl, 1998).

2.5.3.6 Top Bar Effect

The effect of vertical position of reinforcement on bond properties is well acknowledged in the studies of deformed bars. Generally, top-cast bars have bond properties inferior to those of bottom-cast bars. The poorer bond qualities of the top-cast bars resulted from the greater settlement of the concrete beneath the top-cast bars and from a lower tensile strength of the concrete at the top of the casting (Wan et al., 2002a). The current ACI318 code provision requires that development length be increased by 30% for a horizontal reinforcement having more than 300 mm of concrete below it. However, the top bar effect is not included in the transfer and

development length equation of the current code provisions.

Petrou et al. (2000) and Wan et al. (2002b) showed that slip of top-cast strands at transfer of prestress is consistently higher than that of bottom-cast strands in pretensioned concrete piles. The observed top-bottom slip ratio ranged from 1.03 to over 3.0. Since slip is a powerful indicator of transfer length, an excessive transfer length was estimated for the top-cast strands.

Peterman (2007) and Carroll (2009) suggested that the top-strand effect rely on the amount of concrete above the strand rather than the amount of concrete below the strand.

2.5.3.7 Time-Dependent Effect

Transfer length varies with time, especially during the first days after transfer. As time elapses, beneficial and detrimental effects occur simultaneously on transfer bond. The causes of the detrimental effects are time-dependent losses such as creep and relaxation. Concrete clamping the strand is generally subjected to high local stresses and strains beyond its elastic limit. The steady transverse crack growth probably results in the stress redistribution and weakens concrete confinement. This bond creep increases transfer length over time (Barnes et al., 2003). On the other hand, the beneficial effects come from shrinkage and concrete properties developing with time. Prestress is usually released before the concrete gains its design value. Concrete strength gradually increases and it might heal the initial transverse cracks (fib, 2000). Shrinkage also provides additional radial compressive stresses on the strand. These opposite effects are a possible reason why a majority of the increase in transfer length occurs during the first days after transfer (fib, 2000).

Kaar et al. (1963) reported transfer lengths of prestressing strands with the various diameters of 6.4 mm, 9.5 mm, 12.7 mm, and 15.2 mm over a period of 1 year. The average increase was 6% for all diameters of the strand. They stated that the increase in transfer length with time was irrelevant to concrete compressive strength at time of transfer. Cousins et al. (1990b) measured transfer lengths of uncoated strands and epoxy coated strands periodically up to 1 year after release. Transfer lengths increased by 5.4% for uncoated strands and 11.7% for epoxy coated strands in average. The majority of the increases occurred within the first 90 days. Oh and Kim (2000) found that transfer length increased by 2~3% at 7 days after the time of release and by 5% at 90 days. Barnes et al. (2003) observed 10 to 20% increases in transfer length over time. The most part of the increase took place within the first 28 days.

2.5.3.8 Prestress Release Method

In practice, prestress is usually suddenly released by flame cutting or disk cutting. Gradual release requires a large-scale mechanical device to control the movement of pretensioned strands and a space to install it. It is widely accepted that the sudden release method results in a longer transfer length than the gradual release method. In general, a dynamic impact generated by sudden release at one end of a pretensioned concrete member has no effect on transfer length at the opposite end. The adjacent end where prestress is released is called cut end while the far end is called dead end.

Kaar et al. (1963) reported that transfer lengths at cut ends is 20% longer than at dead ends for strands of 6.4 mm, 9.5 mm, and 12.7 mm diameter, and 30% longer for 15.2 mm diameter strand. Zia and Mostafa (1977) formulated respective

equations for sudden release and gradual release, equation (2.30) and (2.31). The equation for sudden release has a coefficient of 1.5 with respect to the term $f_{pi}d_b/f'_{ci}$ while a coefficient of 1.3 for gradual release. It implies 15% increase in transfer length at cut end. Russell and Burns (1997) observed visible transverse cracks that completely propagated through some test specimens with a 15.2 mm diameter strand due to sudden release. However, an average increase in transfer length was marginal for 15.2 mm diameter strands. On the other hand, 34% increase in average transfer length was found for 12.7 mm diameter strands. Sudden release raised a degree of scatter for strands of both diameters. Oh and Kim (2000) also indicated that transfer length at cut end increased by 16 and 13% for 12.7 mm and 15.2 mm strand respectively. On the other hand, Barnes et al. (2003) stated that the release method has no effect on transfer lengths of the specimens with concrete release strengths greater than 48 MPa and bright strands. For the specimens with rusted strands, sudden release increased transfer length by 30 to 50%. Eurocode2 reflects the effect of release method by adopting the factor, α_1 . The value of the factor α_1 is 1.25 for sudden release, which increases transfer length by 25%.

3. High Strength Prestressing Strand

3.1 Introduction

For several decades, prestressed concrete structures have been fabricated with Grade 1,860 strands. In some countries, however, recent attempts in developing high-strength seven-wire strands which have higher tensile strengths than the conventional Grade 1,860 strands became successful. Japan developed Grade 2,230 MPa strands in the early 2,000s and some researches on Grade 2,069 strands were conducted in the United States (Hill, 2006; and Carroll, 2009). South Korea also succeeded in developing two grades of low-relaxation seven-wire high-strength strand that have the nominal tensile strength of 2,160 MPa and 2,400 MPa. These tensile strengths are increased by about 16% and 29% from that of the Grade 1,860 strands, respectively. The recent revision to KS D 7002 (KATS, 2011) permitted the specifications for the mechanical properties of the high-strength strands and designated them SWPC7CL and SWPC7DL. In this section, the properties of SWPC7CL and SWPC7DL strands are presented.

3.2 Mechanical Properties of High Strength Prestressing Strand

The typical stress-strain curves of high-strength strands are presented in figure 3.1, along with the stress-strain curve of low-relaxation Grade 1,860 strand (SWPC7BL) for comparison. As seen in the figure, prestressing strands have an ambiguous yielding point. Several methods have been in use to determine yielding point of prestressing strands. Two main methods are extension under load (EUL) method and

offset method. In EUL method, the yield strength is determined as the stress occurred when the total strain reaches a specified value of strain. ASTM A416 (ASTM International, 2006) adopts 1% EUL method for seven-wire, uncoated steel strand. In offset method, the yield strength is determined as the intersection of the stress-strain curve and a line which starts at a specified value of strain and lies parallel to the initial linear region of the curve. Eurocode2 uses 0.1% offset method and KCI design code (Korean Concrete Institute, 2012) recommends 0.2% offset method. Figure 3.2 presents these methods applied to the measured stress-strain curves of prestressing strands. It is noteworthy that the three methods give similar yielding points in case of Grade 1860 strand, on the other hand, a large gap occurs among the yielding points by the three methods in case of high-strength strands.

Table 3.1 presents the specifications of KS D 7002 for the mechanical properties of the high strength prestressing strands. Minimum load at 0.2% proof stress means the load corresponding to the yield stress determined by 0.2% offset method. SWPC7BN represents stress-relieved Grade 1,860 strands. The ratio of minimum load at 0.2% proof stress to minimum breaking strength is kept constant as 0.85 for all types of prestressing strands in KS D 7002. On the other hand, ASTM A 416 requires different ratios for each type of prestressing strands: 0.90 for low-relaxation strands and 0.85 for stress-relieved strands. The actual ratios of SWPC7CL and SWPC7DL strands produced in accordance with KS D 7002 also satisfy the requirement of ASTM A 416.

With the increase in tensile strength, yield strength is also elevated but the other mechanical properties remain similar to Grade 1,860 strands. The SWPC7CL and SWPC7DL strands have the same geometric shape, weight, and elastic modulus as Grade 1,860 strands.

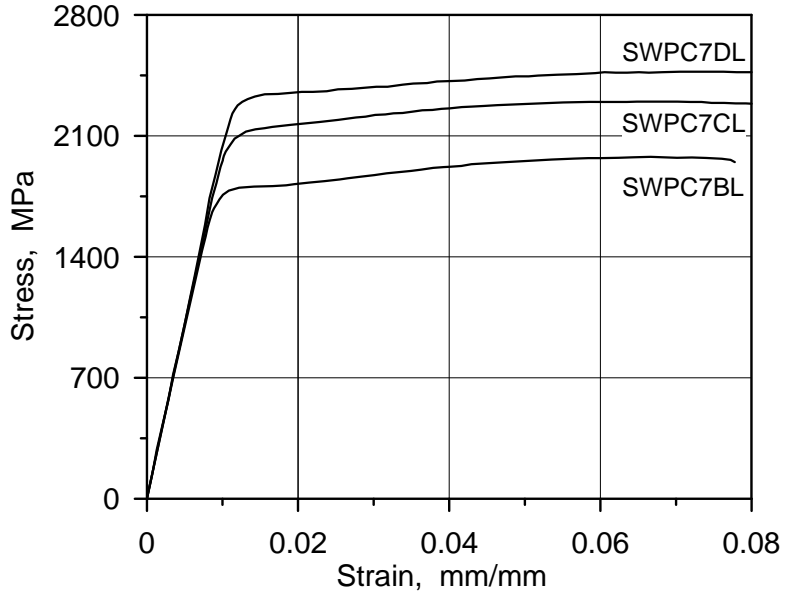


Figure 3.1 Measured stress-strain curves of high strength prestressing strands

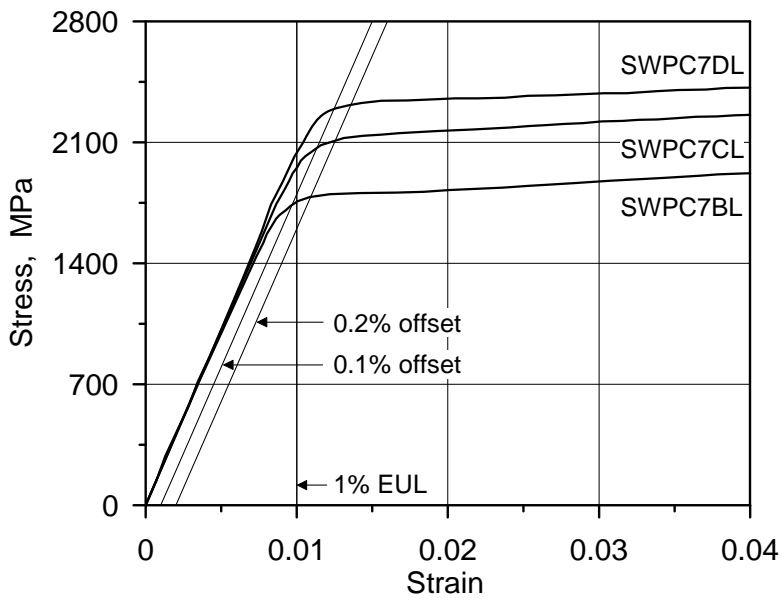


Figure 3.2 Methods of determining yield point of prestressing strand

Table 3.1 Specifications for the mechanical properties of the high strength prestressing strands (KATS, 2011)

Strand designation	Nominal diameter (mm)	Minimum Load at 0.2% proof stress (kN)	Minimum breaking strength (kN)	Minimum Elongation (%)	Maximum Relaxation (%)
SWPC7BN	12.7	156	183	3.5	8.0
	15.2	222	261	3.5	8.0
SWPC7BL	12.7	156	183	3.5	2.5
	15.2	222	261	3.5	2.5
SWPC7CL	12.7	182	214	3.5	2.5
	15.2	255	300	3.5	2.5
SWPC7DL	12.7	202	237	3.5	2.5
	15.2	283	333	3.5	2.5

Table 3.2 and 3.3 summarizes the measured mechanical properties of the SWPC7CL and SWPC7DL strands. They include proportional limit strain ε_{pl} ; elastic modulus E_p ; yield strains ε_{py} and stresses f_{py} determined by 1% EUL, 0.1% offset, and 0.2% offset method; and ultimate strain ε_{pu} and stress f_{pu} . These properties were obtained the data provided by the wire manufacturer. More details of the data process and the analysis procedure can be found in the thesis of Choi (2015).

The same restrictions on total elongation and relaxation loss are imposed on the high-strength strands. The total elongation should be at least 3.5% and the relaxation loss at 1,000 hours after tensioning up to 70% of the minimum breaking strength is required below 2.5% for low-relaxation strands. The tests performed by the strand manufacturer revealed that the total elongation ranged from 6.00% to 9.48% and the relaxation loss was between 0.90% and 1.70% (see Table 3.2 and 3.3).

Table 3.2 Measured mechanical properties of SWPC7CL strand (Choi, 2015)

Strand No.	ε_{pl} (%)	E_p (GPa)	1% EUL	0.1% offset		0.2% offset		f_{pu} (MPa)	ε_{pu} (%)
			f_{py} (MPa)	f_{py} (MPa)	ε_{py} (%)	f_{py} (MPa)	ε_{py} (%)		
1	0.74	195.8	1,895	1.13	2,019	1.25	2,064	2,240	6.65
2	0.73	200.9	1,923	1.11	2,028	1.23	2,073	2,235	8.16
3	0.76	202.6	1,921	1.09	2,002	1.22	2,057	2,235	6.76
4	0.91	198.4	1,939	1.14	2,066	1.26	2,104	2,250	7.70
5	0.90	196.5	1,937	1.15	2,064	1.27	2,098	2,249	6.32
6	0.79	194.0	1,896	1.15	2,037	1.27	2,081	2,253	6.75
7	0.85	201.2	1,949	1.11	2,040	1.23	2,074	2,220	8.04
8	0.71	196.9	1,905	1.12	2,011	1.25	2,060	2,218	6.49
9	0.80	201.7	1,868	1.05	1,923	1.19	2,002	2,202	7.14
10	0.90	204.2	1,984	1.12	2,082	1.24	2,117	2,283	8.20
11	0.82	207.9	1,995	1.10	2,071	1.22	2,114	2,283	8.35
12	0.87	201.1	1,944	1.13	2,066	1.25	2,108	2,281	8.35
13	0.92	200.2	1,947	1.12	2,035	1.24	2,072	2,169	9.48
14	0.81	200.0	1,937	1.11	2,021	1.23	2,062	2,169	9.19
Avg.	0.82	200.1	1,931	1.12	2,033	1.24	2,078	2,235	7.68
Std. dev.	0.07	3.6	34	0.03	40	0.02	30	37	1.01

Table 3.3 Measured mechanical properties of SWPC7DL strand (Choi, 2015)

Strand No.	ε_{pl} (%)	E_p (GPa)	1% EUL	0.1% offset		0.2% offset		f_{pu} (MPa)	ε_{pu} (%)
			f_{py} (MPa)	f_{py} (MPa)	ε_{py} (%)	f_{py} (MPa)	ε_{py} (%)		
1	0.91	198.5	1,971	1.23	2,250	1.35	2,288	2,354	8.10
2	0.82	212.4	2,053	1.13	2,191	1.25	2,241	2,340	8.12
3	0.87	198.4	1,940	1.23	2,233	1.35	2,280	2,416	6.37
4	0.97	209.3	2,064	1.17	2,239	1.29	2,282	2,417	6.16
5	0.94	209.8	2,060	1.16	2,225	1.28	2,275	2,418	6.28
6	1.01	199.6	2,000	1.22	2,227	1.34	2,279	2,415	6.66
7	1.00	202.1	2,010	1.20	2,229	1.33	2,277	2,415	6.66
8	0.90	207.5	2,052	1.17	2,226	1.30	2,277	2,415	6.68
9	0.86	209.4	2,055	1.16	2,221	1.29	2,275	2,415	6.68
10	0.84	214.6	2,076	1.13	2,217	1.26	2,268	2,414	6.72
11	0.84	211.0	2,066	1.15	2,224	1.27	2,265	2,414	6.71
12	0.97	208.3	2,059	1.17	2,231	1.29	2,278	2,415	6.71
13	0.88	207.4	2,037	1.16	2,208	1.29	2,269	2,415	6.82
14	0.93	203.5	2,003	1.19	2,218	1.32	2,273	2,414	6.84
15	0.89	215.2	2,096	1.13	2,220	1.26	2,272	2,417	6.74
16	0.89	214.7	2,094	1.14	2,225	1.26	2,273	2,414	6.64
17	0.89	203.9	2,003	1.18	2,210	1.31	2,265	2,414	6.85
18	0.98	207.4	2,051	1.18	2,229	1.30	2,278	2,416	6.87
19	0.91	200.4	1,975	1.21	2,221	1.34	2,274	2,416	6.85
20	0.95	204.7	2,021	1.19	2,224	1.31	2,271	2,415	6.86
21	0.94	207.8	2,053	1.17	2,230	1.30	2,285	2,433	6.00
22	1.01	202.8	2,024	1.20	2,226	1.32	2,281	2,436	7.70
Avg.	0.92	206.8	2,035	1.18	2,224	1.30	2,274	2,411	6.82
Std. dev.	0.06	5.2	40	0.03	12	0.03	9	22	0.53

One of the most critical issues for prestressing steels is the resistance to stress corrosion. This is because a high level of stress causes internal defects of steel which makes the steel more vulnerable to corrosion. If the steel subjected to a high stress is exposed to a corrosive environment, corrosion can be accelerated and it leads to a brittle failure of the steel. ISO 15630-3 (European Committee for Standardization, 2010) defines various test methods for reinforcements and prestressing steel including stress corrosion test. In the test, steel tendon is immersed in the thiocyanate liquid and tensioned with an initial force. And then, the time elapsed up to failure is measured. Table 3.4 presents the minimum requirements for stress corrosion resistance of prestressing steel. It also shows the test results of SWPC7BL, SWPC7CL and SWPC7DL strands conducted by the wire rod manufacturer in accordance with ISO 15630-3. Table 3.4 proves that the SWPC7CL and SWPC7DL strands have the similar resistance to stress corrosion to the current Grade 1,860 strands (Kim et al., 2014).

Table 3.4 Stress corrosion test of high strength prestressing strands (Kim et al., 2014)

Type of strand	Number of specimen	Minimum lifetime to failure (hour)	Median lifetime to failure (hour)
ISO15630-3 requirement	6	2.0	5.0
SWPC7BL	12	2.9	7.9
SWPC7CL	12	3.3	12.2
SWPC7DL	12	2.7	7.7

4. Experimental Program

4.1 Introduction

This chapter provides detailed descriptions of the experiments performed in this study. Sixty six beams with a rectangular section were fabricated through 10 test series. The purpose of the first 7 series was to investigate the effect of test variables on transfer length of Grade 1,860 strands and the rest of the batches focused on transfer length of Grade 2,400 strands. Before the main experiments to evaluate the effects of the test variables, a preliminary test was conducted to explore a feasibility of ERSGs in measuring transfer length. The results of the preliminary test indicated that ERSGs can give reliable measurements. Based on this conclusion, ERSGs were adopted in the main experiments. All the experiments were conducted in fields.

The descriptions given in this chapter include test variables, properties of materials used in the experiments, fabrication of test specimens, instrumentation and test procedure. Section 4.2 provides detailed descriptions of transfer length test for Grade 1,860 strands and Section 4.3 deals with transfer length test for Grade 2,400 strands in detail.

4.2 Transfer Length Test for Grade 1,860 Strands

4.2.1 Test Variables

In this experimental work, the effects of 9 test variables on transfer length of Grade 1,860 strands were assessed: initial prestress, strand diameter, cover depth, cross section size, strand spacing, curing condition, debonding, reinforcement spacing, and prestress release method. Some of the test variables have been traditionally treated as major factors but the others have not. The major factors were reassessed based on behavior of the strand and the effects of new factors were examined.

Initial prestress and strand diameter are fundamental factors to influence transfer length. These variables were reevaluated based on strand strain distribution within the transfer zone. The strands with a diameter of 12.7 mm and 15.2 mm were tensioned up to two different levels. After anchorage seating loss, the residual stress in the strands were approximately 50% or 70% of their tensile strength.

In aspect of bond mechanics, cover depth plays a role to confine the strand. To fully develop the bond capacity, concrete cover should be preserved from splitting cracks. Concrete cover depths from the closet concrete face to the centroid of the strand were considered in a range of 30 mm to 60 mm, which includes the minimum cover depth of 40 mm recommended by the ACI318 code provision.

A strand located concentrically in a rectangular cross section is surrounded by the same cover depth towards the four sides of the cross section. Comparison between the test results of cover depth and cross section size will enhance the understanding of the concrete confining action. The cross section sizes were determined in order that the specimens for cross section size have the same cover depths as the

specimens for cover depth.

Strand spacing is also related to the concrete confining action. The stress state of the concrete between two strands is influenced by both strands. Center-to-center spacings ranged from 45 mm to 90 mm were considered, which includes the reduced strand spacing of 50 mm recommended by the ACI318 code provision.

Accelerated curing methods are commonly used for quality control and to shortening construction periods at large construction sites or fabrication yards. Effects of curing methods on transfer length inclusive of high temperature steam curing and conventional ambient curing methods were taken into account.

Debonding technique is used to reduce excessive stresses in the concrete due to prestressing in practice and to minimize stress disturbance in experiments. A few experimental researches investigated the effect of debonding. In this experimental program, PVC sleeves with a length of 80 mm were provided at both ends of most of the specimens.

In concrete structures, prestressing strands are arranged among several layers of reinforcing bars. Several investigations have been conducted on the effect of the strand spacing and the transverse stirrups but did not on the longitudinal reinforcing bars. Center-to-center spacings of reinforcing steel bars ranged from 60 mm to 90 mm.

Except for special cases, sudden release methods that involve the cutting of strands are typical at construction sites, resulting in significant dynamic impact on structural members. The effects of sudden release methods on transfer lengths were investigated through comparison of transfer lengths at cut and dead ends. For all specimens in this experiment, prestress was suddenly released at one end of the specimens.

As explained above, the values for the test variables were selected to be in accordance with standard industrial practice. The test variables and their values considered in this study are summarized in Table 4.1. The designation system of the test specimens are presented in Figure 4.1. For example, N45S150-B70F-C60-1 means that the design compressive strength of the concrete is 45 MPa; the specimen is steam-cured; the cross section is 150 by 150 mm; a 15.2 mm Grade 1,860 strand was prestressed and the residual prestress after seating loss was 70% of its tension strength; the strand was fully bonded; the minimum distance from the centroid of the strand to the closest concrete surface was 60 mm; and the specimen was the first specimen among the identical specimens.

Table 4.2 lists test variables considered in each test series. Test series 1 is a preliminary test to investigate the applicability of ERSGs. DEMEC gauges, ERSGs for concrete, ERSGs for strand were attached together on the specimens. The readings of the instrumentations will be discussed in Chapter 5.

Table 4.3 through 4.7 summarizes the information on the test variables and conditions of each individual specimen. Geometric configuration including cross sectional dimensions and positions of strand and reinforcing bars are illustrated in Figure 4.2.

Table 4.1 Test variables for Grade 1,860 strands

Test variables		Value	Designation
Concrete	Design compressive strength (MPa)	45	N45
		35	N35
	Curing condition	Steam curing	S
		Air curing	A
Section	Cross section size (mm×mm)	60×60	60
		90×90	90
		120×120	120
		150×150	150
		200×200	200
	Cover depth (mm)	30	C30
45		C45	
60		C60	
Strand	Nominal tensile strength (MPa)	1,860	B
	Nominal diameter (mm)	15.2	–
		12.7	12
	Center-to-center spacing (mm)	45	S45
		60	S60
		75	S75
90		S90	
Initial prestress (% of f_{pu})	70	70	
	50	50	
Debonding	Full-bonded	F	
	Debonded	–	
Reinforcement	Center-to-center spacing (mm)	60	R60
		75	R75
		90	R90

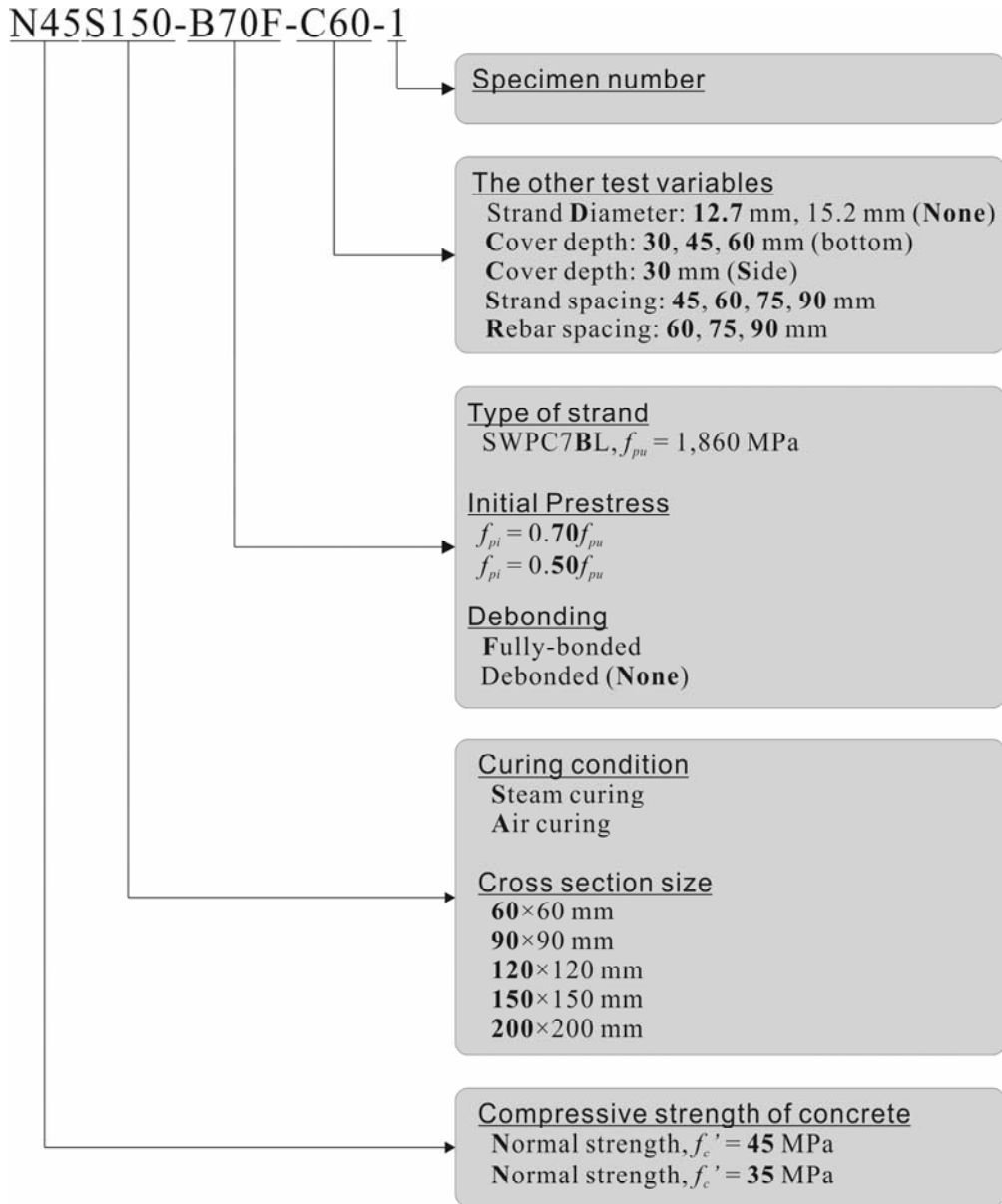


Figure 4.1 Specimen designation for transfer length test of Grade 1,860 strands

Table 4.2 Test variables considered in each test series

Test series	Test variables
1	preliminary test
2	center-to-center spacing of reinforcements
3	center-to-center spacing of prestressing strands
4	cover depth and cross section size
5	cover depth, cross section size, initial prestress, diameter of prestressing strand, and debonding
6	cover depth, cross section size, initial prestress, and diameter of prestressing strand
7	curing condition

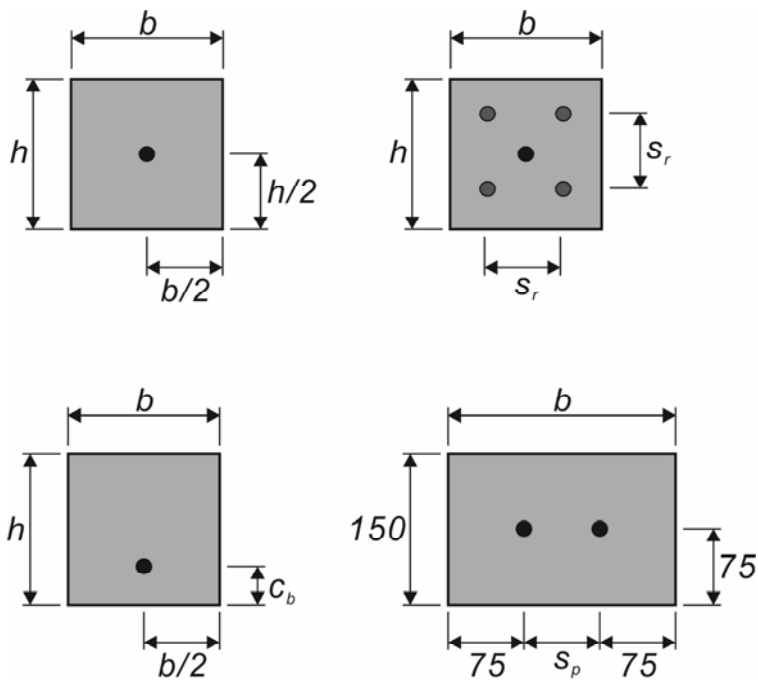


Figure 4.2 Illustrative cross sections of test specimens with Grade 1,860 strands

Table 4.3 Specimens of test series 1~3

No.	Specimen ID	f'_c (MPa)	f_{pu} (MPa)	f_{pj}/f_{pu}	b (mm)	h (mm)	d_b (mm)	c_b (mm)	s_p (mm)	s_r (mm)	l_{db} (mm)	curing
1-1	N45S150-B70F-1	45	1,860	0.75	150	150	15.2	–	–	–	–	steam
1-2	N45S150-B70F-2	45	1,860	0.75	150	150	15.2	–	–	–	–	steam
1-3	N45S150-B70F-3	45	1,860	0.75	150	150	15.2	–	–	–	–	steam
2-1	N45S150-B70F-4	45	1,860	0.75	150	150	15.2	–	–	–	–	steam
2-2	N45S150-B70F-R60	45	1,860	0.75	150	150	15.2	–	–	60	–	steam
2-3	N45S150-B70F-R75	45	1,860	0.75	150	150	15.2	–	–	75	–	steam
2-4	N45S150-B70F-R90	45	1,860	0.75	150	150	15.2	–	–	90	–	steam
3-1	N45S150-B70F-S45	45	1,860	0.75	195	150	15.2	–	45	–	–	steam
3-2	N45S150-B70F-S60	45	1,860	0.75	210	150	15.2	–	60	–	–	steam
3-3	N45S150-B70F-S75	45	1,860	0.75	225	150	15.2	–	75	–	–	steam
3-4	N45S150-B70F-S90	45	1,860	0.75	240	150	15.2	–	90	–	–	steam

Table 4.4 Specimens of test series 4

No.	Specimen ID	f'_c (MPa)	f_{pu} (MPa)	f_{pj}/f_{pu}	b (mm)	h (mm)	d_b (mm)	c_b (mm)	s_p (mm)	s_r (mm)	l_{db} (mm)	curing
4-1	N45S150-B70F-C30	45	1,860	0.75	150	150	15.2	30	–	–	–	steam
4-2	N45S150-B70F-C30S	45	1,860	0.75	150	150	15.2	30	–	–	–	steam
4-3	N45S150-B70F-C45	45	1,860	0.75	150	150	15.2	45	–	–	–	steam
4-4	N45S150-B70F-C60	45	1,860	0.75	150	150	15.2	60	–	–	–	steam
4-5	N45S120-B70F	45	1,860	0.75	120	120	15.2	–	–	–	–	steam
4-6	N45S90-B70F	45	1,860	0.75	90	90	15.2	–	–	–	–	steam
4-7	N45S60-B70F	45	1,860	0.75	60	60	15.2	–	–	–	–	steam

Table 4.5 Specimens of test series 5

No.	Specimen ID	f'_c (MPa)	f_{pu} (MPa)	f_{pj}/f_{pu}	b (mm)	h (mm)	d_b (mm)	c_b (mm)	s_p (mm)	s_r (mm)	l_{db} (mm)	curing
5-1	N45S150-B70F-5	45	1,860	0.75	150	150	15.2	–	–	–	–	steam
5-2	N45S200-B70-1	45	1,860	0.75	200	200	15.2	–	–	–	80	steam
5-3	N45S150-B70-1	45	1,860	0.75	150	150	15.2	–	–	–	80	steam
5-4	N45S120-B70-1	45	1,860	0.75	120	120	15.2	–	–	–	80	steam
5-5	N45S90-B70-1	45	1,860	0.75	90	90	15.2	–	–	–	80	steam
5-6	N45S150-B70-C60-1	45	1,860	0.75	150	150	15.2	60	–	–	80	steam
5-7	N45S150-B70-C45-1	45	1,860	0.75	150	150	15.2	45	–	–	80	steam
5-8	N45S150-B50-1	45	1,860	0.54	150	150	15.2	–	–	–	80	steam
5-9	N45S120-B50-1	45	1,860	0.54	120	120	15.2	–	–	–	80	steam
5-10	N45S90-B50-1	45	1,860	0.54	90	90	15.2	–	–	–	80	steam
5-11	N45S150-B70-D12-1	45	1,860	0.75	150	150	12.7	–	–	–	80	steam
5-12	N45S150-B50-D12	45	1,860	0.54	150	150	12.7	–	–	–	80	steam

Table 4.6 Specimens of test series 6

No.	Specimen ID	f'_c (MPa)	f_{pu} (MPa)	f_{pj}/f_{pu}	b (mm)	h (mm)	d_b (mm)	c_b (mm)	s_p (mm)	s_r (mm)	l_{db} (mm)	curing
6-1	N45S200-B70-2	45	1,860	0.75	200	200	15.2	–	–	–	80	steam
6-2	N45S150-B70-2	45	1,860	0.75	150	150	15.2	–	–	–	80	steam
6-3	N45S120-B70-2	45	1,860	0.75	120	120	15.2	–	–	–	80	steam
6-4	N45S90-B70-2	45	1,860	0.75	90	90	15.2	–	–	–	80	steam
6-5	N45S150-B70-C60-2	45	1,860	0.75	150	150	15.2	60	–	–	80	steam
6-6	N45S150-B70-C45-2	45	1,860	0.75	150	150	15.2	45	–	–	80	steam
6-7	N45S150-B50-2	45	1,860	0.54	150	150	15.2	–	–	–	80	steam
6-8	N45S120-B50-2	45	1,860	0.54	120	120	15.2	–	–	–	80	steam
6-9	N45S90-B50-2	45	1,860	0.54	90	90	15.2	–	–	–	80	steam
6-10	N45S150-B70-D12-2	45	1,860	0.54	150	150	12.7	–	–	–	80	steam
6-11	N45S90-B70-D12	45	1,860	0.75	90	90	12.7	–	–	–	80	steam

Table 4.7 Specimens of test series 7

No.	Specimen ID	f'_c (MPa)	f_{pu} (MPa)	f_{pj}/f_{pu}	b (mm)	h (mm)	d_b (mm)	c_b (mm)	s_p (mm)	s_r (mm)	l_{db} (mm)	curing
7-1	N45A150-B70	45	1,860	0.75	150	150	15.2	–	–	–	80	air
7-2	N35A150-B70	35	1,860	0.75	150	150	15.2	–	–	–	80	air
7-3	N35A120-B70	35	1,860	0.75	120	120	15.2	–	–	–	80	air
7-4	N35A150-B50	35	1,860	0.54	150	150	15.2	–	–	–	80	air
7-5	N35A150-B70-D12	35	1,860	0.75	150	150	12.7	–	–	–	80	air

4.2.2 Material Properties

4.2.2.1 Concrete

Three types of concrete mix proportions were used for the fabrication of the test specimens. Detailed concrete mix proportion is provided in Table 4.8. Two of three were prepared for concrete with design compressive strength of 45 MPa. The only difference between the two mix proportions was slag replacement ratio: 50% in the test series 1~4 and 0% in the test series 5~7. Water-to-binder ratio was kept as being 32%. The last type of the concrete mix proportions was used for concrete with design compressive strength of 35 MPa. These mix proportions were originally designed for 50 m concrete box girders and piers of the Incheon bridge. The concrete was mixed in the concrete batching plant located inside the Incheon bridge construction site and transported by a remicon truck. For all types of the concrete mix proportions, typical Type I Portland cement was used and the maximum aggregate size was 20 mm. Target slump was 180 mm with a range of ± 25 mm. For fluidity of concrete, high-range water-reducer (HRWR) was used.

Table 4.8 Concrete mix proportion for tests of Grade 1,860 strands

Test series	f'_c (MPa)	Unit weight (kg/m ³)					
		Water	Cement	Slag	Sand	Gravel	HRWR
1~4	45	160	250	250	679	994	6.5
5~7	45	160	500	–	679	994	6.5
7	35	164	216	216	763	964	5.2

More than fifteen 150×300 mm cylinders were fabricated in every test series for compression strength test at time of prestress and ages of 7, 14, and 28 days. The

same curing method as used for the test specimens of the relevant test series was applied to the cylinders. Table 4.9 summarizes the average concrete compressive strengths and elastic moduli measured at time of transfer and after 28 days. In all test series, concrete successfully gained or closely approached its design compressive strength. Complete results of compression strength test can be found in Appendix A.

Table 4.9 Average compressive strength and elastic moduli of concrete at transfer and after 28 days (test series 1~7)

Test series	f'_c (MPa)	At transfer			After 28 days		
		t_i (day)	f'_{ci} (MPa)	E_{ci} (MPa)	t (day)	f_{cu} (MPa)	E_c (MPa)
1	45	2	32.8	27,077	30	53.6	29,351
2	45	3	32.9	24,793	30	44.7	31,736
3	45	2	32.3	23,377	30	50.2	27,333
4	45	2	38.8	26,134	33	47.1	26,735
5	45	2	36.5	25,977	30	54.6	29,332
6	45	2	29.0	23,674	28	42.3	25,813
7	45	7	34.2	24,200	31	47.5	28,266
	35	13	30.7	21,255	31	36.0	26,902

4.2.2.2 Prestressing Strand and Reinforcing Steel Bars

In this experimental work, uniaxial tension test of prestressing strand was not performed. Instead, the mechanical properties were obtained from the mill test certificate issued by the strand manufacturer. It includes the test results of samples of the prestressing strands used in this experiment. Table 4.10 summarizes the mechanical properties of Grade 1,860 strands with the nominal diameter of 12.7 mm

and 15.2 mm used in this experiment.

Table 4.10 Mechanical properties of Grade 1,860 strand

Mechanical properties	Nominal diameter of strand (mm)	
	12.7	15.2
Breaking strength (kN)	191	267
Tensile strength (MPa)*	1,993	1,936
Load at 0.2% proof stress (kN)	170	248
Yield strength (MPa)*	1,775	1,798
Elastic modulus (GPa)	200	200
Elongation (%)	6.9	3.7
Diameter (mm)	12.6	15.13
Difference between center wire diameter and diameter of any outer wire (mm)	0.14	0.19
Diameter of center wire (mm)*	4.29	5.17
Diameter of outer wire (mm)*	4.15	4.98
Area of strand (mm ²)*	95.8	137.9
Unit weight (kg/km)	779	1,106
Pitch length (mm)	176.4	243.6
Lay angle (deg)*	8.55	7.46

* means the values calculated from the measured properties

Some properties in Table 4.10 were calculated using other measured ones. Diameters of center wire and outer wire were obtained from the diameter of strand and the difference between center wire diameter and diameter of any outer wire. Diameter of each wire gave the respective circular area. The circular area of the center wire and 6 outer wires were summed to obtain the area of strand. The tensile strength and the yield strength were calculated by dividing the breaking strength and

the load at 0.2% proof stress by the area of strand. The lay angle between the helix and the longitudinal axis of the strand can be found by using the fact that helical outer wires wrapping the center wire complete a full rotation with respect to the longitudinal axis through traveling the pitch length. Elastic modulus was set as being 200 GPa.

Reinforcing steel bars arranged in the specimens of the test series 2 had the diameter of 16 mm and the specified yield strength of 400 MPa.

4.2.3 Fabrication of Test Specimens

All specimens had a length of 3,000 mm which is long enough to imply full transfer length at both cut and dead ends. Information on cross section of each specimen is given in Table 4.3~7. During the experiment, the strands were kept free of water and rust, and no additional surface treatments were applied.

Two sets of steel prestressing beds that were 5.2 m in length, 2.7 m in width and 1.5 m in height from ground were prepared. Perforated steel plates were fixed at both ends of each bed to allow strands to pass through and pipelines for steam curing were installed at the long lateral side of each bed. Drawings and pictures of the prestressing beds are presented in figure 4.3 and 4.4. Surface-coated wood forms were used for concrete pouring and particular attention was paid to the flatness of bottom surface.

For the ease and security of steel gauge attachment, all gauges were first bonded on strand surfaces and the strands were then placed through the perforations at the ends of the prestressing beds. ERSGs were attached to the exposed portions of strands as well as the parts of the strands to be embedded in concrete for

comparisons with load cell readings. Load cells were installed only at the cut ends. Prestressing force corresponding to more than 75% of the strand tensile strength was applied by hydraulic jacks, which allowed the initial prestress of $0.70f_{pu}$ after anchorage seating loss.

Thermocouples were installed in the prestressing beds and embedded in the specimens to measure temperatures outside and inside the specimens. Absolute sheltering of the entire prestressing beds followed concrete placement, and high temperature steam was applied for about 17 hours afterwards. During the time of curing completion, cylinders were tested to attain the point when specimens had achieved 70% of design compressive strength for termination of the curing process. After that, the forms were disassembled; and DEMEC and concrete gauges were attached to the concrete surface. To measure strand end slip, LVDTs were installed at both ends of each specimen with jigs that were specially fabricated for protection against impacts of sudden prestress release. The process of prestress release was performed at one end after the completion of curing by sudden cutting using a disk cutter.

The whole procedure of the specimen fabrication is pictured in figure 4.5 and the test set-up is illustrated in figure 4.6.

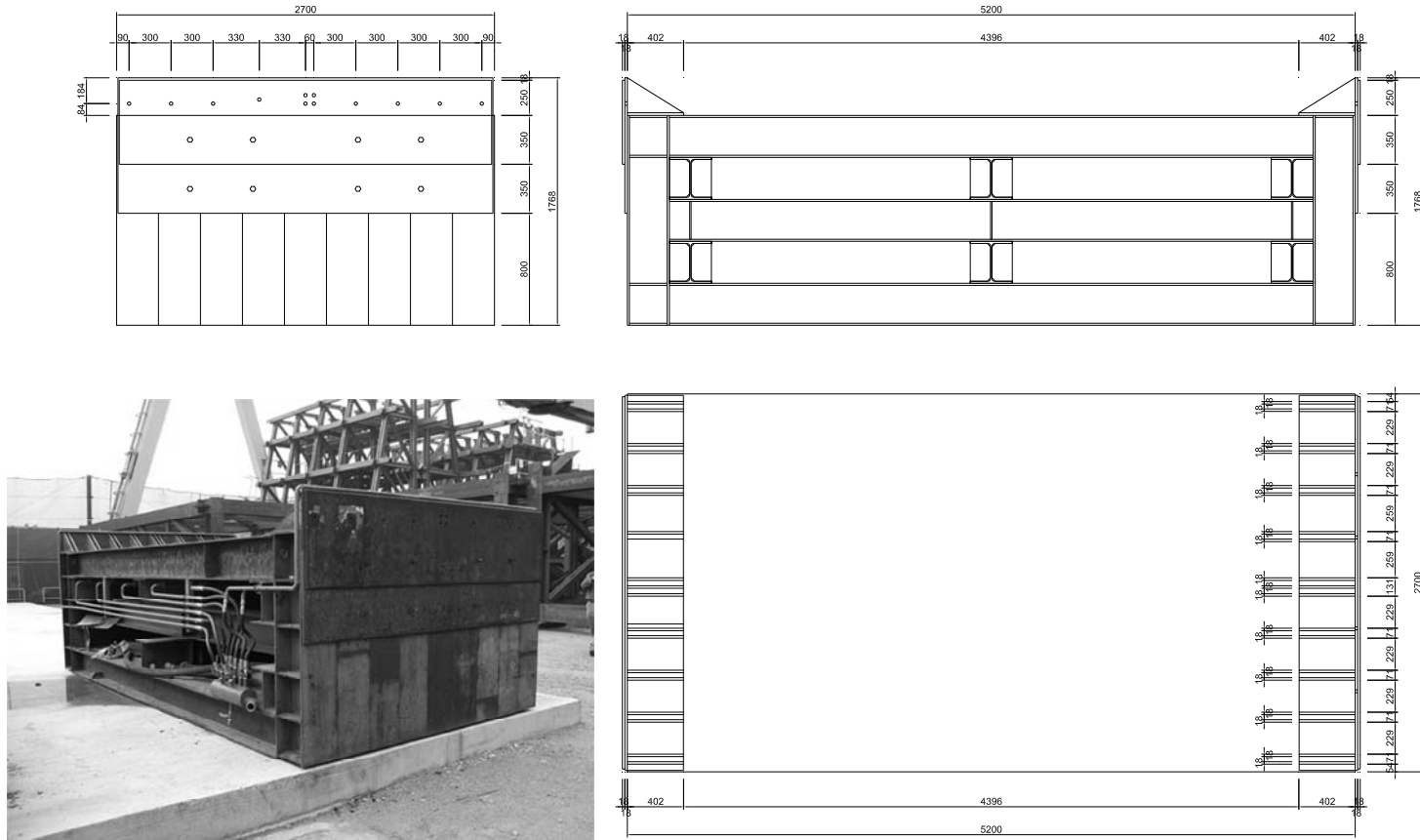


Figure 4.3 Drawings and picture of prestressing bed 1

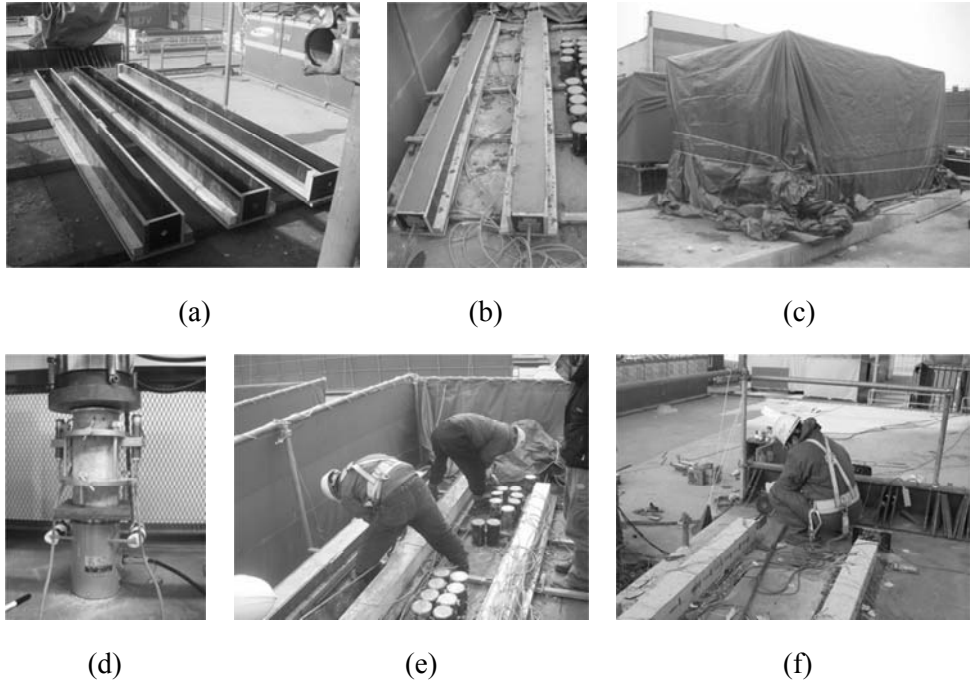


Figure 4.5 Procedure of specimen fabrication: (a) formwork; (b) concrete placement; (c) steam curing; (d) compressive strength test; (e) form removal; and (f) prestress release by disk cutting

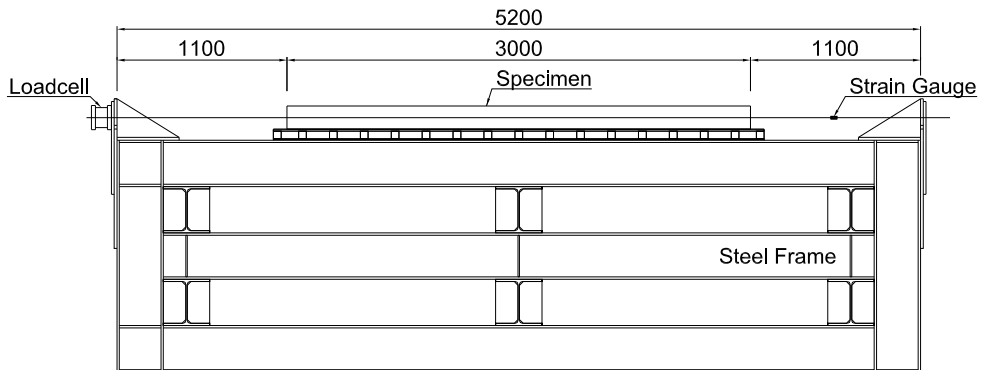


Figure 4.6 Set-up of transfer length test (Grade 1,860 strand)

4.2.4 Instrumentation

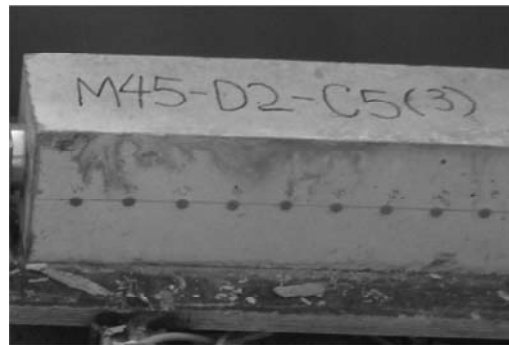
For all gauge types, two gauges were attached at the same location each at opposite face of a specimen or a strand; and measurements of the two were averaged. The data acquisition system collected data from the instrumentations every 10 seconds before and after prestress release.

4.2.4.1 DEMEC gauge

Pin-punched disks for DEMEC readings were attached to both the lateral concrete faces of the specimens of the test series 1, along the length, parallel to the strand. The gauge used for experiments had a precision of ± 20 microstrain and a resolution of 7 microstrain. DEMEC gauge may not yield the same results when operated by different operators, so two operators repeated the measurements for the same location at least once and then averaged them to reduce measurement error. The reference gauge length was 150 mm but overlapped readings were taken every 50 mm for better accuracy.



(a)



(b)

Figure 4.7 DEMEC gauge: (a) digital dial gauge; and (b) disks

4.2.4.2 ERSGs for strand and concrete

Because a prestressing strand consists of seven twisted wires, each wire is twisted at a unique angle at a section relative to the longitudinal direction and different wires may yield different deformations. To adjust the effect of this configuration, as seen in figure 4.8, deviated angles were reflected in data treatment and two gauges each having a gauge length of 5 mm were attached to arbitrarily selected wires at each longitudinal location in such a way that two helical wires were un-gauged on both sides of a gauged helical wire.

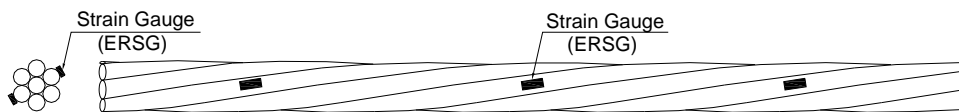


Figure 4.8 Strain gauge attachments on helical wires of strand

In order to protect the gauge from damage and moisture during concrete placement, the gauge protection procedure consisted of two steps. First step was to apply a liquid coating material that consists of xylene and polyurethane over the attached gauge and to let it dry for about 20 minutes. After that, 1 mm thick insulation tape was wrapped over the gauge area. A lot of effort was made to reduce the wrapped area and to have the helical shape of seven-wire strand appeared over the tape.

The similar procedure was applied for ERSGs attached on concrete surface. The gauge length of ERSG was 5 mm for strand and 60 mm for concrete, respectively. ERSGs for strand and concrete s are pictured in figure 4.9.

The locations of ERSGs' placement for all test series are illustrated in figure 4.10

to 4.13. In order to capture the variation in strain profile for identifying the end of transfer zone, the initial location of ERSGs was determined based on the estimations from the empirical equations and later modified in several times to obtain better measurements for the subsequent test. For test series 1, ERSGs and DEMEC gauges were arranged in three patterns (see figure 4.10). The specimen N45S150-B70F-1 had the same arrangement of ERSG for concrete and strand. ERSGs for concrete and DEMEC gauges were attached together on the longitudinal line parallel to the centroid of the strand. The minimum spacing of the gauges was 150 mm.

For the specimen N45S150-B70F-2, half the number of ERSGs was provided for the strand and thus the spacing of the ERSGs for strand was doubled. The reduced number of the ERSGs was intended to investigate the effect of the gauge installation on transfer bond. The arrangements of ERSGs for concrete and DEMEC gauges were identical to that of the specimen N45S150-B70F-1.

On the surface of the specimen N45S150-B70F-3, only DEMEC gauges were attached with the spacing of 50 mm, which is the common practice in transfer length tests. ERSGs were installed on the strand at the center of the specimen.

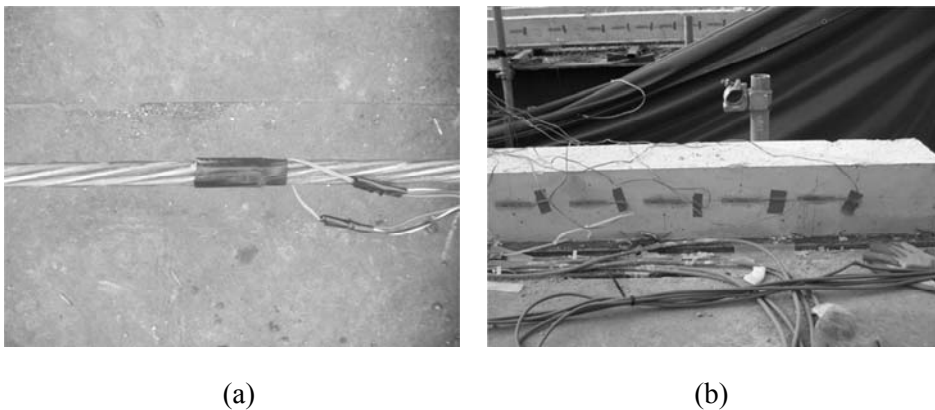
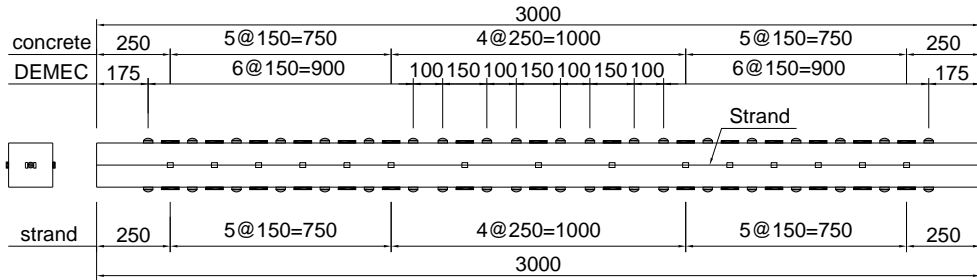
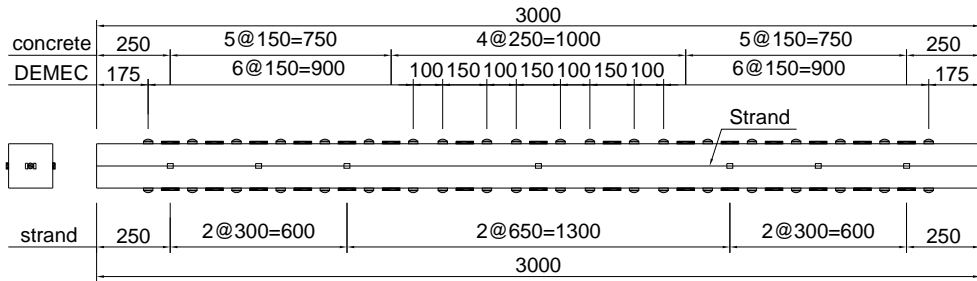


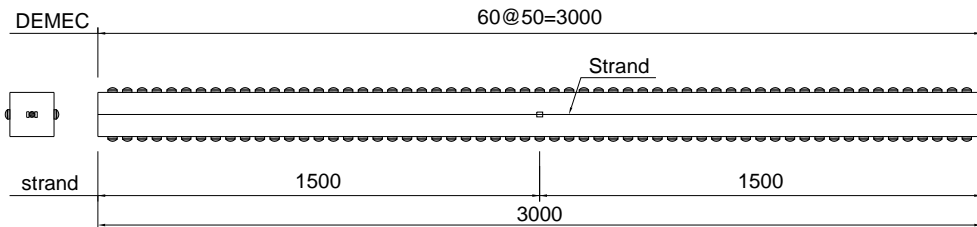
Figure 4.9 Instrumentation: (a) ERSG for strand; and (b) ERSG for concrete



(a)



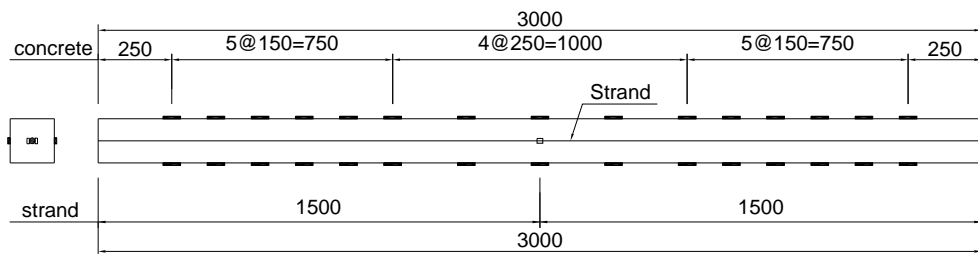
(b)



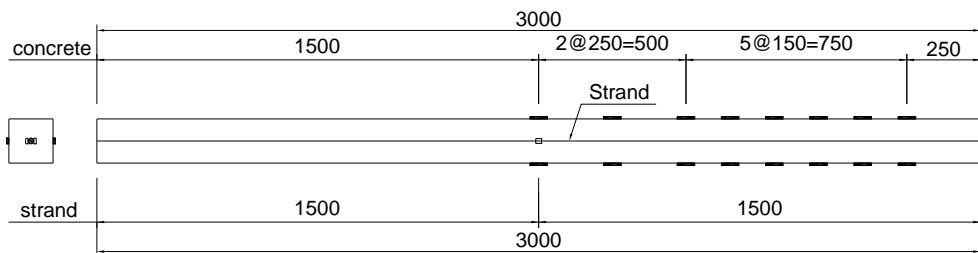
(c)

Figure 4.10 Gauge arrangements of the specimens of the test series 1: (a) N45S150-B70F-1; (b) N45S150-B70F-2; and (c) N45S150-B70F-3
(ERSGs for concrete \blacksquare ; ERSGs for strands \square ; and DEMEC points \blacksquare)

After the test series 1, DEMEC gauges were not used for the strain measurement any longer. From the test series 2 to 4, no ERSGs were placed on the surface of the strand embedded in concrete, except at the center of the specimen. In addition, the full arrangement of ERSGs for concrete spanning the entire length of test specimens was provided for only one or two specimens in each test series. For the rest, ERSGs for concrete were installed on half part of the specimens toward cut end. The half gauge arrangement was because of the limited capacity of the data acquisition system. However, the gauges were fully arranged for the specimens of the test series 5 ~ 10. Figure 4.11 shows the full arrangement and the half one of the test series 2.



(a)

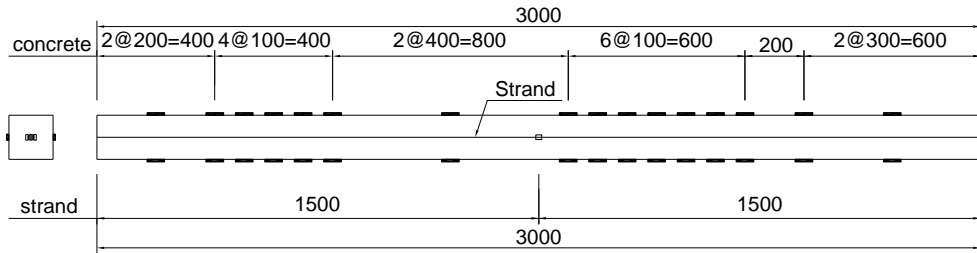


(b)

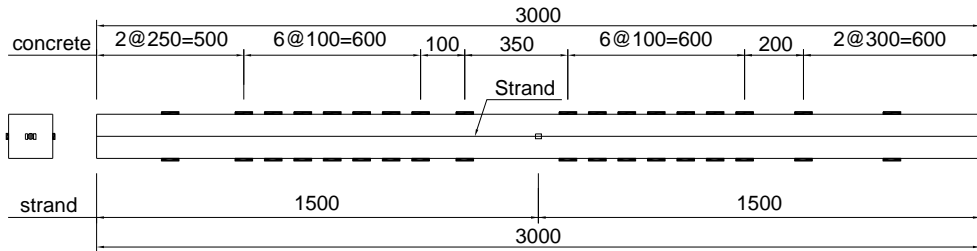
Figure 4.11 Gauge arrangements of the specimens of the test series 2:

(a) N45S150-B70F-4 and N45S150-B70F-R60; and (b) the rest of the specimens (ERSGs for concrete —; and ERSGs for strands □)

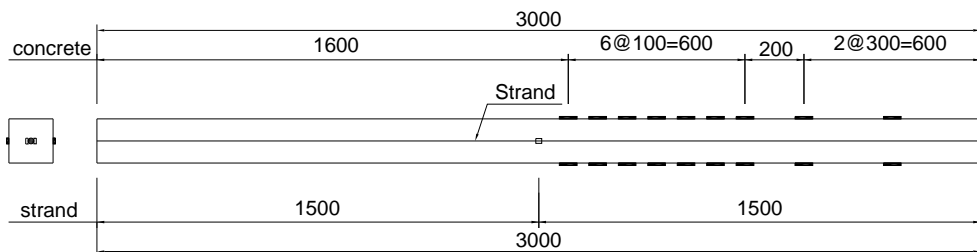
Figure 4.12 presents the gauge locations of the specimen N45S150-B70F-S45 in the test series 3 and the specimen N45S150-B70F-C30 and N45S60-B70F in the test series 4. A typical pattern is also illustrated in Figure 4.12 (c) for the remaining specimens of the test series 3 and 4.



(a)



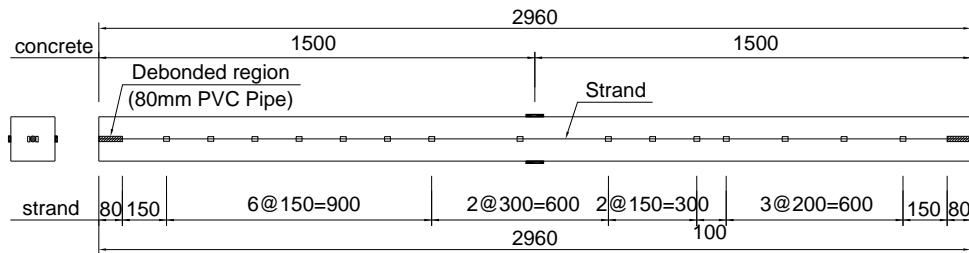
(b)



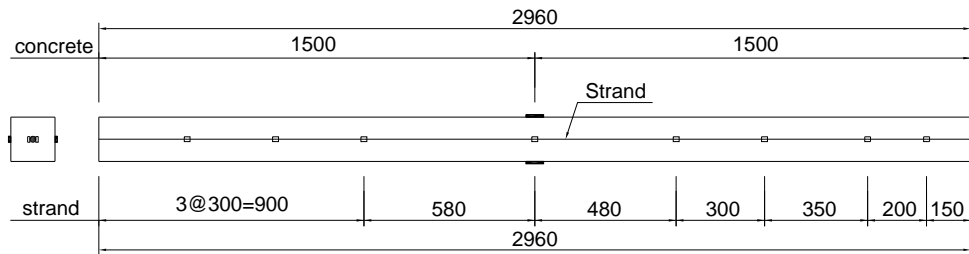
(c)

Figure 4.12 Gauge arrangements of the specimens of the test series 3 and 4: (a) N45S150-B70F-S45; (b) N45S150-B70F-C30 and N45S60-B70F; and (c) the rest of the specimens (ERSGs for concrete \blacksquare ; and ERSGs for strands \square)

For the test series 5 to 7, ERSGs for strand were mainly used to measure transfer length. ERSGs for concrete were attached only at the center of the specimen. The typical gauge arrangement is presented in figure 4.13 (a). Only one exception was made for the specimen N45S150-B70F-5, which had half the number of ERSGs for strand (see figure 4.13(b)).



(a)



(b)

Figure 4.13 Gauge arrangements of the specimens of the test series 5, 6 and 7:

(a) typical pattern; and (b) N45S150-B70F-5

(ERSGs for concrete \blacksquare ; and ERSGs for strands \square)

4.2.4.3 LVDTs for end slip and Load cells

LVDTs were attached to the end faces of the concrete for slip measurement. However, the jig could not protect LVDTs from severe impacts when sudden prestress release was applied. Therefore rare cases of slip measurement by LVDT were successful. Load cells of 200 kN capacity were used to measure the prestressing forces and their data were recorded along with data from other gauges in the data logger. The loadcell and LVDT mounted on the jig are presented in figure 4.14.

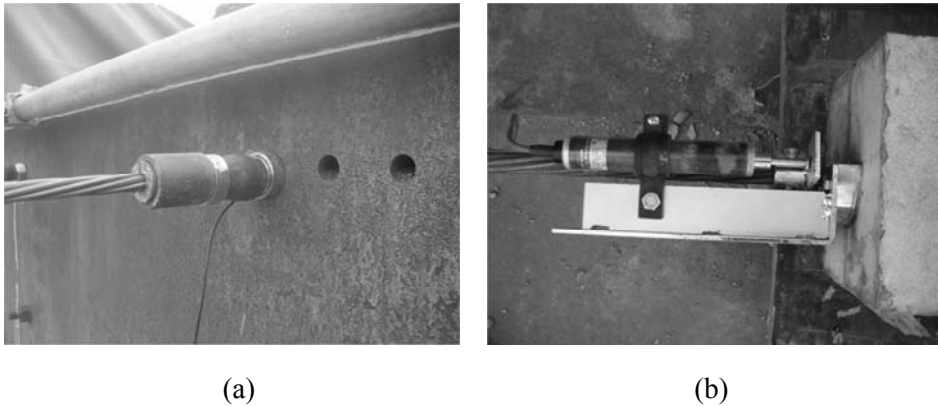


Figure 4.14 Instrumentation of transfer length test for Grade 1,860 strands:

(a) Loadcell; and (b) LVDT for end slip of strand

4.3 Transfer Length Test for Grade 2,400 Strands

4.3.1 Test Variables

For transfer length test of Grade 2,400 strand, the primary concern was whether the current code provisions can provide a sufficient concrete confinement for high strength strand. To evaluate capacity of concrete confinement, concrete compressive strength at transfer, cover depth, and strand spacing were considered as the main test variables. Design concrete compressive strength was 40 MPa and 70 MPa, which will be denoted by normal strength concrete and high strength concrete, respectively, hereafter. When concrete gained approximately 70% of the design compressive strength, prestress was released.

Concrete cover depths from the closet concrete face to the centroid of the strand were considered in a range of 30 mm to 50 mm for high strength concrete and 40 mm to 60 mm for high strength concrete, which includes the minimum cover depth of 40 mm recommended by the ACI318 code provision. Shallower cover depths were examined for high strength concrete because higher concrete compressive strength enhances the capacity of concrete confinement.

Center-to-center strand spacings ranged from 40 mm to 60 mm for high strength concrete and 50 mm to 70 mm for normal strength concrete, which includes the reduced strand spacing of 50 mm recommended by the ACI318 code provision.

The specimens with normal strength concrete were fabricated in the test series 8 and 9. High strength concrete was used for the specimens of the test series 10. For comparison, one specimen with Grade 1,860 strand was fabricated in each test series. Prestress was suddenly released for all specimens.

The transfer length specimens are designated in the same manner as the

specimens with Grade 1,860 strand (see Figure 4.16).

Table 4.12 through 4.14 summarizes the information on the test variables and conditions of each individual specimen. Geometric configuration including cross sectional dimensions and positions of strand and reinforcing bars are illustrated in Figure 4.15.

Table 4.11 Test variables for Grade 2,400 strands

Test variables		Value	Designation	
Concrete	Design compressive strength (MPa)	40	N40	
		70	H70	
	Curing condition	Air curing	A	
Section	Cross section size (mm×mm)	200×200	200	
		Cover depth (mm)	30	C30
			40	C40
			50	C50
60	C60			
Strand	Nominal tensile strength (MPa)	1,860	B	
		2,400	D	
	Nominal diameter (mm)	15.2	–	
	Center-to-center spacing (mm)	40	S40	
		50	S50	
		60	S60	
70		S70		
Initial prestress (% of f_{pu})	70	70		
Debonding	Debonded	–		

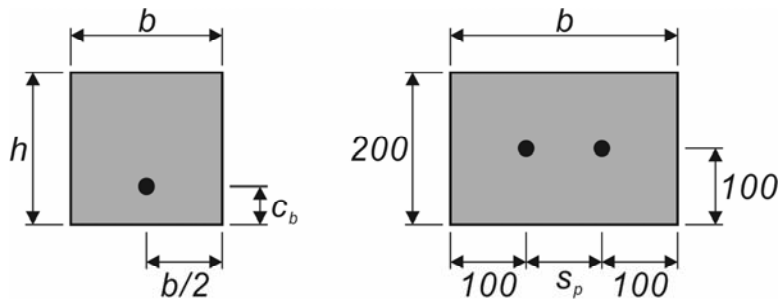


Figure 4.15 Illustrative cross sections of test specimens with Grade 2,400 strands

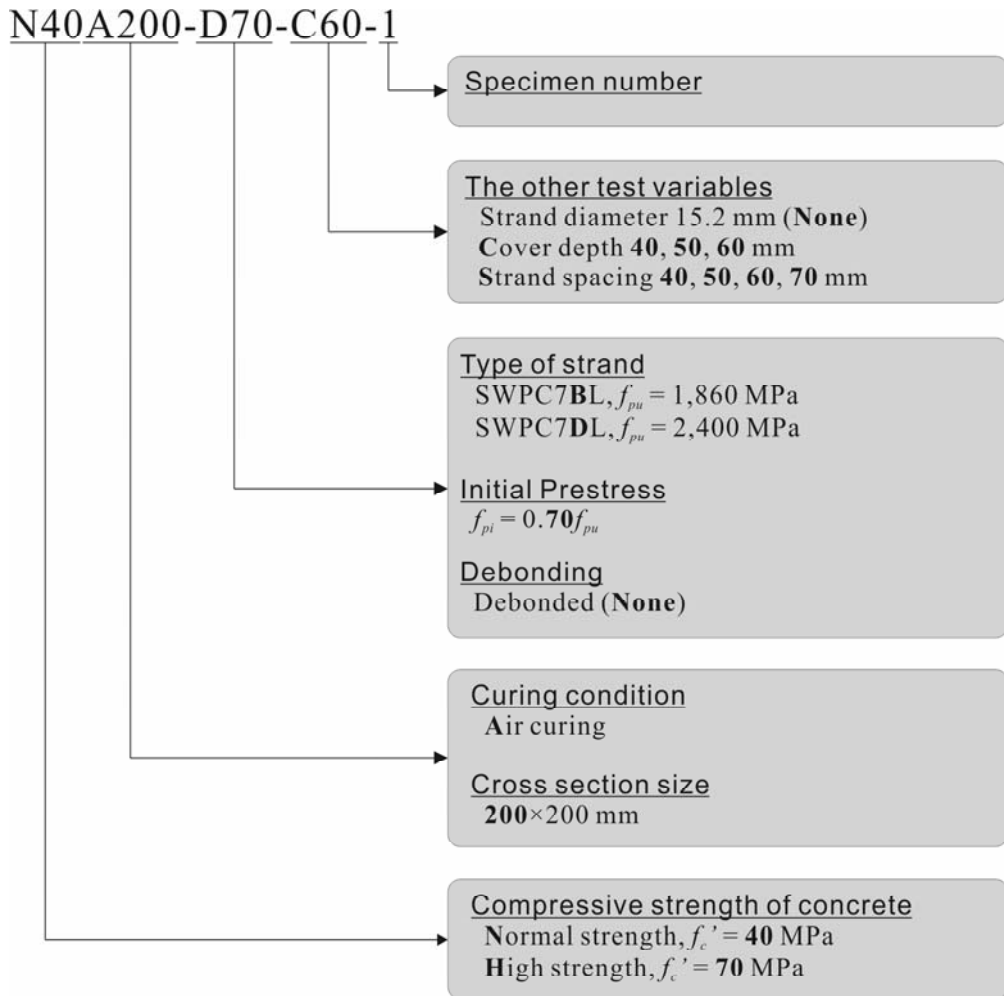


Figure 4.16 Specimen designation for transfer length test of Grade 2,400 strands

Table 4.12 Specimens of test series 8

No.	Specimen ID	f'_c (MPa)	f_{pu} (MPa)	f_{pj}/f_{pu}	b (mm)	h (mm)	d_b (mm)	c_b (mm)	s_p (mm)	s_r (mm)	l_{db} (mm)	curing
8-1	N40A200-D70-C40-1	40	2,400	0.75	200	200	15.2	40	–	–	100	air
8-2	N40A200-D70-C50-1	40	2,400	0.75	200	200	15.2	50	–	–	100	air
8-3	N40A200-D70-C60-1	40	2,400	0.75	200	200	15.2	60	–	–	100	air
8-4	N40A200-B70-C40-1	40	1,860	0.75	200	200	15.2	40	–	–	100	air
8-5	N40A200-D70-S50-1	40	2,400	0.75	250	200	15.2	–	50	–	100	air
8-6	N40A200-D70-S60-1	40	2,400	0.75	260	200	15.2	–	60	–	100	air
8-7	N40A200-D70-S70-1	40	2,400	0.75	270	200	15.2	–	70	–	100	air

Table 4.13 Specimens of test series 9

No.	Specimen ID	f'_c (MPa)	f_{pu} (MPa)	f_{pj}/f_{pu}	b (mm)	h (mm)	d_b (mm)	c_b (mm)	s_p (mm)	s_r (mm)	l_{db} (mm)	curing
9-1	N40A200-D70-C40-2	40	2,400	0.75	200	200	15.2	40	–	–	100	air
9-2	N40A200-D70-C50-2	40	2,400	0.75	200	200	15.2	50	–	–	100	air
9-3	N40A200-D70-C60-2	40	2,400	0.75	200	200	15.2	60	–	–	100	air
9-4	N40A200-B70-C40-2	40	1,860	0.75	200	200	15.2	40	–	–	100	air
9-5	N40A200-D70-S50-2	40	2,400	0.75	250	200	15.2	–	50	–	100	air
9-6	N40A200-D70-S60-2	40	2,400	0.75	260	200	15.2	–	60	–	100	air
9-7	N40A200-D70-S70-2	40	2,400	0.75	270	200	15.2	–	70	–	100	air

Table 4.14 Specimens of test series 10

No.	Specimen ID	f'_c (MPa)	f_{pu} (MPa)	f_{pj}/f_{pu}	b (mm)	h (mm)	d_b (mm)	c_b (mm)	s_p (mm)	s_r (mm)	l_{db} (mm)	curing
10-1	H70A200-D70-C40	70	2,400	0.75	200	200	15.2	30	–	–	100	air
10-2	H70A200-D70-C50	70	2,400	0.75	200	200	15.2	40	–	–	100	air
10-3	H70A200-D70-C60	70	2,400	0.75	200	200	15.2	50	–	–	100	air
10-4	H70A200-B70-C40	70	1,860	0.75	200	200	15.2	40	–	–	100	air
10-5	H70A200-D70-S50	70	2,400	0.75	250	200	15.2	–	40	–	100	air
10-6	H70A200-D70-S60	70	2,400	0.75	260	200	15.2	–	50	–	100	air
10-7	H70A200-D70-S70	70	2,400	0.75	270	200	15.2	–	60	–	100	air

4.3.2 Material Properties

4.3.2.1 Concrete

Normal strength and high strength concrete were used for the fabrication of the test specimens. Design compressive strength of concrete was 40 MPa and 70 MPa, respectively. Detailed concrete mix proportion is provided in Table 4.15. Water-to-binder ratio of the two types of concrete was 31.9% and 22.8%, respectively. Maximum aggregate size was 25 mm for the normal strength concrete and 20 mm for the high strength concrete. The target slump was 120 mm for the normal strength concrete. For high workability, the high strength concrete was controlled to satisfy a slump flow of 600 mm.

Twenty one 150×300 mm cylinders were fabricated in every test series for compression strength test. The cylinders were cured together with the test specimens under the same conditions. In this experiment, steam curing was not applied because it was not assured that the design compressive strength of the high strength concrete would be achieved under the condition of steam curing. After final finishing of concrete surface, the specimens were covered with burlap and kept wet until the form removal. The forms were removed 4~5 days after the concrete placement.

Table 4.15 Concrete mix proportion for tests of Grade 2,400 strands

Test series	f'_c (MPa)	Unit weight (kg/m ³)							
		Water	Cement	Slag	Silica fume	Fly-ash	Sand	Gravel	HRWR
8~9	40	160	426	–		75	754	896	4.0
10	70	155	476	136	68	–	570	939	10.2

Table 4.16 summarizes the average concrete compressive strengths and elastic moduli measured at time of transfer and after 28 days. Because elastic moduli at transfer E_{ci} was not measured, it was assumed to be $E_c \sqrt{f'_{ci}/f'_c}$.

Table 4.16 Average compressive strength and elastic moduli of concrete at transfer and after 28 days (test series 8~10)

Test series	f'_c (MPa)	At transfer			After 28 days		
		t_i (day)	f'_{ci} (MPa)	E_{ci} (MPa)	t (day)	f_{cu} (MPa)	E_c (MPa)
8	40	6	31.2	–	28	39.6	26,600
9	40	16	32.2	–	49	34.3	17,656
10	70	5	46.0	–	30	64.2	28,480

4.3.2.2 Prestressing strand

Table 4.17 summarizes the mechanical properties of low-relaxation Grade 2,400 strands. One size of strand diameter, 15.2 mm, was used for all the test specimens. The mechanical properties of Grade 1,860 strands in this experiment are same to those given in Table 4.10. During the experiment, the strands were kept free of water and rust, and no additional surface treatments were applied.

Table 4.17 Mechanical properties of Grade 2,400 strand

Mechanical properties	Nominal diameter of strand (mm)
	15.2
Breaking strength (kN)	336.8
Tensile strength (MPa)*	2,387
Load at 0.2% proof stress (kN)	316.0
Yield strength (MPa)*	2,239
Elastic modulus (GPa)	200
Elongation (%)	7.5
Diameter (mm)	15.28
Difference between center wire diameter and diameter of any outer wire (mm)	0.14
Diameter of center wire (mm)*	5.19
Diameter of outer wire (mm)*	5.05
Area of strand (mm ²)*	141.1
Unit weight (kg/km)	1.099.5
Pitch length (mm)	223
Lay angle (deg)*	8.20

* The values calculated from the measured properties

4.3.3 Fabrication of Test Specimens

Because transfer lengths of high strength strands are likely to be longer than those of Grade 1,860 strands, a prestressing bed was required to accommodate longer specimens. In this experiment, three types of the prestressing bed were fabricated. Drawings of the prestressing beds are provided in Figure 4.17 and 4.18. Steel I beams were assembled in a rectangular shape to form a frame and additional beams were located inside the frame to reduce the deformation of the bed. Several

stiffeners were welded on the beams to prevent a local buckling due to concentrated loadings.

The test specimens had a length of 4 m and a rectangular cross section of 200×200 mm. In case of the specimens with two strands, the center-to-center spacing of strands was varied while the cover depths were kept constant as 100 mm. Thus, the height of the section remained the same but the width of the section varied depending on the center-to-center spacing of strands.

Prestressing force corresponding to more than 75% of the strand tensile strength was applied by hydraulic jacks, which allowed the initial prestress of $0.70f_{pu}$ after anchorage seating loss. Prestress was suddenly released at one end by flame cutting. The prestressing strands were debonded over 100 mm at both ends.

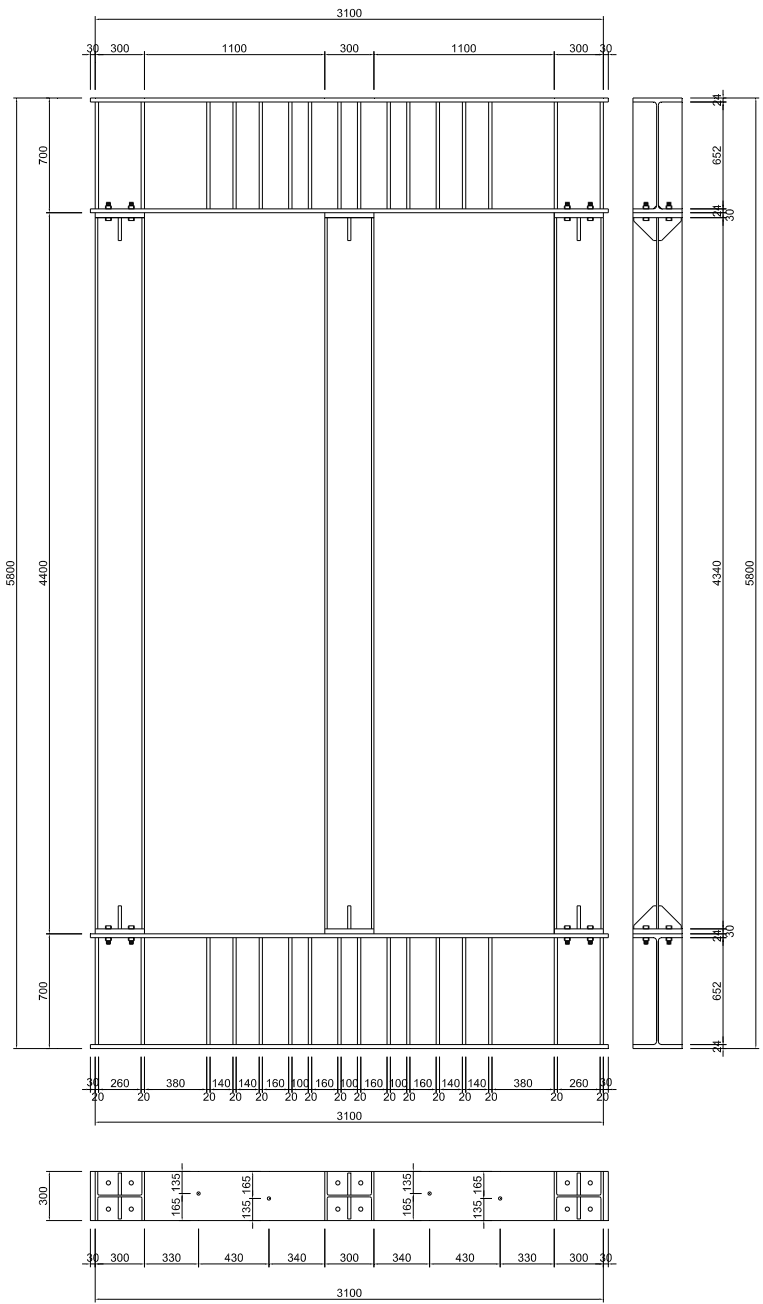


Figure 4.17 Drawing of prestressing bed for transfer length specimens with single prestressing strand

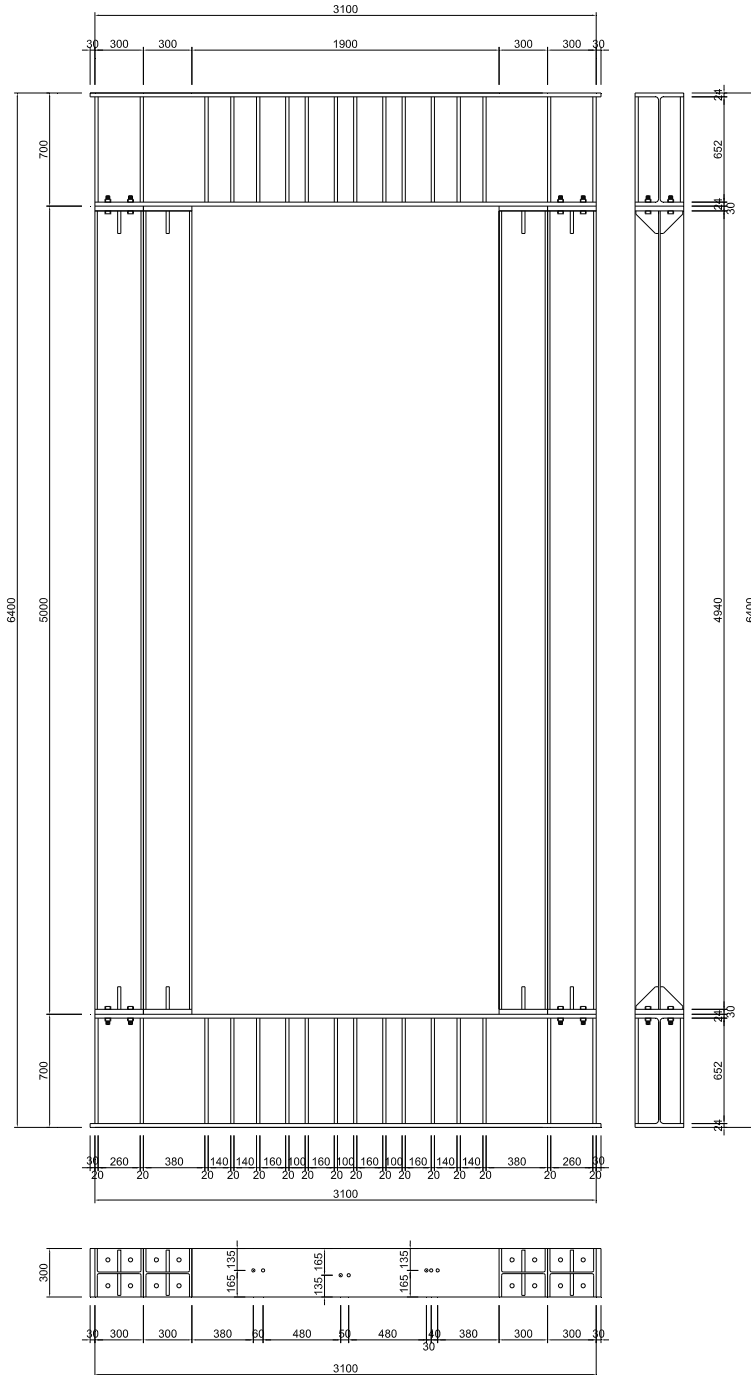
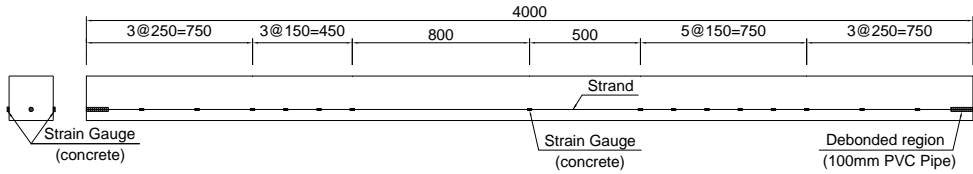


Figure 4.18 Drawing of prestressing bed for transfer length specimens with two prestressing strands

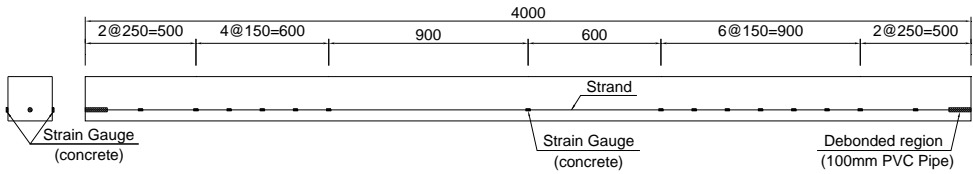
4.3.4 Instrumentation

Concrete strain was measured with ERSGs to obtain transfer length. The location of ERSGs was determined based on the estimations from the ACI318 code and Eurocode2. The gauge spacing was 150 mm for sections where the end of the transfer zone would be located but a wider spacing was provided for the remaining part of the specimen. The gauge arrangement was modified to capture the end of the transfer zone according to concrete compressive strength at transfer and initial prestress as shown in Figure 4.19 and 4.20. ERSGs for concrete were attached on the longitudinal line parallel to the centroid of the strand.

Loadcell with a capacity of 500 kN were placed between the prestressing bed and the anchorage to measure and monitor the prestressing force. Because the cross section of the loadcells was much larger than that of the anchorage, a jig to fix the location of the loadcells against the prestressing bed was required to align the loadcell with the strand. The jigs consisting of 2 seating steel plates and 4 supporting steel bars were fabricated and welded on the prestressing bed (see Figure 4.21 (a)). ERSGs were also installed on the strand surface at the center of the specimen for load measurement. The response of the ERSGs was recorded during tensioning of the strands. At release of prestress, two LVDTs were mounted on the strand at both ends of the specimens to measure end slip (see Figure 4.21 (b)).

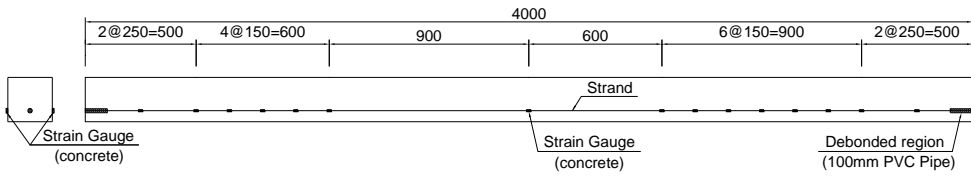


(a)

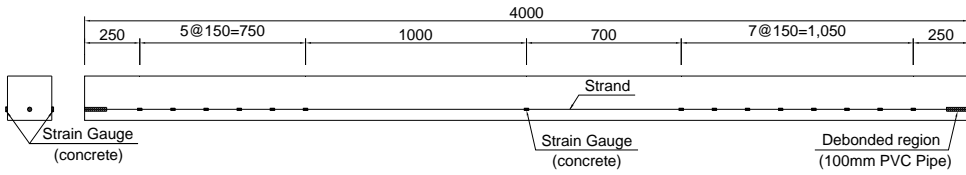


(b)

Figure 4.19 Gauge arrangements of test series 8 and 9: (a) test specimen with Grade 2,400 strands; and (b) test specimen with Grade 1,860 strands



(a)



(b)

Figure 4.20 Gauge arrangements of test series 10: (a) test specimen with Grade 2,400 strands; and (b) test specimen with Grade 1,860 strand



(a)



(b)

Figure 4.21 Instrumentation of transfer length test for Grade 2,400 strands: (a) Loadcell; and (b) LVDT for end slip of strand

5. Experimental Results

5.1 Introduction

Results from the transfer length tests conducted in this experimental program are presented and discussed. The following sections provide detailed descriptions of the entire tests. Section 5.2 discusses the applicability of ERSGs to transfer length test. Section 5.3 analyzed behavior of strands and estimates the residual prestress based on the analytical model proposed by Machida and Durelli (1973), which were simple to use and suitable for the application to this analysis. Section 5.4 identifies the effect of each test variable on the transfer lengths and compares with the predictions of the empirical equations. The complete results for each specimen are given in Appendix B.

5.2 Applicability of ERSGs to Transfer Length Test

5.2.1 Comparison of Strain Measurements using DEMEC and ERSG

DEMEC gauges were applied to the three specimens of the test series 1. Figure 5.1, 5.2, and 5.3 show the results of the specimens. The specimen N45S150-B70F-1 and 2 had 15 measuring points spaced at 150 mm while the specimen N45S150-B70F-3 had 56 measuring points at intervals of 50 mm. In the figures, 1 & 2 and 3 & 4 legends indicate the averages of two measurements on opposite faces by each operator. As seen in these figures, it was impossible to estimate transfer length using DEMEC gauges, because measurements by different operators differed significantly

and furthermore, even a single operator produced inconsistent results between measurements.

This observation is more distinct in Figure 5.1 (b) and 5.3 (b) which is zoomed in to depict a smaller range of strain. Slight measurement variations within small strain levels caused undesirable results. Inherent errors in DEMEC gauges are too large to yield accurate measurements of small strains. It should be noted that the poor results with DEMEC gauges may come from only tests conducted with the specimens and experimental conditions similar to this study.

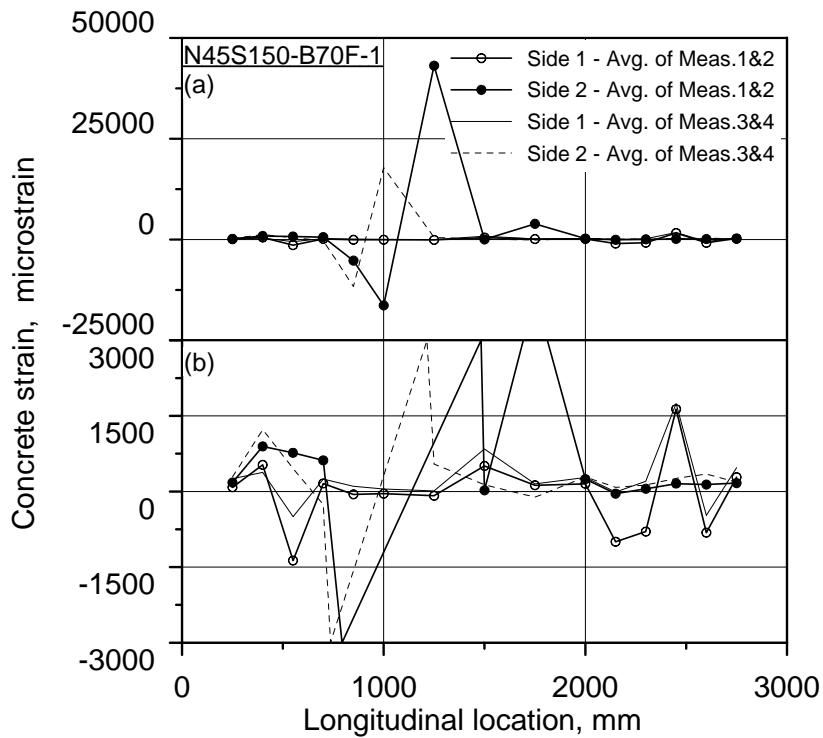


Figure 5.1 Concrete strains of N45S150-B70F-1 measured by DEMEC gauges along specimen length: (a) full range; and (b) magnified

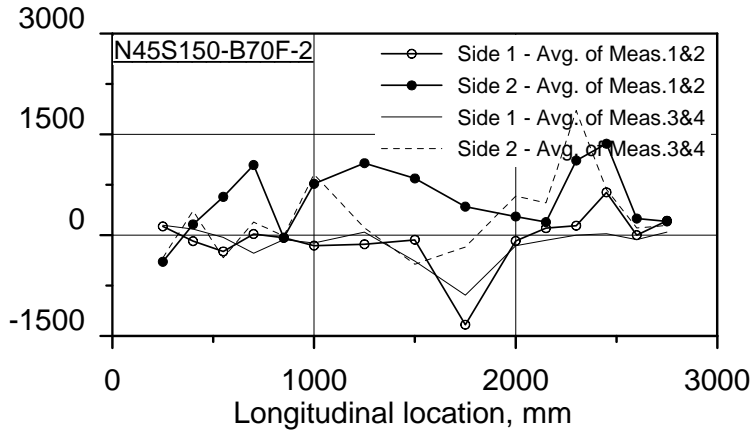


Figure 5.2 Concrete strains of N45S150-B70F-2 measured by DEMEC gauges along specimen length

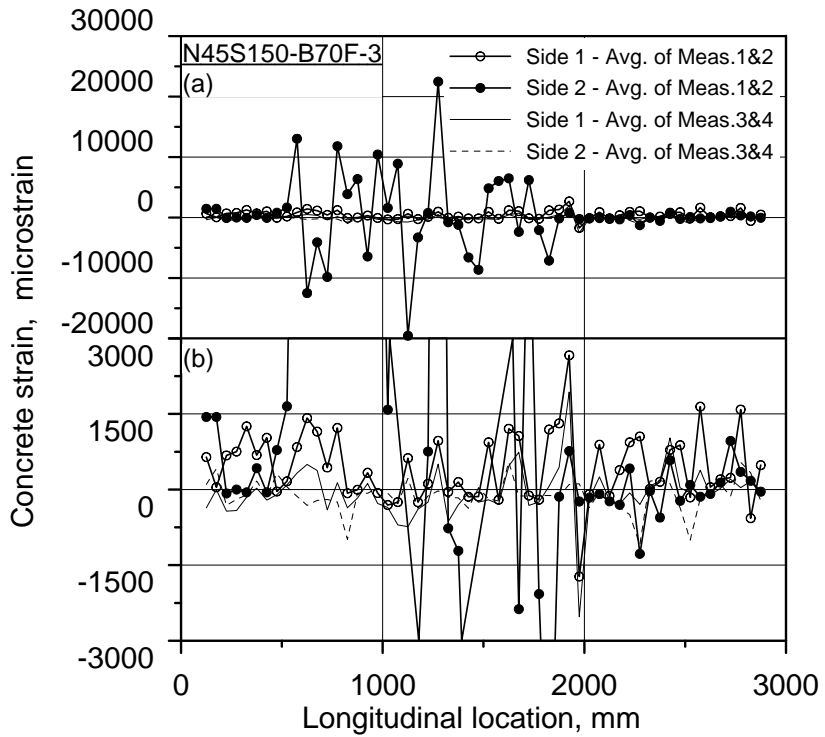


Figure 5.3 Concrete strains of N45S150-B70F-3 measured by DEMEC gauges along specimen length: (a) full range; and (b) magnified

Figure 5.4 and 5.5 are strain measurements taken by ERSGs that were attached directly on both concrete and strand for specimens N45S150-B70F-1 and N45S150-B70F-2, respectively. The upper plot in each figure shows strain readings in strands immediately after release, with the tensile strain in the strand just before release used as a reference. The lower plot on the same graph depicts concrete strains measured after release.

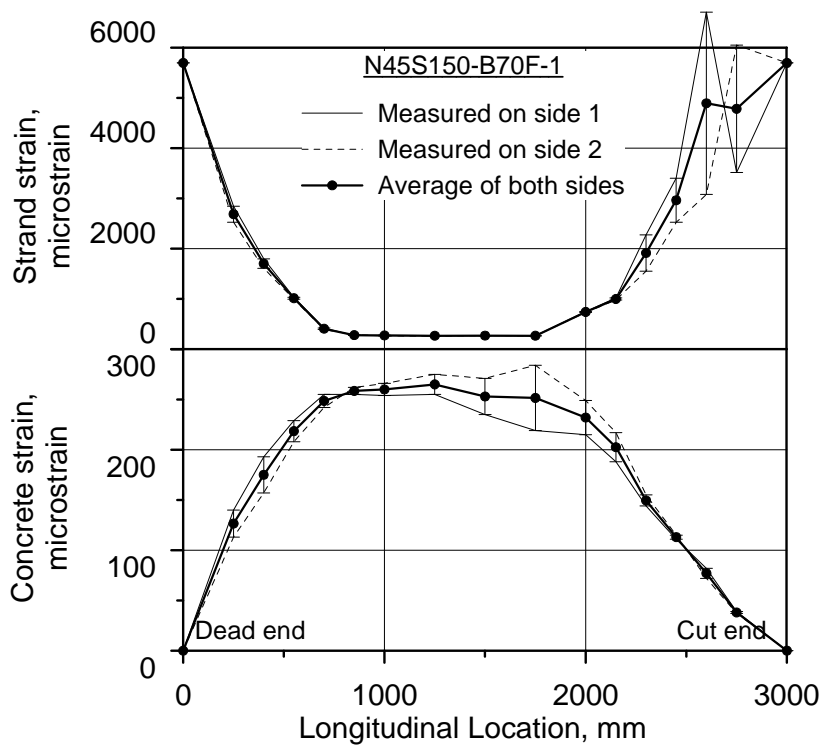


Figure 5.4 Strain profile measured by ERSGs for the specimen N45S150-B70F-1 with 15 gauges attached to strand

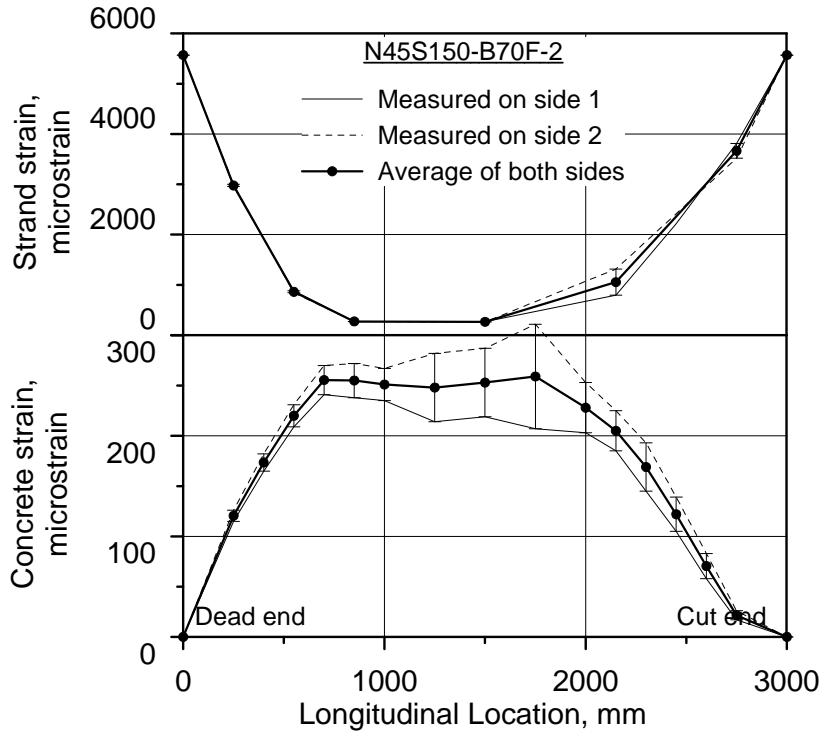


Figure 5.5 Strain profile measured by ERSGs for the specimen N45S150-B70F-2 with 7 gauges attached to strand

Taken as a whole, all plots are distinguished from plots for DEMEC gauge giving acceptable trends capturing theoretical strain variation with distinct components of strain profile including portion of increasing or decreasing strains, initiation of strain plateau and the range of strain plateau required for determination of transfer length. Although the use of ERSGs gives satisfactory transfer length, in order to apply this method to common specimens and test conditions, it is necessary to investigate the applicability and credibility of their measurements in detail.

5.2.2 Applicability of ERSGs for Strand

Russell and Burns (1993) pointed out four problems of ERSG for strand. First of all, each wire of seven-wire strand experiences a slightly different strain condition. Secondly, a large percentage of ERSGs in transfer zone are destroyed at transfer. Thirdly, ERSGs' presence on strand interferes with bond, at least locally. Lastly, ERSGs are difficult to protect during casting.

However, it can be said that these problems can be solved. For the first problem, a couple of gauges were attached on a location, each on a different helical wire of strand with a gap of two helical wires on both sides of a gauged wire. Measured values were averaged to become a representative of strain at the location as seen in Figure 5.4 and 5.5. In Figure 5.6, the averaged strain profile of strand is compared with that of concrete with respect to relative strain, which is normalized to the averaged strain over the strain plateau zone. These averaged values proved to give a curve almost identical to that of concrete strain. The second and fourth problem did not occur in the experimental program. Figure 5.4 and 5.5 show that ERSGs in transfer zone functioned normally and gave stable measurement during release. And for the third problem, analysis follows below.

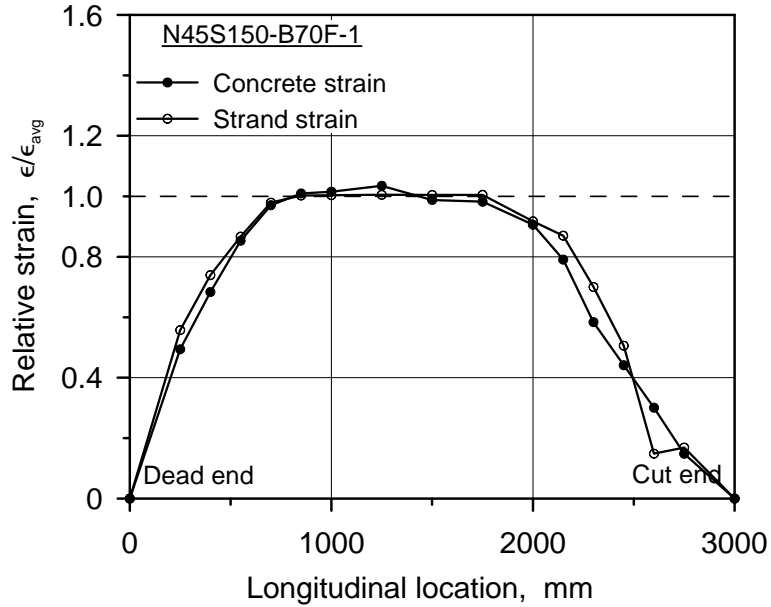


Figure 5.6 Comparison of strain profiles obtained by ERSGs on concrete and strands

5.2.2.1 Loss of Bonds due to Gauge Attachment

To investigate the influence of strain gauges attached to a strand, the two specimens N45S150-B70F-1 and N45S150-B70F-2 were considered. The only difference between the specimens N45S150-B70F-1 and N45S150-B70F-2 in Figure 5.4 and 5.5 is the number of gauges attached to the strand, 6 and 2 gauges in the transfer zone, respectively, with concomitant differences in gauge spacing at 150 mm and 300 mm, respectively. The concrete and strand strain profiles of the specimens N45S150-B70F-1 and N45S150-B70F-2 are compared in Figure 5.7. The two specimens exhibited only negligible differences between the concrete strain profiles. Also the values of the measured strand strains were almost identical except some points near the cut end. As shown in Figure 5.4, a dynamic impact induced by

sudden release can greatly affect the variation in the strand strains in some limited distance. Therefore, the discrepancy between the strand strains near the cut end does not imply any deterioration of transfer bond. Based on the observations in Figure 5.4, 5.5 and 5.7, it can be concluded that strand gauges employed in this experiment does not significantly disturb the bond behavior of strands and concrete.

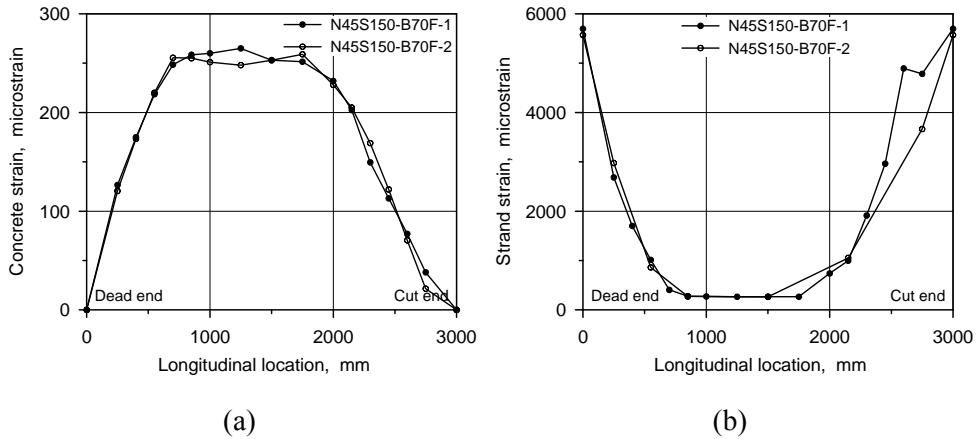


Figure 5.7 Influence of number of ERSGs attached to strand surface on: (a) concrete strain profile; and (b) strand strain profile.

Besides the issue of transfer bond, number of gauges can have another crucial effect on transfer length. Transfer length is determined from the measured strain profiles in Figure 5.4 and 5.5. Gauge interval, mainly ruled by number of gauges, has the conflicting effect with number of gauges. Less gauges, and thus longer interval, may preserve bonds but cannot capture the end of transfer region accurately. The vise-versa may have the opposite effect. Transfer lengths of N45S150-B70F-1, N45S150-B70F-2, and N45S150-B70F-4 measured by ERSGs for strand at cut ends showed an effect of gauge intervals on estimation of transfer length. Transfer length increased by 185 mm at the cut end when gauge interval was doubled from 150 mm

to 300 mm. ERSGs' interval of 150 mm is sparser in comparison with the intervals of DEMEC gauge points, generally 50 mm. When connecting successive measured points linearly, sparser interval only causes the problem of longer transfer length because the strain profile always have decreasing slope in the close vicinity of the transfer length. If the error is in an acceptable range, the transfer length can be thought conservative, which is similar to that the longer transfer length caused by measurement with DEMEC gauge is generally accepted as conservative. Wan et al. (2002b) used reinforcing bars on which ERSGs were attached at 150 ~ 250 mm interval for measuring transfer length of concrete piles and reported that the error was within 75 ~ 150 mm. Judging from the strain distribution curves connecting the measured points of 150 mm interval, the error does not seem to be in excess of a reasonable range. Despite the limited test data, it can be concluded that ERSGs are feasible to obtain the transfer lengths of pretensioned strands.

5.2.2.2 Stability under High Temperatures

Figure 5.8 shows the temperature history during the steam curing process, which was measured in the curing chamber and inside the specimen. Although the maximum temperature applied for 8 hours was 60 °C, concrete specimens experienced temperature histories ranging from 4 °C to 73 °C, the latter of which is close to the gauge's service limit of 80 °C. For reference, to investigate the effects of humidity and temperature during the steam curing process, the strain changes of a bare strand were monitored and are given in Figure 5.9 (a). This plot indicates that humidity and temperature do not have any effects during the steam curing process. On the other hand, as seen in Figure 5.9 (b), for specimen N45S150-B70F-1

significant malfunctions were observed in several gauges that were embedded in concrete and exposed to temperatures that were about 10 °C higher than those outside the concrete. However, as can be seen in the same plot, all of these strain gauges gave stable values after the termination of the curing process, so their readings could be used for the estimation of transfer length. Figure 5.9 (c) and (d) shows specimen N45S150-B70F-2 and N45S150-B70F-4, which was subjected to the same curing process as the specimen N45S150-B70F-1. Most of the ERSGs did not show any signs of malfunction. From these observations, it can be concluded that ERSGs can be used even during high-temperature curing processes.

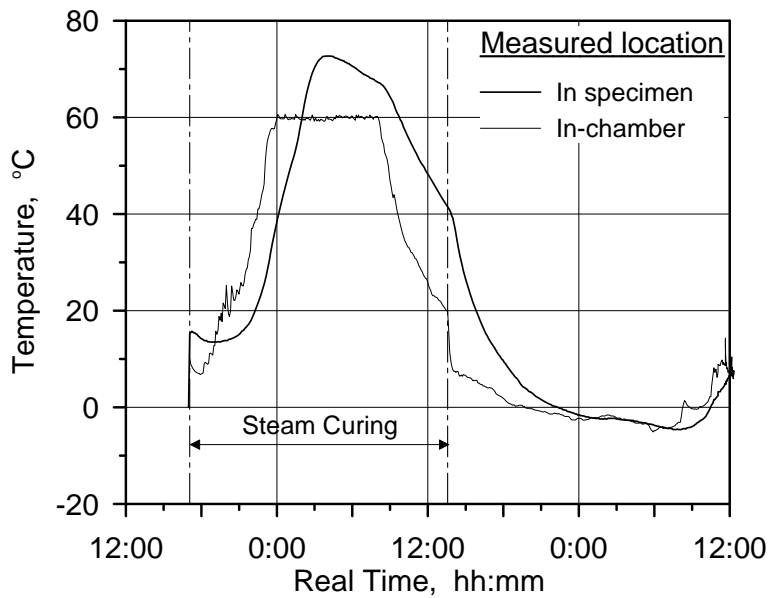
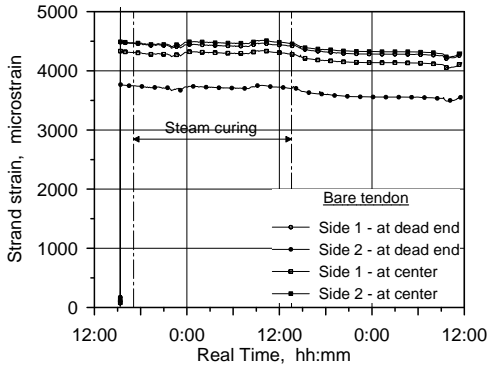
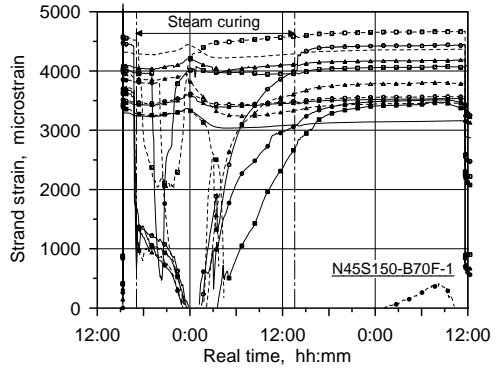


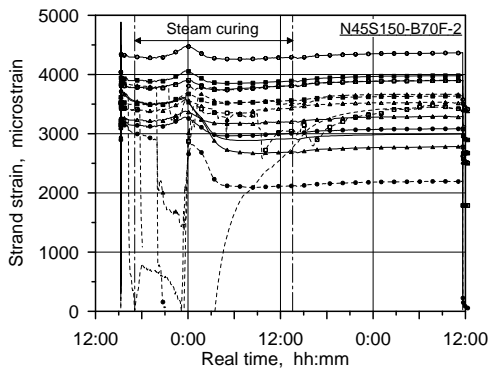
Figure 5.8 Temperatures inside and outside the specimen during steam curing



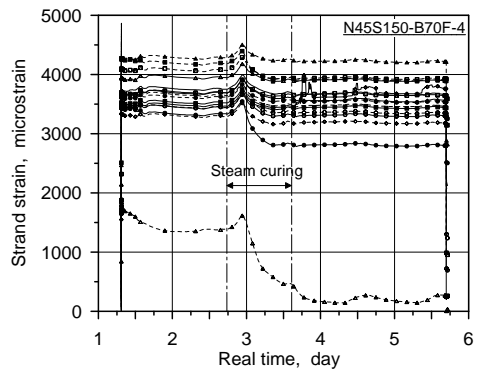
(a)



(b)



(c)



(d)

Figure 5.9 Strain histories during steam curing: (a) bare strand; (b) N45S150-B70F-1; (c) N45S150-B70F-2; and (d) N45S150-B70F-4

5.3 Estimation of Initial Prestress

5.3.1 Behavior of Seven-Wire Strand Subject to Axial and Torsional Displacement

Based on the geometric considerations of a seven-wire strand, Machida and Durelli (1973) proposed explicit expressions for internal forces acting on each wire, which include axial force, bending moment, and twisting moment. To derive the equations for the internal forces, they made several assumptions that:

- (1) each helical wire has a circular cross section in a plane normal to its longitudinal axis;
- (2) diameter of each wire is small in comparison with the pitch of the helix;
- (3) each helical wire is in contact with the two adjacent wires, with the center wire, or with both center and adjacent wires;
- (4) there is no friction between the adjacent wires; and
- (5) the radial dimensions of the cross section in the unloaded strand and its position with respect to the center wire remain constant under load;

The last assumption implies that the deformation due to the contact force and Poisson's effect induced by the axial strain is ignored. Machida and Durelli (1973) stated that the last assumption is valid if the third assumption is reasonable because the deformation of a wire is restrained by the center wire and the neighbor helical wires. Thus, the axial lines of helical wire remain on the same cylinder before and after deformation. This cylinder is the reference cylinder and has a radius of R as shown in Figure 5.10.

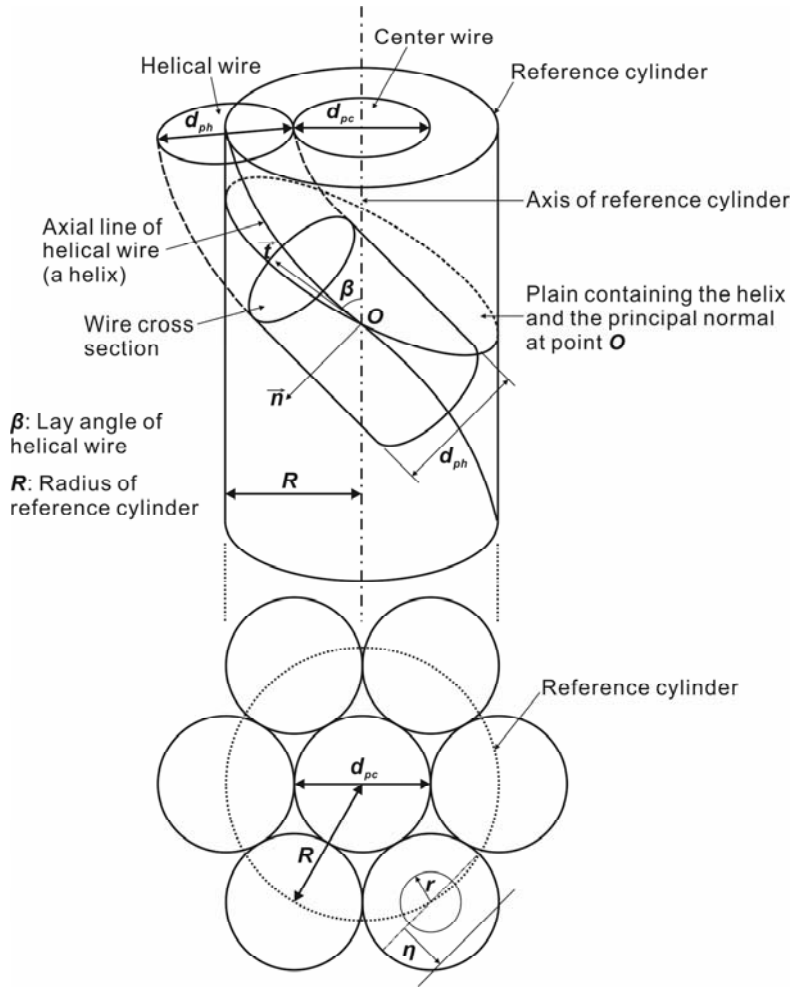


Figure 5.10 Geometry of a helical wire wrapped around a center wire (Machida and Durelli, 1973)

When a seven-wire strand is under tension, the axial line of a helical wire, helix \overline{EF} , is deformed to helix $\overline{EF'}$ accompanying an axial displacement along the axial direction of the strand and a rotation around the axis of the strand (see Figure 5.11). Four types of force are involved in the axial displacement and rotation of each wire: axial force, bending moment acting on the plane containing the axial line of

the wire, twisting moment around the axis of the strand, and contact force. With the assumption of no friction between the wires and no radial deformations of the cross section, the contact force has a negligible effect on the deformations of the wires. Consequently, the helical wires are subjected by axial force, bending moment and twisting moment and the center wire is subjected to axial force and twisting moment.

Machida and Durelli (1973) derived the deformations from the geometric considerations of the seven-wire strand and linearly approximated them by ignoring higher order terms and small quantities. And then, by assuming that the strand is in elastic state, the internal forces acting on each wire were formulated in terms of the axial strain and the rotation. The equations for the wire responses corresponding to each internal force are briefly introduced.

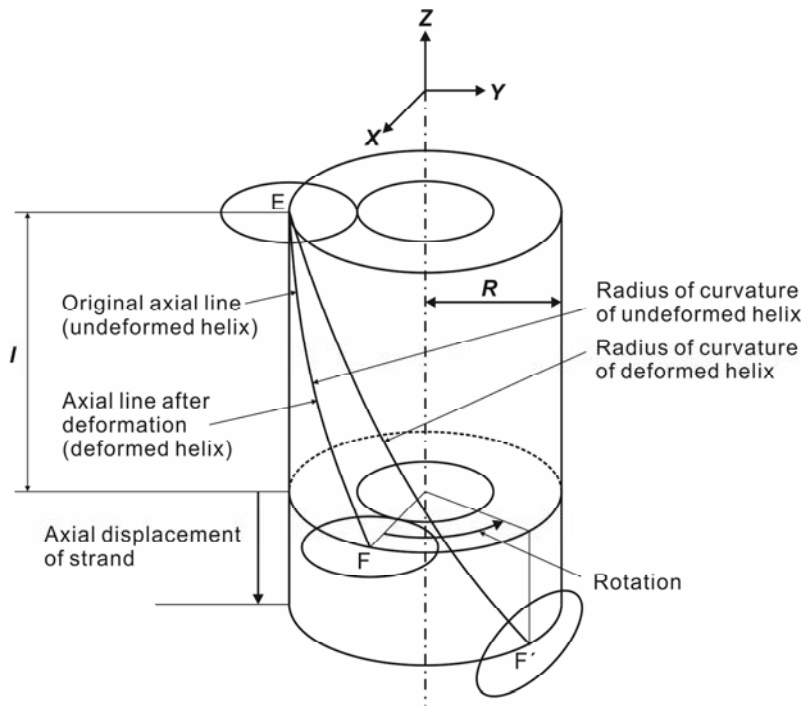


Figure 5.11 Elongation and rotation in a helical wire (Machida and Durelli, 1973)

The responses of the center wire to the axial force P_c are given as follows:

$$\varepsilon_z^{ac} = \varepsilon \quad (5.1a)$$

$$\sigma_z^{ac} = E_p \varepsilon_z^{ac} \quad (5.1b)$$

$$P_c = A_{pc} E_p \varepsilon_z^{ac} \quad (5.1c)$$

where, ε_z^{ac} and σ_z^{ac} is an axial strain and normal stress resulted from P_c in the center wire, respectively; ε is an axial displacement per unit length; and A_{pc} is a cross sectional area of the center wire.

On the other hand, the responses of the helical wire to the axial force P_h are:

$$\varepsilon_s^{ah} = \varepsilon \cos^2 \beta + \gamma \sin^2 \beta \quad (5.2a)$$

$$\sigma_s^{ah} = E_p \varepsilon_s^{ah} = E_p (\varepsilon \cos^2 \beta + \gamma \sin^2 \beta) \quad (5.2b)$$

$$P_h = A_{ph} \sigma_s^{ah} = A_{ph} E_p (\varepsilon \cos^2 \beta + \gamma \sin^2 \beta) \quad (5.2c)$$

where, ε_s^{ah} and σ_s^{ah} is an axial strain, normal stress resulted from P_h in the helical wire, respectively; γ is normalized rotation per the undeformed pitch length of the strand; β is lay angle of the helical wire; and A_{ph} is a cross sectional area of the helical wire.

For given ε and γ , a bending moment M acting on the helical wire and the resulting normal stress and axial strain are:

$$\varepsilon_s^{bh} = \frac{2(\varepsilon - \gamma)\eta}{R} \cos^2 \beta \sin^2 \beta \quad (5.3a)$$

$$\sigma_s^{bh} = E_p \varepsilon_s^{bh} = \frac{2E_p(\varepsilon - \gamma)\eta}{R} \cos^2 \beta \sin^2 \beta \quad (5.3b)$$

$$M = \frac{2E_p I(\varepsilon - \gamma)}{R} \cos^2 \beta \sin^2 \beta \quad (5.3c)$$

where, ε_s^{bh} and σ_s^{bh} is an axial strain and normal stress resulted from M in the helical wire, respectively; η is a distance on the transverse cross section of helical wire from the neutral axis for bending (see Figure 5.10); and I is moment of inertia of the cross section of the helical wire.

For twisting moment T_c acting on the center wire, the corresponding strain and stress are computed by:

$$\gamma_{z\theta}^{tc} = \frac{2\pi\gamma r}{p} \quad (5.4a)$$

$$\tau_{z\theta}^{tc} = G_p \gamma_{z\theta}^{tc} \quad (5.4b)$$

$$T_c = G_p I_p^c \frac{2\pi\gamma}{p} \quad (5.4c)$$

where, $\gamma_{z\theta}^{tc}$ and $\tau_{z\theta}^{tc}$ is a shear strain and shear stress on the transverse cross section of the center wire; r is a radial distance on the transverse cross section of helical wire from the centroid (see Figure 5.10); p is pitch length of the helical wire; G_p is shear modulus; and I_p^c is polar moment of inertia of the cross section of the center wire.

The relationships of twisting moment T_h acting on the helical wire and the resulting shear strain and shear stress are given by:

$$\gamma_{p\theta}^{th} = \frac{(\gamma - \varepsilon)r}{4R} \sin 4\beta \quad (5.5a)$$

$$\tau_{p\theta}^{th} = G_p \gamma_{p\theta}^{th} = \frac{G_p (\gamma - \varepsilon)r}{4R} \sin 4\beta \quad (5.5b)$$

$$T_h = \frac{G_p I_p^h (\gamma - \varepsilon)r}{4R} \sin 4\beta \quad (5.5c)$$

where, $\gamma_{s\theta}^{th}$ and $\tau_{s\theta}^{th}$ is a shear strain and shear stress on the transverse cross section of the helical wire.

Since the strand is in elastic state, the total axial force is the sum of P_c and the component of P_h in the z -direction:

$$P = P_c + 6P_h \cos \beta = C_A \varepsilon + C_B \gamma \quad (5.6a)$$

with

$$C_A = A_{pc} E_p + 6A_{ph} E_p \cos^3 \beta \quad (5.6b)$$

$$C_B = 6A_{ph} E_p \sin^2 \beta \cos \beta \quad (5.6c)$$

Similarly, the total twisting moment around the longitudinal axis of the strand is given by:

$$T = T_c + 6(T_h \cos \beta - M \sin \beta + P_h R \sin \beta) = C_C \varepsilon + C_D \gamma \quad (5.7a)$$

with

$$C_C = 6A_{ph}RE_p \sin \beta \cos^2 \beta - \frac{3G_p I_p^h \sin 4\beta \cos \beta}{2R} - \frac{12E_p I \cos^2 \beta \sin^3 \beta}{R} \quad (5.7b)$$

$$C_D = 6A_{ph}RE_p \sin^3 \beta + \frac{3G_p I_p^h \sin 4\beta \cos \beta}{2R} + \frac{12E_p I \cos^2 \beta \sin^3 \beta}{R} + \frac{2\pi G_p I_p^c}{p} \quad (5.7c)$$

Using equation (5.6a) and (5.7a), ε and γ can be expressed in terms of total axial force and twisting moment:

$$\varepsilon = \frac{C_D}{C_A C_D - C_C C_B} P - \frac{C_B}{C_A C_D - C_C C_B} T \quad (5.8a)$$

$$\gamma = -\frac{C_C}{C_A C_D - C_C C_B} P + \frac{C_A}{C_A C_D - C_C C_B} T \quad (5.8b)$$

5.3.2 Estimation of Prestress at Each Fabrication Stage

5.3.2.1 Relationship between Measured Strain, Axial Force, and Twisting Moment

ERSGs for strand are attached on the surface of the helical wires along their axial lines. Since ERSG measure an axial strain, a measured axial strain is the sum of the strains from two sources: axial force and bending moment. It is given by the sum of equation (5.2a) and (5.3a):

$$\varepsilon_p^h = \varepsilon \cos^2 \beta + \gamma \sin^2 \beta + \frac{2(\varepsilon - \gamma)\eta}{R} \cos^2 \beta \sin^2 \beta \quad (5.9)$$

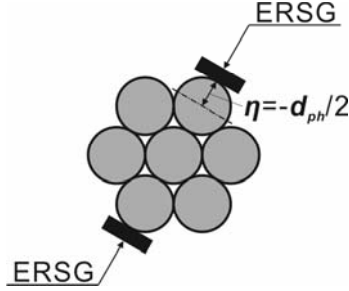


Figure 5.12 Installation locations of ERSGs on the transverse cross section of the strand

As shown in Figure 5.12, ERSGs are installed on the surface of the helical wire that is opposite to the contact point with the center wire. At the installation location, η equals $-d_{ph}/2$. Hence, equation (5.9) becomes:

$$\begin{aligned} \varepsilon_p^h &= \varepsilon \cos^2 \beta + \gamma \sin^2 \beta - \frac{(\varepsilon - \gamma)d_{ph}}{R} \cos^2 \beta \sin^2 \beta \\ &= C_E \varepsilon + C_F \gamma \end{aligned} \quad (5.10a)$$

with

$$C_E = \varepsilon \cos^2 \beta \left(1 - \frac{d_{ph}}{R} \sin^2 \beta \right) \quad (5.10b)$$

$$C_F = \gamma \sin^2 \beta \left(1 + \frac{d_{ph}}{R} \cos^2 \beta \right) \quad (5.10c)$$

Substituting equation (5.8a) and (5.8b) into (5.10a) gives:

$$\varepsilon_p^h = C_G P + C_H T \quad (5.11a)$$

with

$$C_G = \frac{C_E C_D - C_F C_C}{C_A C_D - C_C C_B} \quad (5.11b)$$

$$C_H = \frac{C_F C_A - C_E C_B}{C_A C_D - C_C C_B} \quad (5.11c)$$

All the constants C_A , C_B , C_C , C_D , C_E , C_F , C_G , and C_H can be computed from the mechanical properties of the strand. Equation (5.11) indicates that the axial force P can be obtained from the measured strain ε_p^h and the twisting moment T .

In this experiment, the strands were tensioned with a hydraulic jack of 300 kN capacity, which is used in a common industrial practice (see Figure 5.13). It is equipped with a dial or digital gauge to show a value of applied load but displays no information on the twisting moment or the rotation of the strand.

According to equation (5.8a), (5.8b), and (5.11a), a twisting moment will develop during the tensioning if the rotation of the strand is restrained. Full restraining causes no rotation but the maximum twisting moment, while no restraining allows the maximum rotation but no twisting moment. During the strands were tensioned, a considerable rotation of the strand was actually observed with a naked eye. It means that the hydraulic jack was not capable of fully restraining the rotation.

Here, it is assumed that the twisting moment develops proportionally to the tensile force acting on the strand. Consequently, the total axial force P is expressed by the strain in the helical wire ε_p^h only:

$$\varepsilon_p^h = (C_G + C_H K)P \quad (5.12a)$$

$$P = \frac{\varepsilon_p^h}{C_G + C_H K} \quad (5.12b)$$

With

$$T = KP \quad (5.12c)$$



Figure 5.13 Hydraulic jack for single strand

The linear relationship between the axial force and the twisting moment can be proved by the linear response of the strain in the helical wire to the axial force. Figure 5.14 shows the test result measured in the specimen N45S150-B70F-2. The figure proves the high degree of linearity between the axial force and the strand strain ($r^2 = 0.9999$). The value of K was estimated to be 0.379 mm by linear regression analysis. Figure 5.14 includes two limit conditions of rotation: full restraint and no restraint. The strains in helical wire and center wire under these limit

conditions are marked with dotted black and gray lines, respectively. The measured strains are between the two limit conditions of the helical wire. The strain in the center wire is higher than that of the helical wires because the center wire is subjected to higher axial force and no bending moment. The strain difference between the center wire and the helical wire is very slight under the condition of $\gamma = 0$ but large under the condition of $T = 0$. The total axial force divided by the axial stiffness was almost similar to the values of the strain in the fully restrained helical wires. Figure 5.14 clearly shows that the strain measured on the outside surface of the helical wire significantly varies depending on the rotational restraint.

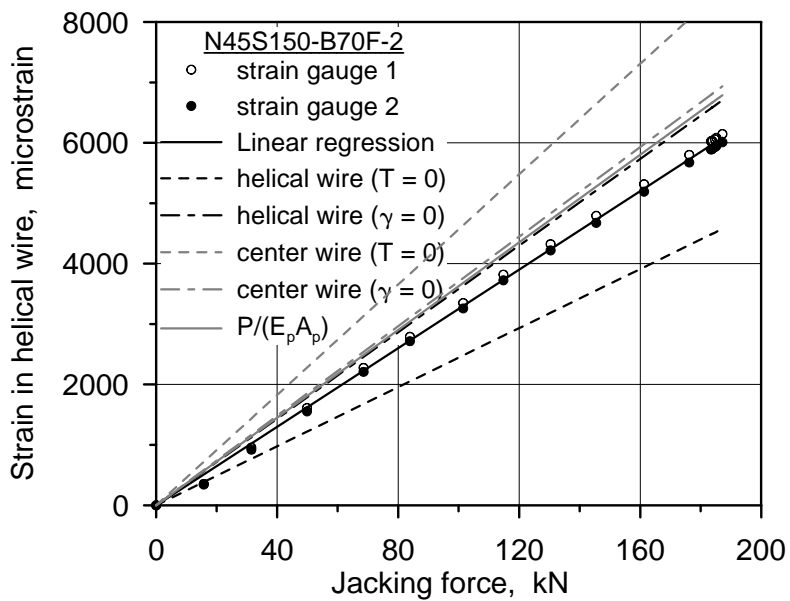


Figure 5.14 Measured strand strain with respect to jacking force (N45S150-B70F-2)

5.3.2.2 Jacking Force and Anchorage Seating Loss

The prestressing force was controlled by the load indicator equipped in the hydraulic jack and increased up to the target value. Figure 5.15 shows the target values and the actual values of the prestressing force applied to the SWPC7BL strands. In average, the actual prestressing forces reached close to their target values. Based on the observation, the jacking force was assumed to be same as the target value of the prestressing force for the strands with no load cell.

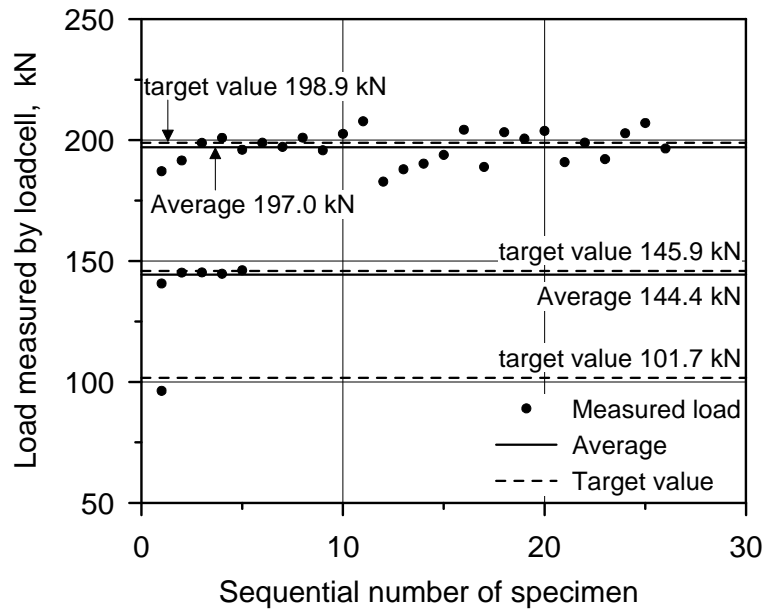


Figure 5.15 Comparison of the target values and the actual values of the prestressing force

The load cells used in the test of Grade 2,400 strands did not provide reliable results in spite of the effort to attach the jig for better measurement. To compensate for the credibility of the load measurement, the elongation of the strand was also

measured with a steel ruler, which is a common practice in fields to inspect the applied force. The SWPC7DL strands were tensioned in 6 steps to measure the elongation. The prestressing force of 44.2 kN was applied at each step and 38.9 kN at the last step. Figure 5.16 presents the strand strains measured during tensioning the strand of the specimen N40A200-D70-S50-1. The figure clearly shows that the strand strains linearly increase during each step and remain constant between the steps, which implies the load was well controlled by the hydraulic jack.

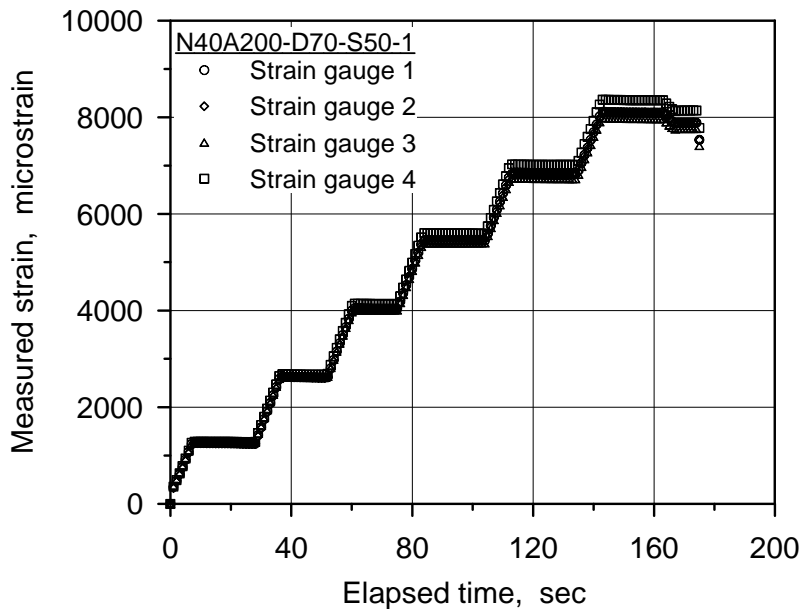
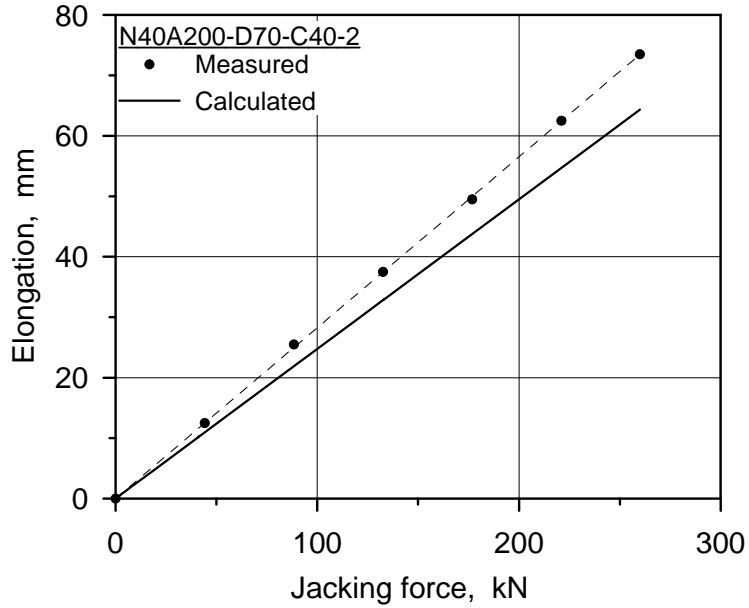


Figure 5.16 Strand strain measured during jacking with respect to elapsed time (N40A200-D70-S50-1)

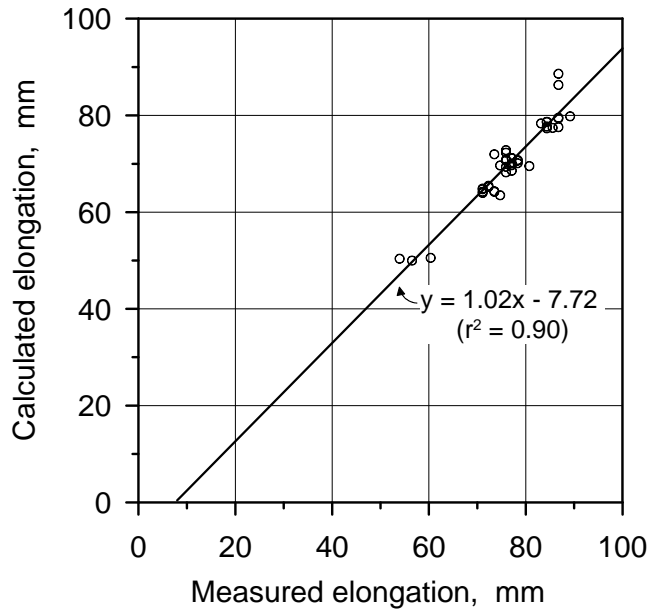
The elongation of the strand can be computed from the strain in the center wire. For calculating the elongation, a distance was considered between the anchorage fixed at the prestressing bed and the jaws inside the hydraulic jack. The distance varied depending on the length of the prestressing bed. Figure 5.17 (a) shows the

measured and calculated elongation for the specimen N40A200-D70-C40-2. The calculated elongation is slightly shorter than the measured one because of the deformation of the prestressing bed. In Figure 5.17 (b), a comparison is made between the measured and calculated elongations for all the specimens in the test series 8, 9, and 10. The best fit curve had the coefficient of determination of 0.90 and the slope of 1.02. It did not pass through the origin because the measured elongation was generally longer. The data in Figure 5.17 (b) are tabularized in Table 5.1 and 5.2.

After the prestressing force reached the target value, the strand was seated into the wedge of the anchorage. At this time, some amount of loss occurs. Figure 5.16 shows that the measured strain decreased after the maximum value maintained for a while. It is assumed that the strand is rotationally restrained during the seating with the same degree as when it was tensioned. Figure 5.18 compares the measured and calculated prestressing forces after seating for the test series 1 ~ 7. The best fit curve had the coefficient of determination of 0.99 and the slope of 1.00. Thus, it can be said that the two values were almost identical.



(a)



(b)

Figure 5.17 Comparison of the measured and calculated elongation for: (a) N40A200-D70-C40-2; and (b) all the specimens in the test series 8, 9, and 10

Table 5.1 Comparison of the measured and calculated elongations of the strands tensioned in the prestressing bed for transfer length specimens with single strand

Strand type	Specimen ID	Mea. (mm)	Cal. (mm)	Cal./Mea.
SWPC 7DL	N40A200-D70-C40-1	71.1	64.2	0.90
	N40A200-D70-C50-1	72.3	65.5	0.91
	N40A200-D70-C60-1	71.1	64.9	0.91
	N40A200-D70-C40-2	73.5	64.3	0.88
	N40A200-D70-C50-2	71.1	64.0	0.90
	N40A200-D70-C60-2	72.3	65.2	0.90
	H70A200-D70-C30	73.5	64.2	0.87
	H70A200-D70-C40	71.1	64.7	0.91
	H70A200-D70-C50	74.7	63.5	0.85
	Average	72.3	64.5	0.89
	Standard deviation	1.3	0.6	0.02
SWPC 7BL	N40A200-B70-C40-1	56.5	50.0	0.88
	N40A200-B70-C40-2	53.9	50.4	0.93
	H70A200-B70-C40	60.4	50.5	0.84
	Average	56.9	50.3	0.88
	Standard deviation	2.7	0.2	0.04

Table 5.2 Comparison of the measured and calculated elongations of the strands tensioned in the prestressing bed for transfer length specimens with two strands

Strand type	Specimen ID	Mea. (mm)	Cal. (mm)	Cal./Mea.	
SWPC 7DL	N40A200-D70-S50-1	75.9	70.7	0.93	
		75.9	72.3	0.95	
	N40A200-D70-S60-1	75.9	70.8	0.93	
		73.5	72.0	0.98	
	N40A200-D70-S70-1	77.1	69.7	0.90	
		75.9	72.8	0.96	
	N40A200-D70-S50-2	78.3	70.6	0.90	
		77.1	70.1	0.91	
	N40A200-D70-S60-2	80.7	69.5	0.86	
		78.3	70.1	0.90	
	N40A200-D70-S70-2	77.1	68.6	0.89	
		75.9	68.2	0.90	
	H70A200-D70-S40	77.1	71.1	0.92	
		78.3	70.8	0.90	
	H70A200-D70-S50	75.9	69.4	0.91	
		77.1	71.2	0.92	
	H70A200-D70-S60	75.9	70.7	0.93	
		74.7	69.6	0.93	
		Average	76.7	70.5	0.92
		Standard deviation	1.5	1.2	0.03

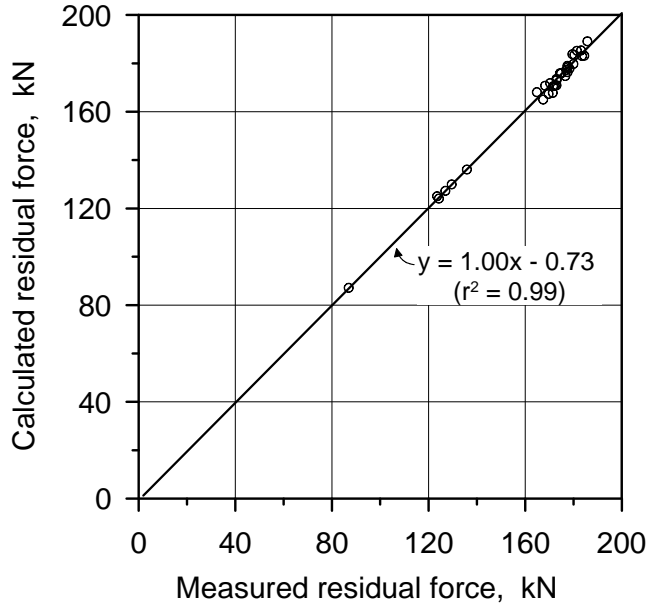


Figure 5.18 Comparison of the measured and calculated residual prestressing force after seating

5.3.2.3 Time-Dependent Losses and Prestress just before Release

The strands experience additional variations from the initial strains including relaxation, concrete shrinkage, and deformation of prestressing bed after the anchorage seating. It is assumed that an additional rotation of the strands is not allowed because they are anchored at both ends of the prestressing bed.

Since equation (5.8a) and (5.8b) are linear equations, the increments of the strains can be written as:

$$\Delta\varepsilon = \frac{C_D}{C_A C_D - C_C C_B} \Delta P - \frac{C_B}{C_A C_D - C_C C_B} \Delta T \quad (5.13a)$$

$$\Delta\gamma = -\frac{C_C}{C_A C_D - C_C C_B} \Delta P + \frac{C_A}{C_A C_D - C_C C_B} \Delta T \quad (5.13b)$$

Substituting $\Delta\gamma = 0$ into equation (5.13a) and (5.13b) yields:

$$\Delta T = \frac{C_C}{C_A} \Delta P \quad (5.13a)$$

$$\Delta P = C_A \Delta \varepsilon \quad (5.13b)$$

From equation (5.10a), the increment of the strain $\Delta \varepsilon_p^h$ is given by:

$$\Delta \varepsilon_p^h = C_E \Delta \varepsilon \quad (5.14)$$

Thus, ΔP becomes:

$$\Delta P = \frac{C_A}{C_E} \Delta \varepsilon_p^h \quad (5.15)$$

The variation in the prestressing force between seating and release can be computed from the measured strand strain using equation (5.15). Figure 5.19 compares the measured and calculated prestressing forces just before release for the test series 1 ~ 7. The best fit curve had the coefficient of determination of 0.91 and the slope of 0.95.

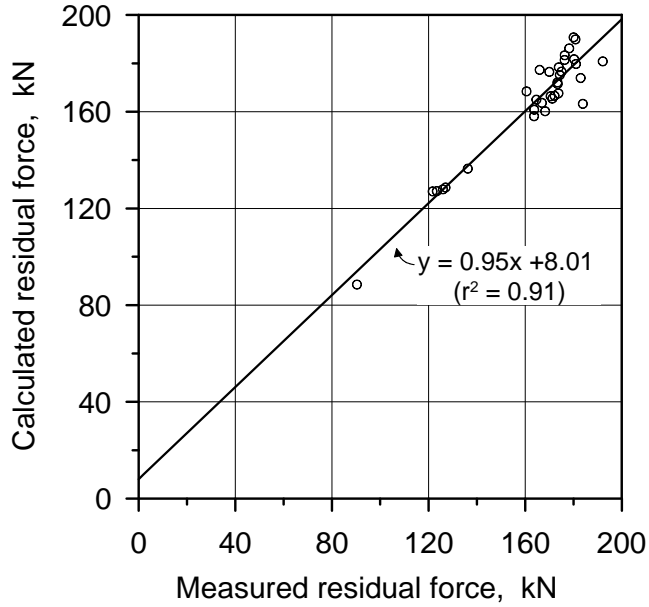


Figure 5.19 Comparison of the measured and calculated residual prestressing force just before release

5.3.2.4 Loss due to Elastic Shortening of Specimen and Initial Prestress

As the prestressing force is introduced into the specimen, the specimen is deformed and this shortening reduces the prestressing force. The prestress loss due to the elastic shortening of the specimen Δf_{pi3} can be computed by:

$$\Delta f_{pi3} = \frac{n\rho_p \left(1 + \frac{e_p^2}{r_c^2}\right) f_{pj} - n \frac{M_d}{I_c} e_p}{1 + n\rho_p \left(1 + \frac{e_p^2}{r_c^2}\right)} \quad (5.16)$$

where, e_p is the eccentricity of the centroid of the strand; I_c and r_c is

moment of inertia and radius of gyration of the cross section of the concrete member, respectively; and M_d is the moment due to the self-weight.

At this stage, since the strands were cut, the load cells and ERSGs cannot provide the residual stress in the strand embedded in the specimen. Instead, the estimated initial prestress can be evaluated by comparing the concrete strain in the strain plateau zone because the deformation of concrete specimens is caused by the initial prestress. Figure 5.20 compares the measured and calculated concrete strain at the center of the specimen just after release for all of the test series. The best fit curve had the coefficient of determination of 0.85 and the slope of 1.12.

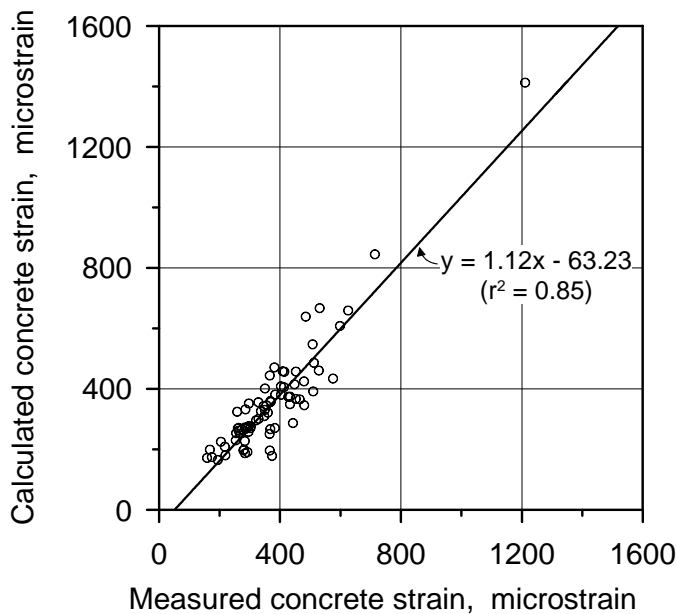


Figure 5.20 Comparison of the measured and calculated concrete strain at the center of the specimen just after release

Tables 5.3 through 5.9 summarize the strand stresses and the prestress losses at

each fabrication stage. In the tables, Δf_{pi1} , Δf_{pi2} , and Δf_{pi3} represent the anchorage seating loss, the time-dependent loss between anchorage seating and detensioning and the loss due to elastic shortening of specimen. Also, f_{pi1} is the residual prestress equal to $f_{pj} - \Delta f_{pi1}$, f_{pi2} is the residual prestress equal to $f_{pi1} - \Delta f_{pi2}$, and f_{pi} is the initial prestress equal to $f_{pi2} - \Delta f_{pi3}$.

Table 5.3 Stress in strand and prestress losses at each fabrication stage (test series 1 and 2)

(Unit: MPa)

Specimen ID	f_{pi}	Δf_{pi1}	f_{pi1}	Δf_{pi2}	f_{pi2}	Δf_{pi3}	f_{pi}	f_{pi}/f_{pu}
N45S150-B70F-1	1,424	137	1,287	39	1,249	52	1,196	0.64
N45S150-B70F-2	1,358	113	1,244	24	1,220	51	1,169	0.63
N45S150-B70F-3	1,390	135	1,254	44	1,211	–	–	–
N45S150-B70F-4	1,457	142	1,316	9	1,307	59	1,248	0.67
N45S150-B70F-R60	1,443	149	1,293	36	1,257	57	1,200	0.65
N45S150-B70F-R75	1,430	143	1,288	46	1,242	56	1,185	0.64
N45S150-B70F-R90	1,458	190	1,268	35	1,233	56	1,177	0.63

Table 5.4 Stress in strand and prestress losses at each fabrication stage (test series 3 and 4)

(Unit: MPa)

Specimen ID	f_{pi}	Δf_{pi1}	f_{pi1}	Δf_{pi2}	f_{pi2}	Δf_{pi3}	f_{pi}	f_{pi}/f_{pu}																																																																																																					
N45S150-B70F-S45	1,420	171	1,249	-11	1,260	48	1,231	0.66																																																																																																					
	1,443	101	1,342	44	1,297				N45S150-B70F-S60	1,470	162	1,308	15	1,293	47	1,283	0.69	1,443	96	1,346	-20	1,367	N45S150-B70F-S75	1,507	179	1,328	23	1,306	43	1,277	0.69	1,443	137	1,306	-29	1,335	N45S150-B70F-S90	1,326	96	1,231	43	1,187	37	1,156	0.62	1,443	157	1,285	87	1,199	N45S150-B70F-C30	1,363	120	1,243	-90	1,333	106	1,228	0.66	N45S150-B70F-C30S	1,443	141	1,302	19	1,283	102	1,182	0.64	N45S150-B70F-C45	1,380	166	1,214	27	1,188	70	1,118	0.60	N45S150-B70F-C60	1,406	151	1,255	18	1,237	58	1,179	0.63	N45S120-B70F	1,482	144	1,338	11	1,327	86	1,241	0.67	N45S90-B70F	1,370	150	1,220	26	1,194	125	1,069	0.57	N45S60-B70F	1,474	172	1,302	23
N45S150-B70F-S60	1,470	162	1,308	15	1,293	47	1,283	0.69																																																																																																					
	1,443	96	1,346	-20	1,367				N45S150-B70F-S75	1,507	179	1,328	23	1,306	43	1,277	0.69	1,443	137	1,306	-29	1,335	N45S150-B70F-S90	1,326	96	1,231	43	1,187	37	1,156	0.62	1,443	157	1,285	87	1,199	N45S150-B70F-C30	1,363	120	1,243	-90	1,333	106	1,228	0.66	N45S150-B70F-C30S	1,443	141	1,302	19	1,283	102	1,182	0.64	N45S150-B70F-C45	1,380	166	1,214	27	1,188	70	1,118	0.60	N45S150-B70F-C60	1,406	151	1,255	18	1,237	58	1,179	0.63	N45S120-B70F	1,482	144	1,338	11	1,327	86	1,241	0.67	N45S90-B70F	1,370	150	1,220	26	1,194	125	1,069	0.57	N45S60-B70F	1,474	172	1,302	23	1,279	242	1,037	0.56										
N45S150-B70F-S75	1,507	179	1,328	23	1,306	43	1,277	0.69																																																																																																					
	1,443	137	1,306	-29	1,335				N45S150-B70F-S90	1,326	96	1,231	43	1,187	37	1,156	0.62	1,443	157	1,285	87	1,199	N45S150-B70F-C30	1,363	120	1,243	-90	1,333	106	1,228	0.66	N45S150-B70F-C30S	1,443	141	1,302	19	1,283	102	1,182	0.64	N45S150-B70F-C45	1,380	166	1,214	27	1,188	70	1,118	0.60	N45S150-B70F-C60	1,406	151	1,255	18	1,237	58	1,179	0.63	N45S120-B70F	1,482	144	1,338	11	1,327	86	1,241	0.67	N45S90-B70F	1,370	150	1,220	26	1,194	125	1,069	0.57	N45S60-B70F	1,474	172	1,302	23	1,279	242	1,037	0.56																								
N45S150-B70F-S90	1,326	96	1,231	43	1,187	37	1,156	0.62																																																																																																					
	1,443	157	1,285	87	1,199				N45S150-B70F-C30	1,363	120	1,243	-90	1,333	106	1,228	0.66	N45S150-B70F-C30S	1,443	141	1,302	19	1,283	102	1,182	0.64	N45S150-B70F-C45	1,380	166	1,214	27	1,188	70	1,118	0.60	N45S150-B70F-C60	1,406	151	1,255	18	1,237	58	1,179	0.63	N45S120-B70F	1,482	144	1,338	11	1,327	86	1,241	0.67	N45S90-B70F	1,370	150	1,220	26	1,194	125	1,069	0.57	N45S60-B70F	1,474	172	1,302	23	1,279	242	1,037	0.56																																						
N45S150-B70F-C30	1,363	120	1,243	-90	1,333	106	1,228	0.66																																																																																																					
N45S150-B70F-C30S	1,443	141	1,302	19	1,283	102	1,182	0.64																																																																																																					
N45S150-B70F-C45	1,380	166	1,214	27	1,188	70	1,118	0.60																																																																																																					
N45S150-B70F-C60	1,406	151	1,255	18	1,237	58	1,179	0.63																																																																																																					
N45S120-B70F	1,482	144	1,338	11	1,327	86	1,241	0.67																																																																																																					
N45S90-B70F	1,370	150	1,220	26	1,194	125	1,069	0.57																																																																																																					
N45S60-B70F	1,474	172	1,302	23	1,279	242	1,037	0.56																																																																																																					

Table 5.5 Stress in strand and prestress losses at each fabrication stage (test series 5)

(Unit: MPa)

Specimen ID	f_{pi}	Δf_{pi1}	f_{pi1}	Δf_{pi2}	f_{pi2}	Δf_{pi3}	f_{pi}	f_{pi}/f_{pu}
N45S150-B70F-5	1,443	162	1,281	18	1,262	55	1,207	0.65
N45S200-B70-1	1,443	146	1,297	-31	1,328	34	1,294	0.70
N45S150-B70-1	1,455	124	1,331	-62	1,393	60	1,333	0.72
N45S120-B70-1	1,478	195	1,283	4	1,279	83	1,196	0.64
N45S90-B70-1	1,385	130	1,255	-3	1,258	132	1,125	0.60
N45S150-B70-C60-1	1,443	153	1,290	23	1,267	59	1,208	0.65
N45S150-B70-C45-1	1,443	165	1,278	-14	1,292	77	1,215	0.65
N45S150-B50-1	1,021	119	901	6	895	39	857	0.46
N45S120-B50-1	1,053	132	921	38	883	57	825	0.44
N45S90-B50-1	1,054	114	940	19	921	97	824	0.44
N45S150-B70-D12-1	1,523	105	1,419	11	1,408	43	1,364	0.73
N45S150-B50-D12	1,523	104	1,420	95	1,324	41	1,283	0.69

Table 5.6 Stress in strand and prestress losses at each fabrication stage (test series 6 and 7)

(Unit: MPa)

Specimen ID	f_{pi}	Δf_{pi1}	f_{pi1}	Δf_{pi2}	f_{pi2}	Δf_{pi3}	f_{pi}	f_{pi}/f_{pu}
N45S200-B70-2	1,443	182	1,261	-4	1,265	35	1,230	0.66
N45S150-B70-2	1,443	154	1,289	85	1,204	57	1,147	0.62
N45S120-B70-2	1,394	198	1,195	31	1,165	82	1,083	0.58
N45S90-B70-2	1,471	207	1,265	3	1,261	143	1,119	0.60
N45S150-B70-C60-2	1,443	148	1,295	6	1,289	66	1,223	0.66
N45S150-B70-C45-2	1,443	185	1,258	6	1,252	81	1,172	0.63
N45S150-B50-2	1,058	134	924	-5	929	44	885	0.48
N45S120-B50-2	1,050	154	896	-17	913	64	849	0.46
N45S90-B50-2	1,058	125	934	-5	939	106	833	0.45
N45S150-B70-D12-2	1,006	98	908	-36	944	32	912	0.49
N45S90-B70-D12	1,526	107	1,419	-4	1,423	120	1,303	0.70
N45A150-B70	1,502	155	1,347	36	1,312	61	1,251	0.67
N35A150-B70	1,426	190	1,235	-29	1,264	66	1,198	0.64
N35A120-B70	1,443	153	1,290	-39	1,329	102	1,226	0.66
N35A150-B50	1,058	3	1,056	-34	1,090	57	1,033	0.56
N35A150-B70-D12	1,523	1	1,523	-44	1,567	58	1,508	0.81

Table 5.7 Stress in strand and prestress losses at each fabrication stage (test series 8)

(Unit: MPa)

Specimen ID	f_{pi}	Δf_{pi1}	f_{pi1}	Δf_{pi2}	f_{pi2}	Δf_{pi3}	f_{pi}	f_{pi}/f_{pu}
N40A200-D70-C40-1	1,841	162	1,679	-6	1,685	91	1,595	0.66
N40A200-D70-C50-1	1,841	149	1,692	-56	1,748	81	1,667	0.69
N40A200-D70-C60-1	1,841	152	1,690	-61	1,750	70	1,681	0.70
N40A200-B70-C40-1	1,449	132	1,317	-26	1,344	69	1,274	0.68
N40A200-D70-S50-1	1,841	131	1,710	81	1,630	38	1,561	0.65
	1,841	154	1,687	119	1,568			
N40A200-D70-S60-1	1,841	160	1,681	43	1,638	37	1,557	0.65
	1,841	191	1,650	101	1,549			
N40A200-D70-S70-1	1,841	158	1,683	135	1,548	35	1,546	0.64
	1,841	146	1,696	82	1,613			

Table 5.8 Stress in strand and prestress losses at each fabrication stage (test series 9)

(Unit: MPa)

Specimen ID	f_{pi}	Δf_{pi1}	f_{pi1}	Δf_{pi2}	f_{pi2}	Δf_{pi3}	f_{pi}	f_{pi}/f_{pu}
N40A200-D70-C40-2	1,841	143	1,699	17	1,681	115	1,566	0.65
N40A200-D70-C50-2	1,841	133	1,708	162	1,545	90	1,455	0.61
N40A200-D70-C60-2	1,841	151	1,690	177	1,513	77	1,436	0.60
N40A200-B70-C40-2	1,449	136	1,313	-36	1,349	89	1,261	0.68
N40A200-D70-S50-2	1,841	130	1,711	15	1,696	51	1,591	0.66
	1,841	148	1,693	105	1,588			
N40A200-D70-S60-2	1,841	136	1,706	386	1,320	43	1,404	0.59
	1,841	141	1,700	124	1,576			
N40A200-D70-S70-2	1,841	150	1,691	190	1,501	45	1,506	0.63
	1,841	127	1,714	115	1,600			

Table 5.9 Stress in strand and prestress losses at each fabrication stage (test series 10)

(Unit: MPa)

Specimen ID	f_{pi}	Δf_{pi1}	f_{pi1}	Δf_{pi2}	f_{pi2}	Δf_{pi3}	f_{pi}	f_{pi}/f_{pu}
H70A200-D70-C30	1,841	132	1,709	83	1,627	96	1,531	0.64
H70A200-D70-C40	1,841	146	1,695	64	1,631	83	1,549	0.65
H70A200-D70-C50	1,841	103	1,696	38	1,658	72	1,587	0.66
H70A200-B70-C40	1,449	163	1,286	75	1,211	58	1,153	0.62
H70A200-D70-S40	1,841	163	1,679	125	1,554	36	1,487	0.62
	1,841	206	1,636	144	1,491			
H70A200-D70-S50	1,841	135	1,706	76	1,631	37	1,609	0.67
	1,841	132	1,709	49	1,661			
H70A200-D70-S60	1,841	136	1,705	157	1,549	37	1,527	0.64
	1,841	138	1,703	132	1,572			

5.4 Transfer Length

5.4.1 Determination of Transfer Length

Since transfer length is defined as a distance required to develop an effective prestress in a prestressing steel (ACI Committee 318, 2011), it is determined from a strain profile measured along the longitudinal location of a pretensioned concrete member. In the strain profile, a constant strain zone, which is called strain plateau, indicates the full transfer of prestress. Strictly speaking, transfer length is the distance from the end of the pretensioned concrete member to the first point of the strain plateau. However, it is generally difficult to find the exact location of the first point because the measured strain profile asymptotically approaches the strain plateau. Nevertheless, it is generally difficult to find the exact location of the first point because the measured strain profile asymptotically approaches the strain plateau.

There are several reasons for this ambiguity. The first reason is the random errors due to the nonhomogeneous nature of concrete and the limited precision of the measurements (Deatherage and Burdette, 1994). The errors can occur at every measuring point. To reduce the deviations, Russell and Burns (1993) suggested a smoothing technique of replacing a reading with the average of the reading and the two neighbor readings. It is illustrated in Figure 5.21 and the averaging is taken by equation (5.17):

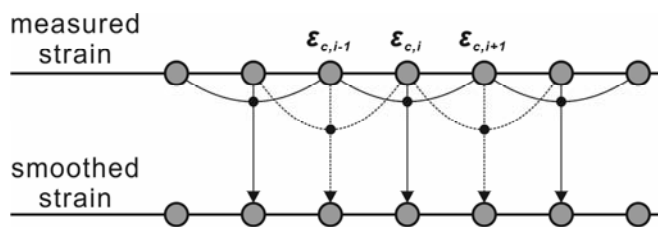


Figure 5.21 Illustration of smoothing technique

$$\varepsilon_{c,i} = \frac{\varepsilon_{c,i-1} + \varepsilon_{c,i} + \varepsilon_{c,i+1}}{3} \quad (5.17)$$

The second reason was an averaging effect that comes from the gauge length of the instrumentations. In case of using DEMEC gauges, the gauge length ranges from 150 to 250 mm. ERSGs used in this experiment had the gauge length of 60 mm for concrete and 5 mm for strand. This effect is magnified by the smoothing technique because it averages the averaged readings once again and lengthens the gauge length.

Two types of methods to determine transfer length can be found in the literature: slope-intercept method and average maximum strain (AMS) method. The AMS is the average of all strains contained on or near the plateau of the full prestressing force. In the slope-intercept method, transfer length is determined as an intersection of the AMS and a line that best fit the measured strains in the transfer zone. Figure 5.22 (a) shows the example of the slope-intercept method.

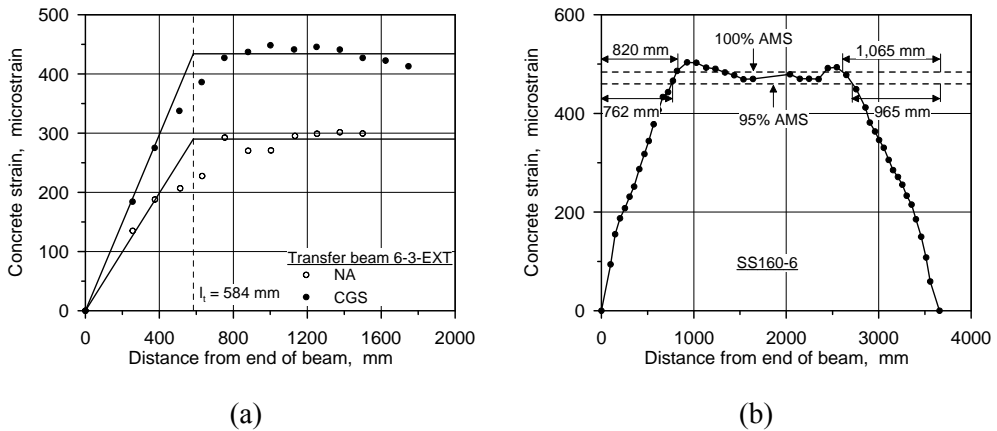


Figure 5.22 Determination of transfer length from the measured strain profile: (a) slope-intercept method (Deatherage and Burdette, 1994); and (b) AMS method (Russell and Burns, 1997)

This method is based on the assumption of the uniform bond stress within the transfer zone. Applying the method to a curvilinear strain profile may produce inaccurate transfer length. Deatherage and Burdette (1994) and Carroll (2009) adopted the slope-intercept method to obtain transfer length.

On the other hand, the AMS method uses the strain profile instead of the fitted line. Thus, it can be applied to any type of strain profile. Russell and Burns (1993) suggested that a lower AMS would be desirable than 100% AMS to compensate for the averaging effects that comes from the long gauge length and the smoothing technique. Even though an ideal strain profile has a distinct end of the transfer zone, the averaging effects rounded it as shown in Figure 5.23. Eventually, the transfer length becomes longer. The reduced AMS makes the transfer length closer to the ideal transfer length.

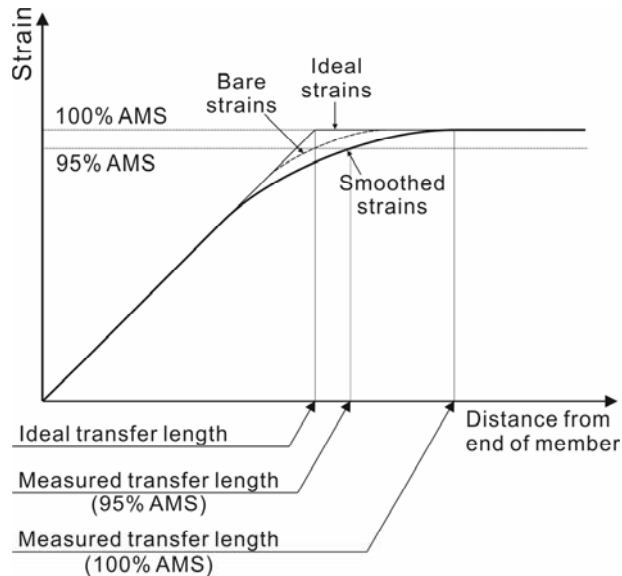


Figure 5.23 Effect of smoothing on measured transfer length

(Russell and Burns, 1993)

Many researchers (Russell and Burns, 1993; Oh and Kim, 2000) adopted 95% AMS method and some (Cousins et al., 1990) used 100% AMS method. Kose and Burkette (2005) applied a multiplier of 0.90 to convert the transfer lengths determined by 100% AMS method into those by 95% AMS method.

In this study, 95% AMS method was adopted to obtain transfer lengths from the measured strain profiles. For strand gauges, the averaging effects are negligible because strand gauge is a short and concentrated measuring tool. Instead, strand gauges are attached at interval wider than that of DEMEC gauges. Equating the transfer length with the distance to the first measurement point of strain plateau will result in the longest transfer length because this method implies a linear interpolation between measurements, which ignores the shape of the strain curve asymptotically approaching the strain plateau. A simple way to reduce the error is to lower the strain plateau line such as 95% AMS method. In Table 5.10 through 5.13, the transfer lengths measured by 95% AMS method are tabularized. The strain profiles can be found in Appendix B.

Table 5.10 Measured transfer length (test series 1 ~ 4)

Specimen ID	f'_{ci} (MPa)	f_{pi} (MPa)	Measured transfer length (mm)	
			Dead end	Cut end
N45S150-B70F-1	32.8	1,196	658 672*	1,103 1,116*
N45S150-B70F-2	32.8	1,169	638 721*	1,104 1,285*
N45S150-B70F-4	32.9	1,248	526	1,110
N45S150-B70F-R60	32.9	1,200	500	1,041
N45S150-B70F-R75	32.9	1,185	–	927
N45S150-B70F-R90	32.9	1,177	–	718
N45S150-B70F-S45	32.3	1,231	991	965
N45S150-B70F-S60	32.3	1,283	–	1,012
N45S150-B70F-S75	32.3	1,277	–	831
N45S150-B70F-S90	32.3	1,156	–	1,210
N45S150-B70F-C30	38.8	1,228	562	820
N45S150-B70F-C30S	38.8	1,182	–	739
N45S150-B70F-C45	38.8	1,118	–	680
N45S150-B70F-C60	38.8	1,179	–	902
N45S120-B70F	38.8	1,241	–	607
N45S90-B70F	38.8	1,069	–	717
N45S60-B70F	38.8	1,037	575	1,306

Note: Transfer lengths were measured from the concrete strain profile.

*Transfer length was measured from the strand strain profile.

Table 5.11 Measured transfer length (test series 5 ~ 6)

Specimen ID	f'_{ci} (MPa)	f_{pi} (MPa)	Measured transfer length (mm)	
			Dead end	Cut end
N45S150-B70F-5	36.5	1,207	811	840
N45S200-B70-1	36.5	1,294	946	949
N45S150-B70-1	36.5	1,333	698	826
N45S120-B70-1	36.5	1,196	963	1,067
N45S90-B70-1	36.5	1,125	698	1,815
N45S150-B70-C60-1	36.5	1,208	1009	935
N45S150-B70-C45-1	36.5	1,215	783	805
N45S150-B50-1	36.5	857	668	660
N45S120-B50-1	36.5	825	839	833
N45S90-B50-1	36.5	824	589	709
N45S150-B70-D12-1	36.5	1,364	556	770
N45S150-B50-D12	36.5	1,283	595	830
N45S200-B70-2	29.0	1,230	846	891
N45S150-B70-2	29.0	1,147	800	822
N45S120-B70-2	29.0	1,083	874	913
N45S90-B70-2	29.0	1,119	877	810
N45S150-B70-C60-2	29.0	1,223	841	953
N45S150-B70-C45-2	29.0	1,172	822	1,006
N45S150-B50-2	29.0	885	770	787
N45S120-B50-2	29.0	849	681	801
N45S90-B50-2	29.0	833	707	675
N45S150-B70-D12-2	29.0	912	779	692
N45S90-B70-D12	29.0	1,303	919	772

Note: All the transfer lengths were measured from the strand strain profile.

Table 5.12 Measured transfer length (test series 7 ~ 8)

Specimen ID	f'_{ci} (MPa)	f_{pi} (MPa)	Measured transfer length (mm)	
			Dead end	Cut end
N45A150-B70	34.2	1,251	626*	754*
N35A150-B70	30.7	1,198	814*	935*
N35A120-B70	30.7	1,226	653*	735*
N35A150-B50	30.7	1,033	661*	756*
N35A150-B70-D12	30.7	1,508	838*	1,075*
N40A200-D70-C40-1	31.2	1,595	642	907
N40A200-D70-C50-1	31.2	1,667	619	1,202
N40A200-D70-C60-1	31.2	1,681	764	774
N40A200-B70-C40-1	31.2	1,274	575	644
N40A200-D70-S50-1	31.2	1,561	880	1,430
N40A200-D70-S60-1	31.2	1,557	731	870
N40A200-D70-S70-1	31.2	1,546	638	1,276

Note: Transfer lengths were measured from the concrete strain profile.

*Transfer length was measured from the strand strain profile.

Table 5.13 Measured transfer length (test series 9 ~ 10)

Specimen ID	f'_{ci} (MPa)	f_{pi} (MPa)	Measured transfer length (mm)	
			Dead end	Cut end
N40A200-D70-C40-2	32.2	1,566	564	848
N40A200-D70-C50-2	32.2	1,455	552	677
N40A200-D70-C60-2	32.2	1,436	589	799
N40A200-B70-C40-2	32.2	1,261	399	487
N40A200-D70-S50-2	32.2	1,591	694	904
N40A200-D70-S60-2	32.2	1,404	1,618	1,060
N40A200-D70-S70-2	32.2	1,506	1,080	1,117
H70A200-D70-C30	46.0	1,531	477	681
H70A200-D70-C40	46.0	1,549	458	709
H70A200-D70-C50	46.0	1,587	324	876
H70A200-B70-C40	46.0	1,153	411	576
H70A200-D70-S40	46.0	1,487	526	669
H70A200-D70-S50	46.0	1,609	523	614
H70A200-D70-S60	46.0	1,527	393	997

Note: All the transfer lengths were measured from the concrete strain profile.

5.4.2 Effect of Test Variables on Transfer Length

In this section, an effect of each test variable is analyzed based on a comparison of the measured transfer lengths. To reasonably evaluate an effect of a specific test variable, the comparison was made among the specimens that have the identical conditions except for the test variable under investigation. Initial prestress and concrete compressive strength at transfer cannot be exactly identical for the comparable specimens. Their effects on transfer length were first evaluated and the transfer lengths were adjusted to exclude their effects when investigating the effects of the other test variables.

5.4.2.1 Initial Prestress

Grade 1,860 strand

In average, the residual strand stress just after detensioning was approximately 63% of the nominal tensile strength of strand. Several specimens in the test series 5 and 6 were subjected to a lower level of prestressing force, approximately 45% of the nominal tensile strength of strand. Table 5.14 summarizes the two groups of specimens prestressed with the high and low level of prestressing force. In the table, the transfer length at cut end of the specimen N45S90-B70-1 was abnormally high because the cut end of the specimen was broken into pieces at detensioning. The dimension of the cross section was not enough to absorb the energy due to the sudden release of the prestressing force. This abnormal transfer length was excluded from the analysis.

Table 5.14 Influence of initial prestress on transfer length

Specimen ID	f_{pi} / f_{pu}	Transfer length (mm)		Ratio		ACI318 Eq. (12-4)
		Dead	Cut	Dead	Cut	
N45S150-B70-1	0.72	698	826	1.05	1.25	960
N45S150-B50-1	0.46	668	660	1.00	1.00	617
N45S150-B70-2	0.62	800	822	1.04	1.04	826
N45S150-B50-2	0.48	770	787	1.00	1.00	638
N45S120-B70-1	0.64	963	1,067	1.15	1.28	862
N45S120-B50-1	0.44	839	833	1.00	1.00	595
N45S120-B70-2	0.58	874	913	1.28	1.14	780
N45S120-B50-2	0.46	681	801	1.00	1.00	612
N45S90-B70-1	0.61	698	1,815*	1.18	–	811
N45S90-B50-1	0.44	589	709	1.00	–	594
N45S90-B70-2	0.60	877	810	1.24	1.20	806
N45S90-B50-2	0.45	707	675	1.00	1.00	600
Average	0.63			1.16	1.18	
	0.45			1.00	1.00	

*This transfer length was excluded from the analysis.

The transfer lengths were increased by 16% at dead end and 18% at cut end as the initial prestress was increased by 38%. The increasing ratio of the transfer length is similar to that of $\sqrt{f_{pi}}$. According to Balázs (1992), transfer length has different relationships with initial prestress depending on bond-slip relationship of strand. In the analysis by Balázs, the bond-slip relationship varied with the coefficient a . If $a=0$, equations (2.10) and (2.11) gives a constant bond stress and a linear distribution of strand stress within the transfer zone, respectively. Equation (2.13) yields transfer length proportional to initial prestress. If $a=1/3$, bond stress distribution is linear and strand stress distribution is parabolic within the transfer zone. Transfer length is proportional to a square root of initial prestress. Thus, the relationship observed in this experiment implies the linear bond stress distribution

and parabolic strand stress distribution within the transfer zone of the specimens.

The transfer lengths listed in Table 5.14 are plotted on a bar chart in Figure 5.24. The figure also include the transfer lengths predicted by the two equations of the ACI318 code, $f_{pe}d_b/21$ and $50d_b$. The transfer lengths of the specimens with the low initial prestress and the specimens with small dimensions of cross section exceed the predictions by both equations of the ACI318 code provisions.

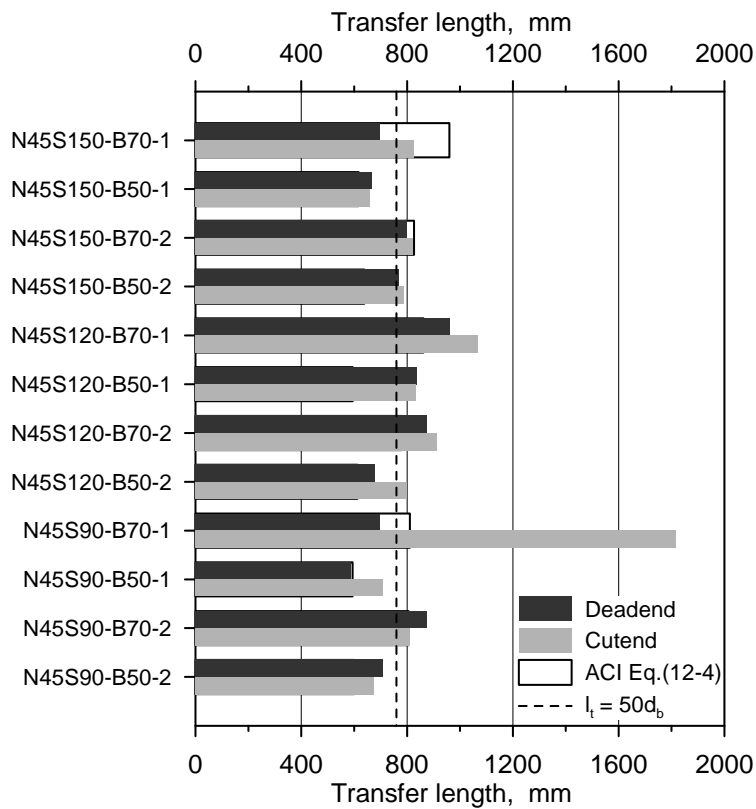


Figure 5.24 Influence of initial prestress on transfer length

High Strength Strand

Table 5.15 and Figure 5.25 compare the effect of the initial prestress on transfer lengths of high strength strands. The transfer lengths were increased by 21% at dead end and 46% at cut end as the initial prestress was increased by 28%. At dead end, the average increasing ratio of the transfer length was slightly lower than that of f_{pi} . Except one case, however, the increasing ratios of transfer length were similar to that of $\sqrt{f_{pi}}$ as shown in Table 5.15. On the other hand, the average increasing ratio of transfer length at cut end was much larger than that of f_{pi} . It implies that the dynamic impact induced by sudden release of prestress was greater than the increase in the initial prestress.

Table 5.15 Influence of initial prestress on transfer length of high strength strand

Specimen ID	f_{pi} (MPa)	Transfer length (mm)		Ratio		ACI318 Eq. (12-4)
		Dead	Cut	Dead	Cut	
N40A200-B70-C40-1	1,274	575	644	1.00	1.00	918
N40A200-D70-C40-1	1,595	642	907	1.12	1.41	1,160
N40A200-B70-C40-2	1,261	399	487	1.00	1.00	908
N40A200-D70-C40-2	1,566	564	848	1.41	1.74	1,160
H70A200-B70-C40	1,153	411	576	1.00	1.00	831
H70A200-D70-C40	1,549	458	709	1.11	1.23	1127
Average	1,229			1.00	1.00	
	1,570			1.21	1.46	

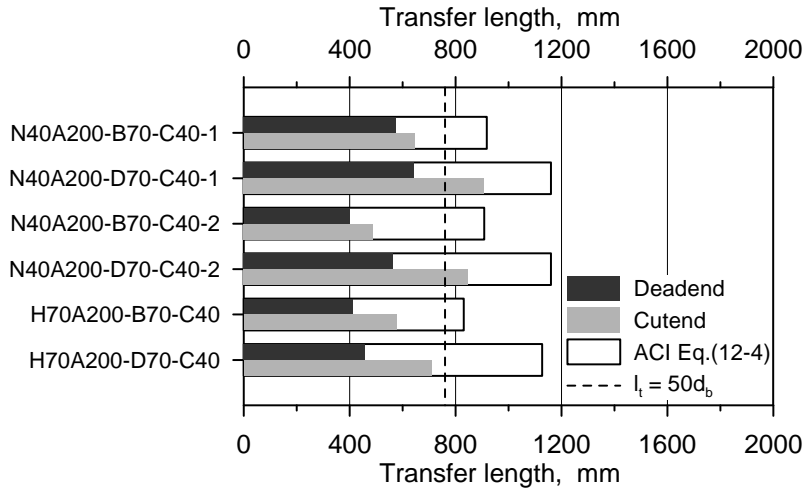


Table 5.25 Influence of initial prestress on transfer length of high strength strand

5.4.2.2 Concrete Compressive Strength at Transfer

Concrete compressive strength at transfer f'_{ci} has been acknowledged as a highly influential factor to transfer length. Concrete compressive strength greatly affects the resistance of concrete to relative deformation of a strand embedded in the concrete. In most empirical equations, transfer length is inversely proportional to $(f'_{ci})^k$ as shown in Table 2.1. The value of k is usually 1, 1/2, or 2/3.

Table 5.16 and 5.17 list the transfer lengths of the comparable specimens in two categories: specimens with a single strand and two strands. Because each specimen had an individual initial prestress, the transfer lengths were normalized with respect to $\sqrt{f_{pi}}$ using the relationship between transfer length and initial prestress. In the tables, the specimens had the concrete compressive strength at transfer ranged from 31.2 MPa to 46.0 MPa. In Table 5.17, the transfer length at dead end of the specimen N40A200-D70-S60-2 was abnormally high because the strain plateau zone was not

well defined. The strain distribution between both transfer zones was inclined and it caused much longer transfer length at dead end than those of the comparable specimens. This abnormal transfer length was excluded from the analysis.

Averaging all the normalized transfer length, the normalized transfer length was decreased by 23% at dead end and 9% at cut end as the concrete compressive strength at transfer increased from 32.2 MPa to 46.0 MPa. Averaging the normalized transfer lengths at both ends, the increasing ratios of the normalized transfer length are similar to that of $1/\sqrt{f'_{ci}}$. It implies that transfer length is inversely proportional to $\sqrt{f'_{ci}}$.

Interestingly, the normalized transfer length for $f'_{ci} = 31.2$ MPa was increased by 24% at dead end and 22% at cut end in comparison with $f'_{ci} = 32.2$ MPa. Since the concrete compressive strengths at transfer are almost the same, there might be another reason for these considerable increases in transfer length. A possible explanation is the longer curing period. A larger shrinkage strain might provide a beneficial effect on the shorter transfer lengths.

The transfer lengths listed in Table 5.16 and 5.17 are also plotted on bar charts in Figure 5.26 and 5.27, respectively. It can be seen in the figures that the equation $l_t = 50d_b$ can be unconservative for the transfer length of the high-strength strands, even though high strength concrete is employed. All of the transfer lengths at dead end fell below the ACI318-11 Eq. (12-4) but two transfer lengths at cut end exceed the predictions and four approached the predictions.

Table 5.16 Influence of concrete compressive strength at transfer on transfer length of specimens with a single strand

Specimen ID	f'_{ci} (MPa)	Transfer length (mm)		$l_t/\sqrt{f_{pi}}$ (mm·MPa ^{-0.5})		Ratio	
		Dead	Cut	Dead	Cut	Dead	Cut
N40A200-D70-C40-1	31.2	642	907	16.1	22.7	1.13	1.06
N40A200-D70-C40-2	32.2	564	848	14.2	21.4	1.00	1.00
H70A200-D70-C40	46.0	458	709	11.6	18.0	0.82	0.84
N40A200-D70-C50-1	31.2	619	1,202	15.2	29.4	1.05	1.66
N40A200-D70-C50-2	32.2	552	677	14.5	17.8	1.00	1.00
H70A200-D70-C50	46.0	324	876	8.1	22.0	0.56	1.24
N40A200-B70-C40-1	31.2	575	644	16.1	18.0	1.43	1.31
N40A200-B70-C40-2	32.2	399	487	11.2	13.7	1.00	1.00
H70A200-B70-C40	46.0	411	576	12.1	17.0	1.08	1.24
Average	31.2					1.20	1.34
	32.2					1.00	1.00
	46.0					0.82	1.11

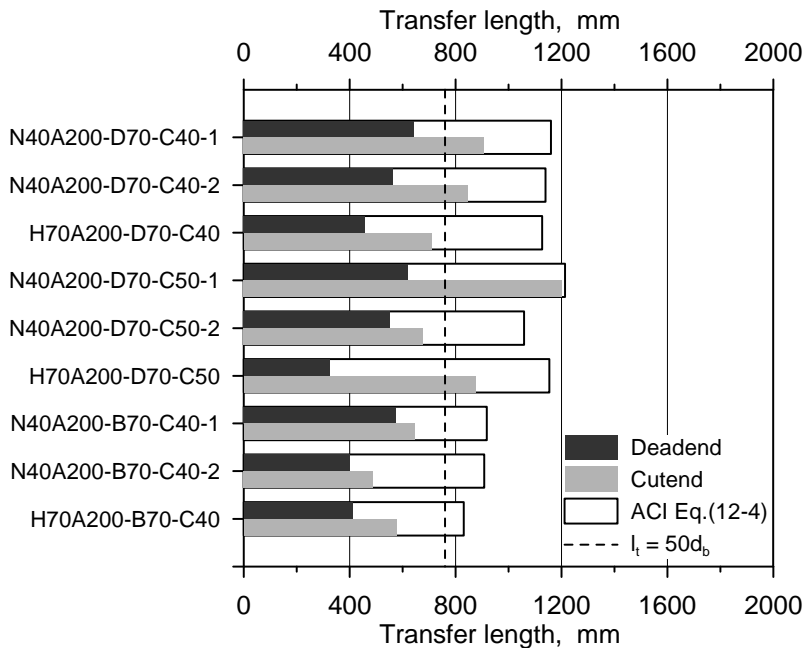


Figure 5.26 Influence of concrete compressive strength at transfer on transfer length of specimens with a single strand

Table 5.17 Influence of concrete compressive strength at transfer on transfer length of specimens with two strands

Specimen ID	f'_{ci} (MPa)	Transfer length (mm)		$l_t/\sqrt{f_{pi}}$ (mm·MPa ^{-0.5})		Ratio	
		Dead	Cut	Dead	Cut	Dead	Cut
N40A200-D70-S50-1	31.2	880	1,430	22.3	36.2	1.28	1.60
N40A200-D70-S50-2	32.2	694	904	17.4	22.7	1.00	1.00
H70A200-D70-S50	46.0	523	614	13.0	15.3	0.75	0.67
N40A200-D70-S60-1	31.2	731	870	–	22.0	–	0.78
N40A200-D70-S60-2	32.2	1,618*	1,060	–	28.3	–	1.00
H70A200-D70-S60	46.0	393	997	–	25.5	–	0.90
Average	31.2					1.28	1.19
	32.2					1.00	1.00
	46.0					0.75	0.79

*This transfer length was excluded from the analysis.

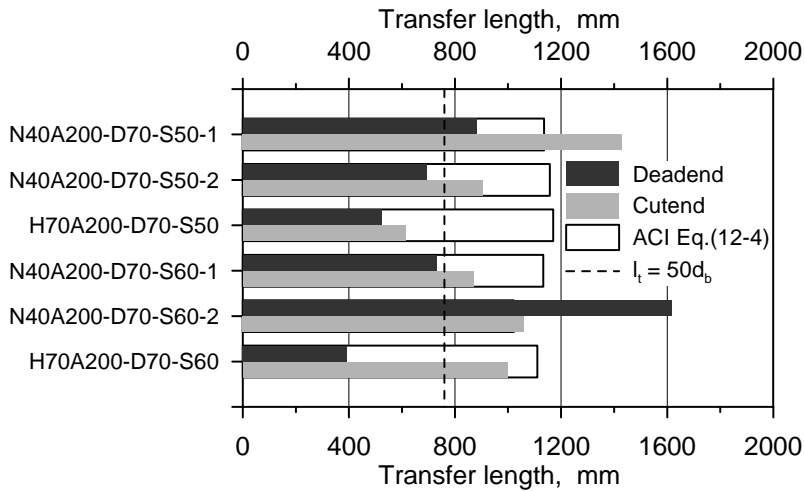


Figure 5.27 Influence of concrete compressive strength at transfer on transfer length of specimens with two strands

5.4.2.3 Strand Diameter

Strand diameter is the factor that determines the contact area of the strand to the surrounding concrete. Thus, it has been generally accepted that transfer length increases proportionally to the strand diameter. However, the opposite trend was reported in some studies (Deatherage and Burdette, 1994; Kose and Burkette, 2005; and Carroll, 2009). According to fib (2000), transfer length is proportional to strand diameter if bond stress is constant along the transfer zone and the amount of the bond stress is independent of strand diameter.

Table 5.18 lists the comparable specimens regarding the effect of the strand diameter. Because each specimen had an individual initial prestress and concrete compressive strength at transfer, the transfer lengths were normalized with respect to $\sqrt{f_{pi}/f'_{ci}}$ using the relationships previously obtained.

Table 5.18 Influence of strand diameter on transfer length

Specimen ID	d_b (mm)	Transfer length (mm)		$l_t/\sqrt{f_{pi}/f'_{ci}}$ (mm)		Ratio	
		Dead	Cut	Dead	Cut	Dead	Cut
N45S150-B70-1	15.2	698	826	115.5	136.7	1.00	1.00
N45S150-B70-2	15.2	800	822	127.1	130.7		
N45S150-B70-D12-1	12.7	556	770	90.9	125.9	0.75	0.94
N45S90-B70-1	15.2	698	1,815*	–	–	1.00	1.00
N45S90-B70-2	15.2	877	810	141.2	130.4		
N45S90-B70-D12	12.7	919	772	137.0	115.2	0.97	0.88
Average	15.2					1.00	1.00
	12.7					0.86	0.91

* This transfer length was excluded from the analysis.

In average, the normalized transfer lengths of 12.7 mm diameter strand were

shorter than those of 15.2 mm diameter strand. The decreasing ratio of the normalized transfer length was 0.86 at dead end and 0.91 at cut end, which is slightly higher than that of the strand diameter, 0.84, but their differences are negligible. It implies that transfer length is approximately proportional to strand diameter.

The transfer lengths listed in Table 5.18 are plotted on a bar chart in Figure 5.28. It can be seen that both equations of the ACI318 code provisions gave the unconservative transfer lengths for the specimens with 12.7 mm diameter strand.

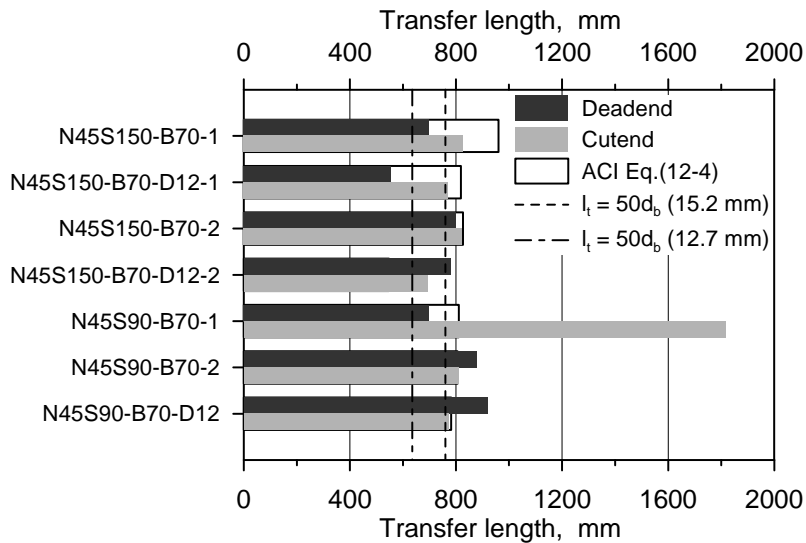


Figure 5.28 Influence of strand diameter on transfer length

In summary, the effects of initial prestress, concrete compressive strength at transfer, and strand diameter can be expressed as the following relationship:

$$l_t \propto \sqrt{\frac{f_{pi}}{f'_{ci}}} d_b \quad (5.18)$$

This relationship is the same as the equation (2.29) proposed by Oleśniewicz (1975). The proportionality constant in the equation is given as relative transfer length Ψ . Oleśniewicz stated that the relative transfer length had the value of 10, 7, and 13 for average, lower bound, and upper bound. Hereafter, relative transfer lengths will be compared to evaluate the effects of the test variables on transfer length.

5.4.2.4 Cover Depth and Cross Section Size

A primary purpose of concrete cover depth is to prevent a splitting crack from developing along the strand. For most specimens in this experiment, no visible splitting cracks were observed on the surface of the specimens. Three specimens, however, suffered an explosive damage near the cut end at release of prestress. The damaged specimens had a shallow cover depth or small cross section sizes.



(a)



(b)

Figure 5.29 Damage due to sudden release of prestress: (a) N45S150-B70F-C30S;
and (b) N45S60-B70F

Figure 5.29 shows the pictures of the damaged specimens due to the sudden release. The side concrete cover at the cut end of the specimen N45S150-B70F-C30S fell apart from the specimen (see Figure 5.29 (a)). A part of the specimens N45S60-B70F and N45S90-B70-1 was totally exploded within some distance from the cut end (see Figure 5.29 (b)). The transfer length at cut end of the specimen N45S150-B70F-C30S was not significantly affected by the damage but excessively longer transfer lengths were measured at the cut ends of the other two specimens. These abnormal transfer lengths were not included in the analysis.

Grade 1,860 strand

Table 5.19 and 5.20 list the transfer lengths of the comparable specimens regarding the effect of cover depth in two categories: fully bonded and partially debonded strands. The considered clear cover depth ranged from 22.4 mm to 67.4 mm.

The transfer lengths in each category presented conflicting trends on the effect of the cover depth. For fully bonded strands, the relative transfer lengths at dead end did not vary over the range of the cover depth. But a significant reduction occurred at cut end, which contradicts the tendency reported in the literature (fib, 2000; Oh and Kim, 2000).

The test results of partially debonded strands showed that the shallower clear cover depths of 37.4 mm and 52.4 mm caused longer transfer lengths but the maximum transfer length was measured at the clear cover depths of 52.4 mm.

The transfer lengths listed in Table 5.19 and 5.20 are also plotted on bar charts in Figure 5.30 and 5.31, respectively.

Table 5.19 Influence of cover depth on transfer length of fully bonded Grade 1,860 strand

Specimen ID	c_c (mm)	Transfer length (mm)		Ψ		Ratio	
		Dead	Cut	Dead	Cut	Dead	Cut
N45S150-B70F-1	67.4	658	1,103	7.2	12.1	1.00	1.00
N45S150-B70F-2	67.4	638	1,104	7.1	12.2		
N45S150-B70F-4	67.4	526	1,110	5.6	11.9		
N45S150-B70F-C60	52.4	–	902	–	10.8	–	0.90
N45S150-B70F-C45	37.4	–	680	–	8.4	–	0.69
N45S150-B70F-C30	22.4	562	820	6.6	9.6	1.00	0.77
N45S150-B70F-C30S	22.4	–	739	–	8.8		

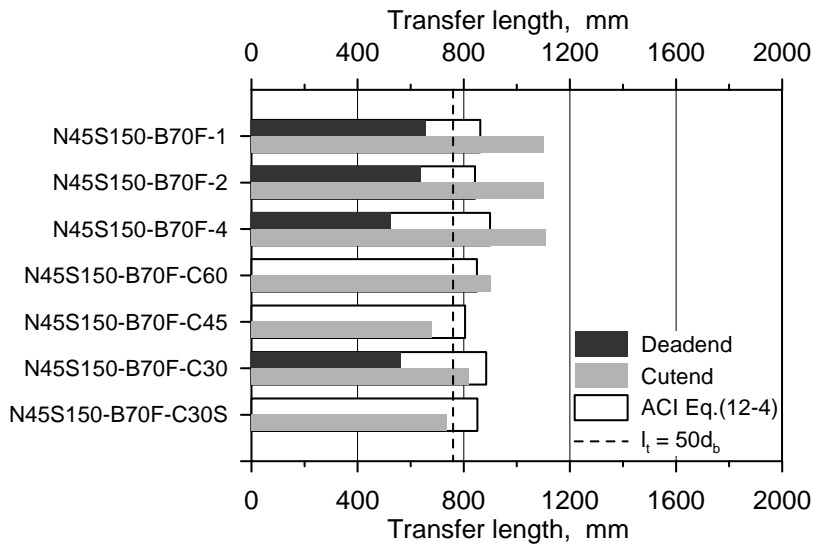


Figure 5.30 Influence of cover depth on transfer length of fully bonded Grade 1,860 strand

Table 5.20 Influence of cover depth on transfer length of partially debonded Grade 1,860 strand

Specimen ID	c_c (mm)	Transfer length (mm)		Ψ		Ratio	
		Dead	Cut	Dead	Cut	Dead	Cut
N45S150-B70-1	67.4	698	826	7.6	9.0	1.00	1.00
N45S150-B70-C60-1	52.4	1,009	935	11.6	10.7	1.52	1.19
N45S150-B70-C45-1	37.4	783	805	9.0	9.2	1.18	1.02
N45S150-B70-2	67.4	800	822	8.4	8.6	1.00	1.00
N45S150-B70-C60-2	52.4	841	953	8.6	9.7	1.02	1.12
N45S150-B70-C45-2	37.4	822	1,006	8.6	10.5	1.02	1.21
Average	67.4					1.00	1.00
	52.4					1.27	1.16
	37.4					1.10	1.11

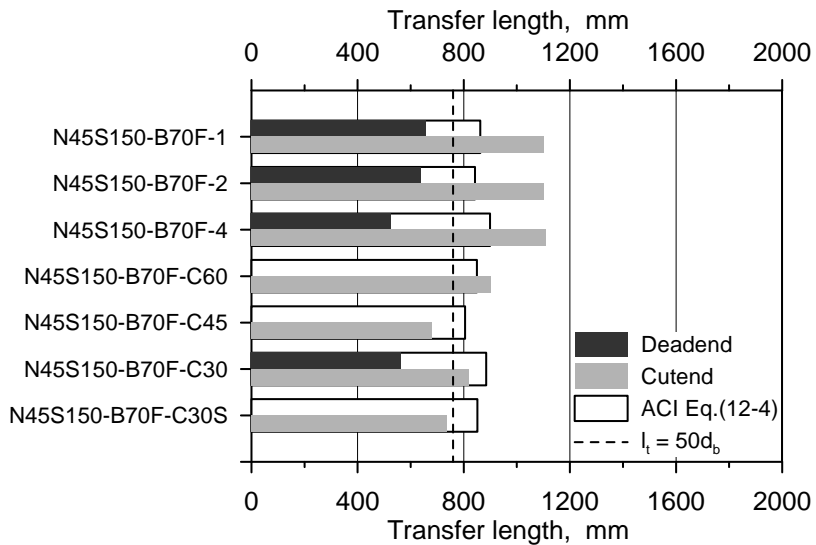


Figure 5.31 Influence of cover depth on transfer length of partially debonded Grade 1,860 strand

Table 5.21 and 5.22 list the transfer lengths of the comparable specimens regarding the effect of cross section size in two categories: fully bonded and partially debonded strands. The considered cross section size ranged from 60 mm to 200 mm.

The transfer lengths in each category presented inconclusive trends on the effect of the cross section, similarly to the cover depth. For fully bonded strands, the transfer lengths at dead end slightly increased over the range of the cross section size. But a significant reduction occurred at cut end. Table 5.22 showed the inconsistent test results for partially debonded strands.

The transfer lengths listed in Table 5.21 and 5.22 are also plotted on bar charts in Figure 5.32 and 5.33, respectively.

It can be concluded that sufficient concrete confinement was provided for the specimens and radial cracks were not significantly developed around strand because no visible splitting cracks were observed on the concrete surface and most relative transfer lengths fell between the upper and lower bound value.

In addition, no general trend was found in the range of the cover depth considered in this experiment. It means that there were no detrimental effects for smaller values of the cover depth.

Table 5.21 Influence of cross section size on transfer length of fully bonded Grade 1,860 strand

Specimen ID	b and h (mm)	Transfer length (mm)		Ψ		Ratio	
		Dead	Cut	Dead	Cut	Dead	Cut
N45S150-B70F-1	150	658	1,103	7.2	12.1	1.00	1.00
N45S150-B70F-2	150	638	1,104	7.1	12.2		
N45S150-B70F-4	150	526	1,110	5.6	11.9		
N45S120-B70F	120	–	607	–	7.1	–	0.59
N45S90-B70F	90	–	717	–	9.0	–	0.75
N45S60-B70F	60	575	1,306*	7.4	–	1.11	–

* This transfer length was excluded from the analysis.

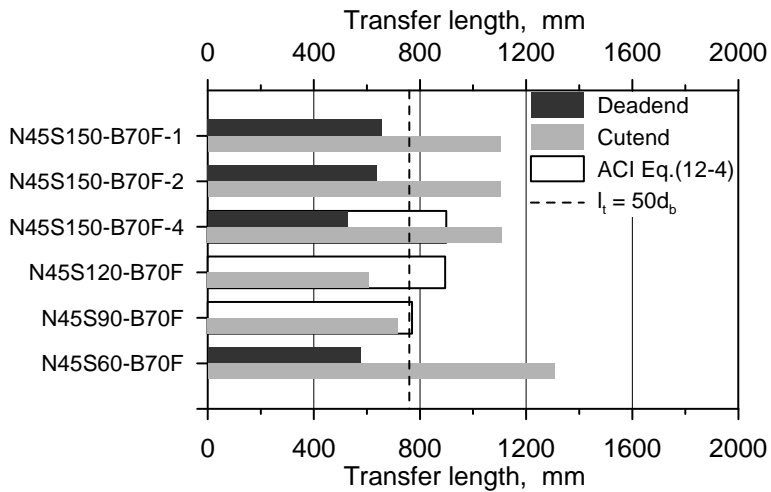


Table 5.32 Influence of cross section size on transfer length of fully bonded Grade 1,860 strand

Table 5.22 Influence of cross section size on transfer length of partially debonded Grade 1,860 strand

Specimen ID	b and h (mm)	Transfer length (mm)		Ψ		Ratio	
		Dead	Cut	Dead	Cut	Dead	Cut
N45S200-B70-1	200	946	949	10.5	10.5	1.38	1.17
N45S150-B70-1	150	698	826	7.6	9.0	1.00	1.00
N45S120-B70-1	120	963	1,067	11.1	12.3	1.46	1.36
N45S90-B70-1	90	698	1,815*	8.3	–	1.09	–
N45S200-B70-2	200	846	891	8.6	9.0	1.02	1.05
N45S150-B70-2	150	800	822	8.4	8.6	1.00	1.00
N45S120-B70-2	120	874	913	9.5	9.9	1.12	1.14
N45S90-B70-2	90	877	810	9.3	8.6	1.11	1.00
Average	200					1.20	1.11
	150					1.00	1.00
	120					1.29	1.25
	90					1.10	1.00

* This transfer length was excluded from the analysis.

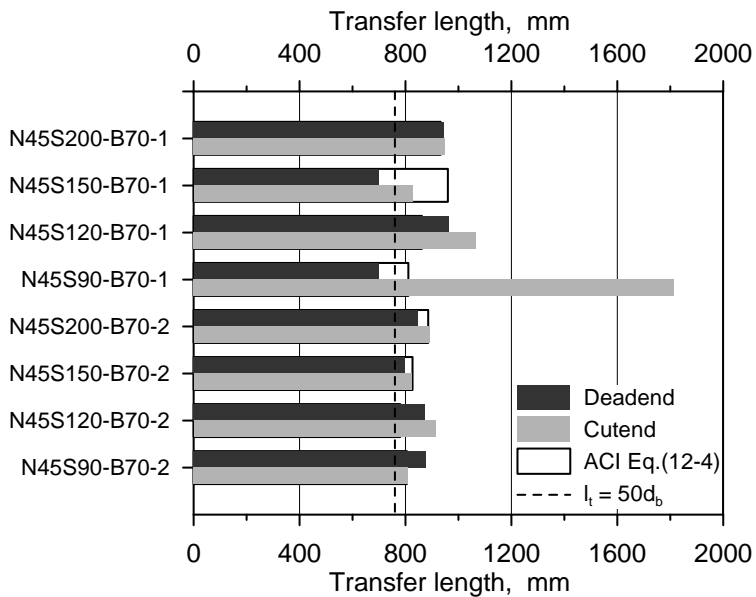


Table 5.33 Influence of cross section size on transfer length of partially debonded Grade 1,860 strand

High Strength Strand

Table 5.23 and 5.24 list the transfer lengths of the comparable specimens regarding the effect of cover depth in two categories: normal strength concrete and high strength concrete. The considered clear cover depth was in the range of 22.4 mm to 52.4 mm.

For normal strength concrete, decrease in the clear cover depth from 52.4 mm to 42.4 mm reduced the transfer length at dead end by 15% but raised the transfer length at cut end by 9%. The further decrease in the clear cover depth did not affect the transfer length.

For high strength concrete, the transfer lengths at dead end increased as the clear cover depth decreased but the opposite trend was seen at cut end.

The transfer lengths listed in Table 5.23 and 5.24 are also plotted on bar charts in Figure 5.34 and 5.35, respectively.

A general trend was not found in the range of the concrete cover depth considered in this experiment. Hence, the current code provisions regarding cover depth can be applied to high strength strand. Many of relative transfer lengths, however, fell below the lower bound value. When comparing with ACI318-11 Eq. (12-4), the measured transfer lengths were much smaller than the predicted values as shown in Figure 5.34 and 5.35. It should be noted that all specimens were cured with air curing condition. Air curing condition can reduce transfer length considerably. Detailed discussion on the effect of curing condition will be given in 5.4.2.6.

Table 5.23 Influence of cover depth on transfer length of high strength strand embedded in normal strength concrete

Specimen ID	c_c (mm)	Transfer length (mm)		Ψ		Ratio	
		Dead	Cut	Dead	Cut	Dead	Cut
N40A200-D70-C60-1	52.4	764	774	6.8	6.9	1.23	0.64
N40A200-D70-C50-1	42.4	619	1,202	5.5	10.8	1.00	1.00
N40A200-D70-C40-1	32.4	642	907	5.9	8.3	1.06	0.77
N40A200-D70-C60-2	52.4	589	799	5.8	7.8	1.07	1.19
N40A200-D70-C50-2	42.4	552	677	5.4	6.6	1.00	1.00
N40A200-D70-C40-2	32.4	564	848	5.3	8.0	0.99	1.21
Average	52.4					1.15	0.91
	42.4					1.00	1.00
	32.4					1.02	0.99

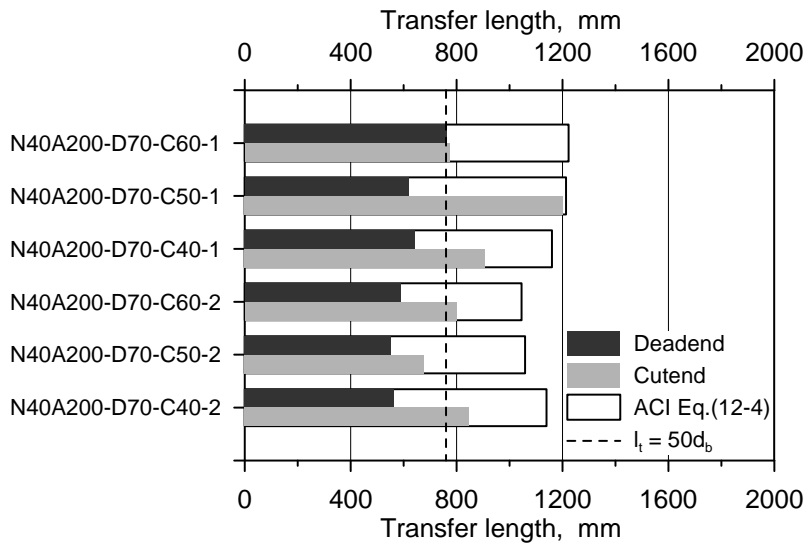


Table 5.34 Influence of cover depth on transfer length of high strength strand embedded in normal strength concrete

Table 5.24 Influence of cover depth on transfer length of high strength strand embedded in high strength concrete

Specimen ID	c_c (mm)	Transfer length (mm)		Ψ		Ratio	
		Dead	Cut	Dead	Cut	Dead	Cut
H70A200-D70-C50	42.4	324	876	3.6	9.8	1.00	1.00
H70A200-D70-C40	32.4	458	709	5.2	8.0	1.43	0.82
H70A200-D70-C30	22.4	477	681	5.4	7.7	1.50	0.79

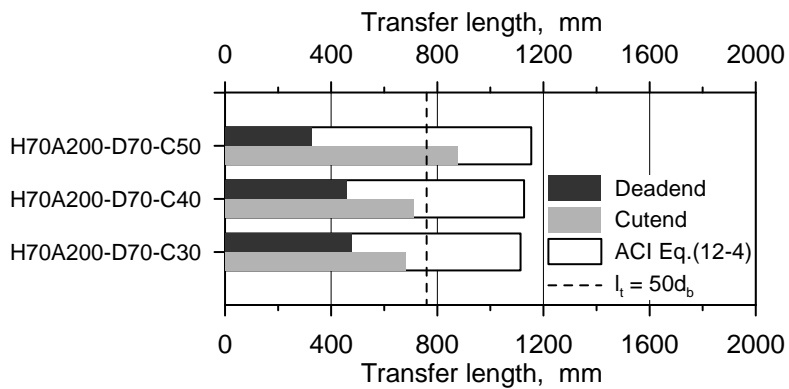


Table 5.35 Influence of cover depth on transfer length of high strength strand embedded in high strength concrete

5.4.2.5 Strand Spacing

Grade 1,860 strand

Table 5.25 lists the transfer lengths of the comparable specimens regarding the effect of strand spacing. The considered center-to-center spacing ranged from 45 mm to 90 mm. The transfer lengths presented no clear trends with the center-to-center spacing of the strands. The transfer lengths listed in Table 5.25 are also plotted on bar charts in Figure 5.36.

Table 5.25 Influence of strand spacing on transfer length of fully bonded Grade 1,860 strand

Specimen ID	s_p (mm)	Transfer length (mm)		Ψ		Ratio	
		Dead	Cut	Dead	Cut	Dead	Cut
N45S150-B70F-S45	45	991	965	10.6	10.3	1.00	1.00
N45S150-B70F-S60	60	–	1,012	–	10.6	–	1.03
N45S150-B70F-S70	75	–	831	–	8.7	–	0.84
N45S150-B70F-S90	90	–	1,210	–	13.4	–	1.29

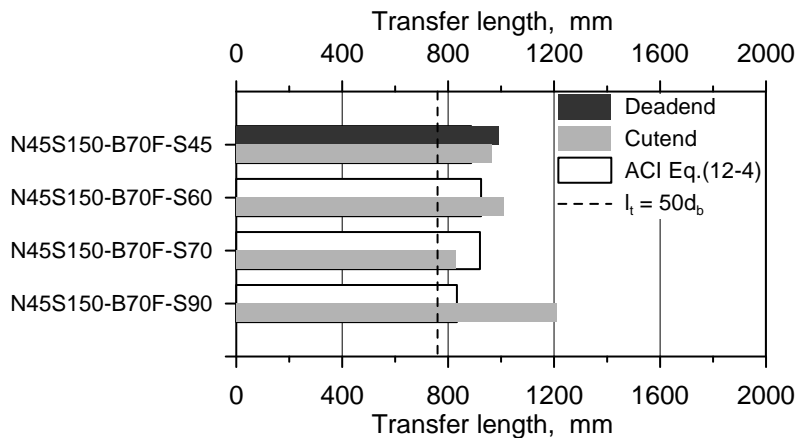


Table 5.36 Influence of strand spacing on transfer length of fully bonded Grade 1,860 strand

High Strength Strand

Table 5.26 and 5.27 list the transfer lengths of the comparable specimens regarding the effect of strand spacing in two categories: normal strength concrete and high strength concrete. The considered center-to-center spacing ranged from 40 mm to 70 mm.

The transfer lengths presented no clear trends with the center-to-center spacing of the strands. Smaller spacing of strands causes longer transfer length at dead end for high strength concrete but the same trend was not found in the other test conditions.

The transfer lengths listed in Table 5.26 and 5.27 are also plotted on bar charts in Figure 5.37 and 5.38, respectively.

In conclusion, no harmful effects on transfer length were found for the center-to-center spacing considered in this experiment. This conclusion agrees with the findings in several researches (Cousins et al. 1993 and 1994; Deatherage and Burdette, 1994; and Russell and Burns, 1993 and 1996).

Table 5.26 Influence of strand spacing on transfer length of high strength strand embedded in normal strength concrete

Specimen ID	s_p (mm)	Transfer length (mm)		Ψ		Ratio	
		Dead	Cut	Dead	Cut	Dead	Cut
N40A200-D70-S50-1	50	880	1,430	8.1	13.2	1.00	1.00
N40A200-D70-S60-1	60	731	870	6.8	8.1	0.83	0.61
N40A200-D70-S70-1	70	638	1,276	5.9	11.9	0.73	0.90
N40A200-D70-S50-2	50	694	904	6.5	8.4	1.00	1.00
N40A200-D70-S60-2	60	1,618*	1,060	–	10.5	–	1.25
N40A200-D70-S70-2	70	1,080	1,117	10.3	10.7	1.60	1.27
Average	50					1.00	1.00
	60					0.83	0.93
	70					1.16	1.08

* This transfer length was excluded from the analysis.

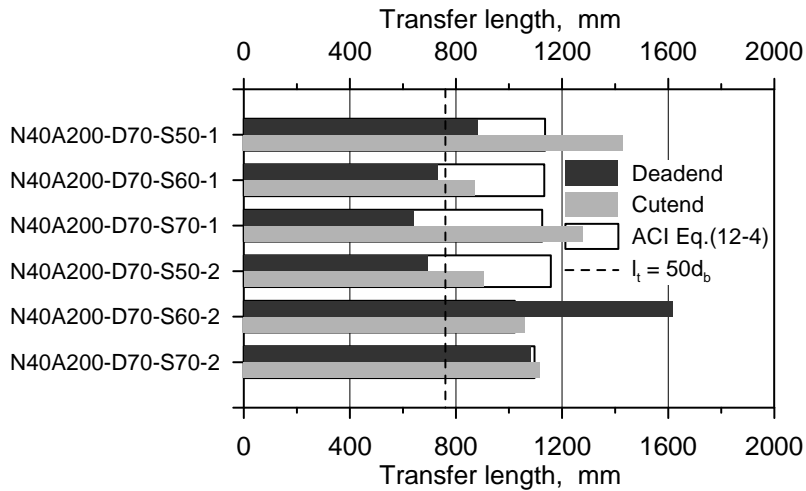


Figure 5.37 Influence of strand spacing on transfer length of high strength strand embedded in normal strength concrete

Table 5.27 Influence of strand spacing on transfer length of high strength strand embedded in high strength concrete

Specimen ID	s_p (mm)	Transfer length (mm)		Ψ		Ratio	
		Dead	Cut	Dead	Cut	Dead	Cut
H70A200-D70-S40	40	526	669	6.1	7.7	1.05	1.13
H70A200-D70-S50	50	523	614	5.8	6.8	1.00	1.00
H70A200-D70-S60	60	393	997	4.5	11.3	0.77	1.67

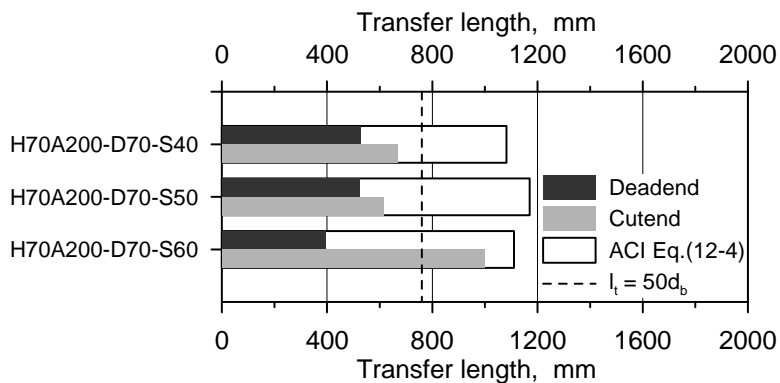


Figure 5.38 Influence of strand spacing on transfer length of high strength strand embedded in high strength concrete

5.4.2.6 Curing Condition

To investigate the effects of curing conditions on transfer length, the effects of conventional atmospheric curing were compared with those of high temperature steam curing. Figure 5.39 shows ambient and inside temperatures that were measured during a 12-hour atmospheric curing process. During this process, no other means of curing were applied except sheltering to avoid direct sunshine to and evaporation from the specimens. Transfer lengths measured under these two different curing conditions for specimens N45S150-B70-1, N45S150-B70-2, and

N45A150-B70, which were fabricated under identical test conditions, are given in Table 5.28. For the steam cured specimens N45S150-B70-1 and N45S150-B70-2, detensioning work was performed at concrete ages of approximately two days with concrete compressive strength of 36.5 MPa and 29.0 MPa, respectively. On the other hand, the air cured specimen N45A150-B70 was detensioned at seven days with concrete compressive strengths of 34.2 MPa. The air cured specimen showed approximately 7% shorter transfer length than the steam cured specimen at the cut end and approximately 15% shorter transfer length at the dead end. Transfer length calculation using ACI 318-11 Eq. (12-4) yields conservative transfer lengths at both ends. This experimental observation indicates that accelerated fabrication by steam curing processes can result in longer transfer lengths than conventional air curing methods.

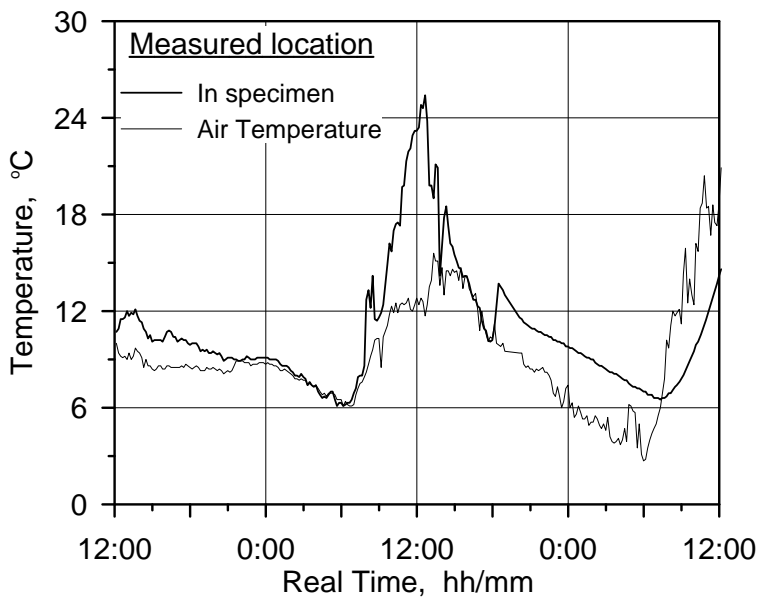


Figure 5.39 Temperatures inside and outside specimen during air curing

Table 5.28 Influence of curing conditions on transfer length

Specimen ID	Curing	Transfer length (mm)		Ψ		Ratio	
		Dead	Cut	Dead	Cut	Dead	Cut
N45S150-B70-1	steam	698	826	7.6	9.0	1.00	1.00
N45S150-B70-2	steam	800	822	8.4	8.6		
N45A150-B70	air	626	754	6.8	8.2	0.85	0.93

5.4.2.7 Debonding

The relative transfer lengths of the specimens with the identical conditions except for debonding were compared in Table 5.29. The specimens with partially debonded strand have 22% shorter transfer lengths at cut end. At dead end, however, the opposite tendency of 16% increase was found. The decrease in transfer length due to debonding has also been reported by Russell and Burns (1997). In their report, 12.7 mm strands with 203 mm sleeve had shorter transfer lengths by approximately 45%.

Figure 5.40 show that the ACI 318-11 equations estimate much shorter transfer lengths at cut end of fully bonded strands.

Table 5.29 Influence of debonding on transfer length

Specimen ID	Debond-ing	Transfer length (mm)		Ψ		Ratio	
		Dead	Cut	Dead	Cut	Dead	Cut
N45S150-B70F-1	No	658	1,103	7.2	12.1	1.00	1.00
N45S150-B70F-2	No	638	1,104	7.1	12.2		
N45S150-B70F-4	No	526	1,110	5.6	11.9		
N45S150-B70F-5	No	811	840	7.6	9.0		
N45S150-B70-1	Yes	698	826	7.6	9.0	1.16	0.78
N45S150-B70-2	Yes	800	822	8.4	8.6		

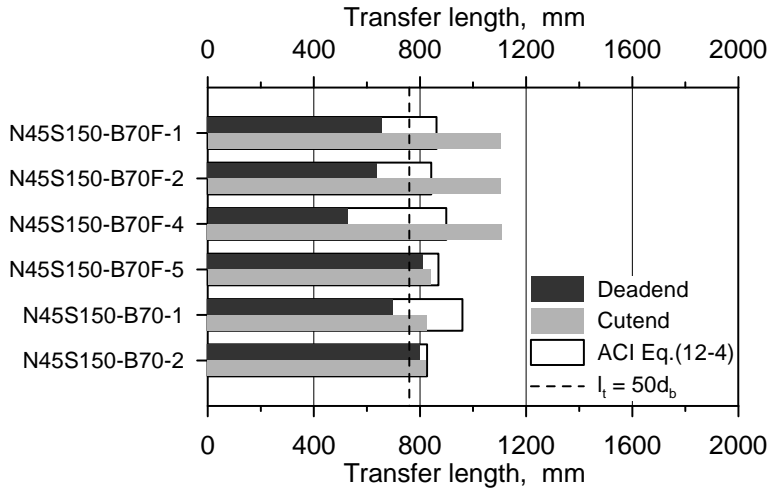


Figure 5.40 Influence of debonding on transfer length

5.4.2.8 Reinforcement Spacing

Little attention has been paid to the effect of the adjacent reinforcement. The considered spacing of reinforcing bars was 60 mm, 75 mm, and 90 mm, which provided the horizontal distance of 14.5 mm, 22.0 mm, and 29.5 mm between the center of reinforcing bars and the strand, respectively. Table 5.30 and Figure 5.41 clearly show the effect of the reinforcement spacing. The transfer lengths at cut end decreased as the reinforcement spacing increased.

Table 5.30 Influence of reinforcement spacing on transfer length

Specimen ID	s_r (mm)	Transfer length (mm)		Ψ		Ratio	
		Dead	Cut	Dead	Cut	Dead	Cut
N45S150-B70F-R60	60	500	1,041	5.5	11.4	1.00	1.00
N45S150-B70F-R75	75	–	927	–	10.2	–	0.90
N45S150-B70F-R90	90	–	718	–	7.9	–	0.70

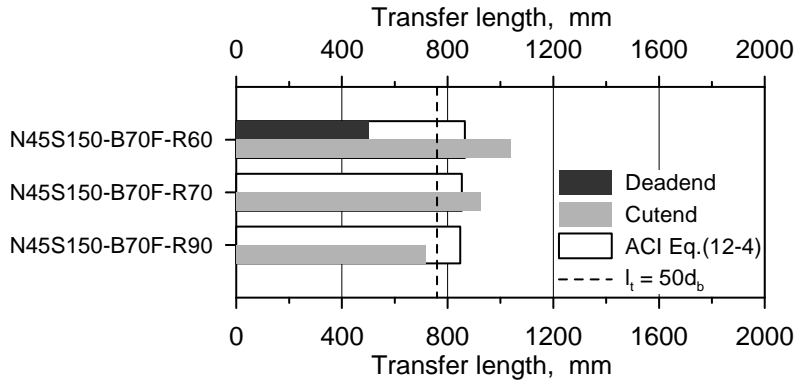


Figure 5.41 Influence of reinforcement spacing on transfer length

5.4.2.9 Prestress Release Method

Generally, sudden release causes a longer transfer length than gradual release. Eurocode2 requires that transfer length be increased by 25% in case of sudden release. To investigate the effect of prestress release method, ratio of transfer length at cut end to transfer length at dead end was obtained for each test specimen. The specimens were divided into 5 groups according to concrete compressive strength, tensile strength of strand, curing condition, partial debonding, and cutting method. The designation of each group followed the system of specimen ID. For example, N45-S-B-F means the group of the steam cured specimens with concrete compressive strength of 45 MPa and fully bonded Grade 1,860 strand.

It should be noted that two types of sudden release method were used in this experiment. The strands were cut by disk cutting in the test series 1 through 7 and by flame cutting in the test series 8 through 10. Flame cutting was done by oxygen-acetylene torch, which heats strand up to the rupture. Thus, the strands actually failed after softening and yielding in tension from the heat (Russell and Burns, 1997).

Figure 5.42 presents the ratio of transfer length at cut end to transfer length at dead end, $l_{t,c}/l_{t,d}$, for all the specimens. It is apparent that the ratios are greater than 1.0 for most of the specimens.

Table 5.31 lists the average value of $l_{t,c}/l_{t,d}$ in each group. Comparing the group N45-S-B with N45-S-B-F, the average ratio dramatically decreased from 1.67 to 1.07 by adopting debonded regions at both ends of the specimens. The debonding reduced transfer lengths at cut end by 22% but increased those at dead end by 16%, which greatly decreased the average ratio.

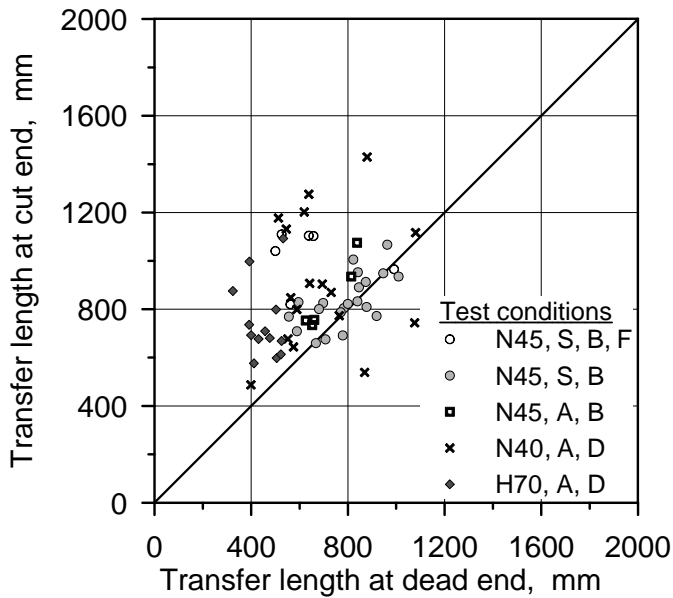


Figure 5.42 Influence of prestress release method on transfer length

Comparing the group N35-A-B with N45-S-B, the average ratio slightly increased due to the curing condition. Air curing decreased transfer length at dead end and at

cut end however this effect was more remarkable at dead end, which increased the average ratio.

Comparing the group N30-A-D with the steam cured groups of partially debonded Grade 1,860 strand, the average ratio significantly increased. Two test conditions were changed: tensile strength of strand and cutting method. It can be said that higher initial press and flame cutting method inflicted more damage on the cut ends of the specimens.

The transfer length difference between dead end and cut end was worsened for high strength concrete. The reduction in transfer length due to the high compressive strength of concrete was greater at dead end than at dead end.

Totally, the sudden release method resulted in 35% longer transfer length at cut end than transfer length at dead end.

Table 5.31 Influence of prestress release method on transfer length

Designation	test series	f'_c (MPa)	f_{pu} (MPa)	Curing	Debonding	Cutting	$l_{t,c}/l_{t,d}$
N45-S-B-F	1~4	45	1,860	steam	N	disk	1.67
N45-S-B	5, 6	45	1,860	steam	Y	disk	1.07
N35-A-B	7	35	1,860	air	Y	disk	1.18
N40-A-D	8, 9	40	2,400	air	Y	flame	1.42
H70-A-D	10	70	2,400	air	Y	flame	1.72
Average							1.35

5.4.3 Comparison with Empirical Equations

In this section, all the transfer length data are compared with the predictions by several empirical equations including the current code provisions. The data include the transfer lengths measured by ERSGs for strand as well as the test results of Grade 2,400 strand, the equations have not been applied to these data.

5.4.3.1 ACI318-11 (2011)

Figure 5.43 compares the test results and the prediction by the ACI318 Eq. (12-4). When calculating the equation, the value of f_{pi} was used instead of f_{pe} . It can be seen that the measured transfer lengths are roughly gathered into three groups. Moreover, the discrepancy increases as the transfer length increases because the equation disregarded the effect of concrete compressive strength. As mentioned in Section 2.5.1.1, ACI318 Eq. (12-4) was formulated by fitting best the test results available at that time. The equation yields lower estimates for the first group, estimates close to average values for the second group, and higher estimates for the third group. It means that ACI318 Eq. (12-4) can give unreasonable results for higher transfer lengths.

Figure 5.44 shows the comparison of the test results with the prediction of the ACI318 equation for shear design, $50d_b$. In the figure, the measured transfer lengths exactly fall into two groups, which represents two strand diameters of 12.7 mm and 15.2 mm, because this equation assumes the constant strand stress of 1,050 MPa. Since the prediction of the equation is affected only by strand diameter, it is unreasonable to apply the equation to high strength strand.

It should be noted that the specimens with the high-strength strands were cured in the atmospheric curing condition. As discussed in the previous section, the atmospheric curing is favorable to transfer length. Thus, the ACI318-11 Eq. (12-4) can be unconservative for steam cured members with the high-strength strands.

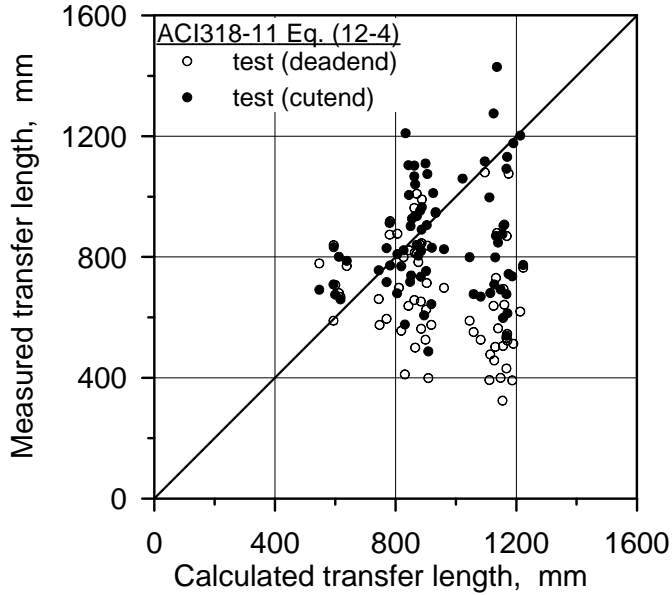


Figure 5.43 Comparison of the measured transfer lengths and the predictions by the ACI318-11 Eq.(12-4) (2011)

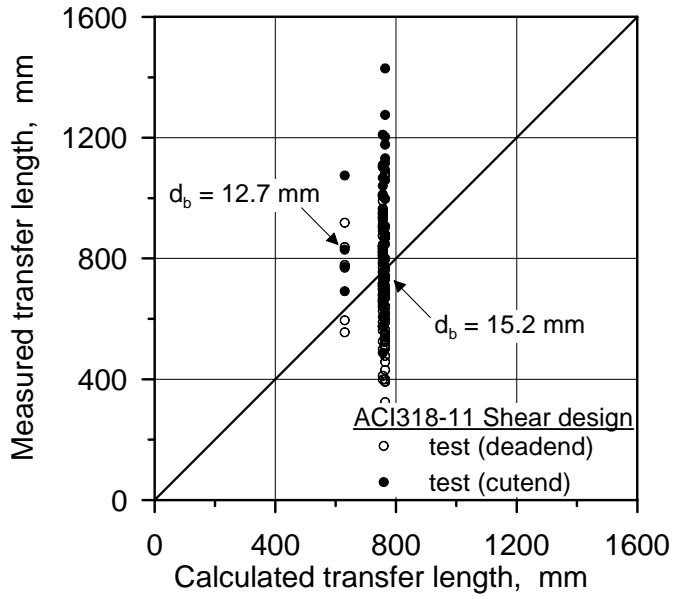


Figure 5.44 Comparison of the measured transfer lengths and the predictions by the ACI318-11 Shear design (2011)

5.4.3.2 Eurocode2 (2004)

Figure 5.45 presents the average transfer lengths calculated in accordance with Eurocode2. A good bond situation was assumed. To obtain transfer lengths at cut end, transfer lengths at dead end were multiplied by a factor of 1.25. Most of the test results fall below the prediction by Eurocode2. It can be said that Eurocode2 provisions are safe and acceptable for design of pretensioned concrete members containing ordinary Grade 1,860 strand as well as Grade 2,400 strand.

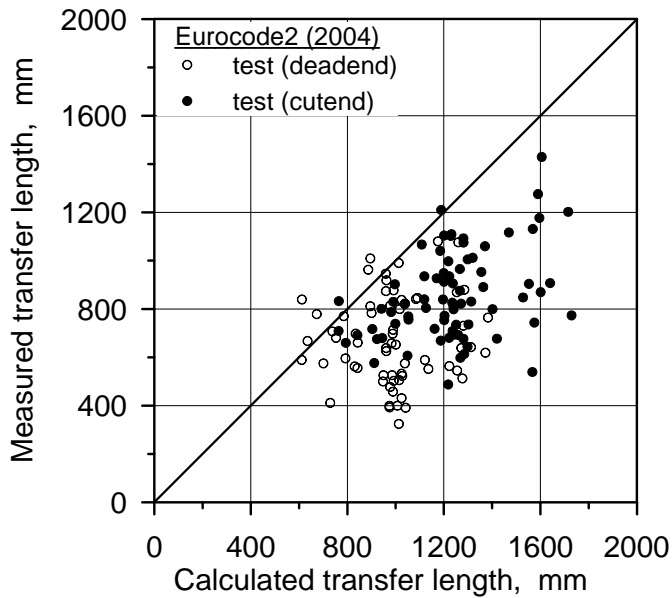


Figure 5.45 Comparison of the measured transfer lengths and the predictions by the Eurocode2 (2004)

5.4.3.3 Oleśniewicz (1975)

Figure 5.46 shows the measured transfer lengths and the results calculated by equation (2.29). The two results are compared in terms of $d_b \sqrt{f_{pi}/f_{ci}'}$. The slopes of the lines are 10 for average, 13 for upper bound, and 7 for lower bound value. Most of the test results fall between the upper and lower bound. Several transfer lengths at dead end are located below the lower bound. Most of the points outside the bound represent the transfer lengths measured in the test series 7, 8, 9, and 10. The common test condition of these test series is curing condition. It exhibits the beneficial effect of air curing condition on transfer length.

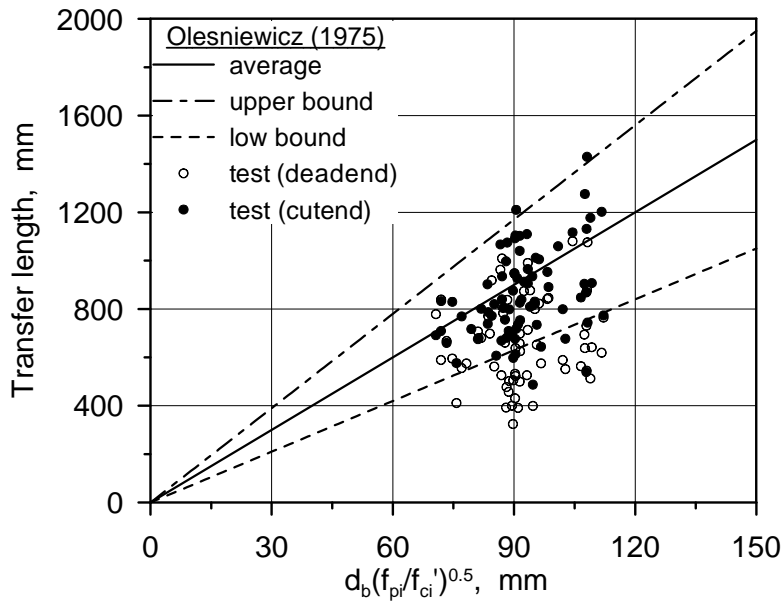


Figure 5.46 Comparison of the measured transfer lengths and the predictions by Oleśniewicz (1975)

5.4.3.4 Zia and Mostafa (1977)

Figure 5.47 shows the measured transfer lengths and the results calculated by equations (2.30) and (2.31). The two results are compared in terms of $(f_{pi}/f'_{ci})d_b$. The slopes of the lines are 1.3 for gradual release and 1.5 for sudden release. The ratio of the two slopes is 1.15; however the resulting transfer length ratio of the two release methods is lower because each equation has a y-intercept. The transfer length ratio calculated by the equations was 1.08 in average, which is much lower than the measured ratio of 1.35 in this experiment.

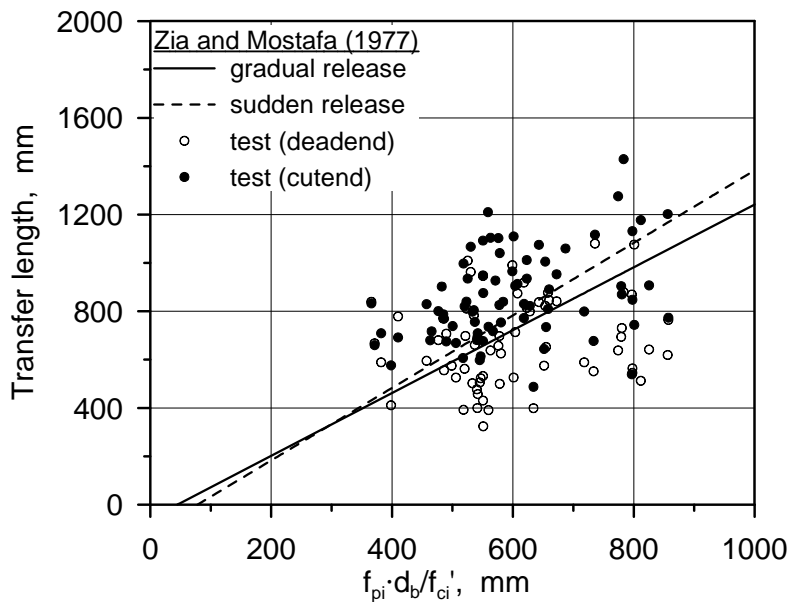


Figure 5.47 Comparison of the measured transfer lengths and the predictions by Zia and Mostafa (1977)

5.4.3.5 Balázs (1992)

Figure 5.48 shows the measured transfer lengths and the results calculated by equation (2.13). The two results are compared in terms of $d_b \sqrt[3]{f_{pi}^3 / f_{ci}^2}$. The slopes of the lines are 3.15 for average, 4.44 for upper bound, and 2.49 for lower bound value. Overall trend is similar to that of Oleśniewicz's model because both equations have similar mathematical forms. Most of the test results fall between the upper and lower bound. Several transfer lengths at dead end are located below the lower bound. More points exist outside the bound than Oleśniewicz's model.

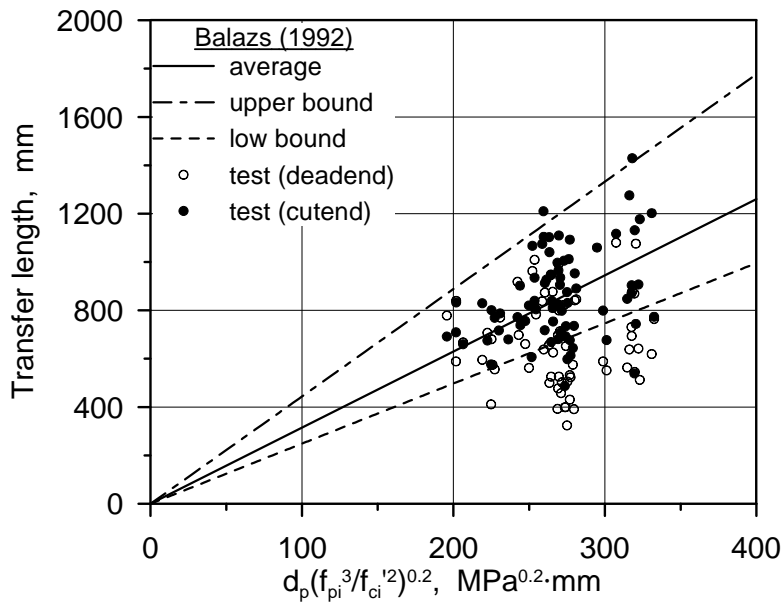


Figure 5.48 Comparison of the measured transfer lengths and the predictions by Balázs (1992)

5.4.3.5 Mitchell et al. (1993)

Figure 5.49 shows the measured transfer lengths and the results calculated by equation (2.35). The two results are compared in terms of $f_{pi}d_b\sqrt{20/f'_{ci}}$. The slope of the line is 0.048 for average value. This model is a variant of ACI318 Eq. (12-4) taking into account the effect of concrete compressive strength at transfer. It can be seen that incorporating the term of $\sqrt{20/f'_{ci}}$ into the equation allowed more reasonable predictions. There is no grouping of the test results in the figure. Also the equation consistently predicts average values over the whole range of the test variables considered in this experiment and the discrepancy does not increase for high transfer lengths.

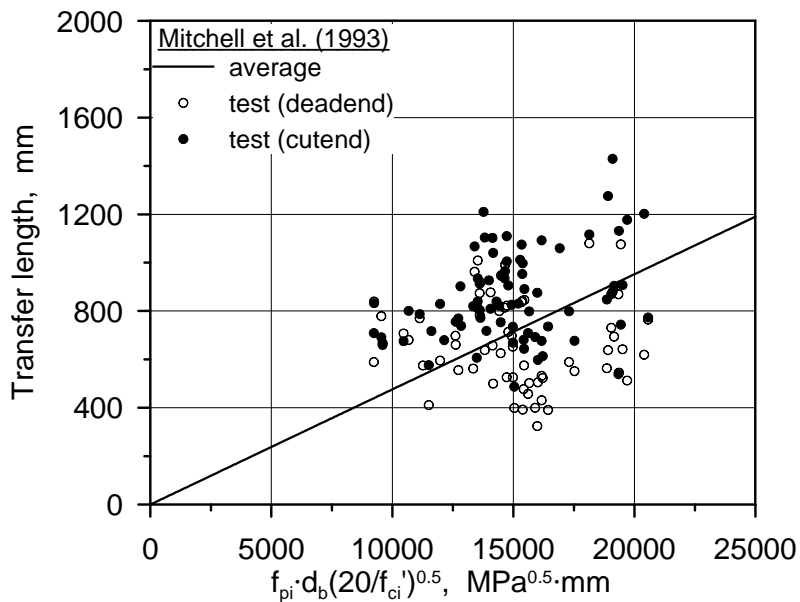


Figure 5.49 Comparison of the measured transfer lengths and the predictions by Mitchell et al. (1993)

5.4.3.6 Mahmoud et al. (1999)

Figure 5.50 shows the measured transfer lengths and the results calculated by equation (2.50). The two results are compared in terms of $f_{pi}d_b/f_{ci}^{0.67}$. The slope of the line is 0.417 for average value. Overall trend is similar to that of Mitchell et al.'s model because both equations have similar mathematical forms. The main difference is the power of concrete compressive strength at transfer. It relates to the assumption of the relationship between transfer length and uniform bond stress. In the range of concrete compressive strength considered in this experiment, the two equations showed no significant differences.

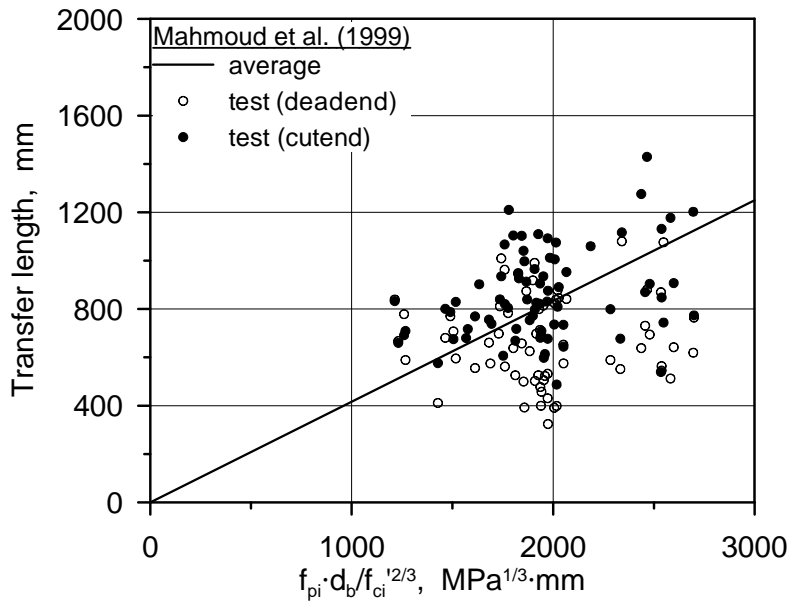


Figure 5.50 Comparison of the measured transfer lengths and the predictions by Mahmoud et al. (1999)

5.4.3.7 Barnes et al. (2003)

Figure 5.51 shows the measured transfer lengths and the results calculated by equation (2.51). The two results are compared in terms of $f_{pi}d_b/f_{ci}^{0.5}$. The slopes of the lines are 0.13 for average, 0.22 for upper bound, and 0.06 for lower bound value. Generally, the equation yields much lower predictions. It is likely to result from the size effect of the specimens in their experiment. They created multiple transfer zones in full-scale AASHTO type I girders that had a height of 711 mm, a bottom flange width of 406 mm, and a length of 12.19 m or 16.46 m. Russell and Burns (1993) reported the large cross section and multiple strands can significantly reduce transfer lengths.

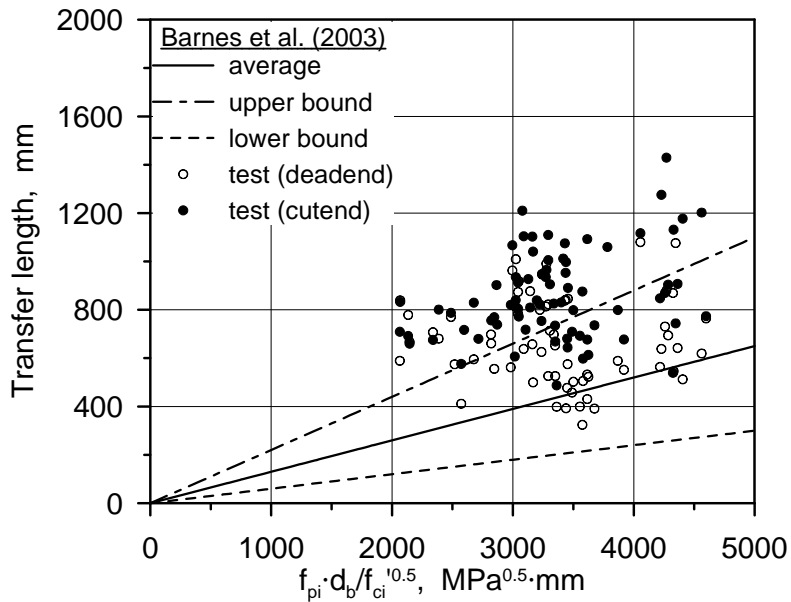


Figure 5.51 Comparison of the measured transfer lengths and the predictions by Barnes et al. (2003)

5.4.3.8 Kose and Burkette (2005)

Figure 5.52 shows the measured transfer lengths and the results calculated by equation (2.52). The two results are compared in terms of $f_{pi} \cdot (25.4 - d_b)^2 / f_{ci}^{r0.5}$. The slope of the line is 0.045 for average. In general, the equation gives higher estimates rather than averages because the model was tuned to represent the 95 % confidence interval for the data used in their study. Some points are located far from the model prediction. These points represent the test results of the specimen with 12.7 mm diameter strand. Because transfer length is proportional to $(25.4 - d_b)^2$ in the equation, smaller diameter yielded longer transfer length. This relationship does not fit the transfer lengths measured in this experiment.

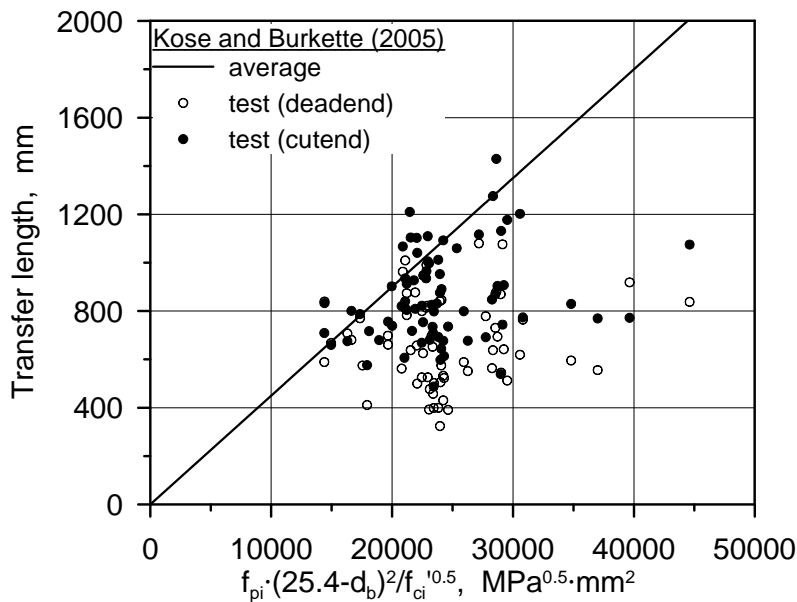


Figure 5.52 Comparison of the measured transfer lengths and the predictions by Kose and Burkette (2005)

5.4.3.9 Marti-Vargas et al. (2007b)

Figure 5.53 shows the measured transfer lengths and the results calculated by equation (2.54). The two results are compared in terms of $f_{pi} d_b / f_{ci}^{0.67}$. The slopes of the lines are 1.0 for average, 1.5 for upper bound, and 0.5 for lower bound value. Overall trend for average values is similar to those of Mitchell et al.'s model and Mahmoud et al.'s model because the equations have similar mathematical forms. Most of the test results fall between the upper and lower bound. Some test results are beyond the upper bound. The majority of the points over the upper bound represent the transfer lengths at cut end. Even though this model was devised for Grade 1,860 strand with 12.7 mm diameter, the equation gives reasonable results for 15.2 mm strand.

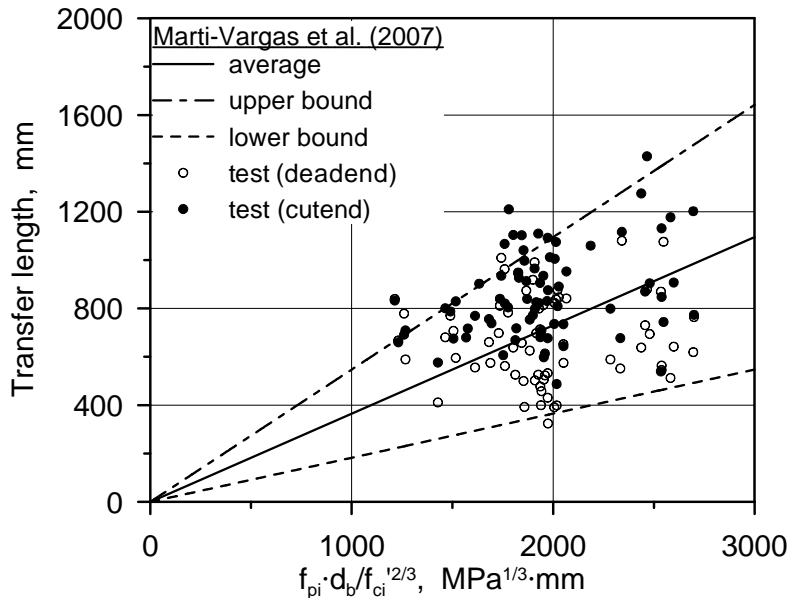


Figure 5.53 Comparison of the measured transfer lengths and the predictions by Marti-Vargas et al. (2007b)

5.5 Concluding Remarks

An extensive experimental program was conducted to measure transfer length of pretensioned concrete members. Strand strains were measured on the helical wires with electrical resistance strain gauges (ERSGs). Applicability of ERSGs to transfer length test and analytical model for behavior of strand were discussed. Provided that specimens and experimental conditions are similar to this experiment, DEMEC gauges cannot yield reliable results when measuring low concrete strains, while ERSGs clearly and accurately measured strain due to prestressing. At least two strain gauges are required at each measuring location to obtain correct strain profiles. In addition to accuracy, other issues should be discussed before applications of ERSGs to tests of transfer length. In this study, loss of bond stresses due to the attachment of steel surface gauges, reliability of measurements on concrete surfaces, and stability of ERSGs under conditions of high temperature were considered. It was concluded that a suitable interval (150 mm) of steel surface gauges did not deteriorate bond between concrete and strand to the extent of affecting test results, that measurements on concrete and steel surface gave almost the same results for 150 mm square sections, and that steel surface gauges yielded stable measurements during high-temperature curing. Thus, the use of ERSGs under these conditions yields reliable measurements of transfer length. ERSGs can also be used to measure prestressing forces and replace load cells through a series of calculations. Using the analytical model proposed by Machida and Durelli (1973), the behavior of the strand and the residual prestressing force were reasonably estimated through the whole fabrication stages.

In order to resolve the discrepancies in the predictions of the existing empirical

equations, test variables currently known as affecting transfer length were reevaluated and test variables not considered in the previous experimental research were examined. The effects of initial prestress, concrete compressive strength at transfer, and strand diameter could be accounted for by the equation proposed by Oleśniewicz. It implies a linear distribution of bond stress and a parabolic distribution of strand strain. No systematic trends were found in the ranges of cover depth, cross sectional size, and strand spacing considered in this study. It means that there were no harmful effects for smaller values. The effects of these factors were negligible if conforming to the current code provisions. Steam curing processes can result in longer transfer lengths than conventional air curing methods. Debonding reduced transfer lengths by 22% at cut end but increased by 16% at dead end. The reinforcing bars in the vicinity of the strand affected the transfer lengths at cut end. In average, sudden release method resulted in 35% longer transfer length at cut end.

Transfer lengths of high-strength strands that have been recently developed were evaluated. Higher initial prestress of Grade 2,400 strand increased transfer length by 21% at dead end and 46% at cut end. The relationship proposed by Oleśniewicz was valid for dead end, however the difference between transfer lengths at dead and cut end was magnified. The current code provisions provided conservative estimates for transfer length of high strength strand. Curing method might result in the underestimation of transfer lengths. No splitting cracks were observed for the specimens and no systematic trends were found in the ranges of cover depth and strand spacing considered in this study. The cover depth and strand spacing of the current code are also feasible to high strength strand.

6. Bond-Slip-Strain Model of Prestressing Strand

6.1 Introduction

The transfer length is defined as the distance over which a strand should be bonded to concrete so as to develop an effective prestress in the prestressing of steel (ACI Committee 318, 2011). A large number of experiments have been performed for the purpose of directly determining the transfer length under specific experimental conditions (Cousins et al., 1986; Castrodale et al., 1988; Brook et al., 1988; Russell and Burns, 1993; Mitchell et al., 1993; Cousins et al., 1993; Deatherage et al., 1994; Russell and Burns, 1997; Barnes et al., 1999; and Oh and Kim, 2000). In these experiments, attempts were made to identify the effects of test variables on the transfer length and, based on the test results, several empirical equations were proposed to best fit the measured transfer lengths (Guyon, 1953; Zia and Mostafa, 1977; Cousins et al., 1986; and Brook et al., 1988). However, such an approach has a fundamental limitation in that the experimental conditions impose restrictions on its application.

Essentially, a prestressing force is transferred to the concrete by the bond stress in the transfer zone of the pretensioned member, and thus the transfer length can be determined from the bond-slip relationship. Balázs (1992) obtained an analytical solution for the governing equation of prestress transfer using the bond-slip relationship and proposed equations for the transfer length. The bond-slip relationship in the study was assumed to be in the form of a power function to approximate previous test results (Balázs, 1992). Den Uijl (1998) performed a series

of experiments that simulated the bond situations of strands and proposed a bond-slip-strand stress (or strain) relationship. In addition, the bond mechanism of the prestressing strand was classified into four categories: adhesion bond, lack-of-fit effect, Poisson effect, and pitch effect. Nitsch (2001) drew another bond-slip-stress relationship from his experimental results. The relationship was divided into three parts: constant part by basic friction, stress dependent part by Hoyer effect, and slip dependent part by lack-of-fit effect. In the aforementioned relationship, the bond stress was expressed as the sum of each mechanism.

Test specimens for the evaluation of the transfer length are designed to accommodate transfer zones in both ends. While such specimens are similar to axially tensioned members with reinforcing bars, the bond situation is different when considering a strand moving into a concrete member. The strain distribution in the transfer zone would be affected by some test variables. If the test variables have no effect on the bond characteristics, the distribution should vary according to a unique bond-slip relationship. In the case of a conventional deformed reinforcing bar, however, it was reported that different bond-slip relationships could be observed even under identical material and specimen configuration conditions (Shima et al., 1987). Shima et al. (1987) solved this problem by considering the strains of the reinforcing bar. Herein, the strain was regarded as an indicator of damage of the concrete surrounding the reinforcing bar (Shima et al., 1987).

On the other hand, there have been no experimental observations that the same phenomenon, that is, different bond-slip relationships under the same material and specimen configuration conditions, could occur for strands. The distribution of the change in the strain of a strand in the transfer zone is dependent on both the boundary values and the curve shape between the boundaries (see Figure 6.1).

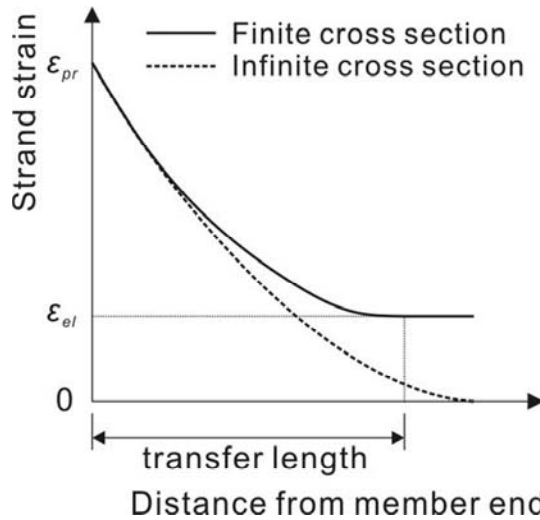


Figure 6.1 Deviation of strain curves in transfer zone due to boundary condition

The left boundary value at the end of the member is determined from the level of the prestressing force, while the right boundary value at the beginning of the transfer zone is the elastic strain of the member due to the prestressing force. The curve shape is affected by the bond characteristics between the concrete and the strand. Variations in the cover depth, the dimensions of the cross section, and the level of prestressing force have little effect on the bond characteristics, but cause changes in both boundaries, unless they result in splitting cracks. In this case, the curve shape should remain unchanged and follow an identical bond-slip relationship. The curve shape, however, changes because of the boundaries as shown in Figure 6.1. The dotted line in the figure indicates the variation in the strand strain, where the member section is infinite and the elastic strain approaches zero. A smaller member section leads to larger elastic strain, and thus, a discrepancy occurs between the dotted and solid lines. This discrepancy is largest at the boundary of the transfer zone. Therefore, unchanged bond characteristics can yield different bond-slip

relationships for a strand.

In this Chapter, a bond-slip-strain relationship is derived from the test results and equations are proposed for the distributions of the bond stress, slip, and strand strain within the transfer zone, as well as the transfer length.

6.2 Bond Stress and Slip of Test Specimens

6.2.1 Test Specimens Included in This Analysis

Some of the test specimens were excluded from the analysis because (1) only concrete strains were measured, or (2) because the specimens seemed to have bond deficiencies. The bond stress distributions in the specimens excluded from and included in the analysis are compared in Figure 6.2. In the longitudinal axis of Figure 6.2, x is the distance from the point where the transfer zone begins to the member end. While the bond stress of the specimen N45S150-B70-1, N45S150-B70-C45-2, N45S120-B70-2, and N35A150-B70-D12 continuously increases up to the member end, the specimens N45S150-B70-C60-1, N45S90-B50-1, N45S120-B50-1, and N45S120-B70-1 converge to lower values. They were fabricated from the same batch as specimen N45S150-B70-1 and can be expected to have almost the same bond strength and compressive strength for the concrete. It can be deduced that the lower bond strength was caused by a bond problem resulting from defects during the fabrication process or a shortage of the cover depth. The measurements on the cut end sides were also excluded from the analysis not to consider an effect of dynamic impact. The test specimens included in the analysis are listed in Table 6.1.

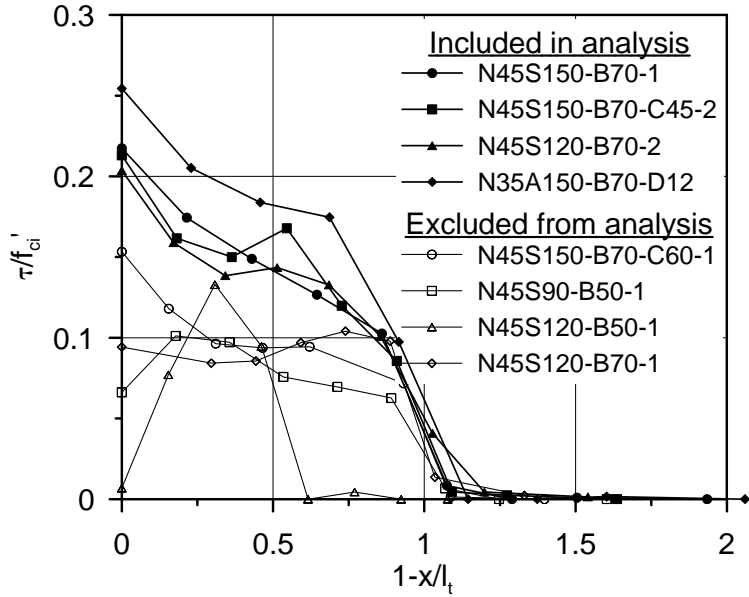


Figure 6.2 Bond stress distributions of the test specimens excluded from and included in the analysis

Table 6.1 Test specimens included in the analysis

No.	Test series	Specimen ID
1	1	N45S150-B70F-1
2	5	N45S150-B70-D12-1
3	5	N45S150-B50-D12
4	5	N45S150-B70-1
5	5	N45S150-B50-1
6	6	N45S150-B70-2
7	6	N45S150-B50-2
8	6	N45S150-B70-C60-2
9	6	N45S150-B70-C45-2
10	6	N45S120-B70-2
11	6	N45S120-B50-2
12	7	N45A150-B70
13	7	N35A150-B70
14	7	N35A120-B70
15	7	N35A150-B50
16	7	N35A150-B70-D12

6.2.2 Calculation of Bond Stress and Slip

In this study, local bond stresses and slips were calculated using tendon strain measurements. It is assumed that bond loss due to the installation of strain gauges on the strands can be ignored to obtain the bond stress and slip from the measured strand strains. This issue was discussed in Section 5.2.2.1 and the conclusion was drawn that the strain gages attached on a strand had little effect on the transfer lengths. In some studies where strain gauges were used on reinforcement, researchers succeeded in either formulating bond-slip relationships (Shima et al., 1987).

The distribution of the change in the strain of a strand was approximated by piecewise cubic Hermite interpolating polynomial (PCHIP) curves, where interpolation is performed between two adjacent measured points using a cubic polynomial and the first derivative is made to be continuous at each point. The first derivative of the strain curve was used to calculate the bond stress. A comparison between a linear interpolation and a PCHIP curve for the measured values of the test specimen N45S150-B70F-1 is presented in Figure 6.3.

The slip at a point in a member is obtained by integrating the relative difference of the concrete and strand strain. As described previously, however, only strand strains were measured for the test specimens analyzed in this experiment. Therefore, it is assumed that the distribution of concrete and strand strains have a similar shape. This assumption has been sufficiently proven in Section 5.2.2.

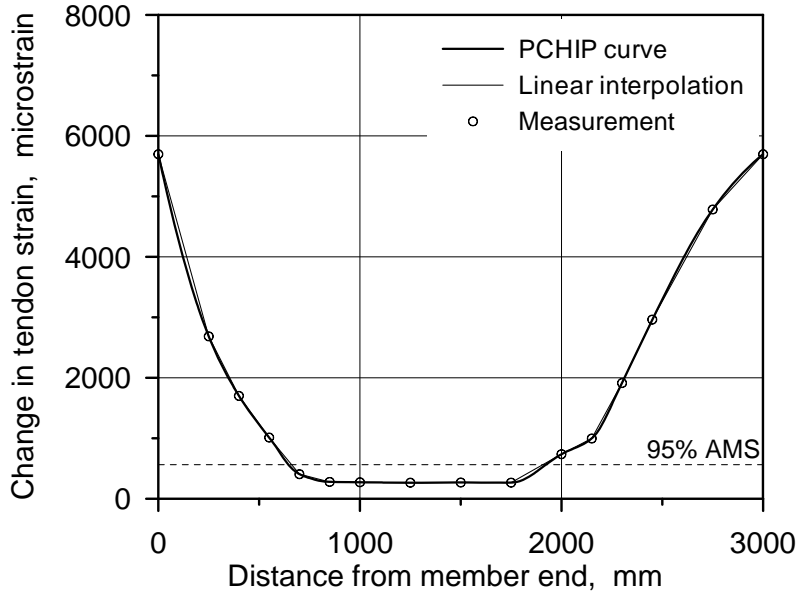


Figure 6.3 Curve fitting for measured strain values of specimen N45S150-B70F-1

6.3 Bond-Slip-Strain Relationship

6.3.1 Derivation of the Relationship between Bond, Slip, and Strain

To obtain a bond-slip-strain relationship for a strand, a basic form of the equation is adopted from the model devised by Shima et al. (1987). The bond stress in the model is composed of a slip function, $f(s_n)$, and a strain function, $g(\varepsilon_s)$, as follows:

$$\tau_b = \tau_0 \cdot g(\varepsilon_s) = (f'_c \cdot f(s_n)) \cdot g(\varepsilon_s) = f'_c \cdot \frac{f(s_n)}{1 + \varepsilon \times 10^5} \quad (6.1)$$

where, τ_0 is bond stress when strain of reinforcing bar is zero. The slip function

$f(s_n)$ represents the bond stress when the strain of the reinforcing bar is zero. It was derived from the test results of the specimens with very short embedment length, which allowed small strain and large slip. The strain function $g(\varepsilon_s)$ represents the effect of the bar strain on the bond stress, which was experimentally identified by the test results of the specimens with various experimental conditions.

It is assumed that the above relationship is applicable to a strand except the slip function. Under this assumption, a distinction between the bond characteristics of the reinforcing bar and the strand is made only by the slip function in the proposed model. Two modifications to equation (6.1) are made so as to apply the formula to a prestressing strand: replacing the design compressive strength and reinforcement strain by the compressive strength at detensioning and the change in the strain of the strand due to detensioning $\Delta\varepsilon_{pr}$ respectively.

$$\tau_b = f'_{ci} \cdot \frac{f(s_n)}{1 + \Delta\varepsilon_{pr} \times 10^5} \quad (6.2)$$

Shown in Figure 6.4 is the relationship between $(\tau_b/f'_{ci}) \cdot (1 + \Delta\varepsilon_{pr} \times 10^5)$ and s_n for all specimens. A linear relationship with a slope of 0.987 is evident. Therefore, the slip function can be simply expressed as $f(s_n) = a_0 s_n$ with $a_0 = 1$. Incorporating the slip function into equation (6.2) gives the following equation:

$$\frac{\tau_b}{f'_{ci}} = \frac{a_0 \cdot s_n}{1 + \Delta\varepsilon_{pr} \times 10^5} = \frac{1.0 \times 10^3 (s/d_b)}{1 + \Delta\varepsilon_{pr} \times 10^5} \quad (6.3)$$

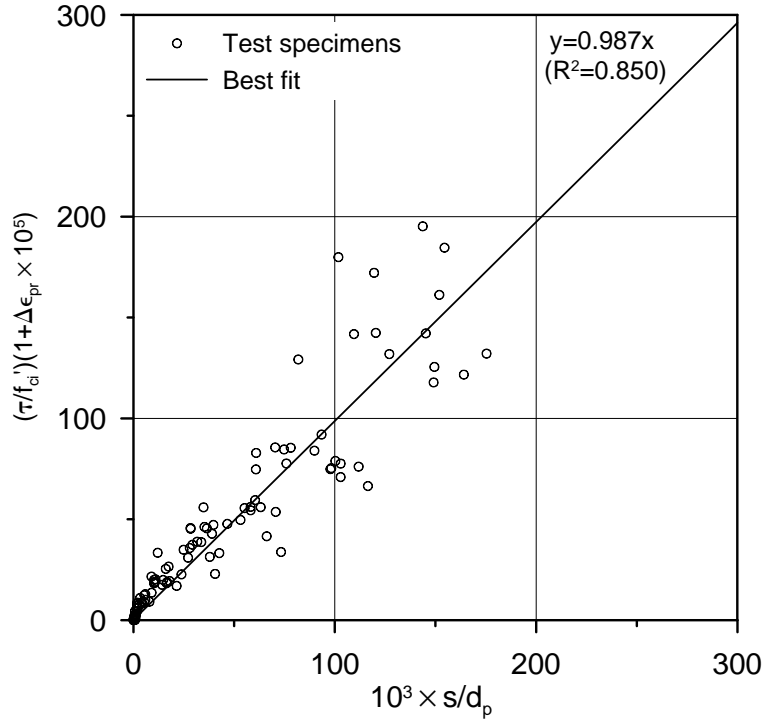


Figure 6.4 Transfer bond-slip-strain relationship of the pretensioned tendon

The bond stress is proportional to the first derivative of $\Delta\epsilon_{pr}$, while slip is given in its integral form. If $\Delta\epsilon_{pr}$ is assumed to be a quadratic polynomial with respect to the longitudinal location x as equation (6.4), an analytical expression for $\Delta\epsilon_{pr}$ can be derived from equation (6.3).

$$\Delta\epsilon_{pr} = a_1x^2 + a_2x + a_3 \quad (6.4)$$

As shown in Figure 6.5, $\Delta\epsilon_{pr}$ equals a_3 at $x=0$, which means that a_3 represents the elastic strain of the member due to the prestressing force at the level

of the strand centroid. The residual strand strain just after detensioning can be expressed as follows:

$$\varepsilon_p = -\varepsilon_{pr} + \Delta\varepsilon_{pr} = a_1x^2 + a_2x + a_3 - \varepsilon_{pr} = a_1x^2 + a_2x + (\varepsilon_{el} - \varepsilon_{pr}) \quad (6.5)$$

where, the minus sign implies tension.

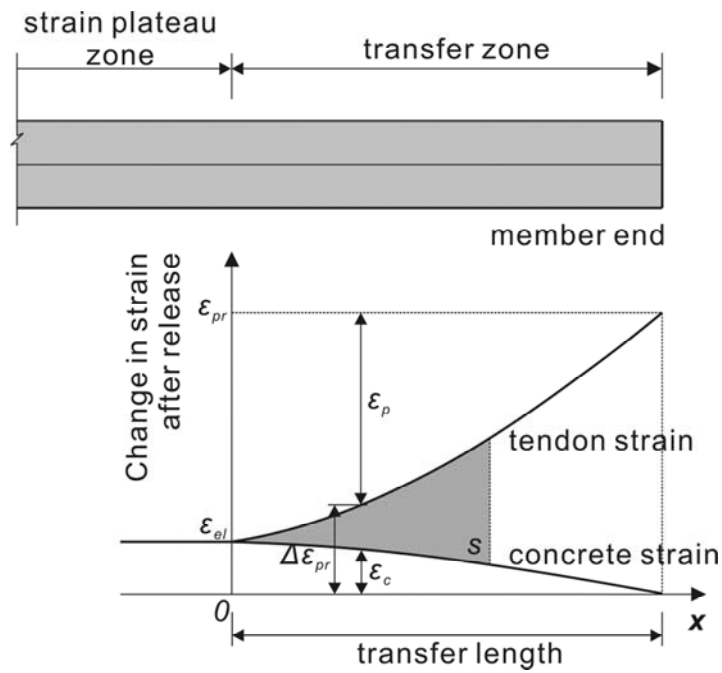


Figure 6.5 Strain distributions of the tendon and concrete along the transfer zone

6.3.2 Bond Stress Distribution

The bond stress can be derived from the equilibrium condition along the strand within the distance dx (fib, 2000):

$$\tau_b = \frac{E_p A_p}{\pi d_b} \frac{d\varepsilon_p}{dx} = \frac{E_p A_p}{\pi d_b} (2a_1 x + a_2) \quad (6.6)$$

Two characteristics distinguish equation (6.6) from previous formulae (Guyon, 1953; Cousins et al., 1990a; Balazs, 1992; fib, 2000) for the bond stress distribution. Firstly, the bond stress is not zero at $x=0$, where the transfer zone begins. At this point, however, the bond stress should be zero because, theoretically, there is no slip at all. This phenomenon can be explained by referring to the adhesion bond. Adhesion stands for the contributions to elastic bond, which refers to the deformation of the cementitious layer around the strand (fib, 2000). The adhesion bond prevents relative displacement until some critical stress is reached (Russell and Burns, 1993). At the critical stress, the contribution of the adhesion bond to the bond stress reduces to zero and rigid-brittle behavior is exhibited (Russell and Burns, 1993). Nitsch (2001) also mentioned that the constant value of bond stress in their models can be attributed to adhesion and friction due to surface roughness.

The behavior of both a strand subjected to prestressing force and the surrounding concrete is shown in Figure 6.6. Herein, x_s , x_{ci} , and x_{cj} are used to denote a point on the strand surface, a point on the inner surface of the concrete in contact with x_s , and a point at some vertical distance, for example, the concrete surface, from x_{ci} before deformation, respectively. Before deformation, the three points were located on the same vertical line. If the prestressing force imposes very small deformation on the concrete, the three points move as shown in Figure 6.6 (b) until the adhesion bond fails. While x_s and x_{ci} move together to x'_s , x_{cj} does not reach x'_{cj} yet. Measurements at x_{cj} will produce the relative displacement of

$x'_{cj} - x_{cj}$, but there is no slip at the strand surface. Once the adhesion bond fails, slip occurs on the interface between the concrete and the strand, and the three points move as shown in Figure 6.6 (c). At this point, the adhesion bond diminishes to zero and its contribution is replaced by that of the other mechanisms such as friction, Hoyer effect, and mechanical interlocking (Russell and Burns, 1993).

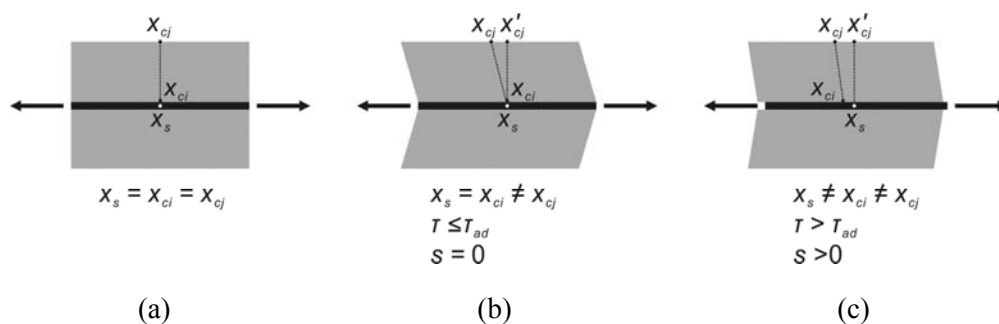


Figure 6.6 Deformation of the concrete surrounding the tendon when slip occurs

Because strains were measured on the strand surface in this experiment, slip remains zero until the bond stress reaches the adhesion bond strength. Slip then jumps to the initial slip value. In accordance with the above description, equation (6.6) should be rearranged as follows:

$$\tau_b(x) = \begin{cases} 0 & (\text{for } x = 0) \\ \frac{E_p A_p}{\pi d_b} (2a_1 x + a_2) & (\text{for } 0 < x \leq l_t) \end{cases} \quad (6.7)$$

where, a_2 corresponds to the adhesion bond strength at the occurrence of the initial slip. The second aspect that distinguishes equation (6.7) from previous

formulae is that the bond stress distribution is assumed to be linear. In previous studies, the bond stress distribution was assumed to take on various forms, such as a constant, a parabola, or a combination of a constant and a linear form (Cousins et al. 1990a). A thick-walled cylinder analysis for a pretensioned member revealed that the bond stress linearly increases within the transfer zone, provided that the concrete confinement is sufficient. Therefore, equation (6.7) can be regarded as an approximated formula for the transfer bond stress of a pretensioned member. The slope a_1 represents the contribution of the other mechanisms to the bond stress after failure of the adhesion bond.

6.3.3 Slip Distribution

If the strain responses of the concrete and strand have a similar shape after detensioning as assumed previously, the ratio of the two curves should be the same at any location. This ratio can be obtained at $x = 0$ as follows:

$$\frac{\varepsilon_c(x)}{\varepsilon_p(x)} = \frac{\varepsilon_c(0)}{\varepsilon_p(0)} = \frac{\varepsilon_{el}}{\varepsilon_{el} - \varepsilon_{pr}} \quad (6.8)$$

Slip can be calculated through the integration of the difference between $\Delta\varepsilon_{pr}$ and ε_c , as shown in Figure 6.5. Brittle failure of the adhesion bond results in the sudden occurrence of the initial slip; the strain difference between the concrete and the strand then has the corresponding initial value. Therefore, slip can be expressed as follows:

$$s(x) = \int_0^x (\Delta \varepsilon_{pr} - \varepsilon_c) + a_4 dx = \begin{cases} 0 & (\text{for } x = 0) \\ \int_0^x (\varepsilon_{pr} + \varepsilon_p - \varepsilon_c) + a_4 dx & (\text{for } 0 < x \leq l_t) \end{cases} \quad (6.9)$$

Substituting equations (6.5) and (6.8) into equation (6.9) gives the following equation for slip

$$s(x) = \frac{\varepsilon_{pr}}{\varepsilon_{pr} - \varepsilon_{el}} \cdot \left(\frac{1}{3} a_1 x^3 + \frac{1}{2} a_2 x^2 \right) + a_4 x + a_5 \quad (6.10)$$

6.3.4 Determination of Coefficients and Transfer Length

Equation (6.3) can be rearranged as follows

$$\tau_b \cdot (1 + \Delta \varepsilon_{pr} \times 10^5) = f'_{ci} \cdot (a_0 \times 10^3) \cdot (s/d_b) \quad (6.11)$$

The terms on the left- and right-hand sides of equation (6.11) can be expressed in terms of x by substituting equations (6.7) and (6.10) into equation (6.11). Both terms should always give the same value over the transfer zone. The coefficients of the equations can be determined by equating each term with the same order as follows:

$$a_1 = \frac{a_0 \pi}{600} \cdot \frac{f'_{ci}}{E_p A_p} \cdot \frac{\varepsilon_{pr}}{\varepsilon_{pr} - \varepsilon_{el}} \quad (6.12)$$

$$a_4 = \frac{100}{a_0 \pi} \cdot \frac{E_p A_p}{f'_{ci}} \left[2a_1 (a_3 + 10^{-5}) + a_2^2 \right] \quad (6.13)$$

$$a_5 = \frac{100}{a_0 \pi} \cdot \frac{E_p A_p}{f'_{ci}} \cdot a_2 (a_3 + 10^{-5}) \quad (6.14)$$

It should be noted that a_2 cannot be determined in the aforementioned manner because equating the second order terms gives the same result as that obtained with the third order terms of equation (6.12). Herein, a_2 is adopted from the model formulated by Den Uijl (1998). In the model, the term corresponding to the adhesion bond was set to be a constant of 3 MPa. Considering the compressive strength of 55 MPa used in Den Uijl's experiments, a_2 is given as follows.

$$\frac{E_p A_p}{\pi d_b} a_2 = \tau_{ad} = 3 \cdot \frac{f'_{ci}}{55} = 0.055 f' \quad (6.15)$$

$$a_2 = \frac{\pi d_b}{E_p A_p} (0.055 f'_{ci}) \quad (6.16)$$

It should be noted that the bond stress was previously assumed to be proportional to the compressive strength, as seen in equation (6.2). Ultimately, all coefficients are calculated. The transfer length is easily obtained from equation (6.17) by applying the condition of $\Delta \varepsilon_{pr} = \varepsilon_{pr}$ at $x = l_t$ to equation (6.4). Transfer length l_t can be expressed as equation (6.18):

$$a_1 l_t^2 + a_2 l_t + (a_3 - \varepsilon_{pr}) = 0 \quad (6.17)$$

$$l_t = \frac{-a_2 \pm \sqrt{a_2^2 - 4a_1(a_3 - \varepsilon_{pr})}}{2a_1} \quad (6.18)$$

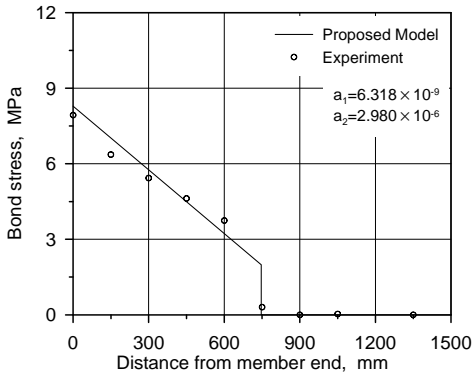
6.3.5 Comparison of the Proposed Model and Experimental Results

The transfer lengths of the test specimens were calculated with the proposed model and a comparison was made between the calculated and measured transfer lengths; the results are shown in Table 6.2. Table 6.2 also includes the calculated results from other existing models. While the results from all of the models in Table 6.2 were in good agreement with the measured values, the estimations from the proposed model are closest to the test results on average and the standard deviation is the smallest. As shown in Figure 6.6, the results obtained with the proposed model also agree well with the measured bond stress, strand strain, slip, and bond-slip relationship for the specimen N45S150-B70-1.

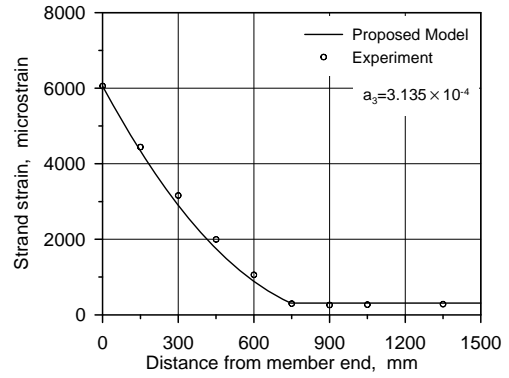
Table 6.2 Comparison of the calculated and measured transfer lengths in this study

(unit: mm)

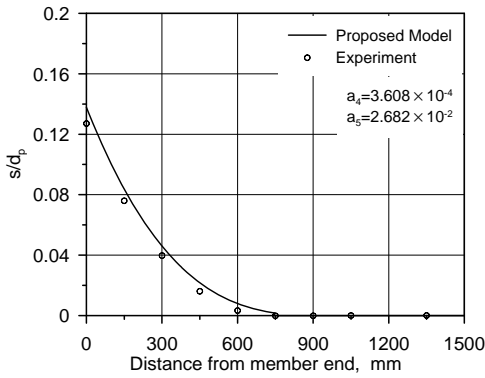
Test specimen	Mea.	Proposed model		ACI 318-11		Zia and Mostafa		Balázs		Mitchell et al.	
		(b)	(b)/(a)	(c)	(c)/(a)	(d)	(d)/(a)	(e)	(e)/(a)	(f)	(f)/(a)
1	661	769	1.16	901	1.36	794	1.20	853	1.29	719	1.09
2	557	651	1.17	832	1.50	629	1.13	725	1.30	630	1.13
3	593	690	1.16	915	1.54	704	1.19	768	1.29	692	1.17
4	698	746	1.07	956	1.37	754	1.08	847	1.21	724	1.04
5	671	579	0.86	640	0.95	466	0.69	666	0.99	484	0.72
6	810	851	1.05	944	1.16	970	1.20	921	1.14	801	0.99
7	760	687	0.90	667	0.88	651	0.86	748	0.98	566	0.75
8	844	851	1.01	946	1.12	978	1.16	922	1.09	803	0.95
9	825	822	1.00	904	1.10	947	1.15	897	1.09	767	0.93
10	876	821	0.94	909	1.04	962	1.10	900	1.03	771	0.88
11	683	676	0.99	663	0.97	670	0.98	745	1.09	562	0.82
12	633	757	1.20	919	1.45	780	1.23	849	1.34	719	1.13
13	817	806	0.99	917	1.12	887	1.09	885	1.08	756	0.93
14	664	682	1.03	702	1.06	651	0.98	754	1.13	579	0.87
15	841	691	0.82	776	0.92	718	0.85	745	0.89	640	0.76
16	655	809	1.23	923	1.41	893	1.36	888	1.36	761	1.16
Avg.	–	–	1.04	–	1.18	–	1.08	–	1.14	–	0.96
Std. dev.	–	–	0.12	–	0.22	–	0.17	–	0.14	–	0.15



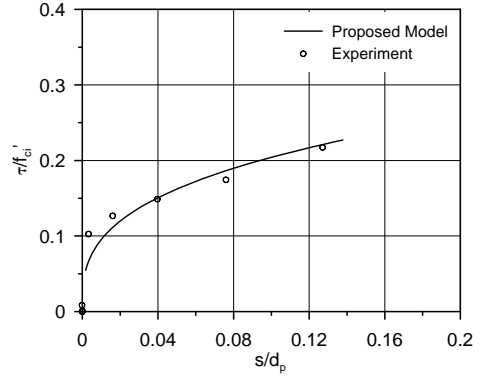
(a)



(b)



(c)



(d)

Figure 6.7 Comparison of the test results and the proposed model for specimen N45S150-B70-1: (a) Bond stress distribution; (b) Strand strain distribution; (c) Slip distribution; and (d) Bond-slip relationship

6.4 Verification of the Proposed Model

To verify the proposed scheme, a comparison was made between the proposed model and the test results from other studies. The test results obtained from rectangular prism members with a single strand were selected for the comparison because such members are similar to the test specimens employed in this study. The comparison results of transfer lengths and slips are summarized in Tables 6.3 through 6.6, and the comparison results of strain or stress distributions are shown in Figure 6.8 through 6.10.

Kim (2000) performed experiments with various test variables and proposed an equation for the transfer length through a nonlinear analysis based on radial concrete cracks. The measured transfer length, slip, and concrete strain at a dead end are compared with the results from the proposed model in Table 6.3, Table 6.4, and Figure 6.8, respectively. As seen in Tables 6.3 and 6.4, the proposed model shows good estimations for the transfer length and slip. In addition, the estimated concrete strains matched very well with measured values, as shown in Figure 6.8. The improved accuracy for the concrete strain distribution when compared to the transfer length is due to the fact that the 95% AMS method generally gives shorter transfer lengths than those determined at the intersection at 100% AMS, that is, elastic strain.

Table 6.3 Comparison of the proposed model and the transfer lengths measured by Kim (2000)

(unit: mm)

Test specimen	Mea. (a)	Cal. (b)	Ratio (b)/(a)	Test specimen	Mea. (a)	Cal. (b)	Ratio (b)/(a)
M12-N-C4-1	535	642	1.20	M15-N-C4-1	754	747	0.99
M12-N-C4-2	602	642	1.07	M15-N-C4-2	781	785	1.01
M12-N-C5-1	512	657	1.28	M15-N-C5-1	680	747	1.10
M12-N-C5-2	527	683	1.30	M15-N-C5-2	609	753	1.24
M12-H-C4-1	455	538	1.18	M15-H-C4-1	675	632	0.94
M12-H-C4-2	501	542	1.08	M15-H-C4-2	610	637	1.04
M12-H-C5-1	434	554	1.28	M15-H-C5-1	548	634	1.16
M12-H-C5-2	483	564	1.17	M15-H-C5-2	492	636	1.29
Average: 1.14, Standard deviation: 0.12							

Table 6.4 Comparison of the proposed model and the slip measured by Kim (2000)

(unit: mm)

Test specimen	Mea. (a)	Cal. (b)	Ratio (b)/(a)	Test specimen	Mea. (a)	Cal. (b)	Ratio (b)/(a)
M12-N-C4-1	1.75	2.05	1.17	M15-N-C4-1	2.43	2.44	1.00
M12-N-C4-2	1.75	2.09	1.19	M15-N-C4-2	1.86	2.57	1.38
M12-N-C5-1	1.97	2.10	1.07	M15-N-C5-1	1.96	2.39	1.22
M12-N-C5-2	2.18	2.17	0.99	M15-N-C5-2	2.14	2.52	1.18
M12-H-C4-1	1.73	1.78	1.03	M15-H-C4-1	1.86	2.10	1.13
M12-H-C4-2	1.76	1.78	1.02	M15-H-C4-2	1.62	2.15	1.33
M12-H-C5-1	1.75	1.83	1.05	M15-H-C5-1	1.50	2.15	1.44
M12-H-C5-2	1.63	1.87	1.14	M15-H-C5-2	1.65	2.12	1.29
Average: 1.16, Standard deviation: 0.14							

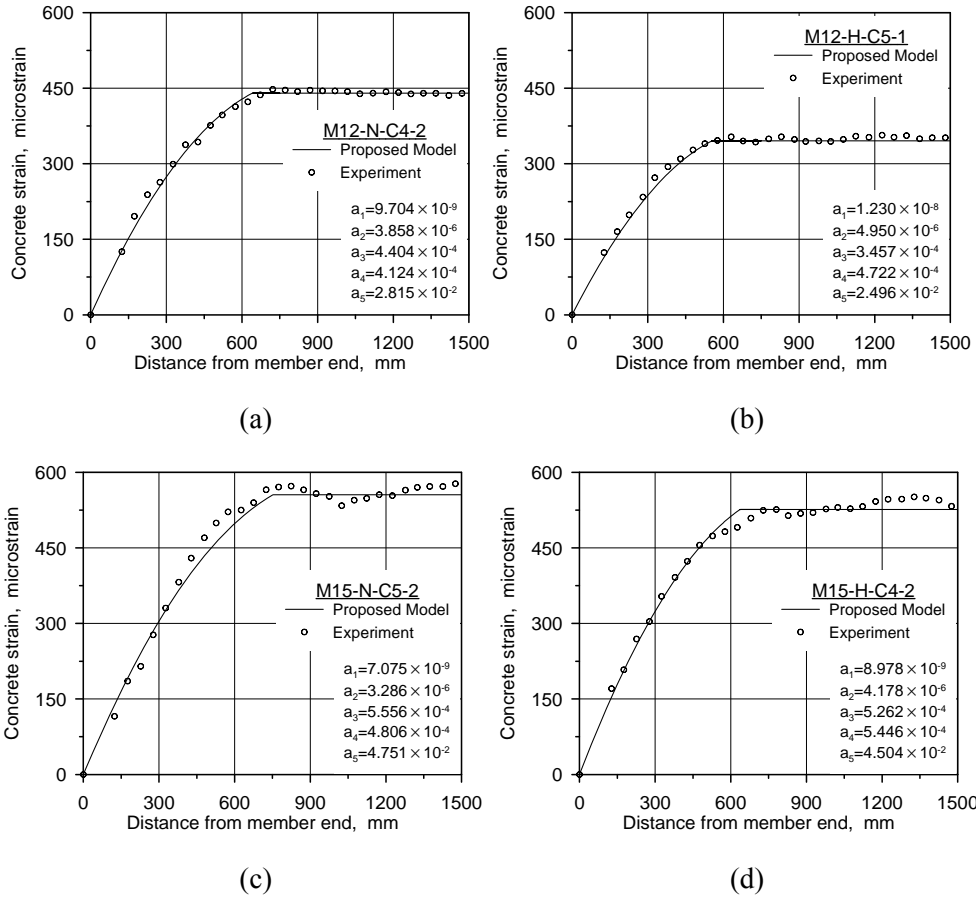


Figure 6.8 Comparison of test results from Kim (2000) and proposed model: (a) M12-N-C4-2; (b) M12-H-C5-1; (c) M15-N-C5-2; and (d) M15-H-C4-2

The estimations from the proposed model and the test results from Mitchell et al. (1993) are compared in Figure 6.9 and Table 6.5. The strands were detensioned by a gradual release method and the transfer lengths in Table 6.5 are the averaged values obtained at both ends. The accuracy of the estimations was similar to that from the experiments of Kim (2000).

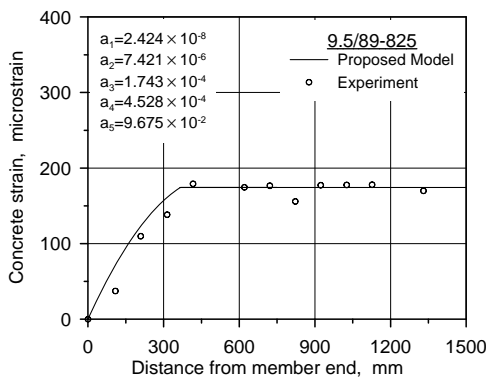
Table 6.5 Comparison of the proposed model and the transfer lengths measured by Mitchell et al. (1993)

(unit: mm)

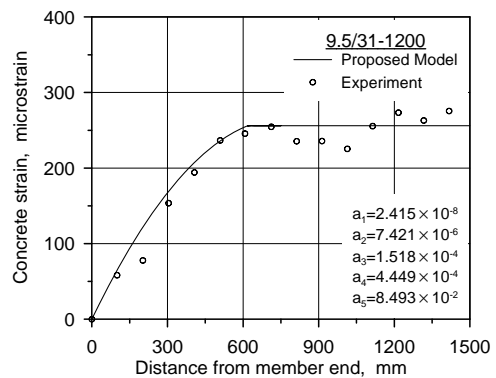
Test specimen	Mea. (a)	Cal. (b)	Ratio (b)/(a)	Test specimen	Mea. (a)	Cal. (b)	Ratio (b)/(a)
9.5/31-1200	506	618	1.22	13/65-850	506	524	1.04
9.5/43-1350	533	538	1.01	13/75-1100	470	498	1.06
9.5/43-1000	432	538	1.25	13/75-950	368	498	1.36
9.5/65-800	303	368	1.22	13/89-950	387	510	1.32
9.5/75-950	355	366	1.03	13/89-650	495	510	1.03
9.5/75-700	355	366	1.03	16/31-1865	804	1010	1.26
9.5/89-825	364	366	1.00	16/31-1500	739	1010	1.37
9.5/89-575	368	366	0.99	16/65-1150	478	599	1.25
13/31-1200	710	884	1.24	16/65-725	486	599	1.23
13/43-1600	584	695	1.19	16/89-975	306	467	1.53
13/43-1250	584	695	1.19	16/89-675	465	467	1.00

Average: 1.17, Standard deviation: 0.15

Note: Measurement was averaged on both sides.



(a)



(b)

Figure 6.9 Comparison of test results from Mitchell et al. (1993) and proposed model: (a) 9.5/89-825; and (b) 9.5/31-1200

The concrete strains and transfer lengths measured by Russell and Burns (1997) are compared with values estimated from the proposed model in Figure 6.10 and Table 6.6. Table 6.6 shows that the proposed model generally underestimated the transfer lengths. This trend was more significant for the SS160 specimen group with a 15.2 mm strand when compared to the SS150 specimen group with a 12.7 mm strand. The same trend is also observed in Figure 6.10 for the concrete strain estimation.

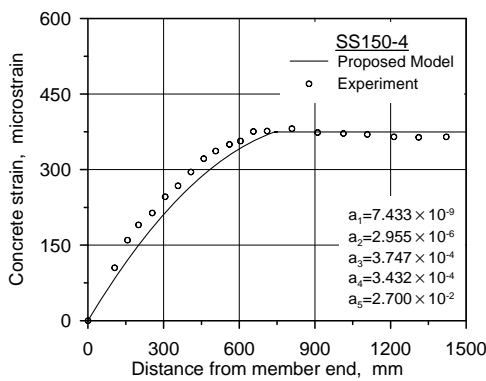
As shown in Tables 6.3 through 6.5, the proposed model underestimated only the test results from Russell and Burns (1997). The measured transfer lengths of the SS160 specimens were longer than those with similar experimental conditions in other studies, i.e., M15-N-C4-1, M15-N-C4-2, 16/31-1865, and 16/31-1500. Russell and Burns (1997) reported that the transfer lengths at the cut end were 34% longer than those at the dead end for the SS150 specimens, but the transfer lengths at both ends were similar for the SS160 specimens. The deviation between the SS160 specimens also seems to be large. While the transfer lengths were much longer for the SS160-2 through SS160-4 specimens, the transfer lengths for the other specimens were relatively close to the estimations. A possible reason for the longer transfer lengths and large deviation could be that the cross section was smaller than that in the other works.

Table 6.6 Comparison of the proposed model and the transfer lengths measured by Russell and Burns (1997)

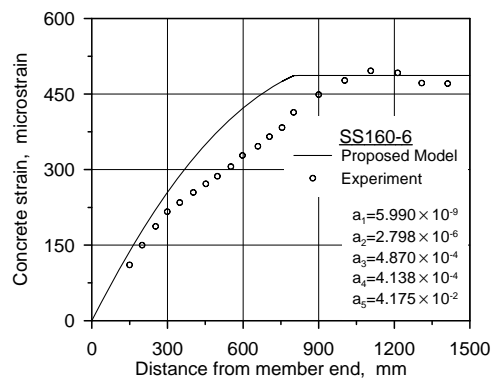
(unit: mm)

Test specimen	Mea. (a)	Cal. (b)	Ratio (b)/(a)	Test specimen	Mea. (a)	Cal. (b)	Ratio (b)/(a)
SS150-3	686	741	1.08	SS160-3	1219	788	0.65
SS150-4	584	741	1.27	SS160-4	1143	788	0.69
SS150-5	864	695	0.80	SS160-5	813	802	0.99
SS150-6	787	695	0.88	SS160-6	965	802	0.83
SS160-1	—	862	—	SS160-7	914	781	0.85
SS160-2	1118	862	0.77	SS160-8	813	781	0.96

Average: 0.89, Standard deviation: 0.18



(a)



(b)

Figure 6.10 Comparison of test results from Russell and Burns (1997) and proposed model: (a) SS150-4; and (b) SS160-6

6.5 Concluding Remarks

A novel bond-slip-strain relationship for a strand was presented from the measurements and equations were proposed for the bond stress, slip, and strand strain within the transfer zone. Model verifications were conducted for steel strands and FRP tendons by comparing the test results from other studies. The proposed model agreed well with the test results for steel strands but was not in good agreement for some types of FRP tendons. More research is needed to modify the model to be validated for FRP tendons. The characteristics of the proposed model are as follows:

1. In the proposed model, the bond stress is obtained by multiplying a slip function and a strain function. The strain function is assumed to be identical to that in the model devised by Shima et al. (1987). The bond behaviors of the strand and reinforcement will be distinguished by the slip function.
2. Sufficient concrete confinement was assumed. Splitting cracks change the bond characteristics, and therefore the model may significantly underestimate the transfer length.
3. The bond stress distribution is linear and begins with an initial value within the transfer zone. The initial value and the slope represent the adhesion bond and the other bond mechanisms, respectively.
4. Slip has a cubic polynomial distribution with an initial value within the transfer zone. The initial value corresponds to the initial value of the bond stress.
5. The strand strain has a quadratic polynomial distribution within the transfer zone. It bends sharply to a value of the elastic strain at the boundary of the

transfer zone, which makes a clear distinction in determining the transfer length. This is different from previous thinking, where the ideal strain distribution would asymptotically approach the elastic strain.

7. Conclusions

7.1 Methodology of Measurement

An extensive experimental program was conducted to measure transfer length of pretensioned concrete members. Strand strains were measured on the helical wires with electrical resistance strain gauges (ERSGs). Applicability of ERSGs to transfer length test and analytical model for behavior of strand were discussed.

1. Provided that specimens and experimental conditions are similar to this experiment, DEMEC gauges cannot yield reliable results when measuring low concrete strains, while ERSGs clearly and accurately measured strain due to prestressing. At least two strain gauges are required at each measuring location to obtain correct strain profiles.
2. In addition to accuracy, other issues should be discussed before applications of ERSGs to tests of transfer length. In this study, loss of bond stresses due to the attachment of steel surface gauges, reliability of measurements on concrete surfaces, and stability of ERSGs under conditions of high temperature were considered. It was concluded that a suitable interval (150 mm) of steel surface gauges did not deteriorate bond between concrete and strand to the extent of affecting test results, that measurements on concrete and steel surface gave almost the same results for 150 mm square sections, and that steel surface gauges yielded stable measurements during high-temperature curing. Thus, the use of ERSGs under these conditions yields reliable measurements of transfer length.

3. ERSGs can also be used to measure prestressing forces and replace load cells through a series of calculations. Using the analytical model proposed by Machida and Durelli (1973), the behavior of the strand and the residual prestressing force were reasonably estimated through the whole fabrication stages.

7.2 Resolution of Discrepancies in Previous Equations

In order to resolve the discrepancies in the predictions of the existing empirical equations, test variables currently known as affecting transfer length were reevaluated and test variables not considered in the previous experimental research were examined.

1. The effects of initial prestress, concrete compressive strength at transfer, and strand diameter could be accounted for by the equation proposed by Oleśniewicz. It implies a linear distribution of bond stress and a parabolic distribution of strand strain.
2. No systematic trends were found in the ranges of cover depth, cross sectional size, and strand spacing considered in this study. It means that there were no harmful effects for smaller values. The effects of these factors were negligible if conforming to the current code provisions.
3. Steam curing processes can result in longer transfer lengths than conventional air curing methods.
4. Debonding reduced transfer lengths by 22% at cut end but increased by 16% at dead end.
5. The reinforcing bars in the vicinity of the strand affected the transfer lengths at

cut end.

6. In average, sudden release method resulted in 35% longer transfer length at cut end.

7.3 Transfer Length of High Strength Strand

Transfer lengths of high-strength strands that have been recently developed were evaluated.

1. Higher initial prestress of Grade 2,400 strand increased transfer length by 21% at dead end and 46% at cut end. The relationship proposed by Oleśniewicz was valid for dead end, however the difference between transfer lengths at dead and cut end was magnified.
2. The current code provisions provided conservative estimates for transfer length of high strength strand. Curing method might result in the underestimation of transfer lengths.
3. No splitting cracks were observed for the specimens and no systematic trends were found in the ranges of cover depth and strand spacing considered in this study. The cover depth and strand spacing of the current code are also feasible to high strength strand.

7.4 Proposal of New Transfer Length Equation

Finally, a novel bond-slip-strain model was proposed based on the actual bond behavior of strand. From the model, simple equations were derived for transfer length, bond stress, slip, and strand strain along the transfer zone. Model

verifications were conducted by comparing the test results from other studies. The proposed model agreed well with the test results.

References

AASHTO. (2010). "AASHTO LRFD Bridge Design Specification," 5th edition, American Association of State Highway and Transportation Officials, Washington, D.C., 1632 pp.

Abdalla, O. A., Ramirez, J. A., and Lee, R. H. (1993). *Strand Debonding in Pretensioned Beams—Precast Prestressed Concrete Bridge Griders With Debonded Strands, Part 2, Final Report: Simply Supported Tests*, Publication No. FHWA/INDOT/JHRP-92-25, School of Civil Engineering of Purdue University and the Indiana Department of Transportation, W.Lafayette, IN., 228 pp.

Abrishami, H. H. and Mitchell, D. (1993). "Bond Characteristics of Pretensioned Strand," *ACI Material Journal*, Vol. 90, No. 3, pp. 228-235.

ACI Committee 318 (2011). "Building Code Requirements for Structural Concrete (ACI318-11) and Commentary", American Concrete Institute, Farmington Hill, MI, 503 pp.

ASTM International. (2006). "Standard Specification for Steel Strand, Uncoated Seven-Wire for Prestressed Concrete," A416/A416M-06, American Society for Testing and Materials, West Conshohocken, PA, 5 pp.

- Balázs, G. L. (1992). "Transfer Control of Prestressing Strands," *PCI Journal*, Vol. 37, No. 6, Nov.-Dec., pp. 60-71.
- Baltay, P. and Gjelsvik, A. (1990). "Coefficient of Friction for Steel on Concrete at High Normal Stress," *Journal of Materials in Civil Engineering*, Vol. 2, No. 1, pp. 46-49.
- Barnes, R. W., Burns, W. H., and Kreger, M. E. (1999). *Development length of 0.6-Inch Prestressing Strand in Standard I-Shaped Pretensioned Concrete Beams*, FHWA/TX-02/1388-1, Austin: Center for Transportation Research, the University of Texas at Austin, Austin, TX, 338 pp.
- Barnes, R. W., Grove, J. W., and Burns, N. H. (2003). "Experimental Assessment of Factors Affecting Transfer Length," *ACI Structural Journal*, Vol. 100, No. 6, pp. 740-748.
- Bogaerts, B. and Brosens, K. (1995). *Ankering van Voorspanstrengen in Geprefabriceerde Vloerelementen*, Graduate Thesis, Katholieke Unversiteit Leuven, Leuven, Belgium, 120 pp.
- Brook, M. D., Gerstle, K. H., and Logan, D. R. (1988). "Effect of Initial Strand Slip on the Strength of Hollow-Core Slabs," *PCI Journal*, Vol. 33, No. 1, pp. 90-111.
- Buckner, C. D. (1995). "A Review of Strand Development Length for Pretensioned Concrete Members," *PCI Journal*, Vol. 40, No. 2, Mar.-Apr., pp. 84-105.

- Burdette, E. G., Deatherage, J. H., and Chew, C. K. (1994). "Development Length and Lateral Spacing Requirements of Prestressing Strand for Prestressed Concrete Bridge Girders," *PCI Journal*, V. 39, No. 1, pp. 70-83.
- Carroll, J. C. (2009). *Grade 300 Prestressing Strand and the Effect of Vertical Casting Position*, PhD Thesis, Virginia Polytechnic Institute and State University, Blacksburg, VA, 337 pp.
- Castrodale, R. W., Burns, N. H., and Kreger, M. E. (1988). *A Study of Pretensioned High Strength Concrete Girders in Composite Highway Bridges – Laboratory Tests*, Research Report 381-3, CTR, the University of Texas at Austin, Austin, TX., 234 pp.
- Choi, E. J. (2015). "Material Modeling of High-Strength Strand and its Impact on Flexural Strength of PSC Members," Master's thesis, Seoul National University, Seoul, South Korea, 53 pp.
- Cousins, T. E., Johnston, D. W., and Zia, P. (1986). *Bond of Epoxy-Coated Prestressing Strand*, FHWA/NC/87-005, Center for Transportation Engineering Studies, North Carolina State University, Raleigh, NC, 370 pp.
- Cousins, T. E., Johnston, D. W., and Zia, P. (1990a). "Transfer and Development Length of Epoxy Coated and Uncoated Prestressing Strand," *PCI Journal*, Vol. 35, No. 4, pp. 92-103.

- Cousins, T. E., Johnston, D. W., and Zia, P. (1990b). "Transfer Length of Epoxy Coated Prestressing Strand," *ACI Material Journal*, Vol. 87, No. 3, pp. 193-203.
- Cousins, T. E., Johnston, D. W., and Zia, P. (1990c). "Development Length of Epoxy Coated Prestressing Strand," *ACI Material Journal*, Vol. 87, No. 4, pp. 309-318.
- Cousins, T. E., Stallings, J. M., and Simmons, M. B. (1993). *Effect of Strand Spacing on Development of Prestressing Strand*, Project No. 65308, Auburn University, Auburn, AL., 150 pp.
- Cousins, T. E., Stallings, J. M., and Simmons, M. B. (1994). "Reduced Strand Spacing in Pretensioned, Prestressing Members," *ACI Structural Journal*, Vol. 91, No. 3, pp. 277-286.
- Deatherage, J. H. and Burdette, E. G. (1994). "Development Length and Lateral Spacing Requirements of Prestressing Strand for Prestressed Concrete Bridge Girders," *PCI Journal*, Vol. 39, No. 1, Jan.-Feb., pp. 70-83.
- Den Uijl, J. A. (1992). "Bond and Splitting Action of Prestressing Strand," *International Conference Bond in Concrete*, Riga, Latvia, pp. 2/79-2/88.
- Den Uijl, J. A. (1996). "Bond of Strands in High Performance Concrete," *4th International Symposium on Utilization of High-strength/High-performance concrete*, Paris, France, pp. 1175-1184.

- Den Uijl, J. A. (1998). "Bond Modelling of Prestressing Strand," Bond and Development of Reinforcement – A tribute to Dr. Peter Gergely, SP180-7, Leon, ed., American Concrete Institute, Farmington Hills, MI, pp. 145-169.
- Den Uijl, J. A. and Bigaj, A. J. (1996). "A Bond Model for Ribbed Bars Based on Concrete Confinement", HERON, Vol. 41, No. 3, pp. 201-226.
- European Committee for Standardization. (2004). "Eurocode 2: Design of Concrete Structures – Part 1-1: General Rules and Rules for Buildings," Brussels, Belgium, 230 pp.
- European Committee for Standardization. (2010). "Steel for the reinforcement and prestressing of concrete - Test methods - Part 3: Prestressing steel," ISO 15630-3:2010, Brussels, Belgium, 38 pp.
- fib, *Bond of Reinforcement in Concrete*, State-of-the-Art Report, Bulletin 10, Task Group Bond Models, Lausanne, Switzerland, 2000, 427 pp.
- Gopalaratnam, V. S. and Shah, S. P. (1985). "Softening Response of Plain Concrete in Direct Tension", ACI JOURNAL, Vol. 82, No. 3, pp. 310-323.
- Gross, S.P. and Burns, N. H. (1995). *Transfer and Development Length of 15.2-mm (0.6-in.) Diameter Prestressing Strand in High Performance Concrete: Results of the Hoblitzell-Buckner Beam Tests*, Research Report 580-2, Center for Transportation Research, The University of Texas at Austin, Austin, TX., 106 pp.

- Grove, J. W. (1998). *Transfer and Development Length of Debonded 0.6-in. (15-mm) Diameter Prestressing Strand in AASHTO Type I Girder Specimens*, Master's Thesis, The University of Texas at Austin, Austin, TX.
- Guyon, Y. (1953). *Prestressed Concrete*, Contractors Record and Municipal Engineering, London, 543 pp.
- Hanson, N. W. (1969). "Influence of Surface Roughness of Prestressing Strand on Bond Performance," *PCI Journal*, Vol. 14, No. 1, pp. 32-45.
- Hanson, N. W., and Kaar, P. H. (1959). "Flexural Bond Tests of Pretensioned Prestressed Beams," *JOURNAL OF THE AMERICAN CONCRETE INSTITUTE*, Vol. 30, No. 7, pp. 783-802.
- Hill, A. T. (2006). *Material Properties of the Grade 300 and Grade 270 Prestressing Strands and Their Impact on the Design of Bridges*, Master's Thesis, Virginia Polytechnic Institute and State University, Blacksburg, VA, 159 pp.
- Hillerborg, A. (1983). "Analysis of One Single Crack," *Fracture Mechanics of Concrete (Developments in Civil Engineering)*, F. H. Wittmann, ed., Vol. 7, Elsevier, pp. 223-249.
- Jabson, H. L. (1997). *Transfer and Development Length of Fully Bonded 0.6-in. (15-mm) Diameter Prestressing Strand in AASHTO Type I Concrete Beams*, Master's Thesis, The University of Texas at Austin, Austin, TX.

Janney, J. R. (1954). "Nature of Bond in Pre-tensioned Prestressed Concrete,"
JOURNAL OF THE AMERICAN CONCRETE INSTITUTE, Vol. 25, No. 9, pp. 717-736.

Janney, J. R. (1963). "Report of Stress Transfer Length Studies on 270 k Prestressing
Strand," *PCI Journal*, Vol. 8, No. 1, pp. 41-45.

Kaar, P., LaFraugh, R., and Mass, M. (1963). "Influence of Concrete Strength on
Strand Transfer Length," *PCI Journal*, Vol. 5, No. 8, pp. 47-67.

KATS. (2011). "Uncoated stress-relieved steel wires and strands for prestressed
concrete," KS D 7002:2011, Korean Agency for Technology and Standards,
Seoul, South Korea, 9 pp.

Kilgore, J. H. (1997). *Transfer and Development Length of Debonded 0.6-in. (15-
mm) Diameter Prestressing Strand in AASHTO Type I Concrete Beam*, Master's
Thesis, The University of Texas at Austin, Austin, TX.

Kim, E. S. (2000). *Analysis of Prestress Transfer Zone and Prediction of Transfer
Length in Pretensioned Prestressed Concrete Member*, PhD Thesis, Seoul
National University, Seoul, Republic of Korea, 186 pp.

Kim, J. K., Seong, T. R., Youn, S. G., Jeon, S. J., and Kim, K. H. (2014). "Stress
Corrosion of PS Strand for Prestressed Concrete," Technical article, *Magazine of
the Korea Concrete Institute*, Vol. 26, No. 4, pp. 45-49. (in Korean)

- Korean Concrete Institute. (2012). "Design Code and Commentary of Concrete Structures," Seoul, Korea, 548 pp. (in Korean)
- Kose, M. M. (1999). *Statistical Evaluation of Transfer and Development Length of Low-Relaxation Prestressing Strands in Standard I-Shaped Pretensioned Concrete Beams*, Ph.D. Thesis, Texas Tech University, Lubbock, TX., 200 pp.
- Kose, M. M. (2007). "Prediction of Transfer Length of Prestressing Strands Using Neural Networks," *ACI Structural Journal*, Vol. 104, No. 2, pp. 162-169.
- Kose, M. M. and Burkette, W. R. (2005). "Formulation of New Development Length Equation for 0.6 in. Prestressing Strand," *PCI Journal*, Vol. 50, No. 5, pp. 96-105.
- Lane, S. N. (1998). *A New Development Length Equation for Pretensioned Strands in Bridge Beams and Piles*, Research Report FHWA-RD-98-116, Structure Division, Federal Highway Administration, McLean, VA., 131 pp.
- Machida, S. and Durelli, A. J. (1973). "Response of A Strand to Axial and Torsional Displacements," *Journal Mechanical Engineering Science*, Vol. 15, No. 4, pp. 241-251.
- Mahmoud, Z. I., Rizkalla, S. H., and Zaghoul, E. R. (1999). "Transfer and Development Lengths of Carbon Fiber Reinforced Polymers Prestressing Reinforcement," *ACI Structural Journal*, Vol. 96, No. 4, pp. 594-602.

Martí-Vargas, J. R., Arbeláez, C. A., Serna-Ros, P., and Castro-Bugallo, C. (2007a). "Reliability of Transfer Length Estimation from Strand End Slip", *ACI Structural Journal*, Vol. 104, No. 4, pp. 487-494.

Martí-Vargas, J. R., Arbeláez, C. A., Serna-Ros, P., Navarro-Gregori, J., and Pallarés-Rubio, L. (2007b). "Analytical Model for Transfer Length Prediction of 13 mm Prestressing Strand", *Structural Engineering and Mechanics*, Vol. 26, No. 2, pp. 211-229.

Mattock, A. H. (1962). "Proposed Redraft of Section 2611 – Bond of the Proposed Revision of Building Code Requirements for Reinforced Concrete (ACI318-56)," ACI Committee 323 Correspondence.

Mitchell, D., Cook, W. D., Khan, A. A., and Tham, T. (1993). "Influence of High Strength Concrete on Transfer and Development Length of Pretensioned Strand," *PCI Journal*, Vol. 38, No. 3, May-Jun., pp. 52-66.

Nanni, A., Utsunomiya, T., Yonekura, H., and Tanigaki, M. (1992). "Transmission of Prestressing Force to Concrete by Bonded Fiber Reinforced Plastic Tendons," *ACI Structural Journal*, Vol. 89, No. 3, pp. 335-344.

Nitsch, A. (2001). *Spannbetonfertigteile mit teilweiser Vorspannung aus hochfestem Beton*, PhD thesis, Faculty of Civil Engineering, RWTH Aachen University, Aachen, German, 269 pp. (in German)

- Noghabai, K. (1995), *Splitting of Concrete in the Anchorage Zone of Deformed Bars*,
Licenciate Thesis, Luleå University of Technology, Sweden, 131 pp.
- Oh, B. H., and Kim, E. S. (2000). "Realistic Evaluation of Transfer Lengths in
Pretensioned, Prestressed Concrete Members", *ACI Structural Journal*, Vol. 97,
No. 6, pp. 821-830.
- Oh, B. H., Kim, E. S., and Choi, Y. C. (2006) "Theoretical Analysis of Transfer
Lengths in Pretensioned Prestressed Concrete Members", *Journal of Engineering
Mechanics*, ASCE, Vol. 132, No. 10, pp. 1057-1066.
- Oleśniewicz, A. (1975). "Statistical Evaluation of Transmission Length of Strand,"
Research and Design Center for Industrial Building (BISTYP), Warsaw, Poland.
- Over, S. and Au, T. (1965). "Prestress Transfer Bond of Pretensioned Strands in
Concrete," *ACI JOURNAL*, Proceedings Vol. 62, No. 11, pp. 1451-1459.
- Peterman, R. J. (2007). "The effects of As-Cast Depth and Concrete Fluidity on
Strand Bond," *PCI Journal*, Vol. 52, No. 3, pp. 72-101.
- Petrou, M., Wan, B., Joiner, W. S., Trezos, C. G., and Harries, K. A. (2000).
"Excessive Strand End Slip in Prestressed Slip," *ACI Strcutural Journal*, Vol. 97,
No. 5, pp. 774-782.

- Plizzari, G., Schumm, C., and Giuriani, E. (1987). "The effect of Residual Tensile Strength of Cracked Concrete on the Local Bond-Slip Law after Splitting," Politecnico di Milano, Studi E. Recherche, Vol. 9, pp. 129-155.
- Russell, B. W., and Burns, N. H. (1993). *Design Guidelines for Transfer, Development and Debonding of Large Diameter Seven Wire Strands in Pretensioned Concrete Girders*, Research Report FHWA/TX-93 1210-5F, Center for Transportation Research, University of Texas at Austin, 286 pp.
- Russell, B. W., and Burns, N. H. (1996). "Measured Transfer Lengths of 0.5 and 0.6 in. Strands in Pretensioned Concrete," *PCI Journal*, Vol. 41, No. 5, pp. 44-65.
- Russell, B. W., and Burns, N. H. (1997). "Measurement of Transfer Lengths on Pretensioned Concrete Elements", *Journal of Structural Engineering*, ASCE, Vol. 123, No. 5, pp. 541-549.
- Shima, H., Chou, L., and Okamura, H. (1987). "Micro and Macro Models for Bond in RC," *Journal of the Faculty of Engineering*, The University of Tokyo (B), Vol. 39, No. 2, pp. 133-194.
- Stocker, M. F. and Sozen, M. A. (1970). *Investigation of Prestressed Concrete for Highway Bridges – Part V: Bond Characteristics of Prestressing Strand*, Bulletin 503, Engineering Experiment Station, University of Illinois at Urbana-Champaign, Ill., 119 pp.

- Tabatabai, H., and Dickson, T. J. (1993). "The History of the Prestressing Strand Development Length Equation," *PCI Journal*, Vol. 38, No. 6, pp. 64-75.
- Tadros, M. K. and Baishya, M. C. (1996). "Reader Comments: A Review of Strand Development Length for Pretensioned Concrete Members," *PCI Journal*, Vol. 41, No. 2, Mar.-Apr., pp. 120-127.
- Tawfiq, K. S. (1995). "Cracking and Shear Capacity of High Strength Concrete Girders, Final Report," FAMU/FSU College of Engineering, Tallahassee, FL., 145 pp.
- Tepfer, R. (1979). "Cracking of Concrete Cover along Achored Deformed Reinforcing Bars," *Magazine of Concrete Research*, Vol. 31, No. 106, pp. 3-12.
- Wan, B., Harries, K. A., and Petrou, M. F. (2002b). "Transfer Length of Strands in Prestressed Concrete Piles," *ACI Structural Journal*, Vol. 99, No. 5, pp. 577-585.
- Wan, B., Petrou, M. F., Harries, K. A., and Hussein, A. A. (2002a). "Top Bar Effects in Prestressed Concrete Piles," *ACI Structural Journal*, Vol. 99, No. 2, pp. 208-214.
- Weerasekera, R. and Loov, R. E. (1990). *Prestress Transfer Length Predicted by Cohesive Crack Model*, International Conference on Micromechanics of Failure of Quasi-Brittle Materials, Albuquerque, NM, USA, pp. 417-426.

Zia, P. and Mostafa, T. (1977). "Development Length of Prestressing Strands," *PCI Journal*, Vol. 22, No. 5, Sep.-Oct., pp. 54-65.

APPENDIX A
Material Properties

A.1 Concrete

A.1.1 Test Series 1

(unit: MPa)

t (day)	Specimen 1		Specimen 2		Specimen 3		Specimen 4		Average	
	$f_c(t)$	$E_c(t)$	$f_c(t)$	$E_c(t)$	$f_c(t)$	$E_c(t)$	$f_c(t)$	$E_c(t)$	$f_c(t)$	$E_c(t)$
1	32.4	27,397	31.3	26,264	31.8	27,192	–	–	31.8	26,951
2*	30.3	26,644	35.3	27,396	32.8	27,192	–	–	32.8	27,077
8	45.7	27,946	41.8	29,117	46.6	27,362	–	–	44.7	28,142
16	53.2	28,226	52.7	27,706	50.7	27,065	–	–	52.2	27,666
24	53.8	28,800	52.7	29,800	55.1	29,848	–	–	53.8	29,483
30	54.5	28,846	53.4	29,768	52.8	29,440	–	–	53.6	29,351

*time of prestress release

A.1.2 Test Series 2

(unit: MPa)

t (day)	Specimen 1		Specimen 2		Specimen 3		Specimen 4		Average	
	$f_c(t)$	$E_c(t)$	$f_c(t)$	$E_c(t)$	$f_c(t)$	$E_c(t)$	$f_c(t)$	$E_c(t)$	$f_c(t)$	$E_c(t)$
1	24.8	21,342	20.4	18,205	–	–	–	–	22.6	19,773
1.8	32.7	25,373	30.6	23,058	–	–	–	–	31.6	24,216
2	32.8	24,488	31.5	24,566	31.3	24,995	–	–	31.9	24,683
3*	32.6	23,372	34.9	25,199	31.2	25,808	–	–	32.9	24,793
7	36.0	24,823	35.4	25,120	34.5	24,877	–	–	35.3	24,940
15	38.6	26,496	39.2	26,386	40.9	28,009	–	–	39.5	26,963
21	39.1	26,138	38.4	26,998	37.6	25,100	–	–	38.4	26,078
30	41.1	31,736	48.2	44,372	–	–	–	–	44.7	31,736

*time of prestress release

A.1.3 Test Series 3

(unit: MPa)

t (day)	Specimen 1		Specimen 2		Specimen 3		Specimen 4		Average	
	$f_c(t)$	$E_c(t)$	$f_c(t)$	$E_c(t)$	$f_c(t)$	$E_c(t)$	$f_c(t)$	$E_c(t)$	$f_c(t)$	$E_c(t)$
1	30.8	26,066	28.6	25,263	31.9	22,619	29.7	22452	30.3	24,100
2*	32.8	22,112	31.7	23,511	32.5	24,507	–	–	32.3	23,377
7	36.8	25,856	41.1	26,509	37.9	25,396	–	–	38.6	25,920
16	42.5	27,481	46.1	27,009	45.3	25,643	–	–	44.6	26,711
21	49.8	29,456	47.9	27,821	48.9	26,618	–	–	48.9	27,965
30	50.8	27,669	47.0	26,396	52.8	27,932	–	–	50.2	27,333

*time of prestress release

A.1.4 Test Series 4

(unit: MPa)

t (day)	Specimen 1		Specimen 2		Specimen 3		Specimen 4		Average	
	$f_c(t)$	$E_c(t)$	$f_c(t)$	$E_c(t)$	$f_c(t)$	$E_c(t)$	$f_c(t)$	$E_c(t)$	$f_c(t)$	$E_c(t)$
1	37.3	25,247	38.1	27,452	40.5	25,484	37.1	27,700	38.2	26,471
2*	37.8	25,917	40.8	26,290	38.3	27,346	38.2	24,983	38.8	26,134
9	42.5	25,524	41.0	27,161	40.9	26,693	–	–	41.5	26,460
14	46.4	25,747	44.1	26,167	46.6	26,798	–	–	45.7	26,237
23	48.5	26,993	48.1	26,584	52.3	27,130	–	–	49.6	26,902
33	45.6	27,437	48.6	26,898	47.1	25,871	–	–	47.1	26,735

*time of prestress release

A.1.5 Test Series 5

(unit: MPa)

t (day)	Specimen 1		Specimen 2		Specimen 3		Specimen 4		Average	
	$f_c(t)$	$E_c(t)$	$f_c(t)$	$E_c(t)$	$f_c(t)$	$E_c(t)$	$f_c(t)$	$E_c(t)$	$f_c(t)$	$E_c(t)$
2*	37.9	26,784	40.7	25,705	34.6	26,610	–	–	37.7	26,366
	38.1	25,118	33.5	25,424	34.6	26,220	–	–	35.4	25,587
14	51.4	29,709	56.1	30,108	–	–	–	–	53.7	29,909
	51.4	28,508	40.6	28,370	–	–	–	–	46.0	28,439
30	55.5	29,164	57.3	29,634	–	–	–	–	56.4	29,399
	53.0	29,376	52.7	29,156	–	–	–	–	52.9	29,266

*time of prestress release

A.1.6 Test Series 6

(unit: MPa)

t (day)	Specimen 1		Specimen 2		Specimen 3		Specimen 4		Average	
	$f_c(t)$	$E_c(t)$	$f_c(t)$	$E_c(t)$	$f_c(t)$	$E_c(t)$	$f_c(t)$	$E_c(t)$	$f_c(t)$	$E_c(t)$
2*	32.3	25,167	30.5	–	24.2	24,220	–	–	29.0	24,694
	29.9	24,617	30.3	–	26.8	20,691	–	–	29.0	22,654
8	36.1	24,871	38.0	24,682	36.3	25,226	–	–	36.8	24,926
	38.6	24,765	38.7	26,669	37.1	24,469	–	–	38.1	25,301
28	38.2	25,176	43.9	25,082	43.9	25,868	–	–	42.0	25,376
	41.2	25,631	41.2	26,252	45.3	26,867	–	–	42.6	26,250

*time of prestress release

A.1.7 Test Series 7

(unit: MPa)

t (day)	Specimen 1		Specimen 2		Specimen 3		Specimen 4		Average	
	$f_c(t)$	$E_c(t)$	$f_c(t)$	$E_c(t)$	$f_c(t)$	$E_c(t)$	$f_c(t)$	$E_c(t)$	$f_c(t)$	$E_c(t)$
6	19.8	12,840	–	–	–	–	–	–	19.8	12,840
7	23.1	17,883	–	–	–	–	–	–	23.1	17,883
11	31.1	20,768	29.7	20,328	–	–	–	–	30.4	20,548
13*	29.4	21,582	32.0	20,351	30.9	21,743	–	–	30.7	21,225
31	39.2	25,451	41.7	27,007	27.2	28,246	–	–	36.0	26,902

*time of prestress release

(unit: MPa)

t (day)	Specimen 1		Specimen 2		Specimen 3		Specimen 4		Average	
	$f_c(t)$	$E_c(t)$	$f_c(t)$	$E_c(t)$	$f_c(t)$	$E_c(t)$	$f_c(t)$	$E_c(t)$	$f_c(t)$	$E_c(t)$
6	32.5	23,007	–	–	–	–	–	–	32.5	23,007
7*	34.1	23,664	33.3	24,293	35.0	24,645	–	–	34.2	24,200
31	49.4	29,644	51.4	28,161	43.7	26,578	45.6	28,682	47.5	28,266

*time of prestress release

A.1.8 Test Series 8

(unit: MPa)

t (day)	Specimen 1		Specimen 2		Specimen 3		Specimen 4		Average	
	$f_c(t)$	$E_c(t)$	$f_c(t)$	$E_c(t)$	$f_c(t)$	$E_c(t)$	$f_c(t)$	$E_c(t)$	$f_c(t)$	$E_c(t)$
1	20.2	–	20.2	–	19.7	–	–	–	20.0	–
4	27.7	–	25.9	–	25.7	–	–	–	26.4	–
5	27.7	–	30.2	–	28.0	–	–	–	28.6	–
6*	32.4	–	31.0	–	30.3	–	–	–	31.2	–
20	38.2	–	36.5	–	37.6	–	–	–	37.4	–
28	39.8	–	38.8	26,119	40.1	27,081	–	–	39.6	26,600

*time of prestress release

A.1.9 Test Series 9

(unit: MPa)

t (day)	Specimen 1		Specimen 2		Specimen 3		Specimen 4		Average	
	$f_c(t)$	$E_c(t)$	$f_c(t)$	$E_c(t)$	$f_c(t)$	$E_c(t)$	$f_c(t)$	$E_c(t)$	$f_c(t)$	$E_c(t)$
2	19.1	–	19.4	–	19.6	–	–	–	19.4	–
6	23.3	–	24.4	–	23.8	–	–	–	23.9	–
	26.5	–	25.0	–	26.9	–	–	–	26.2	–
8	27.8	–	27.1	–	26.6	–	–	–	27.2	–
11	28.3	–	28.2	–		–	–	–	28.3	–
16*	32.2	–	33.4	–	30.9	–	–	–	32.2	–
49	32.2	14,908	36.1	21,890	34.7	16,171	–	–	34.3	17,656

*time of prestress release

A.1.10 Test Series 10

(unit: MPa)

t (day)	Specimen 1		Specimen 2		Specimen 3		Specimen 4		Average	
	$f_c(t)$	$E_c(t)$	$f_c(t)$	$E_c(t)$	$f_c(t)$	$E_c(t)$	$f_c(t)$	$E_c(t)$	$f_c(t)$	$E_c(t)$
1	32.5	–	32.9	–	33.0	–	–	–	32.8	–
3	42.1	–	39.9	–	41.3	–	–	–	41.1	–
5*	45.8	–	45.8	–	46.2	–	–	–	46.0	–
	43.3	–	45.9	–	48.9	–	–	–	46.0	–
6	45.6	–	48.1	–	47.8	–	–	–	47.1	–
30	64.2	38,085	63.5	25,004	64.8	22,351	–	–	64.2	28,480

*time of prestress release

A.2 Grade 1,860 strand (12.7 mm)

2009-03-13 15:51 FROM:

TO:00221456477

P:2/2

품질시험 · 검사성적서

- ① 시 료 명 : PC 강연선(SWPC 7B1, 12.7mm, 고리제강)
 ② 시료 채취장소 : 인천광역시 연수구 송도동 12-1번지 인천대학교 현장
 ③ 성취 이용목적 : 품질시험용
 ④ 공 사 형 : 인천대학교 현장
 ⑤ 발 주 자 : 인천대학교(주)
 ⑥ 시 공 자 : 삼산JOINT VENTURE
 주 소 : 인천광역시 연수구 송도동 12-1번지
 ⑦ 의뢰인 생 명 : 한중대리인 김동영

⑧ 성적서번호 : TQU-000456

⑨ 접수 일자 : 2009년 02월 09일



귀하가 동시시험 · 검사 의뢰한 각 시료에 대하여는 아래 시험방법에 의하여 시험 · 검사한 성과와 다음과 같이 호신합니다.

성과 결과

시험 · 검사종목	단위	시험구분	시험 · 검사방법	시험 · 검사결과	책임기술자		
					자격종목	성명	서명
인장시험	KN		KS D 7002 : 2002	191	건축품질시험기술사	박연규	우승
1%압구간신축에 대한 하중	KN		KS D 7002 : 2002	176	건축품질시험기술사	박연규	우승
연신율	%		KS D 7002 : 2002	6.9	건축품질시험기술사	박연규	우승
회전저항	mm		KS D 7002 : 2002	12.6	건축품질시험기술사	박연규	우승
회소저항	mm		KS D 7002 : 2002	12.6	건축품질시험기술사	박연규	우승
삼축압축과 축간지압과의 차	mm		KS D 7002 : 2002	0.14	건축품질시험기술사	박연규	우승
인장무거	kg/cm		KS D 7002 : 2002	775	건축품질시험기술사	박연규	우승
코인양자	백		KS D 7002 : 2002	14	건축품질시험기술사	박연규	우승

- 시료채취자 : 삼산JV 윤성중
- 시료채취인허자 : 김리던 박일성
- 시료채취일자 : 2009년 02월 02일

이 시험 · 검사결과는 동초 의뢰사 제출된 시료에 대한 결과이므로 다른 목적으로 이용을 금지합니다.

시험번호	B-40010-026
구분	신민서명
과장	윤성중
검사	박연규

2009년 02월 18일

한국화학시험연구원



주소 : 울산광역시 중구 대문동 411

(전화번호 : 052-220-3166, 김재준)

유의사항 : 책임기술자의 성명과 서명이 기록되지 아니한 경우에는 성과에 대한 보증은 할 수 없습니다.


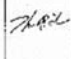






총 1 페이지 중 1 페이지

A.3 Grade 1,860 strand (15.2 mm)

2009-08-13 15:50 FROM:

TO:80221456477

P:1/2

 (주)신진계.류.씨 (주)신진계.류.씨		품질시험 · 검사성적서																		
NO. 155																				
① 시 료 명 :	PC 강연관(SWPC 7BL1 - 15.2mm(은봉))																			
② 시 료 제작 장소 :	인천광역시 연수구 송도동 12-1번지																			
③ 시 료 적용 목적 :	편의시설																			
④ 중 사 명 :	인천테크 빌딩																			
⑤ 발 주 자 :	인천테크 주식회사																			
⑥ 시 공 자 :	삼성 JOINT VENTURE																			
⑦ 의뢰인 :	주 소 : 인천광역시 연수구 송도동 12-1번지 상 명 : 원 동 신 삼성주산(주) 건설주관																			
※ 귀하가 2002. 04. 10일자로 종결사건 - 검사 의뢰한 위 시료에 대하여는 아래 시험방법에 의하여 시험 결과는 다음과 같이 되었습니다.																				
성 과 결 과																				
번 번호	시험 · 검사종목	시험 검사 방법	시험 · 검사결과	제 임 기 속 자																
				과격중속 및 자기중속 번호	성 명	서 명														
1	0.2트랩구연선관에 대한 과중시험		248 248수	보통 품질 시험기속사 9715003002TV	김 용 하															
2	인장하중(KN)		267 267수																	
3	인 장 륜(%)		3.7 3.7수																	
4	직경(mm)	KS D 7002	15.13 $\begin{matrix} +0.2 \\ -0.2 \end{matrix}$																	
5	상선 과 축선 지름차 차(mm)		0.19 0.19수																	
6	연위중량(kg/12m)		1106 1106수																	
7	포염분율(ra)		243.6 $\begin{matrix} 0.04 \\ 0.02 \end{matrix}$																	
※ 시 료 제 의 자 : 삼성JV 공 부 조 ※ 시 료 제 의 회 사 : 김 리 단 공 부 조 ※ 시 료 제 의 일 : 2003. 01. 01																				
<table border="1"> <tr> <td>시험번호</td> <td colspan="3">-</td> </tr> <tr> <td>구 분</td> <td>성 명</td> <td>서 명</td> <td></td> </tr> <tr> <td>확인자</td> <td>김용하</td> <td></td> <td></td> </tr> <tr> <td>감리단</td> <td>김리단</td> <td></td> <td></td> </tr> </table>					시험번호	-			구 분	성 명	서 명		확인자	김용하			감리단	김리단		
시험번호	-																			
구 분	성 명	서 명																		
확인자	김용하																			
감리단	김리단																			
※ 이 시험 · 검사결과는 당초 의뢰한 해당 시료에 대한 결과이므로 다른 목적으로 이용을 금합니다. 2009년 04월 15일 (주)신진계.류.씨 품질시험전문기관 대표 : 김 선 (주)443-812 경기도 화성시 봉곡면 광지의 861-5(12)																				
※ 계약사항 : 책임기술자와 성명표 적명이 기재되지 아니한 경우에는 성과에 대한 보증은 할 수 없습니다.																				

A.4 Grade 2,400 strand



Factory : 127-27 Yusan-Dong Yangsan-City, Kyungnam (626-230), Korea
Tel : 82-55-389-1400-3 Fax : 82-55-389-1404 www.kiswire.com

Mill Test Certificate

To Messrs. 한국건설기술연구원

L/C No. : 201301PCU56200 Coil No. : 1 Sheet No. : 1/1
Commodity : UNCOATED 7-WIRE STRESS RELIEVED STEEL STRAND FOR P.C
Specification : KS D 7002 Grade : SWPC 7D. L
Net. Wt : 1,545kg DATE : 2013/01/25

1. Construction & Dimensions

Item	Unit	Specification	Results		
			1	2	3
Construction(center+outer wire)	-	1+6	1+6	1+6	1+6
Strand diameter(공칭직경)	mm	15.2 +0.4,-0.2	15.28	15.28	15.28
Steel area(공칭단면적)	mm ²	138.70	141.38	141.38	141.40
Lay length(꼬임길이)	mm	182.4~273.6	223.0	223.0	223.0
Weight per 1000m(단위질량)	kg	1101	1099.5	1099.5	1099.5
Difference in wire size(center-outer)	mm	Min. 0.08	0.140	0.140	0.140
Lay Direction(꼬임방향)	-	-	S	S	S

2. Physical Properties

Item	Unit	Specification			
Breaking strength(연선인장하중)	kN	Min. 333	336.2	336.7	337.5
Yield strength at(0.2%)(항복하중)	kN	Min. 283	314.9	316.1	316.9
Elongation in (600mm)(신율)	%	Min. 3.5	7.6	7.9	7.0
Modulus of elasticity(탄성계수)	kN/mm ²	-	200.9	203.9	202.6
Relaxation at(576)hrs (70)% of (B/S)	%	Max. 2.5	0.65	0.65	0.65

3. Chemical Composition (%)

Charge No.	C(x100)	Si(x100)	Mn(x100)	P(x1000)	S(x1000)
SF23763	99	134	51	10	2

4. Finish

Stress relieving : Each strand had been subjected to stress-relieving continuous heat treatment after stranding.

This is to Certify that the above particulars are correct.


CHIEF INSPECTOR OF
KISWIRE LTD.

KISWIRE LTD.

Head Office : 475, Mangmi-Dong, Sooyoung-Ku, Busan, Korea Tel 82-51-754-6007-13, Fax 82-51-757-7379

Seoul Office : 20th floor, Jangkyo Bldg., 1, Jangkyo-Dong, Chung-Ku, Seoul, Korea Tel 82-2-3166-114, Fax 82-2-3166-280



APPENDIX B

Transfer Length Test Results

B.1 Test Series 1

B.1.1 Preliminary Test

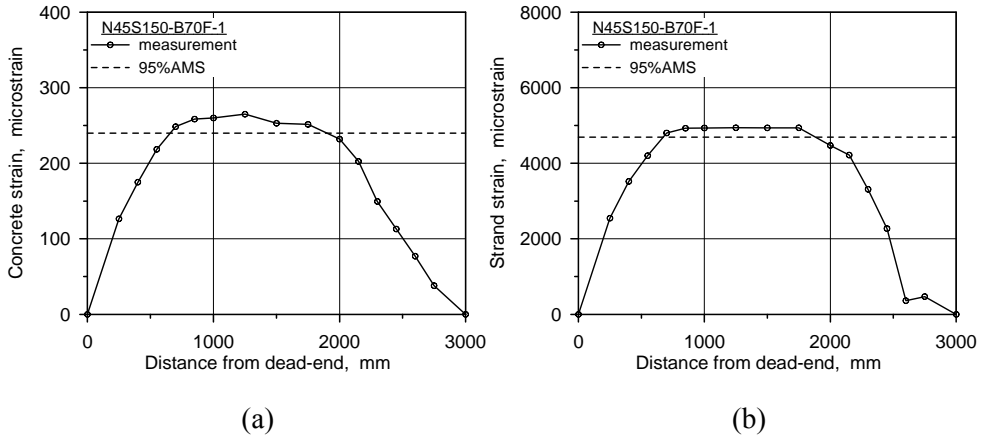


Figure B.1 Strain profiles of the specimens N45S150-B70F-1: (a) concrete strain; and (b) strand strain

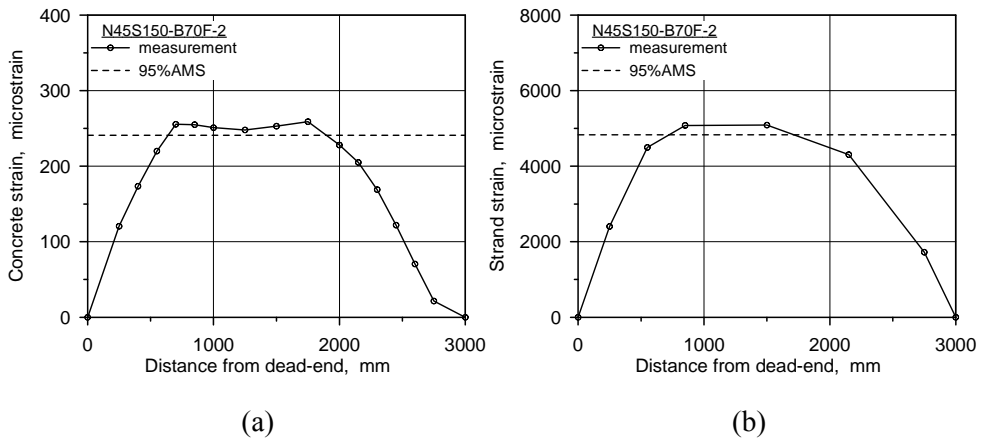
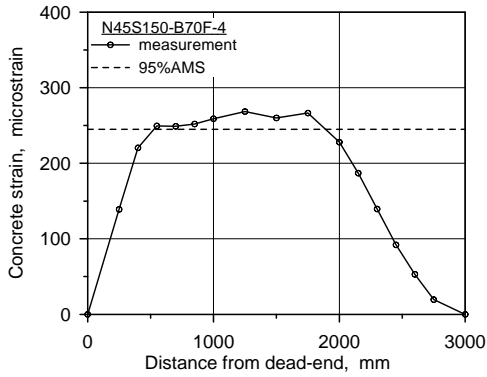


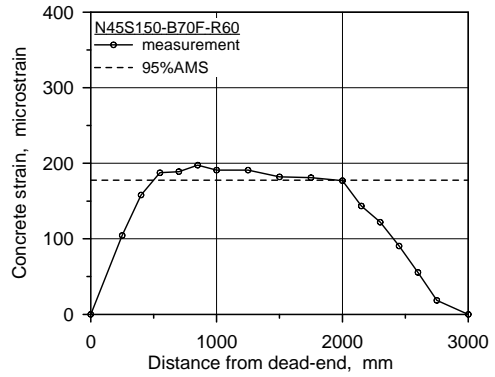
Figure B.2 Strain profiles of the specimens N45S150-B70F-2: (a) concrete strain; and (b) strand strain

B.2 Test Series 2

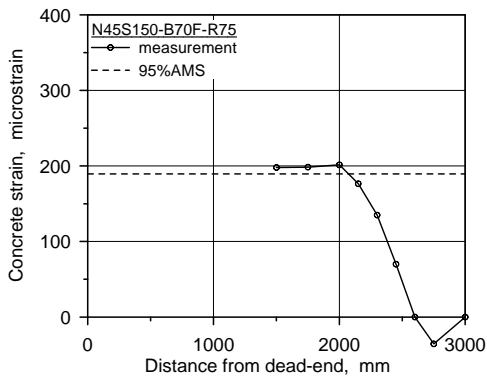
B.2.1 Reinforcement Spacing



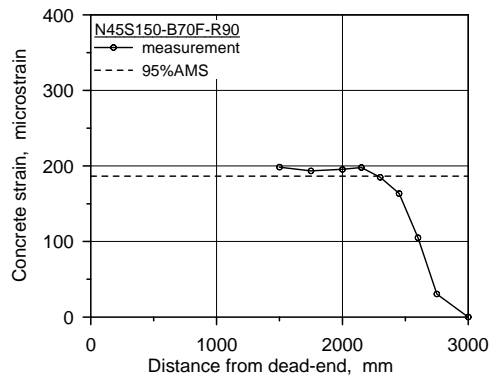
(a)



(b)



(c)



(d)

Figure B.3 Concrete strain profiles of the specimens in test series 2: (a) N45S150-B70F-4; (b) N45S150-B70F-R60; (c) N45S150-B70F-R75; and (d) N45S150-B70F-

R90

B.3 Test Series 3

B.3.1 Strand Spacing

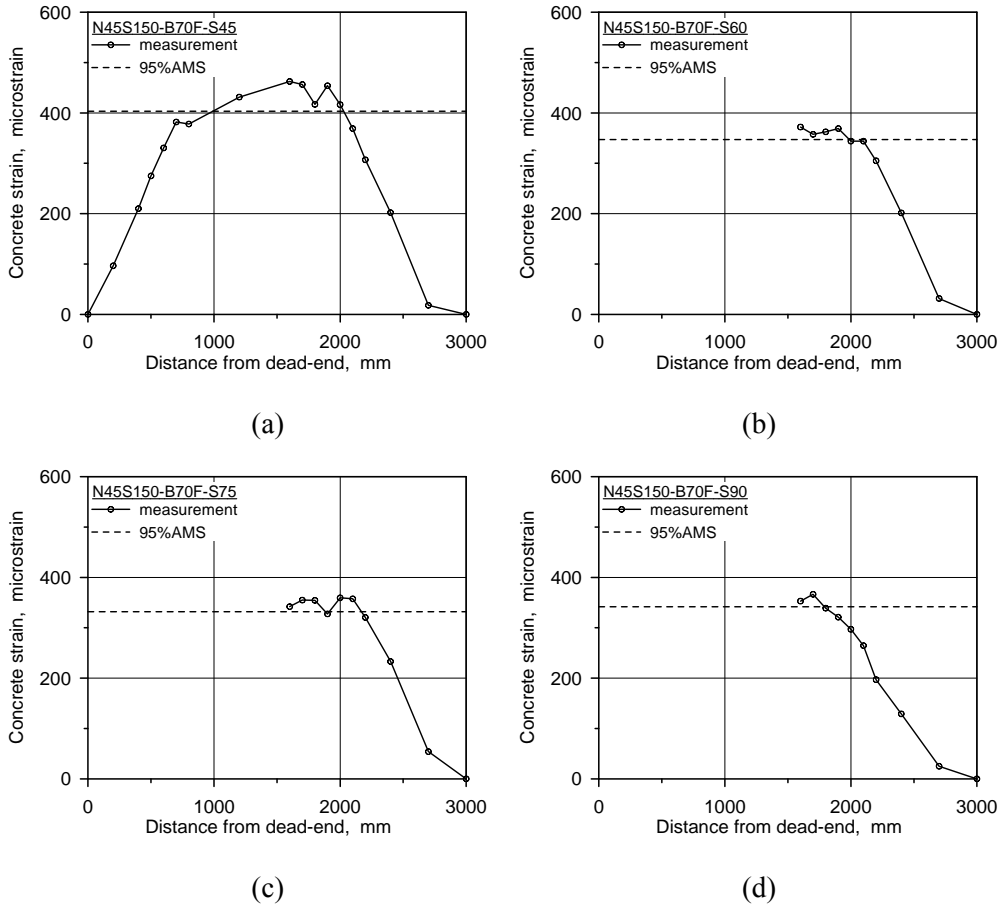
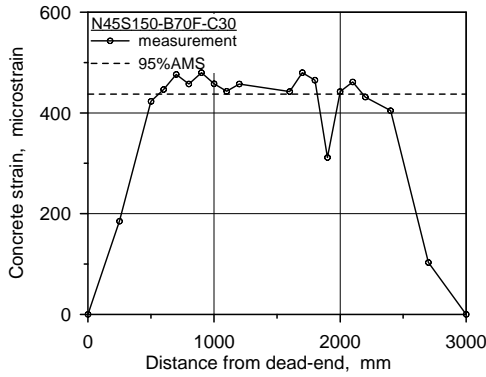


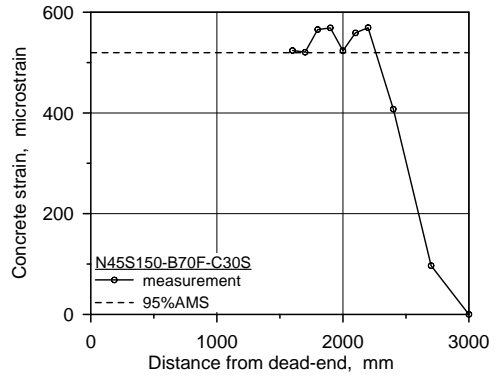
Figure B.4 Concrete strain profiles of the specimens in test series 3: (a) N45S150-B70F-S45; (b) N45S150-B70F-S60; (c) N45S150-B70F-S75; and (d) N45S150-B70F-S90

B.4 Test Series 4

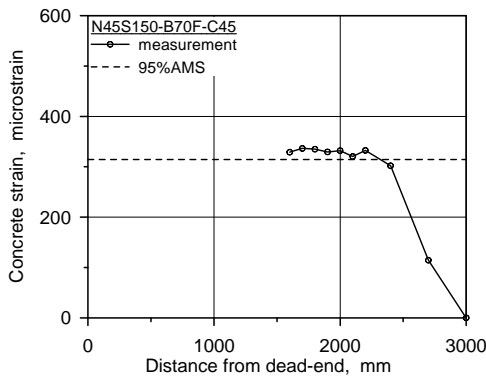
B.4.1 Cover Depth



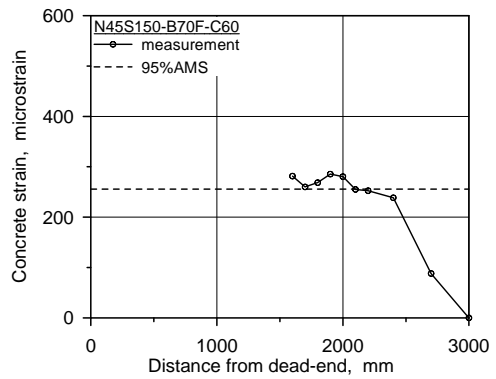
(a)



(b)



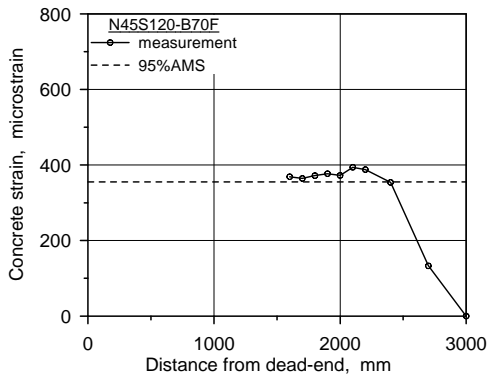
(c)



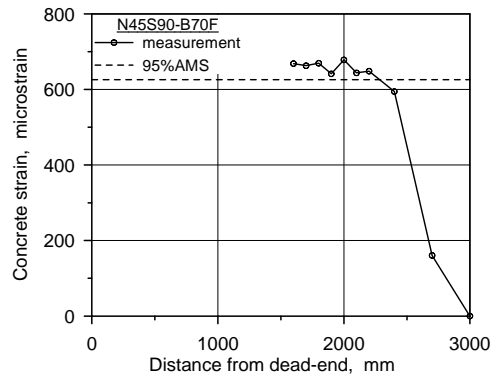
(d)

Figure B.5 Concrete strain profiles of the specimens in test series 4: (a) N45S150-B70F-C30; (b) N45S150-B70F-C30S; (c) N45S150-B70F-C45; and (d) N45S150-B70F-C60

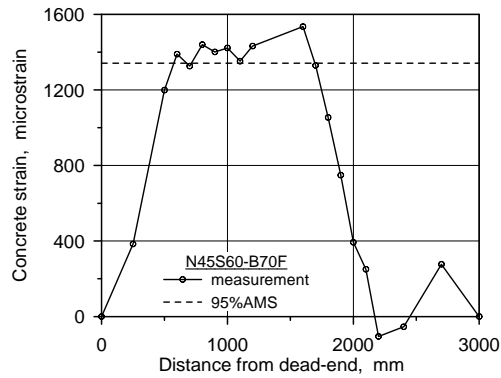
B.4.2 Cross Section Size



(a)



(b)



(c)

Figure B.6 Concrete strain profiles of the specimens in test series 4: (a) N45S120-B70F; (b) N45S90-B70F; and (c) N45S60-B70F

B.5 Test Series 5

B.5.1 Cross Section Size

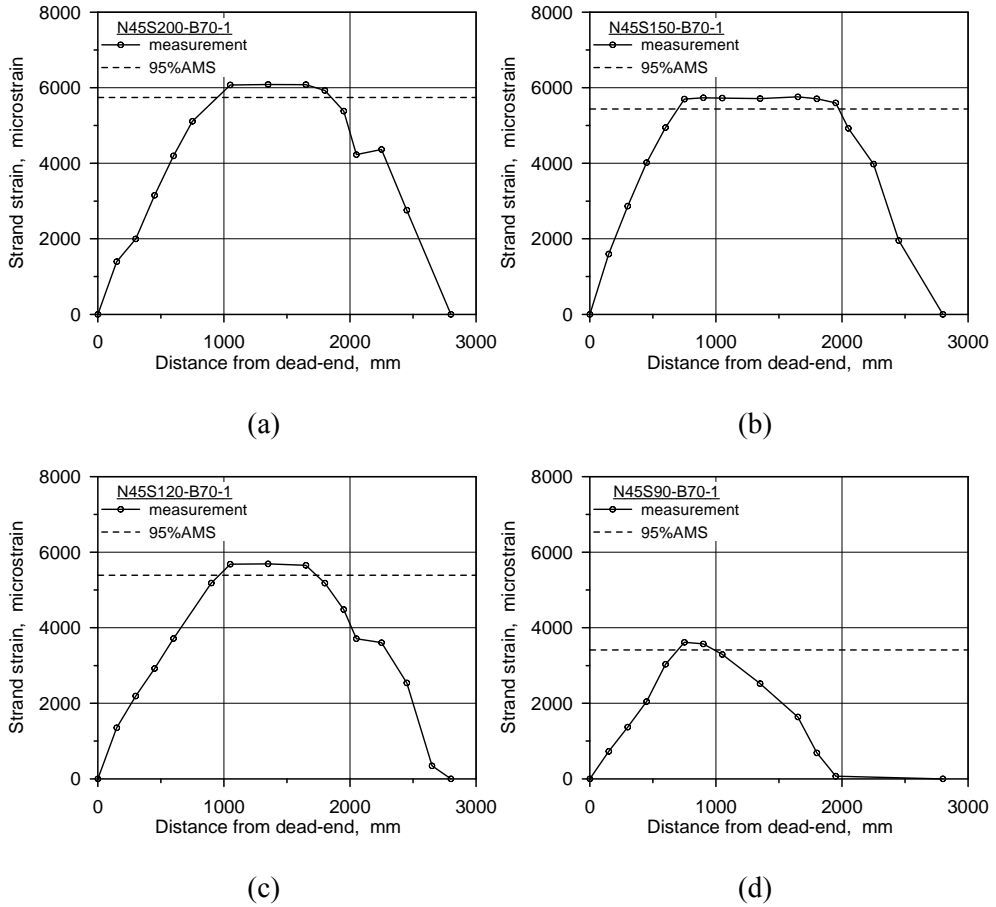


Figure B.7 Strand strain profiles of the specimens in test series 5: (a) N45S200-B70-1; (b) N45S150-B70-1; (c) N45S120-B70-1; and (d) N45S90-B70-1

B.5.2 Cover Depth

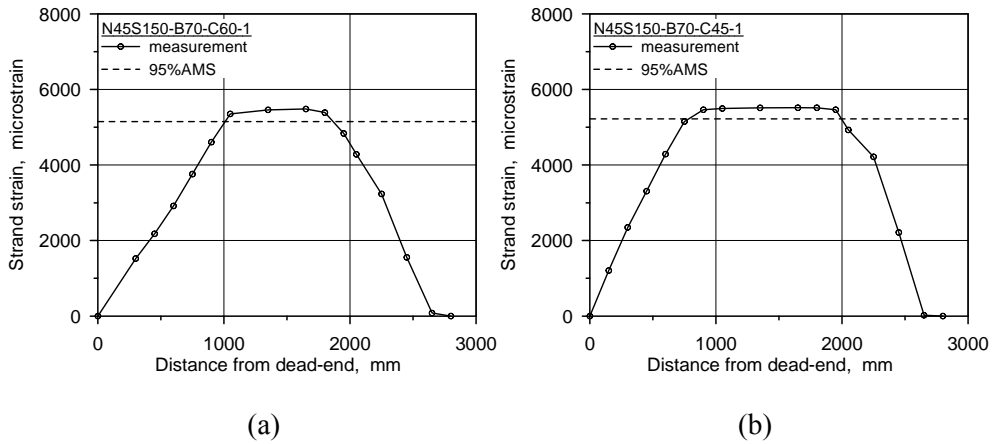


Figure B.8 Strand strain profiles of the specimens in test series 5: (a) N45S200-B70-C60-1; and (b) N45S150-B70-C45-1

B.5.3 Strand Diameter

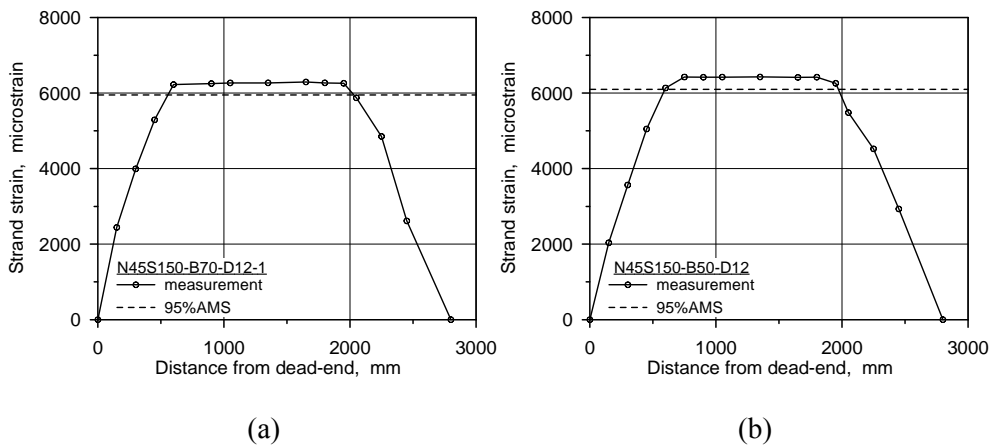


Figure B.9 Strand strain profiles of the specimens in test series 5: (a) N45S150-B70-D12-1; and (b) N45S150-B50-D12

B.5.4 Initial Prestress and Debonding

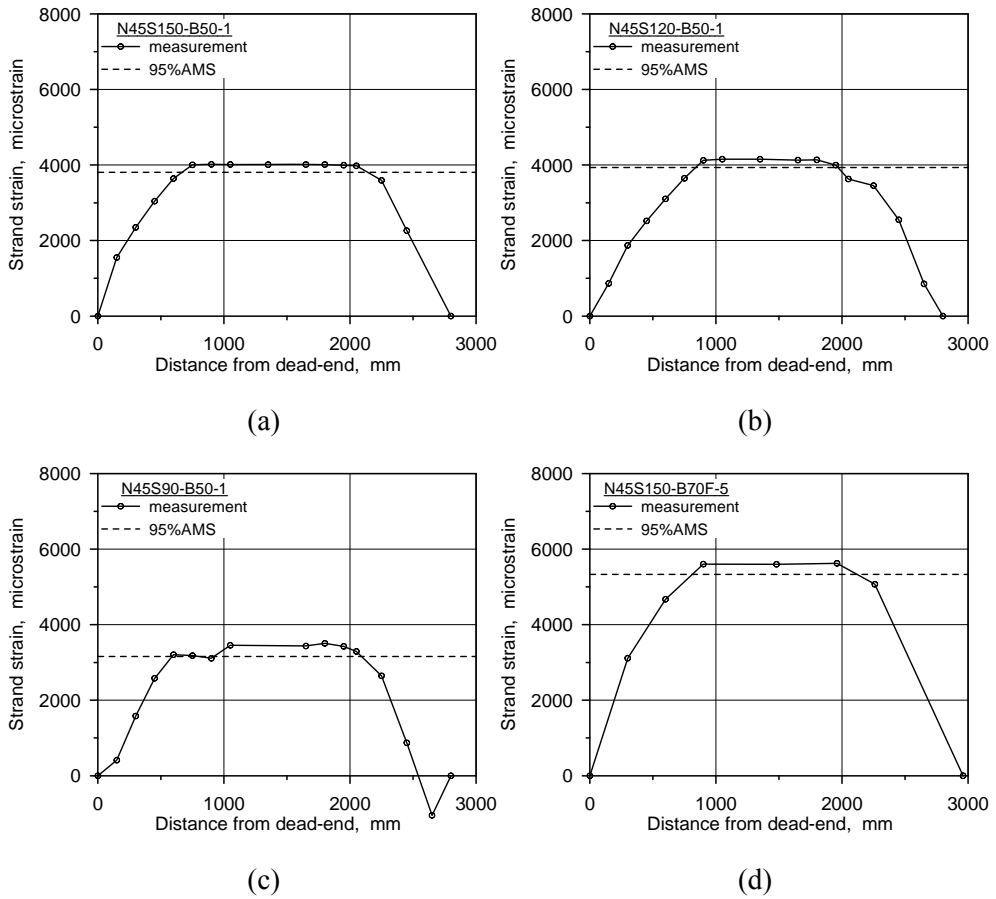


Figure B.10 Strand strain profiles of the specimens in test series 5: (a) N45S150-B50-1; (b) N45S120-B50-1; (c) N45S90-B50-1; and (d) N45S150-B70F-5

B.6 Test Series 6

B.6.1 Cross Section Size

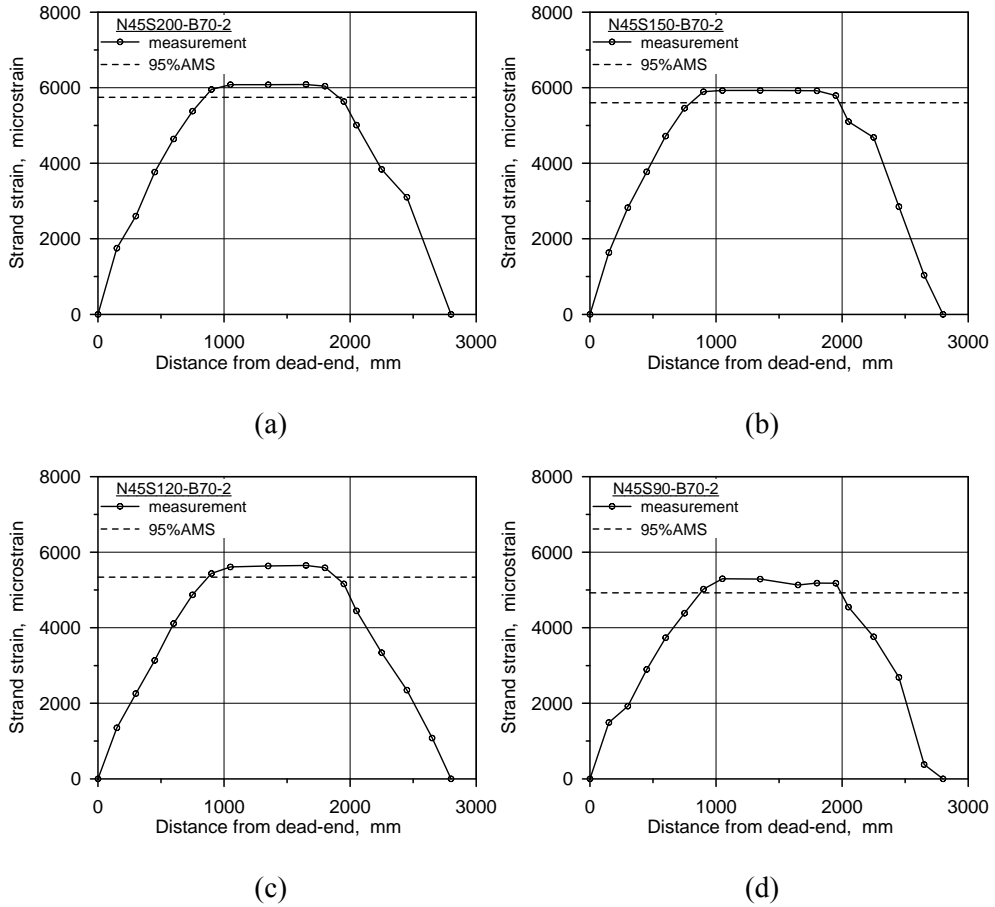


Figure B.11 Strand strain profiles of the specimens in test series 6: (a) N45S200-B70-2; (b) N45S150-B70-2; (c) N45S120-B70-2; and (d) N45S90-B70-2

B.6.2 Cover Depth

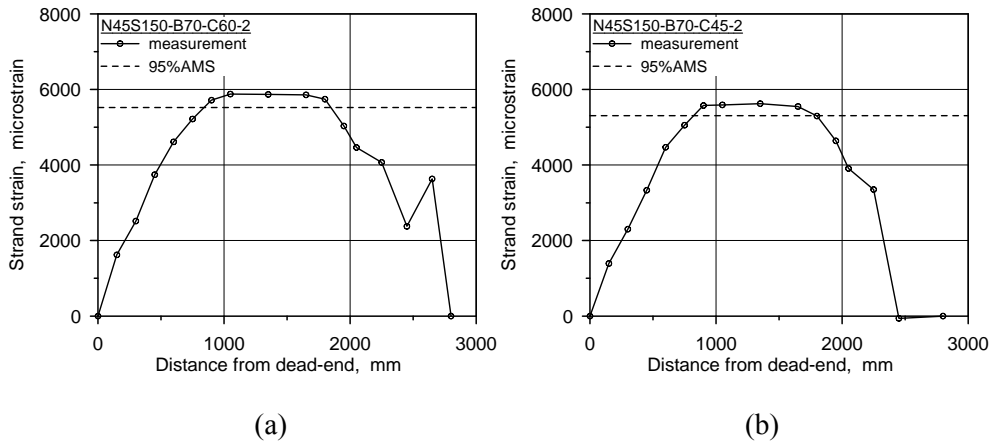


Figure B.12 Strand strain profiles of the specimens in test series 6: (a) N45S200-B70-C60-2; and (b) N45S150-B70-C45-2

B.6.3 Strand Diameter

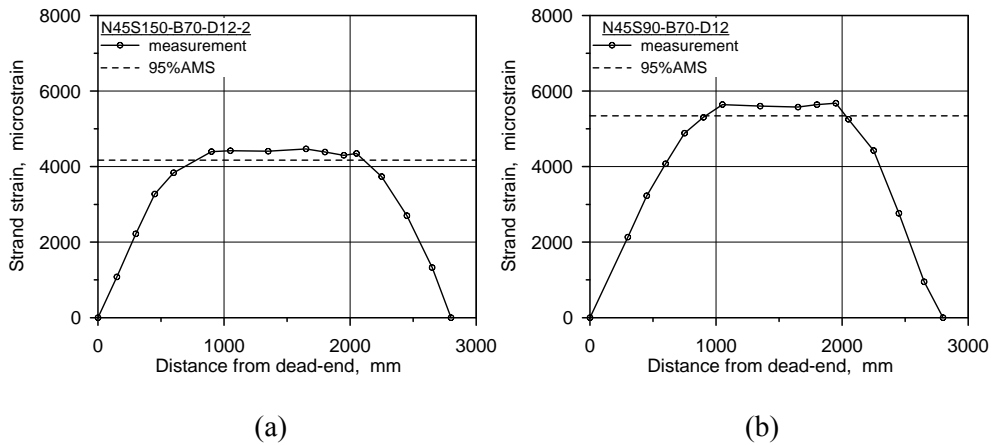


Figure B.13 Strand strain profiles of the specimens in test series 6: (a) N45S150-B70-D12-2; and (b) N45S90-B70-D12

B.6.4 Initial Prestress

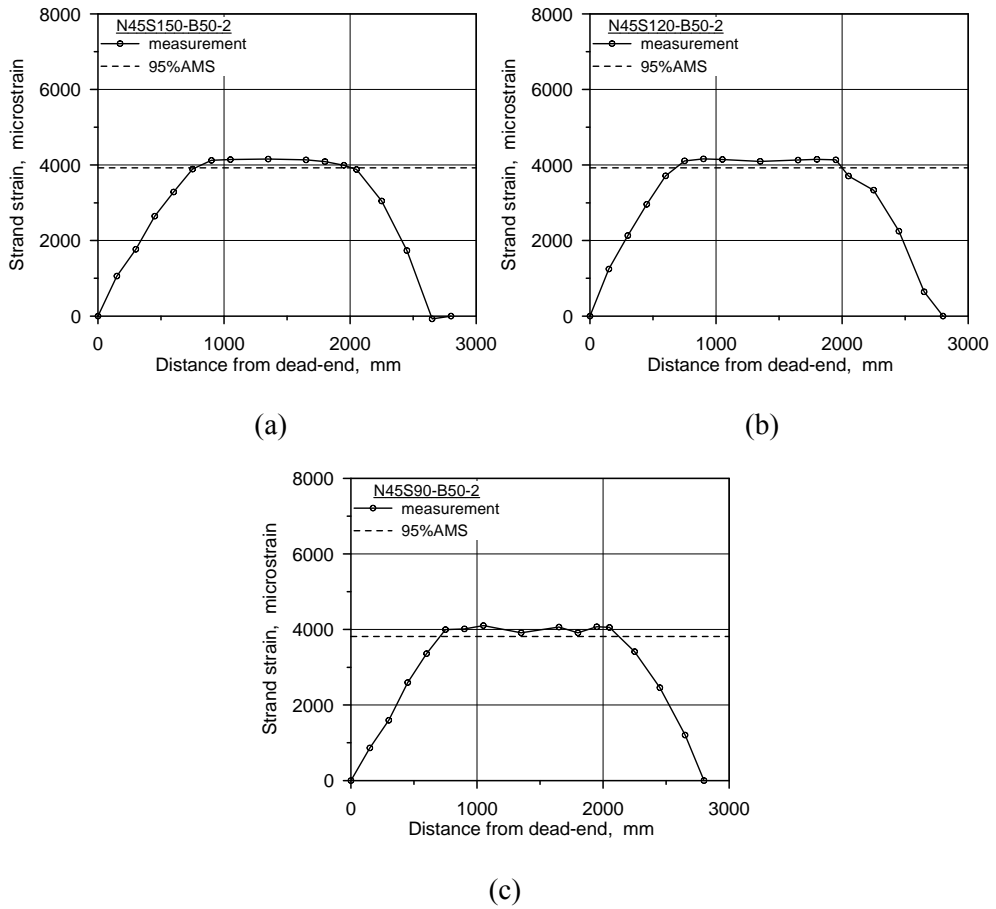


Figure B.14 Strand strain profiles of the specimens in test series 6: (a) N45S150-B50-2; (b) N45S120-B50-2; and (c) N45S90-B50-2

B.7 Test Series 7

B.7.1 Design Concrete Compressive Strength

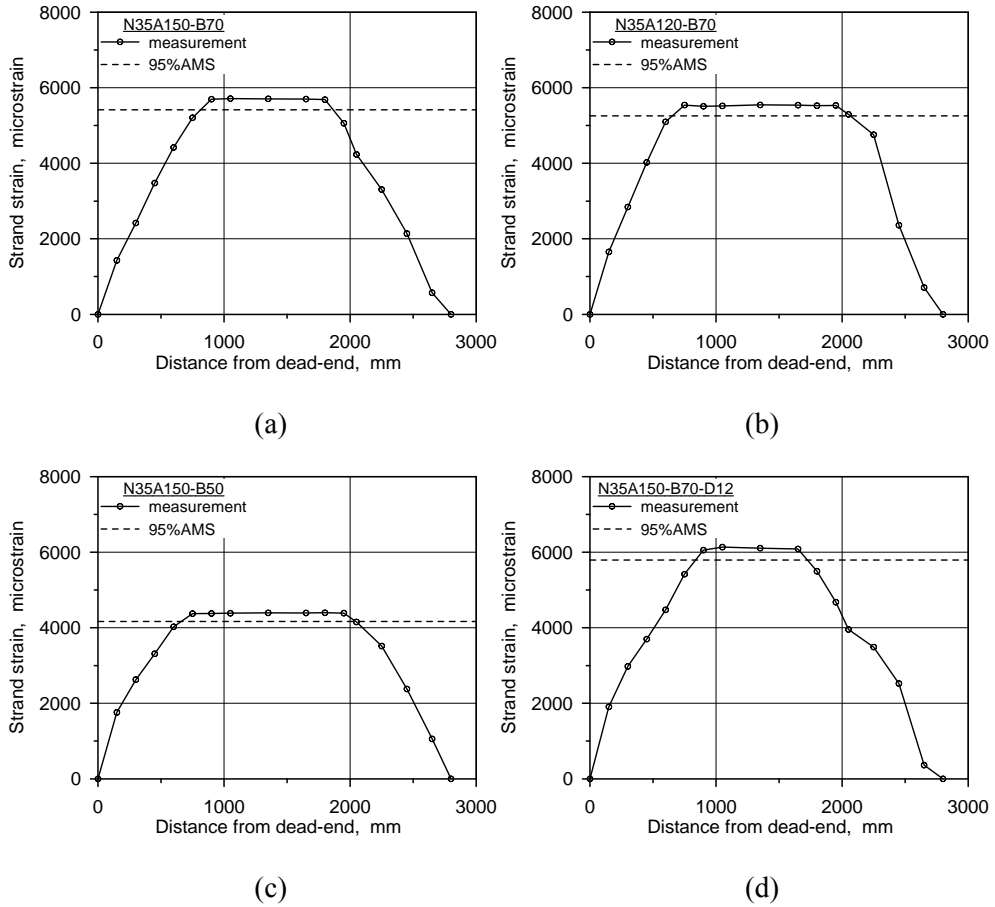


Figure B.15 Strand strain profiles of the specimens in test series 7: (a) N35A150-B70; (b) N35A120-B70; (c) N35A150-B50; and (d) N35A150-B70-D12

B.7.2 Curing Condition

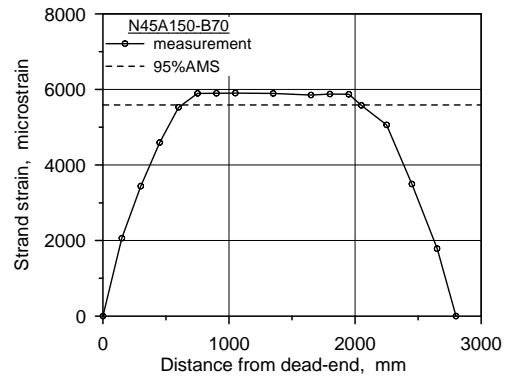
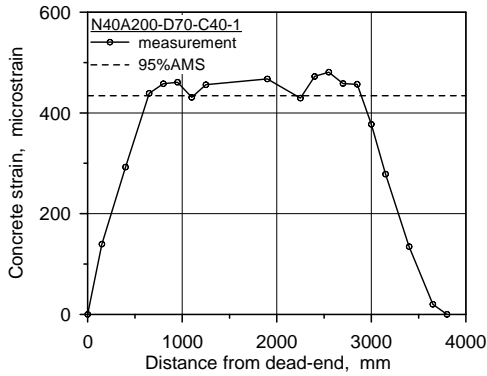


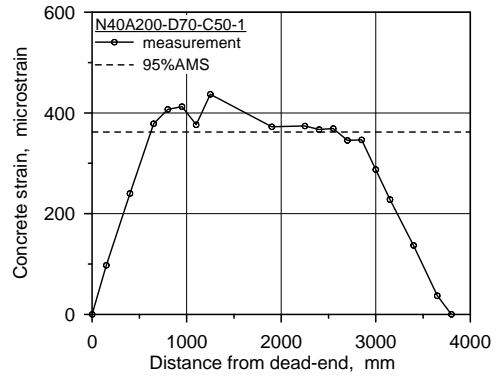
Figure B.16 Strand strain profiles of the specimens N45A150-B70 in test series 7

B.8 Test Series 8

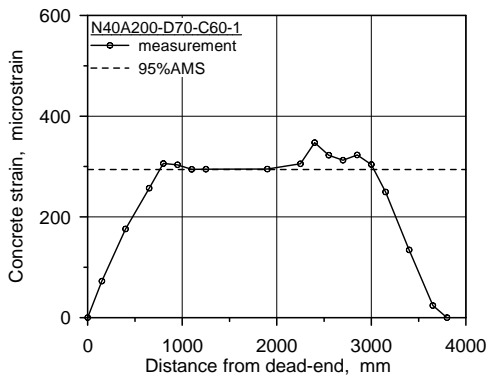
B.8.1 Cover Depth and Tensile Strength of Strand



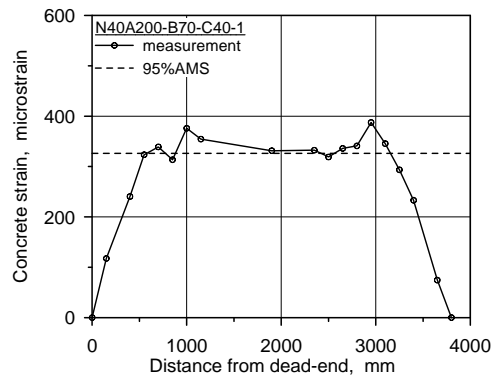
(a)



(b)



(c)



(d)

Figure B.17 Concrete strain profiles of the specimens in test series 8: (a) N40A200-D70-C40-1; (b) N40A200-D70-C50-1; (c) N40A200-D60-1; and (d) N40A200-B70-C40-1

B.8.2 Strand Spacing

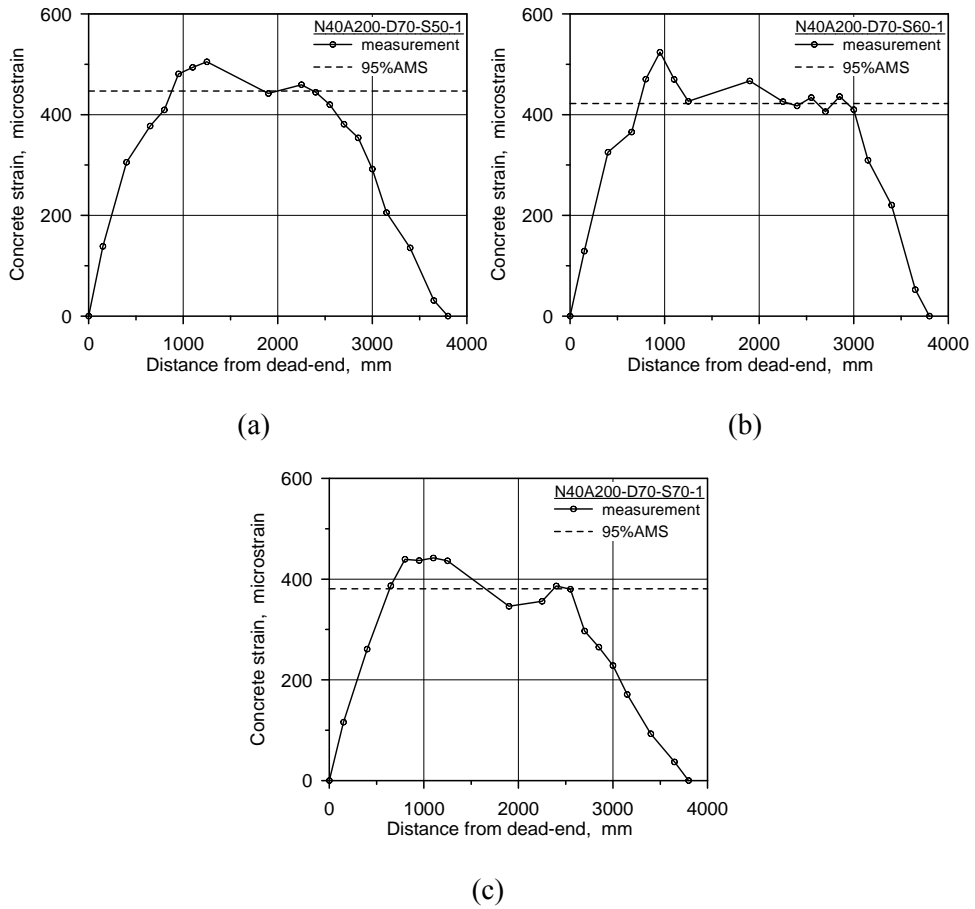
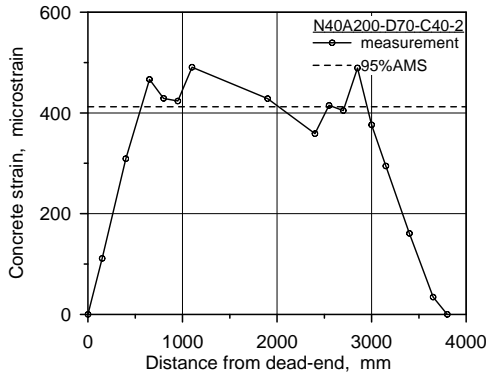


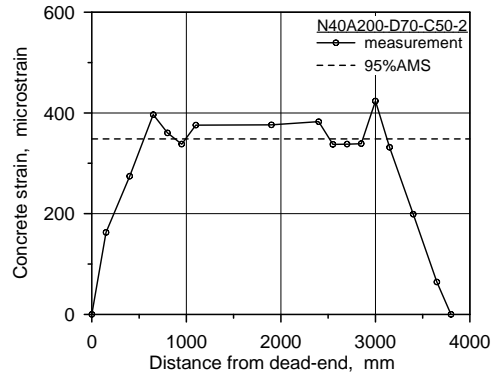
Figure B.18 Concrete strain profiles of the specimens in test series 8: (a) N40A200-D70-S50-1; (b) N40A200-D70-S60-1; and (c) N40A200-S70-1

B.9 Test Series 9

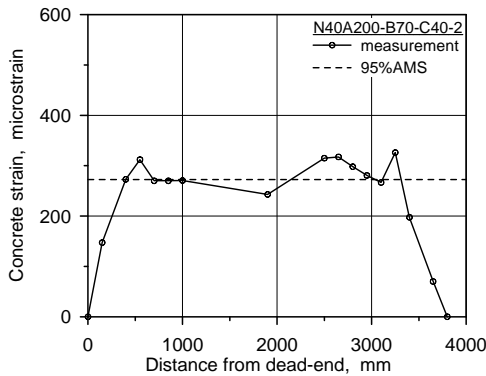
B.9.1 Cover Depth and Tensile Strength of Strand



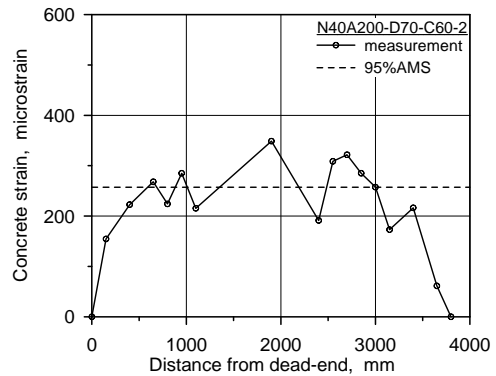
(a)



(b)



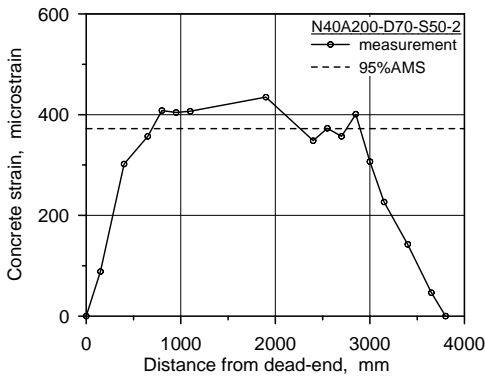
(c)



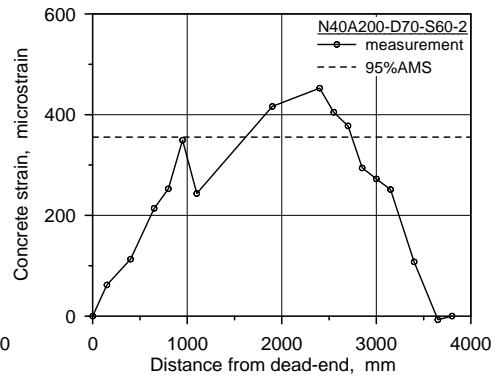
(d)

Figure B.19 Concrete strain profiles of the specimens in test series 9: (a) N40A200-D70-C40-2; (b) N40A200-D70-C50-2; (c) N40A200-D60-2; and (d) N40A200-B70-C40-2

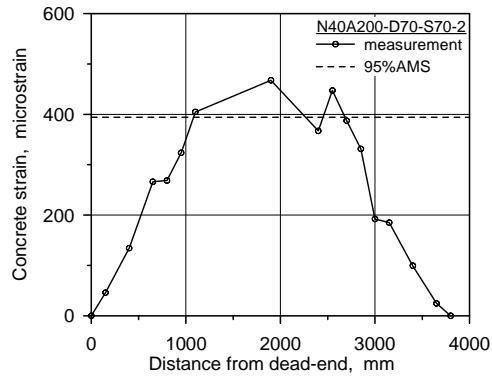
B.9.2 Strand Spacing



(a)



(b)

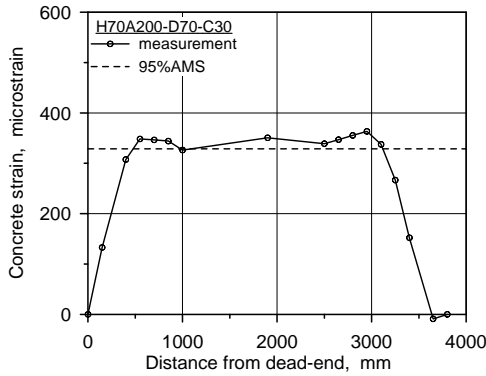


(c)

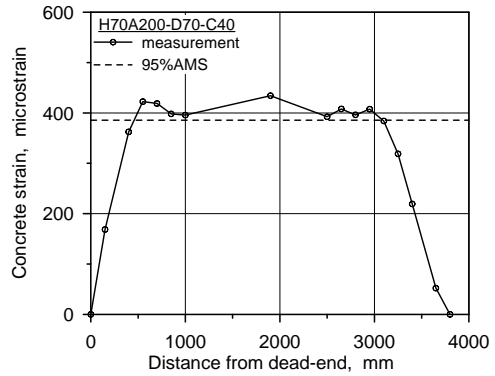
Figure B.20 Concrete strain profiles of the specimens in test series 9: (a) N40A200-D70-S50-2; (b) N40A200-D70-S60-2; and (c) N40A200-S70-2

B.10 Test Series 10

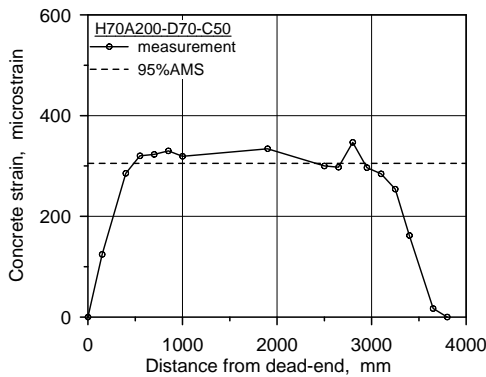
B.10.1 Cover Depth and Tensile Strength of Strand



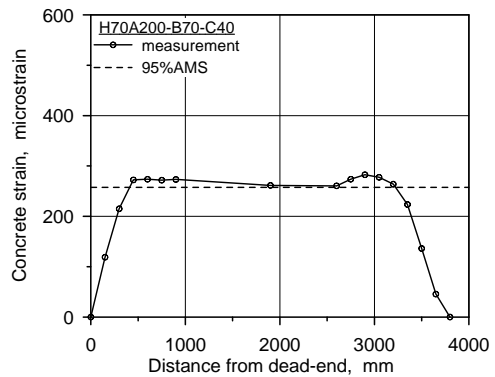
(a)



(b)



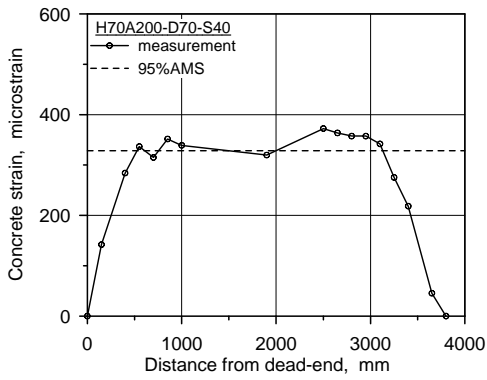
(c)



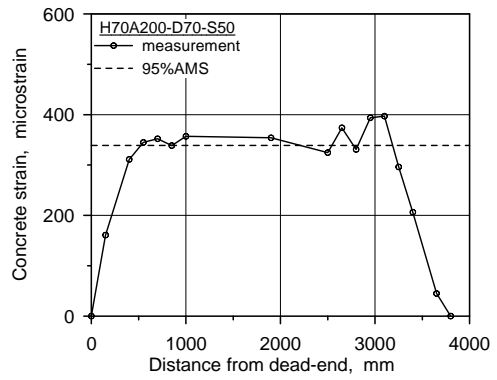
(d)

Figure B.21 Concrete strain profiles of the specimens in test series 10: (a) H70A200-D70-C30; (b) H70A200-D70-C40; (c) H70A200-D50; and (d) H70A200-B70-C40

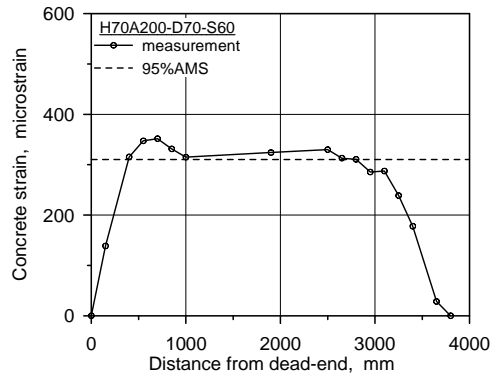
B.10.2 Strand Spacing



(a)



(b)



(c)

Figure B.22 Concrete strain profiles of the specimens in test series 10: (a) H70A200-D70-S40; (b) H70A200-D70-S50; and (c) H70A200-S60

국문초록

프리텐션 프리스트레스트 콘크리트 부재의 전달 영역 거동 및 해석

전달 길이는 유효 프리스트레스 응력을 전달하기 위하여 프리스트레스 강재가 콘크리트에 부착되어야 하는 길이로 정의된다. 전달 영역 내에서는 긴장력의 크기가 작기 때문에 하중이 단부 근처에 작용할 경우 전달 길이 값의 결정에 따라 사용하중 단계에서는 균열 모멘트, 극한하중 단계에서는 전단 강도와 정착 길이 등이 크게 영향을 받을 수 있다.

전달길이를 결정하기 위해 수십년간 다양한 경험식들이 제시되어 왔으나 동일한 조건에 대해서 경험식들의 예측값들이 크게 상이할 수 있음이 잘 알려져 있다. 따라서 전달 길이에 대해 주요 인자로 인식되어온 실험 변수의 영향을 재평가하고 그동안 고려되지 않았던 새로운 실험 변수의 영향을 확인할 필요가 있다. 또한 많은 경험식들은 부착 응력이 일정하다는 가정 하에 구성되었다. 이러한 가정은 부착 응력을 직접 측정하는 것이 아니라 전달 영역 내 콘크리트 변형률이 선형 분포를 갖는다는 관측을 근거로 하였다. 따라서 실제의 부착 거동에 기반한 전달 길이 추정식이 요구된다. 마지막으로 최근 들어 기존 강연선 보다 인장강도가 증진된 고강도 강연선이 개발되었으나 고강도 강연선에 대한 실험은 거의 이루어지지 않았다. 따라서 고강도 강연선에 대한 현 설계기준의 규정과 기존의 이론들이 적합한지 연구가 필요하다.

이러한 연구 목표를 달성하기 위하여 다양한 실험 변수를 고려한 일련의 전달 길이 실험을 수행하였다. 강연선의 꼬여있는 외부 측선에서 변형

를 측정하였으며 측정 방법의 타당성을 우선 논의하였다. 또한 측정된 강연선 변형률로부터 강연선의 거동을 해석하는 방법을 제시하였다. 실험 결과로부터 각 실험 변수의 영향을 파악하고 이를 바탕으로 현 설계기준 및 기존 경험식들을 평가하였다. 최종적으로 실제 강연선 거동을 바탕으로 새로운 부착 모델과 전달 길이 예측식을 제시하였다.

실험 결과 초기 프리스트레스 응력, 콘크리트 압축강도, 강연선 지름의 영향은 Oleśniewicz의 관계식을 이용하여 합리적으로 설명가능하였다. 이것은 전달 영역에서 선형의 부착 응력 분포 및 포물선 형태의 강연선 변형률 분포를 의미하는 것이다. 피복두께, 단면크기, 강연선 간격에 대하여 쪼갬 균열 발생 및 콘크리트 구속력 약화는 뚜렷이 나타나지 않았다. 따라서 현 설계 기준을 만족한다면 이 변수들의 영향은 크지 않은 것으로 판단된다. 이 외에도 양생 방법, 비부착, 철근 간격, 강선 절단 방법에 따른 영향을 파악하였다.

현 설계기준은 고강도 강연선의 전달 길이에 대하여 보수적인 예측값을 주었다. 현 설계기준의 최소 피복두께 및 강연선 간격 규정은 고강도 강연선에도 적용 가능하다. 순간 절단에 의한 양 단부의 전달 길이 차이는 고강도 강연선에서 보다 크게 확대되었다.

실제 측정된 부착 응력 분포로부터 새로운 부착-슬립-변형률 관계를 유도하였다. 이 관계로부터 부착 응력, 슬립, 강연선 변형률에 대한 간단한 형태의 예측식을 제시하였다. 제안 모델 및 예측식들은 프리텐션 부재의 전달 영역 거동의 예측에 유용하게 활용될 수 있을 것으로 판단된다.

주요어 : 프리텐션, 전달 길이, 고강도 강연선, 부착 응력, 강연선 변형률,
부착-슬립-변형률 관계

학 번 : 2009-30232